Design and Synthesis of Novel *Mycobacterium tuberculosis* Pantothenate Kinase and Glutamate Racemase Inhibitors

THESIS

Submitted in partial fulfilment

of the requirements for the degree of

DOCTOR OF PHILOSOPHY

by

PRASANTHI MALAPATI

ID No 2014PHXF0402H

Under the supervision of

D. SRIRAM

BITS Pilani

Pilani | Dubai | Goa | Hyderabad

BIRLA INSTITUTE OF TECHNOLOGY & SCIENCE, PILANI

2017

BIRLA INSTITUTE OF TECHNOLOGY & SCIENCE, PILANI

CERTIFICATE

This is to certify that the thesis entitled "**Design and Synthesis of Novel *Mycobacterium tuberculosis* Pantothenate Kinase and Glutamate Racemase Inhibitors**" and submitted by **PRASANTHI MALAPATI** ID No. **2014PHXF0402H** for award of Ph.D. of the Institute embodies original work done by her under my supervision.

Signature of the supervisor:

Name in capital letters : **D. SRIRAM**

Designation : **Professor**

Date:

Acknowledgement

This thesis is the end of my journey in obtaining my Ph.D. In this wonderful journey there are numerous people whose continuous support, encouragement and guidance helped me to successfully complete my thesis. I would take this opportunity to express my gratitude to each and every one who made my stay in BITS memorable.

My first thanks must go out to my adviser, HOD of pharmacy department ***Prof. D. Sriram*** *for the continuous support of my Ph.D. study and research, for his patience, motivation, enthusiasm and immense knowledge. His guidance helped me in all the time of research and writing of this thesis. Our interactions were always quite informal and friendly. I consider myself quite fortunate to have had such an understanding and caring adviser, throughout the course of my research at the Institute. The work environment given to me under him, the experiences gained from him and his creative working culture are treasured and will be remembered throughout my life.*

I gratefully acknowledge my DAC member ***Prof. Yogeeswari Perumal*** *for her understanding, encouragement and personal attention which have provided good and smooth basis for my Ph.D. tenure.*

I deeply acknowledge and my heartfelt thanks to ***Dr. Balaram Gosh****, Department of Pharmacy, BITS, Pilani-Hyderabad campus, for his valuable suggestions, guidance and precious time which he offered me throughout my research.*

I would like to thank my parents ***Venkateswara Rao*** *and* ***Anasuya****, my husband* ***Venkat*** *and my brother* ***Vishnu*** *who have given their blessings and love for the great desire to see me succeed and get the highest degree in education. It is only their vision, support and encouragement which always helped me in keeping my morale high. I dedicate this thesis to my father for his unconditional love and care.*

I take this opportunity to thank ***Prof. Souvik Bhattacharya****, Vice-Chancellor (BITS) and Director* ***Prof. G Sundar*** *(Hyderabad campus), for allowing me to carry out my doctoral research work in the institute.*

*I am sincerely thankful to **Prof. S.K. Verma**, Dean, Academic Research Division, BITS-Pilani, Pilani and **Dr. Vidya Rajesh**, Associate Dean, Academic Research Division, BITS-Pilani, Hyderabad campus for their co-operation and encouragement at every stage of this research work.*

*I am happy to express my sincere thanks to and **Prof**. **P**. **Yogeeswari** for valuable suggestions, moral support and great discussions during practical sessions.*

*During my research work, I have benefited from discussions with several people, whose suggestions have gone a long way in developing the thesis. I thankful from my bottom of heart to **Prof**. **Punna Rao**, **Dr**. **V**. **Vamsi Krishna, Dr. Swathi Biswas**, **Dr. Sajeli Begum**, **Dr. Onkar Kulkarni**, **Dr. Arti Dhar** department of pharmacy.*

*I take this opportunity to sincerely acknowledge the **Department of Science and Technology** (DST), for providing financial assistance in the form of **DST Inspire fellowship**, JRF. This buttressed me to perform my work comfortably.*

*I sincerely acknowledge the contributions of **Dr Brahmam Medapi, Dr Radhika, Dr Bobesh K Andrews** and **Dr Vijay Soni** towards the successful completion of my thesis.*

*I am very much grateful to all my friends and it's my fortune to gratefully acknowledge the support of some special individuals **Nikhila Meda, Shubham Dwivedi, Shiva Krishna Vagolu, Madhu rekha, Kiran,** for the time they had spent for me and making my stay at campus a memorable one.*

*I express my thanks to laboratory assistants, **Mrs. Saritha**, **Mr. Rajesh**, **Mr. Uppalayya, Mr. Kumar, Mr. Mallesh** and **Mr.Seenu**. I take this opportunity to thank one and all for their help directly or indirectly.*

*Last but not the least I express my sincere gratitude to **almighty God,** for showering me with lots of love and care throughout my life.*

Date ***Prasanthi Malapati***

Abstract

Tuberculosis still remains the leading cause of death worldwide and was unanswered till date. The major hurdles in disease treatment are the genomic changes in bacteria leading to resistance, persistence and co-infection. Available treatment strategies have many drawbacks like longer treatment period, side effects, drug interactions which result in patient noncompliance. In present work we thrived to develop inhibitors against unexplored key targets namely Pantothenate kinase (PanK) and glutamate racemase (GR).

In-house database screening was performed employing e-pharmacophore model for target PanK, a total of 13 compounds were shortlisted, further tested for their inhibitory activities. Unfortunately these compounds failed to act against enzyme due to failure of drug screening model and halted the study.

For GR enzyme, five compound libraries comprising a total of 117 compounds were developed by lead derivatization technique and evaluated them by various biological assays compounds were prepared by lead derivatization approach. In Benzthiazole series, compound **BT_25** (IC_{50} 1.32 ± 0.43 µM) has shown very good activity in all *in vitro* and *in vivo* models. Further evaluation in molecular docking supported that this compound also showed similar interactions with *B. subtilis* and TB bacteria with non competitive mode of inhibition in TB bacteria. In Benzoxazole series compound **BO_22** (IC_{50} 1.1 ± 0.52 µM) showed good *in vitro* and *in vivo* activities and was proven to be the most potent molecule of series. This data was in compliance with the molecular docking and simulation studies. In flourothiazole series, comparing the overall assays tested for, compounds **FT_25** (3.97 ± 0.72 µM) has shown potent activities in enzyme assay as well as against active and dormant culture. In Oxoquinazoline and Indazole series, we were able to identify compounds which have efficacy against both replicating and non-replicating stages of *M. tuberculosis*. **QA_16** (10.1 ± 0.62 µM), **QA_19** (5.23 ± 0.34 µM), **IN_11** (6.32 ± 0.35 µM) and **IN 22** (6.11 ± 0.51 µM) results show that they are equally effective as standard drugs against active stage of tuberculosis, additionally, they have the advantage of potency against the persistent phase of tuberculosis.

List of Tables

LIST OF FIGURES

LIST OF ABBREVIATIONS

µg	:	Microgram
µL	:	Microlitre
µM	:	Micromolar
^{13}C NMR	:	Carbon Nuclear Magnetic Resonance
^{1}H NMR	:	Proton Nuclear Magnetic Resonance
3D	:	Three Dimensional
ANOVA	:	Analysis of Variance
Ala	:	Alanine
Arg	:	Arginine
ATP	:	Adenosine Triphosphate
$(BOC)_2O$	:	Di-tert-butyl dicarbonate
BSA	:	Bovine serum albumin
$CDCl_3$	:	Chloroform deuterated
CysM	:	Cysteine synthase M
CysK	:	Cysteine synthase K
d	:	Doublet
DCM	:	Dichloromethane
dd	:	Doublet of doublet
DMF	:	*N*,*N*-Dimethylformamide
DMSO	:	Dimethyl sulfoxide
DMSO-d_6	:	Dimethyl sulphoxide deuterated
DSF	:	Digital Scanning Flourimeter
DRC	:	Dose Response Curve

E	:	Ethambutol
ESI	:	Electron Spray Ionization
Et_3N	:	Triethylamine
EtOH	:	Ethanol
FDA	:	Food and drug administration
GR	:	Glutamate racemase
H/ INH	:	Isoniazid
HEPES	:	4-(2-Hydroxyethyl)-1-Piperazineethanesulfonic acid
HIV	:	Human Immuno Deficiency Virus
HPLC	:	High Pressure Liquid Chromatography
IC_{50}	:	Half Maximal Inhibitory Concentration
ITC	:	Iso Thermal Calorimetry
J	:	Coupling constant
KCl	:	Potassium chloride
kDa	:	Kilodalton
KOH	:	Potassium hydroxide
LAT	:	Lysine ε-amino transferase
LB	:	Luria Broth
LCMS	:	Liquid chromatography–Mass Spectrometry
LHS	:	Left Hand Side
m	:	Multiplet
M.p	:	Melting point
MDR-TB	:	Multidrug-Resistant Tuberculosis
MeOH	:	Methanol
mg	:	Milligram

MABA	:	Microplate alamar Blue assay
MHz	:	Mega hertz
MIC	:	Minimum Inhibitory Concentration
mL	:	Milliliter
Mmol	:	Millimole
M. tuberculosis	:	*Mycobacterium tuberculosis*
MTT	:	(4,5-Dimethylthiazol-2-yl)-2,5-diphenyltetrazolium bromide
MW	:	Microwave
NaCl	:	Sodium chloride
NADH	:	Nicotinamide Adenine Dinucleotide
nM	:	Nanomolar
NRP	:	non-replicating persistence
OADC	:	Oleic Albumin Dextrose Catalase
OASS	:	O-acetylserine sulfhydrylase
OAT	:	Ornithine aminotransferase
OD	:	Optical density
OPS	:	O-phosphoserine
P	:	Para
PDB	:	Protein Data Bank
PanK	:	Pantothenate kinase
PLP	:	Pyridoxal pyrophosphate
R/Rif	:	Rifampicin
ROI	:	Reactive oxygen intermediate
RNS	:	Reactive nitrogen species
Rpm	:	Rotations per minute

RPMI	:	Roswell Park Memorial Institute
Rt	:	Room temperature
S	:	Singlet
SAR	:	Structure Activity Relationship
SDS-PAGE	:	Sodium Dodecyl Sulphate- Polyacrylamide Gel Electrophoresis
t	:	Triplet
TAE	:	Trisbase, Acetic acid, EDTA mixture
TB	:	Tuberculosis
TFA	:	Trifluoroacetic acid
THF	:	Tetrahydrofuran
TLC	:	Thin-layer chromatography
TMS	:	Trimethylsilane
UV	:	Ultraviolet
WHO	:	World Health Organization
XDR-TB	:	Extensively Drug-Resistant Tuberculosis
XP	:	Extra Precision
Z	:	Pyrazinamide
δ	:	Chemical shift

Introduction Chapter 1

Tuberculosis (TB) is a well known infectious fatal disease from decades. TB is caused by *Mycobacterium tuberculosis* (*M. tuberculosis*) typically affecting the lungs. According to World Health Organization 2016 report, about 1.4 million deaths and 10.4 million new cases resulting from TB infection. This is regardless the timely diagnosis and correct treatment with potent available drugs. **Figure 1.1** illustrates the list of countries with three TB burdens from 2016-20 [WHO Global tuberculosis report, 2016]. *M. tuberculosis* is an obligate aerobic bacillus with the slow rate of division. TB is well known as an air-borne disease which is transmitted as the highly infectious aerosol. The pathogen typically majorly affects lungs, but can also infect other vital parts of the body such as the brain, spinal cord, genital organs, and kidneys. The outcomes from the exposure of the pathogen to the human body range from the destruction of the pathogen by host's immune system to the development of active primary TB by the individual [Flynn J.L. *et al.,* 2001]. However, the majority of individuals infected with *M. tuberculosis* have a non-contagious form of infection, known as latent tuberculosis. This form of infection does not show any symptoms and possess 5-10% risk of development of active TB during the lifetime of an infected individual [Clark-Curtiss J.E.; Haydel S.E., 2003].

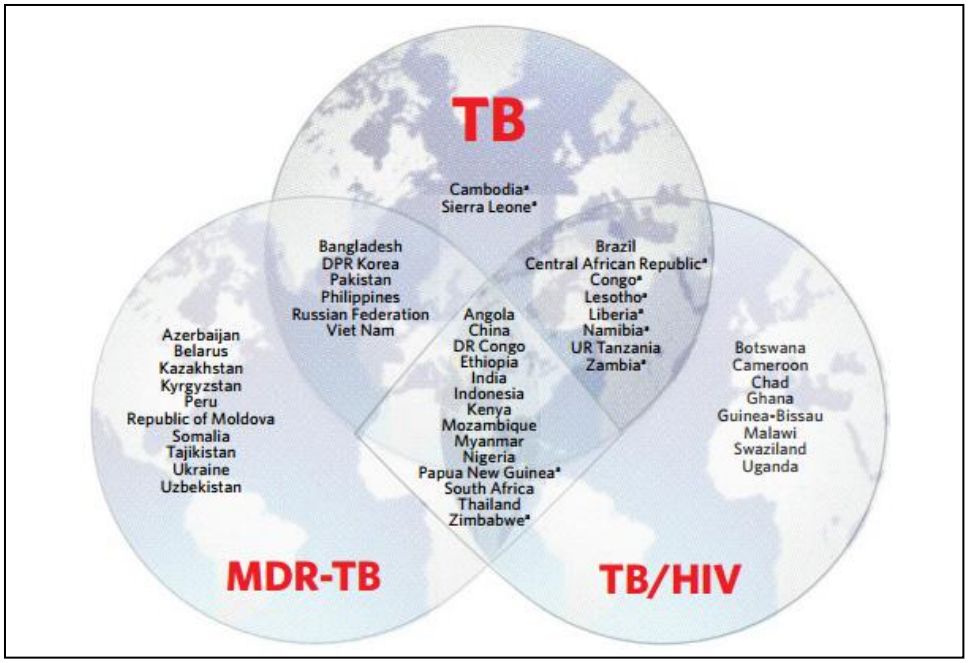

Figure 1.1: Prevalence of TB worldwide

1.1. Pathophysiology of tuberculosis

TB infection begins when the mycobacteria reach the pulmonary alveoli, where they invade and replicate. Macrophages identify the pathogen as foreign material and attempt to eliminate it by phagocytosis. During this process, the bacterium is enveloped by the macrophage and stored temporarily in a membrane-bound vesicle called phagosome. In the process of killing the pathogen, phagosome combines with the lysosome to create a phagolysosome. Within the macrophage the bacteria inhibit many cellular mechanisms preventing the fusion between phagosomes and lysosomes [Houben E.N., *et al*., 2006]. The bacterium is able to reproduce inside the macrophage and will eventually disrupt the immune cell. When a large number of macrophages get infected, they fuse together and form multinucleated giant cells called Langhans cells. These infected macrophages are surrounded by other immune cells creating a compartment called granuloma [Pieters J., *et al*., 2008]. Usually, macrophages, T lymphocytes, B lymphocytes and fibroblasts aggregate to form granulomas, which are surrounded by lymphocytes [Grosset J., *et al*., 2003]. Mostly, the granulomas formed will be suppressed by the host immune system thereby restricting the replication of bacteria. In such cases, the pathogen enters a dormant state within the granulomas, within which the pathogen virulence factors and the host immune response are in balance. Suppression of the immune system leads to the bacterial reactivation and its replication thereby turning into active TB **(Figure 1.2)**.

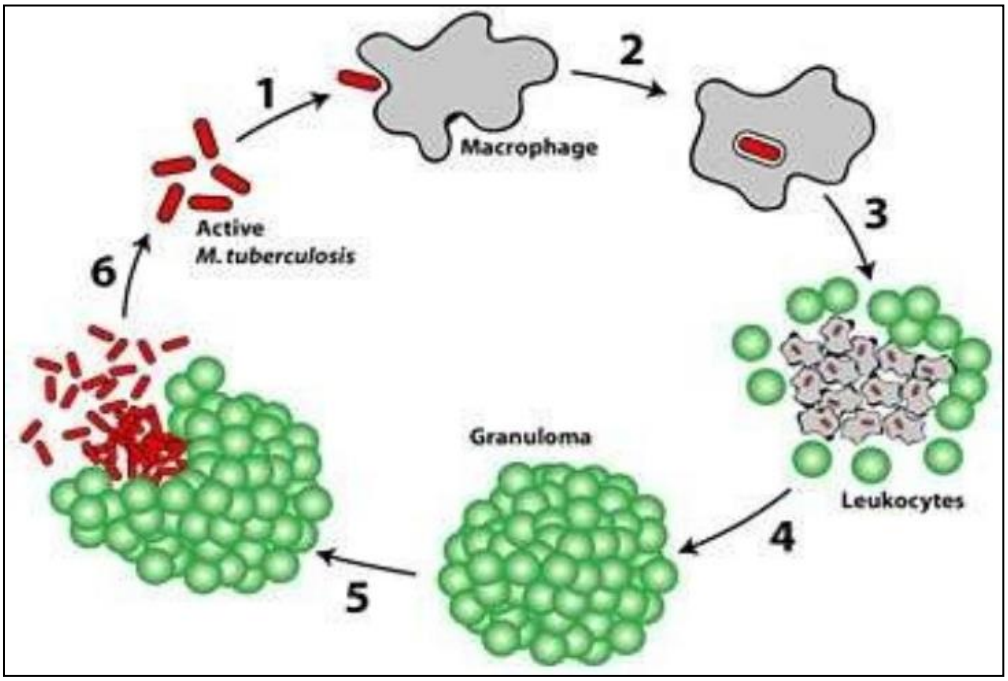

Figure 1.2: Pathogenesis of *M. tuberculosis* [Houben, E.N., *et al*., 2006]

1.2. Existing tuberculosis regimen

WHO recommends a standard regimen of antibiotics in DOTS therapy for newly infected individuals for a period of 6 months which covers 2 phases [Ginsberg, A. M., *et al*., 2007]. The primary phase i.e., Intensive phase treatment involves use of Isoniazid (INH), Rifampicin (RIF), Pyrazinamide (PYZ), Ethambutol (ETH) and Streptomycin for a period of 2 months; the latter phase namely Continuation phase involves use of Isoniazid and Rifampicin for 4 months to completely eliminate bacteria and avoid development of resistance [Dover, L. G., *et al*., 2011]. In case of HIV infected patients with TB, TB therapy is started prior to Clotrimoxazole and antiretroviral therapy. Drugs used for the treatment of Multi-drug resistance (MDR) TB that is resistant to INH and RIF [Green, K., *et al*., 2013] have been classified into 5 groups based on their efficacy. The standard regimen for treatment of MDR TB consists of 8 months of Pyrazinamide, Kanamycin, Ofloxacin, Protionamide, and Cycloserine, followed by 12 months of Ofloxacin, Protionamide, and Cycloserine [WHO Guidelines for treatment of tuberculosis fourth edition-2010, Sharma, S. K., *et al*., 2013].

1.3. Present scenario of resistant tuberculosis

Manmade amplification of TB led to the emergence of resistant forms of TB such as MDR TB and XDR TB. Treatment of MDR strains is limited due to lesser options, expensive, less potency and more side effects. XDR TB [Haydel, S. E., *et a*l., 2010, Parida, S. K., *et al*., 2015] (extensive drug-resistant) [Dheda, K., et al., 2010, O'Donnell, M. R., *et al*., 2013] is MDR TB having additional resistance to any of the Fluoroquinolones (such as Levofloxacin or Moxifloxacin) and to at least one of three injectable second-line drugs (Amikacin, Capreomycin or Kanamycin). The other major problem with TB treatment is persistence i.e., the ability of bacilli to survive in the dormant metabolically inactive stage. One-third of the world population is infected with latent tuberculosis. Most of the drugs available act on metabolically active stages of bacilli [CDC report 2012]. The standard treatment regimen available for latent TB is the use of INH for 6 – 9 months or RIF for 4 months or INH and Rifapentine for 3 months [Jasmer, R. M., 2002]. The current therapies are lengthy and have associated side effects so there is growing need for new antibacterial agents with more efficacy and potency against resistant and persistent TB. The new agents are also expected to lower duration of therapy.

1.4. TB drugs under development pipeline

Due to enormous efforts in the area of TB more than 50 rapid diagnostic tests, 15 vaccine candidates and 2 drugs (Bedaquiline and Delamanid) successfully entered clinical trials in the last decade. Apart from the development of new drugs researchers are focusing on the repurposing of existing drugs for the treatment of susceptible, resistant and latent forms of *M. tuberculosis*. Examples of repurposed drugs include Linezolid, Nitazoxanide, Meropenem-Clavulanate, Sulfamethoxazole and Mefloquine. Linezolid belonging to oxazolidinone class is effective against MDR and XDR forms of TB. But long-term use is restricted due to associated neurotoxicity, which can be overcome by using in combination with Clarithromycin. Another derivative from same class Sutezolid is more attractive due to more tolerance and is under development. Meropenem- Clavulanate and Sulfamethoxazole were also found to be effective against MDR and XDR forms of TB [WHO Global tuberculosis report, 2016].

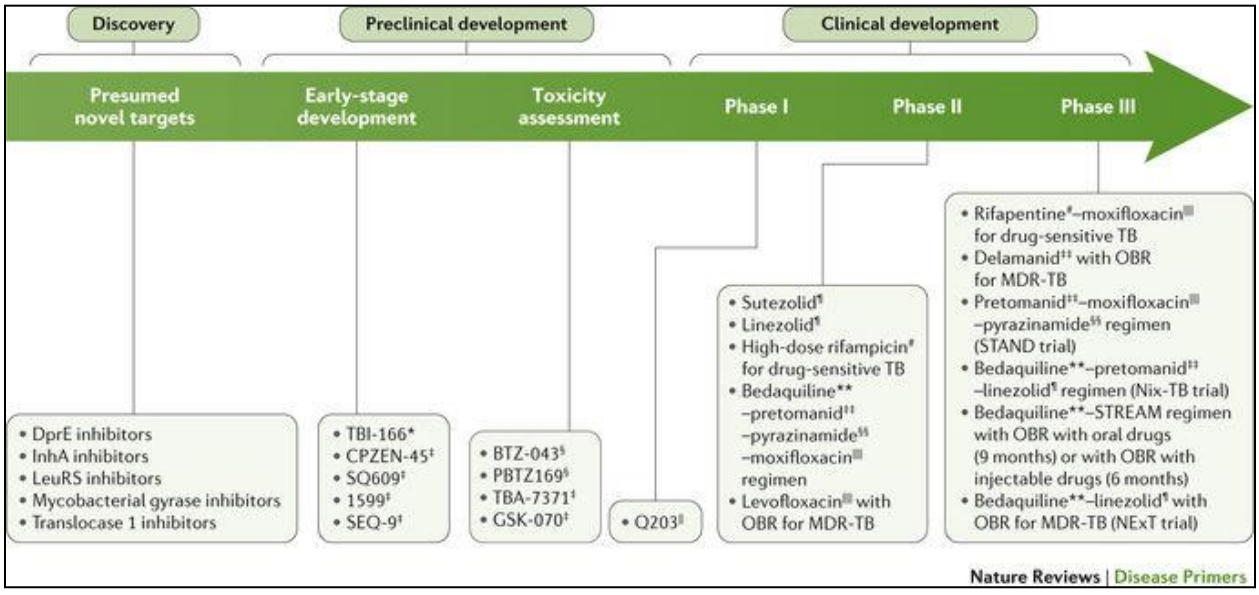

Figure 1.3: Drug development pipeline for TB [Pai M, *et al*., 2016]

Bedaquiline, Delamanid, Pretomanid, Sutezolid, Q203, SQ109 and Benzothiazinones fall under the category of new drugs. Bedaquiline was approved in Dec 2012 by US FDA for treatment of MDR TB. Delamanid and Pretomanid are nitroimidazole derivatives under phase 3 clinical trials. SQ109 is an analogue of Ethambutol and is effective against susceptible and resistant forms of TB. Benzothiazinones are in preclinical phase of development. PBTZ169 a piperazine containing

benzothiazinone is compatible with all TB drugs and appears to have synergies with Bedaquiline and Clofazimine. It is phase I clinical trial for the treatment of susceptible and resistant forms of TB. Q203 belongs to imidazopyridine class is in phase I trials [D'Ambrosio, L., 2015].

Literature review Chapter 2

Detailed literature review was done on two targets involved in the study namely- Thorough literature review was done on two targets involved in the study namely Pantothenate kinase (PanK) and Glutamate racemase (GR). One is involved in the cofactor synthesis and the other in the cell wall synthesis. Bothe the targets are considered to be key enzymes for the persistence of the organism.

2.1. Target I – Pantothenate kinase (PanK)

In pursuit of identifying or selecting targets for novel antimycobacterials, it is very important to limit the choice to those targets that impact viability with the slightest perturbation. Because target-based screening of traditional enzymes has largely proven unsuccessful for antibiotic discovery, different drug exploration strategies can be applied to overcome some of the challenges associated with the failure in activity. One such approach is exploring the targets involved in cofactor synthesis pathways. They are rich sources of potential drug targets, as a single cofactor is used by many proteins in a network.

2.1. 1. Biosynthesis of Coenzyme A mediated by PanK

Coenzyme A (CoA), one such cofactor, is an essential and ubiquitous part of the metabolism of many organisms. CoA functions as an acyl group carrier and carbonyl activating group in numerous reactions central to cellular metabolism, and provides the 4-phosphopantetheine prosthetic group incorporated by carrier proteins that play key roles in fatty acid, polyketide and nonribosomal peptide biosynthesis [Spry, C., *et al*., 2007]. CoA is synthesized *in vivo* from pantothenic acid. The different mechanisms by which organisms obtain the pantothenic acid required for the biosynthesis of CoA and the pathway by which organisms convert pantothenic acid are summarized in (**Figure 2.1**). Many organisms, including animals and several prokaryotic and eukaryotic pathogens, rely on uptake of exogenous pantothenic acid. Some bacteria, fungi and plants, however, are capable of synthesizing pantothenic acid de novo from β-alanine.

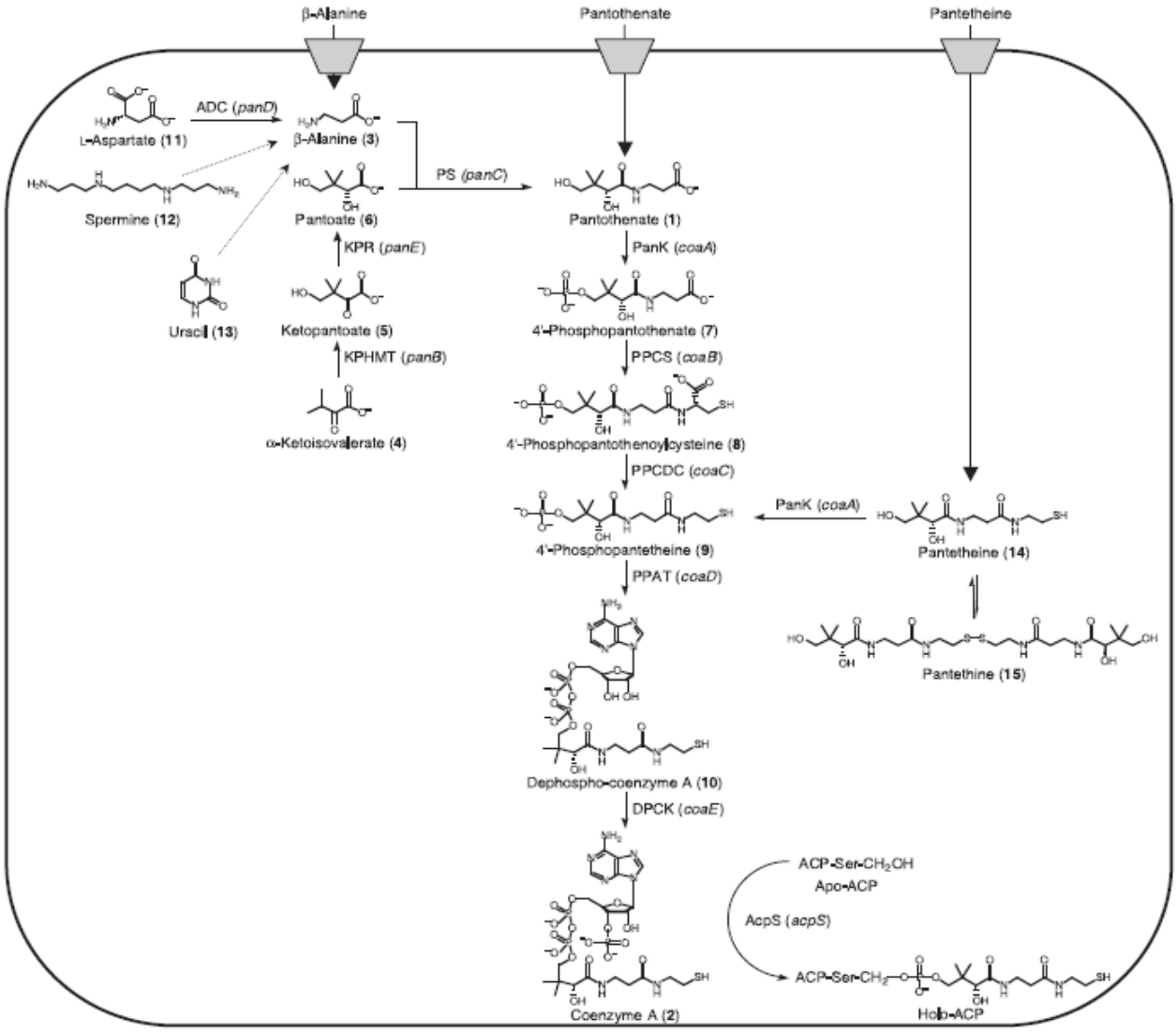

Figure 2.1: Schematic depicting pantothenate uptake, biosynthesis and transformation into CoA via the CoA biosynthesis pathway [Spry, C., *et al.*, 2007]

CoA is synthesized *in vivo* from pantothenic acid by a universal series of five enzymatic steps. The first step of the pathway, and the step that determines the rate of CoA biosynthesis in most organisms, is the PanK-catalyzed phosphorylation of pantothenate to 4-phosphopantothenate. 4-Phosphopantothenate is subsequently condensed with a cysteine molecule by phosphopantothenoylcysteine synthetase (PPCS) to yield 4-phosphopantothenoylcysteine. In the third step of the pathway, the cysteine moiety of 4-phosphopantothenoylcysteine is decarboxylated by phosphopantothenoylcysteine decarboxylase (PPCDC) to produce 4-phosphopantetheine. Phosphopantetheine adenylyltransferase (PPAT) transfers an adenylyl

group to 4-phosphopantetheine, generating dephospho-CoA. Finally, dephospho-CoA is phosphorylated at the 3-position of the ribose, by dephospho-CoA kinase (DPCK), to yield CoA [Spry, C., *et al*., 2007].

Pantetheine and the corresponding disulphide, pantethine is another mechanism for CoA synthesis. The *Escherichia coli* PanK (*E. coli* PanK) has recently been shown to catalyze the phosphorylation of pantetheine, the enzyme binds pantetheine with approximately threefold lower affinity than it does pantothenate [Worthington, A. S., *et al.*, 2006]. There were no reports found regarding similar uptake in *M. tuberculosis.* PanK catalyzes the very first step and also the rate-limiting step in CoA biosynthesis in many bacteria and eukaryotes, feedback regulated by the product of the pathway, CoA and its thioesters [Vallari, D. S., *et al*., 1987]. Inhibition of PanK therefore appears to be a potential target for novel antibacterial agents.

2.1.2. Essentiality of PanK and its characterization

Three types of PanK have been described, which differ in their biochemical and structural characteristics. Type I, encoded by the gene coaA, is found in a large number of bacterial species and is tightly feedback-regulated by CoA and its thioesters. It is exemplified by the extensively studied *E. coli* PanK. The type II enzyme is mostly found in eukaryotes. Humans express four isoforms of the enzyme, named PanK1 to 4. Defects in the panK2 gene have been linked to neurodegenerative disease. Based on sequence and structural homology some bacterial enzymes, such as *Staphylococcus aureus* PanK, are also classified as type II enzymes. Whereas the eukaryotic PanKs are feedback-regulated by CoA, the *Staphylococcus aureus* enzyme is not. Type III, encoded by the gene coaX, is the most widespread type of the enzyme, with homologs present in 12 of the 13 major bacterial groups. It is not inhibited by CoA or its thioesters. Many bacteria have two PanK genes coding for different types of the enzyme [Björkelid, C., *et al*., 2013].

The *M. tuberculosis* genome has both type I and type III PanK genes but it was established that the type I isoform, coaA, is the essential PanK in *M. tuberculosis* [Awasthy, D., *et al*., 2010]. Furthermore, there is low sequence homology between type I and type II PanKs [Leonardi, R., *et al*., 2005]. Hence an opportunity exists for the discovery of *M. tuberculosis* PanK inhibitors that are specific to bacteria and have minimal interaction with the human enzyme.

The foremost crystal structure of PanK is *E. coli* PanK, in complex with CoA, with 5-adenylimidodiphosphate, a non-hydrolysable analogue of ATP, and with ADP as well as

pantothenate. The mode of enzyme action can be explained by initial and end complex. In initial complex, ATP binds to the enzyme where later the pantothenate overlaps with the positions of base, represents the productive mode of binding results in the end complex of ADP and phosphopantothentate. The study of structural comparison of *M. tuberculosis* PanK and *E.coli* PanK revealed the CoA-binding region in *M. tuberculosis* PanK has almost the same structure as that in *E. coli* PanK [Das, S., *et al*., 2006].

Whereas studies on geometric and kinetic aspects of the enzyme activity of both enzymes showed differences. There observed the change in respective locations of reactants, namely ATP and pantothenate and their appropriate products in *M. tuberculosis* PanK; however in *E. coli* PanK are same [Chetnani, B., *et al*., 2009]. Kinetic measurements indicate that *M. tuberculosis* PanK exhibit dual substrate specificity for ATP and GTP, unlike homologous enzyme *E. coli* PanK which shows higher specificity for ATP. This was explained to be arisen to meet the biological necessity during dormant stage where ATP synthesis is down regulated and GTP has to be utilized for its survival [Chetnani, B., *et al*., 2010]. Further analysis through crystal structures of *M. tuberculosis* PanK with pantothenate, pantothenol and N9-Pan (reported as PanK inhibitor of CoA synthesis in *E. coli*) revealed that N9-Pan can behave in a similar manner to pantothenate. Similarly suggesting that these derivatives can be inhibitors of *M. tuberculosis* PanK [Ivey, R. A., *et al*., 2004, Thomas, J., *et al*., 2010 and Chetnani, B., *et al*., 2011].

2.1.3. Reported inhibitors against PanK

Inhibitors discovered with traditional target-driven drug discovery may not optimally inhibit the enzyme predominant in bacterial cell or may not be available at the desired concentration. Therefore Venkataraman., *et al*., considered mechanistic information on scaffolds before optimization using the thermal shift-based MoI (mechanisms of inhibition) assay to screen compounds and identify the true binders and classify inhibitors accordingly [Venkatraman, J., *et al*., 2012]. The first enzyme-engineered inhibitor complex structures of *M. tuberculosis* PanK were determined by Bjorkelid *et.al*., the biochemical characterization of two new classes of inhibitor compounds the triazoles, which are ATP competitors, and the biaryl acetic acids, with a mixed mode of inhibition was carried out and also observed that the binding nature was similar to natural substrate pantothenate and product phosphopantothentate but these inhibitors even though found to be inactive against *M. tuberculosis* in the whole cell assay, they are potent inhibitors of *M. tuberculosis* PanK (**Figure. 2.2 and 2.3**) [Björkelid, C., *et al*., 2013].

Assessment of *M. tuberculosis* PanK vulnerability through Target Knockdown and Mechanistically Diverse Inhibitors was determined, reporting the dual approaches established the poor vulnerability of PanK in *M. tuberculosis.* This study also made evident that for *M. tuberculosis* PanK, a mixed mode of inhibition would most likely result in growth inhibition at a much lower inhibitor concentration [Reddy, B. K., *et al*., 2014].

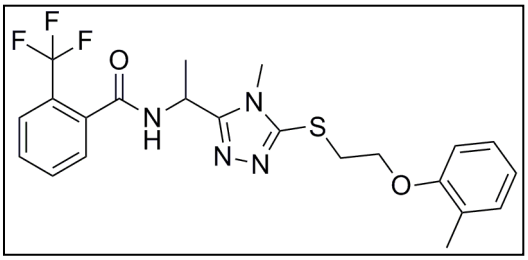

Figure 2.2: Structure of *M. tuberculosis* PanK inhibitor of triazole class [Björkelid, C., *et al*., 2013]

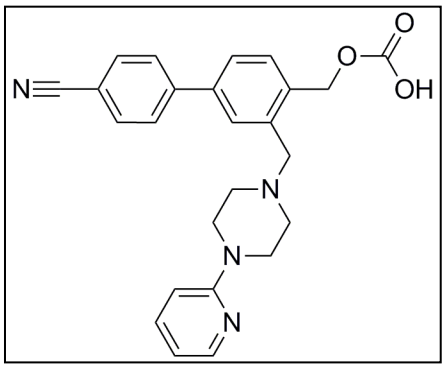

Figure 2.3: Structure of *M. tuberculosis* PanK inhibitor of biaryl class [Björkelid, C., *et al*., 2013]

2.2. Target II – Glutamate racemase

In enzymology, Glutamate racemase (GR) (EC 5.1.1.3) is an enzyme that catalyzes the chemical reaction:

L-glutamate ⟶ D-glutamate

Hence, this enzyme has one substrate, L-glutamate (L-glu), and one product, D-glutamate (D-glu). This enzyme belongs to the family of isomerases, specifically those racemases and epimerases acting on amino acids and derivatives, including proline racemase, aspartate

racemase, and diaminopimelate epimerase [Kim, K.H., *et al*., 2007]. This enzyme participates in glutamate metabolism that is essential for cell wall biosynthesis in bacteria [Sengupta S., *et al*., 2008]. Glutamate racemase performs the additional function of gyrase inhibition, preventing gyrase from binding to DNA [Reece, R.J., *et al*., 1991]. Glutamate racemase serves two distinct metabolic functions: primarily, it is a critical enzyme in cell wall biosynthesis, but also plays a role in gyrase inhibition [Sengupta, S., *et al*., 2008, Reece, R.J., *et al*., 1991]. The ability of GR and other proteins to serve two distinct functions is known as "moon lighting".

2.2.1. Role in bacterial cell wall synthesis

Glutamate racemase is a bacterial enzyme that is encoded by the MurI gene in *M. tuberculosis*. This enzyme is most commonly known as being responsible for the synthesis of bacterial cell walls. Through experimentation it was found that this enzyme is able to construct these cell walls by synthesizing D-glu from L-glu through racemization [Hwang, K.Y., *et al*., 1999]. D-glu is a monomer of the peptidoglycan layer in prokaryotic cell walls. Peptidoglycan is an essential structural component of the bacterial cell wall. The peptidoglycan layer is also responsible for the rigidity of the cell wall [Schleifer, K.H., *et al*., 1972]. This process, in which GR helps catalyze the inter-conversion of glutamate enantiomers, like L-glu, into the essential D-glu, is also cofactor independent. As such it can proceed without needing an additional source, which would bind to an allosteric site, altering the enzyme shape to assist in catalyzing the reaction [Glavas, S., *et al*., 2001]. GR involves a two-step process to catalyze the glutamate enantiomers to D-glu. The first step is a deprotonation of the substrate to form an anion [Glavas, S., *et al*., 2001]. Subsequently the substrate gets reprotonated. Once the glutamate is in the active site of the enzyme it undergoes a very large conformational change of its domains. Due to this main function of biosynthesis of bacterial cell walls GR has been targeted as an antibacterial in drug discovery [Lundqvist, T., *et al*., 2007]. But in case of tuberculosis, the enzyme still remains unexplored which can be potential antimycobacterial drug target.

2.2.2. Moonlighting function of GR

Along with its main function of cell wall biosynthesis, the moonlighting protein GR also functions independently as a gyrase inhibitor [Sengupta, S., *et al*., 2008]. Present in certain forms of bacteria, GR reduces the activity of DNA gyrase by preventing gyrase from binding to DNA [Sengupta, S., *et al*., 2008]. When gyrase binds to DNA, the enzyme decreases the tension in the DNA strands as they are unwound and causes the strands to become supercoiled [Sengupta, S., *et*

al., 2006]. This is a critical step in DNA replication in these cell which results in the reproduction of bacterial cells [Sengupta, S., *et al*., 2008]. The presence of Glutamate racemase in the process inhibits gyrase from effectively binding to DNA by deforming the shape of the enzyme's active site. It essentially disallows gyrase from catalyzing the reaction that coils unwinding DNA strands [Sengupta, S., *et al*., 2008]. This function of GR was discovered experimentally. DNA gyrase was incubated with the MurI enzyme and then added to a sample of DNA; the results of this experiment showed inhibition of supercoiling activity when GR was present. The cell wall biosynthesis function of GR is not directly related to its moonlighting function. The enzyme ability to inhibit gyrase binding can proceed independently of its main function [Sengupta, S., *et al*., 2008]. This means that DNA gyrase, in turn, will not have any effect on GR racemization, which was confirmed in a study of the racemization with and without the presence of DNA gyrase. In an experimental analysis, it was determined that GR employs the use of two different enzymatic active sites for its two functions. This was shown by the inclusion of the racemase substrate L-glu in an assay with the separated gyrase inhibition site. The gyrase inhibition occurs in both supercoiling and relaxing activities of the DNA gyrase, and the study concluded that the inhibition activity was able to proceed, unchanged, in the presence of the racemase substrate [Sengupta, S., *et al*., 2008]. This dictates that the two functions can be carried out independently of each other, on non-overlapping sites, making GR a true moonlighting protein. Mutant forms of MurI that are unable to exhibit their racemase function, no matter how compromised their racemase abilities were, were still proven through a study to be able to perform the DNA gyrase inhibition, with comparable results to a non-mutated form of GR [Sengupta, S., *et al*., 2008].

2.2.3. Relation between racemization and moonlighting functions of GR

Glutamate racemase provides multiple functions for bacterial cells. GR is an enzyme which is primarily known for its role in synthesizing bacterial cell walls. While performing the function of cell wall synthesis, GR also acts as a gyrase inhibitor, preventing gyrase from binding to DNA. The two processes have been shown to be unrelated [Sengupta, S., *et al*., 2008]. In order to ascertain the effects of gyrase inhibition on cell wall synthesis, the efficiency of the conversion of D-glu to L-glu was measured while varying the concentration of DNA gyrase. Conversely, the effects of cell wall production on gyrase inhibition were discovered by varying the concentration of the racemization substrate [Sengupta, S., *et al*., 2008]. The results of these experiments

conclude that there is no significant effect of racemization on gyrase inhibition or vice versa. The two functions of GR acting independent of each other reaffirmed the fact that GR is a moonlighting protein.

2.2.4. Structural insight of *M. tuberculosis* GR

Glutamate racemase is known to use its active site to undergo racemization and participate in the cell wall biosynthesis pathway of bacteria. From previous studies, it is most likely that the active site of GR that performs racemization is not the same active site that undergoes gyrase inhibition. In order to ascertain the effects of gyrase inhibition on cell wall synthesis, the efficiency of the conversion of D-glu to L-glu was measured while varying the concentration of DNA gyrase. Conversely, the effects of cell wall production on gyrase inhibition were discovered by varying the concentration of the racemization substrate. It has been shown that the two functions are neutral to each other. Consequently, a different site of GR, distant from its active site, is involved in interacting with gyrase [Sengupta, S., *et al*., 2008]. Protein crystal structure of GR from *M. tuberculosis* in complex with D-glu was reported (PDB ID: 5HJ7). This work revealed the active site conservation and its differences in other GR structures. Apart from the existing dimer geometrical forms this study revealed that GR of *M. tuberculosis* existed in a different new form and hence reported as a third dimer geometrical arrangement existed till today. The GR is inactive in solution unless the dimer interface is mutated. Furthermore, compounds designed to target other GR enzymes have been screened but do not inhibit mycobacterial GR, suggesting that a new drug design effort will be needed to develop inhibitors.

2.2.5. Reported inhibitors

Glutamate racemase has emerged as a potential antibacterial target since the product of this enzyme, D-glu, is an essential component of bacterial walls. Inhibiting the enzyme will prevent bacterial wall formation and ultimately result in lysis of the bacteria cell by osmotic pressure. Furthermore Glutamate racemase is not expressed nor is the product of this enzyme, D-glu is normally found in mammals, and hence inhibiting this enzyme should not result in toxicity to the mammalian host organism [Ruzheinikov, S.N., *et al*., 2005]. In fact, several different drugs have been reported as GR inhibitors in various bacteria like *Helicobacter pylori* and gram positive bacteria, such as pyrazolopyrimidinediones, pyridodiazepine amine, 8-benzyl pteridine-6,7-diones, dipicolinate and benzoat-3-sulfonate, (2R,4S)-4-substituted D-glutamate analogs, 1-*H*-

benzimidazole-2-sulfonic acid, 2,6 pyridinedicarboxylic acid and 4-hydroxybenzene-1,3-disulfonate (**Figure 2.4)** [Israyilova, A., *et al.,* 2016]. Recent report revealed that β-chloro–D-alanine (BCDA) has showed mechanism-based inactivator of GR of *M. tuberculosis*, thus provides a valuable tool for studying this essential and enigmatic enzyme and a starting point for future GR-targeted antibacterial development [Prosser, G.A., *et al*., 2016].

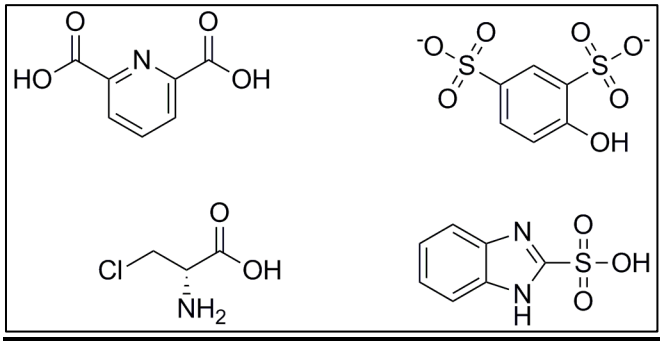

Figure 2.4: Structure of *M. tuberculosis* GR inhibitors [Israyilova, A., *et al.,* 2016]

Objectives and Plan of work Chapter 3

3.1. Objectives

Despite the discovery and availability of cheap and effective methods of treatment, there is an increasing threat from various drug-resistant forms of TB drives the quest for newer, safer, more effective TB treatment regimen. A detailed review of literature enlightened the significance of cofactor and cell wall synthesis pathways and key enzymes involved like Pantothenate kinase (Pank) and Glutamate racemase (GR) respectively. Inhibition of such crucial unexplored targets can be future changer in TB drug discovery. The present study thus focuses on achieving promising mycobacterial cellular potency through developing potential *Mycobacterium tuberculosis* (*M. tuberculosis*) Pank and GR direct inhibitors.

The main objectives of the proposed work are:

1. Design and identification of novel *M. tuberculosis* Pantothenate kinase and Glutamate racemase inhibitors and evaluation of inhibitory potency by enzymatic assay.
2. Random medium-throughput screening of BITS database for lead identification against enzymes.
3. Optimization studies of the selected leads, synthesis of derivatives and characterization of the synthesized compounds.
4. To evaluate the inhibitory potency of the synthesized compounds by *in vitro* enzyme inhibitory assays.
5. Computer-aided evaluation of interaction pattern of protein and ligand using molecular dynamic simulation studies.
6. Evaluate the protein-inhibitor binding followed by characterization of the mode of inhibition using biophysical characterization techniques.
7. *In vitro* anti-mycobacterial screening of the selected compounds using MABA assay.
8. To determine the efficacy of synthesized compounds against stress tolerant *M. tuberculosis*.
9. *In vitro* cytotoxicity studies for all the identified and synthesized compounds.
10. *In vivo* evaluation of anti-mycobacterial potency of the synthesized compounds in *Mycobacterium marinum* (*M. marinum*) induced Zebrafish model.

3.2. Plan of work

The plan of work was classified into the following categories.

3.2.1. Designing of *M. tuberculosis* Pantothenate kinase and Glutamate racemase inhibitors

We have utilized two strategies for designing the inhibitors.

Structure-based drug design approach for Pantothenate kinase

The available inhibitor bound co-crystallized structure of *M. tuberculosis* Pantothenate kinase protein was utilized as a structural framework for virtual screening of BITS *in-house* compounds collection to identify leads.

Random medium-throughput screening for Glutamate racemase

Thermal shift and enzyme assay with sensitive detectors were utilized for rapid screening of in-house BITS database to identify leads that modulate the cell wall synthesis pathway by enzyme inhibition.

3.2.2. Cloning, expression and purification of enzymes

We have planned to perform *in vitro* enzyme assays with Pank purified from *M. tuberculosis* and GR from *Bacillus subtilis (B. subtilis)* based on recent reports (in detail explained in results and discussion section below). The genes coding for the respective enzymes were individually amplified from *M. tuberculosis* H37Rv genomic DNA and *B. subtilis* subsp. *subtilis* 168. Clones were screened by restriction digestion and the resulting construct was transformed into an expression vector with a 6-His-tagged cloned vector and was then transformed into BL21 cells followed by extraction of pure proteins of interest.

3.2.3. *In vitro* enzyme inhibitory potency

The identified leads were further evaluated for their respective enzyme inhibitory potencies employing an *in vitro* assay carried out in 96-well plate.

3.2.4. Synthesis and characterization

The designed molecules were further synthesized in our laboratory utilizing reported methodology available in the literature. All reactions were monitored using thin layer chromatography and LCMS. The synthesized compounds were fully characterized using, ^{1}H-NMR and ^{13}C NMR were recorded and analyzed to confirm the structure of the compounds. The purity of the compounds was evaluated by elemental analysis and HPLC.

3.2.5. Evaluation of protein-inhibitor binding affinity using biophysical technique

The stabilization of top active compounds when bound to protein will be evaluated by thermal shift assay utilizing the differential scanning fluorimetry (DSF) technique.

3.2.6. Molecular dynamic simulation studies

The potent active molecules were subjected to simulation studies to study and analyze the binding and interaction pattern of protein and ligand during simulation.

3.2.7. *In vitro M. tuberculosis* screening

All molecules were further screened for their *in vitro* antimycobacterial activity against *M. tuberculosis* H37Rv by microplate alamar blue assay method.

3.2.8. Evaluation against stress models

The ability of *M. tuberculosis* to survive under stress conditions is considered to be its hallmark. The compounds which invade bacteria in these conditions are in great requirement. The synthesized compounds were tested for *M. tuberculosis* through studies like nutrient starvation, biofilm and further rate and degree of killing bacteria by active compounds was evaluated by time-kill kinetics assay.

3.2.9. *In vivo* anti-mycobacterial screening using adult zebrafish

The synthesized compounds are evaluated for its *in vivo* studies using adult zebrafish model, against *Mycobacterium marinum* strain (ATCC BAA-535) which is a genetic relative of *M. tuberculosis*. The reduction in bacterial count was evaluated by MPN assay.

3.2.10. *In vitro* cytotoxicity screening

All the compounds were also tested for *in vitro* cytotoxicity against RAW 264.7 cell line (mouse leukemic monocyte macrophage) using 3-(4,5-dimethylthiazol-2-yl)-2,5-diphenyltetrazolium bromide (MTT) assay.

Materials and Methods Chapter 4

4.1. Designing novel antagonists of *M. tuberculosis* Pantothenate kinase (PanK)

Structure-based drug design relies on knowledge of the three-dimensional structure of the biological target. We have utilized pharmacophore strategy for identification of leads.

4.1.1. Structure-based drug design approach

In this approach, we described a novel protocol for generating energy-optimized pharmacophore (e-pharmacophore) based on mapping of the energetic terms from the Glide XP scoring function onto atom centers. Beginning with a ligand-receptor complex we refined the ligand pose, computed the Glide XP scoring terms and mapped the energies onto atoms. Then, pharmacophore sites were generated and the Glide XP energies from the atoms that comprised each pharmacophore site were summed. The sites are then ranked based on these energies, and the most favorable sites were selected for the pharmacophore hypothesis [Salam N.K., *et al*., 2009]. Finally, these e-pharmacophores were used as queries for virtual screening.

Protein target for *M. tuberculosis*

In the present study, crystal structures of *M. tuberculosis* Pantothenate kinase in complex with inhibitor (PDB code: 4BFY) were retrieved from protein data bank (PDB) and were utilized for structure-based drug design [Björkelid, C., *et al*., 2013]. Hydrogen atoms, bond orders and formal charges were added using the protein preparation wizard of the maestro software package. Water molecules were removed from the atomic co-ordinates, except which were found to be involved in water-mediated hydrogen bonding interactions between the protein and ligand, thus while preparation of protein, these water molecules were retained. The resulting structure was energy minimized using OPLS_2005 force field [Banks J.L., *et al*., 2005]. Interactions of the ligand with the protein residues in the active site were visualized using ligand interaction diagram in Schrödinger suite version 9.3.

Protein and ligand preparation

The protein files were prepared using protein preparation wizard and impact energy minimization was performed using 500 cycles of steepest descent (SD) and 5000 cycles of conjugate gradient (CG) methods. The optimized potential for liquid simulations (OPLS) 2005 force field was attained. The active site of the proteins was defined and grid files were generated

using receptor grid generation panel. The reference ligand structure of both the proteins was downloaded from PDB and minimized using impact energy minimization with 100 cycles of SD and 500 cycles of CG. The three-dimensional structure of the compounds were retrieved from *in-house* database was employed for the virtual screening. The database compounds were energy minimized and used as a single file using LigPrep (LigPrep v2.2, Schrodinger 2012) module.

Glide XP (Extra-Precision) docking

The generated grid files from the prepared proteins were used for Glide XP docking calculations. The minimized conjugate gradient output of the reference ligand was used. The Write XP descriptor information‖ option and Compute RMSD option were enabled and the settings were kept default for the rest of the parameters. The XP Glide scoring function was used to order the best-ranked compounds and the specific interactions like *π-cation* and *π-π* stacking were analyzed using XP visualizer in Glide module. The input RMSD of the ligand was also ascertained.

E-pharmacophore generation

The pharmacophore hypotheses were created for the reference ligands of both proteins by using the XP descriptor file of the Glide XP output in the docking post-processing tool of the scripts module by using default settings for refinement and scoring. Starting with the refined crystal ligands, pharmacophore sites were automatically generated with Phase using the default set of six chemical features: hydrogen bond acceptor (A), hydrogen bond donor (D), hydrophobic (H), negative ionizable (N), positive ionizable (P), and aromatic ring (R). Hydrogen bond acceptor sites were represented as vectors along the hydrogen bond axis in accordance with the hybridization of the acceptor atom. Hydrogen bond donors were represented as projected points, located at the corresponding hydrogen bond acceptor positions in the binding site. Projected points allowed the possibility for structurally dissimilar active compounds to form hydrogen bonds at the same location, regardless of their point of origin and directionality [Singh K.D., *et al*., 2012]. The reference ligands were docked with Glide module of Schrödinger 9.3 in extra precision mode (XP) and the docked pose was refined and the Glide XP scoring terms were computed to map energies onto the atoms [Friesner R.A., *et al*., 2006]. The pharmacophore sites were generated, and the Glide XP energies from the atoms that comprised each pharmacophore sites were summed up. These sites were then ranked based on the individual energies, and the most favorable sites were selected for the pharmacophore hypotheses.

Preparation of commercial database

BITS *in house* database containing diverse structured compounds were used in this study. Database molecules were prepared using LigPrep and Epik to expand protonation and tautomeric states at pH 7.0 [Shelly J.C., *et al*., 2007]. Conformational sampling was performed for all molecules using the ConfGen search algorithm. We employed ConfGen with the OPLS_2005 force field and a duplicate pose elimination criterion of 1.0Å RMSD to remove redundant conformers. A distance-dependent dielectric solvation treatment was used to screen electrostatic interactions. A maximum relative energy difference of 10.0 kcal/mol was chosen to exclude high energy structures. Using Phase, the database was indexed with the automatic creation of pharmacophore sites for each conformer to allow rapid database alignments and screening.

Molecular docking studies – Virtual screening workflow

For the e-pharmacophore approach, explicit matching was required for the most energetically favorable site (scoring better than 1.0 kcal/mol) that finds matching pharmacophores in the ligands. For filtering the database molecules, a minimum of 3-4 sites was required to match for hypotheses with 4-6 sites. The above criterion was followed in the present work to screen the in-house database. In order of their fitness score, database leads were ranked to measure how well the aligned ligand conformer matched the hypothesis based on RMSD, site matching, vector alignments and volume terms. Database ligands after e-pharmacophore filter were docked into the binding sites of the protein utilizing medium-throughput virtual screening (MTVS) scoring function to estimate protein-ligand binding affinities. Ligands filtered from MTVS were subjected to Glide SP (standard precision) docking. The center of the Glide grid was defined by the position of the co-crystallized ligand. Default settings were used for both the grid generation and docking. Post-docking minimization was implemented to optimize the ligand geometries. Compounds with best docking and Glide scores were then subjected to Glide XP (extra precision) docking. Final short listing of possible lead compounds was based on visual inspection of the important amino acid residues in the active site cleft involved in binding and the hydrophobic interactions. The shortlisted leads were further tested in enzyme assay for their activity to select the final lead as described in next section.

4.1.2. Biological screening of compounds against *M. tuberculosis* Pantothenate kinase

Cloning, expression and purification of *M. tuberculosis* PanK

Cloning, expression and purification of Pantothenate kinase was done as previously reported (Das., *et al*., 2005). The full-length *coaA* gene has been amplified from *M. tuberculosis* H37Rv genomic DNA using forward primer (5'-CACCCATATGTCGCGGCTTAGCGAGCCG-3') and reverse primer (5'-AGCTAAGCTTTTACAGCTTGCGCAGCCGCAG-3'). The amplified gene was inserted into NdeI/HindIII -digested expression vector pQE2 (Novagen) and six histidine residues were added to the N-terminus of the gene product in order to smooth the progress of protein purification process. The recombinant plasmid was transformed into Escherichia coli (E.coli) BL21 cells (Novagen). The cultures were grown in Luria-Bertani broth (Hi-media) medium with 100mg/mL ampicillin at 37 ^{o}C until A_{600} reached a reading of 0.6. Cultures were induced with 0.2 mM isopropyl-d-thiogalactopyranoside (IPTG) further incubated for 7 h. After the incubation cells were centrifuged at 5,000rpm (Sorvall ST 16R centrifuge) for 20 minutes at 4 ^{o}C. Resuspension of cell pellet was carried out in ice-cold lysis buffer (50 mM Tris/HCl, pH 7.5, 300 mM NaCl, 1 mM DTT, 10% glycerol, 1 mM PMSF and 100 mg/mL lysozyme) and lysed by sonication. The crude lysate was centrifuged at 10,000rpm (Sorvall ST 16R centrifuge) for 30 minutes at 4 ^{o}C and the recombinant protein was loaded into a Ni±NTA metal-affinity column (His-bind resin, Novagen). The lysate was washed with wash buffer (lysis buffer containing 10mM imidazole) for 3 times till the unwanted proteins were washed off. The protein of interest bound to Ni beads was collected using elution buffer (lysis buffer containing 300 mM imidazole). The protein was dialysed using filtration buffer (50 mM Tris/HCl, pH 7.5, 500 mM NaCl, 2 mM DTT, 10% glycerol and 1 mM EDTA) overnight at 4^{0}C. The dialyzed protein sample (25 mL) was concentrated to 2 mL and further concentrated to 1 mL using a Millipore concentrator (MWCO-10 kDa). The protein sample was stored at –80 ^{o}C in 0.25 mL aliquots. The purity of the protein was verified by SDS±PAGE analysis (Awasthy., *et al*., 2010).

Biochemical assay for characterization of Pantothenate kinase

M. tuberculosis Pantothenate kinase (PanK) activity was measured as reported (Venkataraman. J., *et al*., 2012) by employing a pyruvate kinase -lactate dehydrogenase (PK-LDH) enzyme coupled assay (**Figure 4.1**). The assay reactions were carried in the 96-well procedure at 25 °C. Pantothenate and ATP Kinetic parameters were determined in 100-µL mixture containing 50 mM PIPES–NaOH (pH 7.0), 25 mM KCl, 0.1 mM EDTA, 20 mM $MgCl_2$, 2 mM DTT, 0.5mM phosphoenol pyruvate (PEP), 0.24 mM NADH, 0.002% Brij and 20 nM PanK (0.75 µg/mL). The

change in the reaction was observed through absorbance at 340 nm (NADH to NAD^+ conversion) for 60 minutes in a SpectraMax M4 (Molecular devices) microplate reader. Determination of K_m for ATP was done by varying ATP concentration from 20 µM to 1 mM and maintaining D-pantothenate at a saturating concentration of 3 mM. A varying concentration of D-pantothenate from 50 µM to 3 mM with maintaining ATP concentration (saturation) of 1 mM was done for calculation of its K_m.

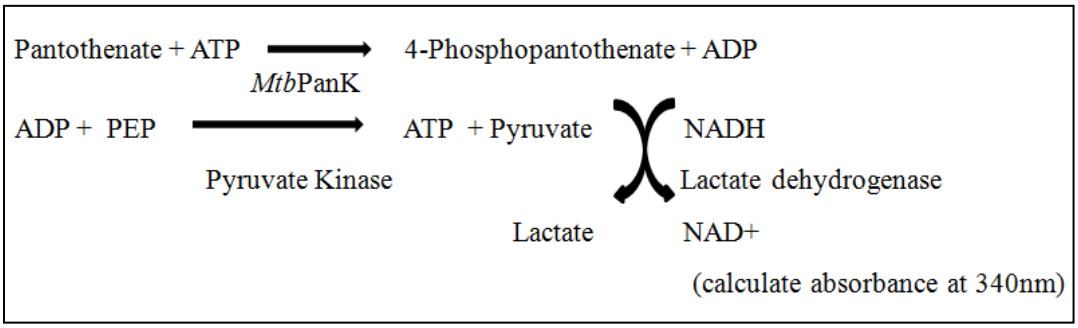

Figure 4.1: Enzyme assay reaction scheme for *M. tuberculosis* Pantothenate kinase (PanK)

4.2. Identification of leads for *M. tuberculosis* Glutamate racemase (GR)

4.2.1. Thermal shift assay (TSA) screening of database compounds

Cloning, expression and purification of *M. tuberculosis* GR

The MurI gene coding for enzyme GR was amplified using *M. tuberculosis* H37Rv genomic DNA and primers (forward primer 5'-GAAGTCATGAATTCGCCGTTG-3') and (reverse primer 5'-AAGATCTCTTCCATGGCCTAATG-3') having RcaI and BglII as restriction sites in order. Pfu DNA polymerase was used to carry out amplification reaction. Recombinant gene was tagged with histidine residues to N-terminus to aid protein purification. RcaI and BglII digested recombinant product was linked to NcoI-BamHI cut pET11d vector (Sengupta., *et al.*, 2006). The recombinant mycobacterial GR was expressed in E.coli BL26 (DE3) strain cells. These cells were grown in Luria-Bertani broth (Hi-media) medium with 100mg/mL ampicillin at 37 ^oC to obtain A_{600} of 0.5. Expression of GR was induced by adding 0.5mM of IPTG and left for incubation for 20 h at 18 ^oC for 20 h followed by centrifugation. Cell pellets were resuspended in buffer A (20 mM sodium phosphate, 30 mM imidazole, 500 mM NaCl, 10%glycerol, 1 mM D, L-glutamate, pH 7 and 4 mM 2-mercaptoethanol) and lysed using sonicator (intermittently cooled with ice). The cell lysate was centrifuged and the supernatant was loaded into a Ni±NTA

metal-affinity column (His-bind resin, Novagen). The column was washed and *M. tuberculosis* GR was eluted with buffer A containing 500 mM imidazole in a linear imidazole gradient. The concentration of GR was done by dialyzing the sample against 2 liters of buffer (20 mM Tris HCl, 100 mM NaCl, 10% glycerol, 4 mM 2-mercaptoethanol and 1mM D, L-glutamate, pH 8.0). The protein sample was stored at –80 ^{o}C in 0.25 mL aliquots. The purity of the protein was determined using SDS±PAGE analysis (Poen, S., *et al*., 2016).

Thermal shift assay

Thermal stability assays were performed using a real-time PCR thermal cycler (Bio-Rad) in 0.2 mL PCR tubes (Bio-Rad) in duplicates. Protein concentration of 0.2 mg/mL *M. tuberculosis* GR, 100 mM Tris HCl, 100 mM NaCl, pH 8.0, 2 mM D-glutamate were mixed in a 25 µL reaction volume with compounds (diluted with DMSO) at appropriate concentrations. The final concentration of DMSO was maintained not more than 2% (v/v). SYPRO orange protein gel stain (Sigma), was used to monitor thermal stability through protein unfolding at a final concentration of 6.25x (the dye available as a DMSO stock marked as "5000x). The sample tubes were sealed properly and heated from 20 to 80 ^{o}C at an interval of 0.02 ^{o}C/s. Changes in fluorescence of SYPRO orange dye indicates the unfolding pattern of protein. T_m values are obtained from the minima of the first derivative (−dF/dt) plots of unfolding protein curves using an in-built function in Bio-Rad prime PCR software [Venkataraman, J., *et al*., 2012]. The detailed procedure of GR protein expression and purification was discussed in below section. The short listed leads were tested for their activity testing in GR enzyme assay and evaluated the correlation of TSA and activity results to finalize the leads.

4.2.2. Glutamate racemase activity enzyme assay

Cloning, expression and purification of *B. subtilis* GR

The recombinant gene (RacE) was obtained by PCR amplification using genomic DNA of *B. subtilis* subsp. *subtilis* 168 with expression plasmid pET28a+ with tag extensions of histidine residues at N-terminus. Enzymes were expressed from *E.coli* BL21 (DE3) at 37 ^{o}C, purified using Ni±NTA metal-affinity column using buffer (20 mM TEA, 10 mM $MgCl_2$, 10 % glycerol, 500 mM NaCl, 50 mM imidazole, 1 mM DTT, 1 mg/mL lysozyme, 0.1 mM phenyl methane

sulfonyl fluoride, pH 7.8). Purity was confirmed using SDS-PAGE. The protein was made into aliquots and stored at -80 ^{o}C [Poen, S., *et. al.*, 2016, Prosser, G.A., *et. al.*, 2016].

Enzyme inhibitory study of *B. subtilis*

Enzyme inhibition studies of test compounds were performed in a 100 µL reaction volume of 100 mM Tris–HCl pH 8.0, 5 mM NAD+, 1 mM D-glutamate, 10 U/mL L-glutamate dehydrogenase (LDH) (all the chemicals were procured from Sigma) and enzyme concentration of 1µM *B. subtilis* GR with varying concentrations of test inhibitor (50 µM to 0.5 µM) monitored at 340 nm using microplate spectrophotometer (Spectromax M4, Molecular devices). IC_{50} of compounds was determined by measuring the NADH formation in the reaction at 340nm [Poen, S., *et. al.*, 2016]. The finalized leads were optimized using medicinal chemistry procedures.

4.2.3. Synthesis and characterization

The top potent lead compounds identified against *M. tuberculosis* GR by the above mentioned strategies were taken up for further lead optimization via synthesis. Lead expansion of the leads was achieved using the subsequent synthetic protocols. Chemicals (reagents and solvents) obtained from commercial sources were used without further purification. The reactions were monitored by thin layer chromatography (TLC) on silica gel 40 F254 (Merck, Darmstadt, Germany) coated on aluminium plates. Compounds were purified by Biotage Isolera flash chromatography. Molecular weights of the synthesized compounds were checked by Shimadzu, LCMS-2020 and the method used was electron spray ionization (ESI-MS) method. All ^{1}H NMR and ^{13}C NMR spectra were recorded on a Bruker AM-400/300 MHz and 100/75 MHz spectrometer, Bruker Bio Spin Corp., Germany using tetramethyl silane (TMS) as an internal standard. Melting points of compounds were reported in degrees Celsius and were uncorrected. Compounds were analyzed for C, H, N using a Vario MICRO cube in CHN mode.

Synthesis of 1-(3-(benzo[*d*]thiazol-2-yl)phenyl)-3-phenylthiourea and urea derivatives as potent *M. tuberculosis* GR inhibitors

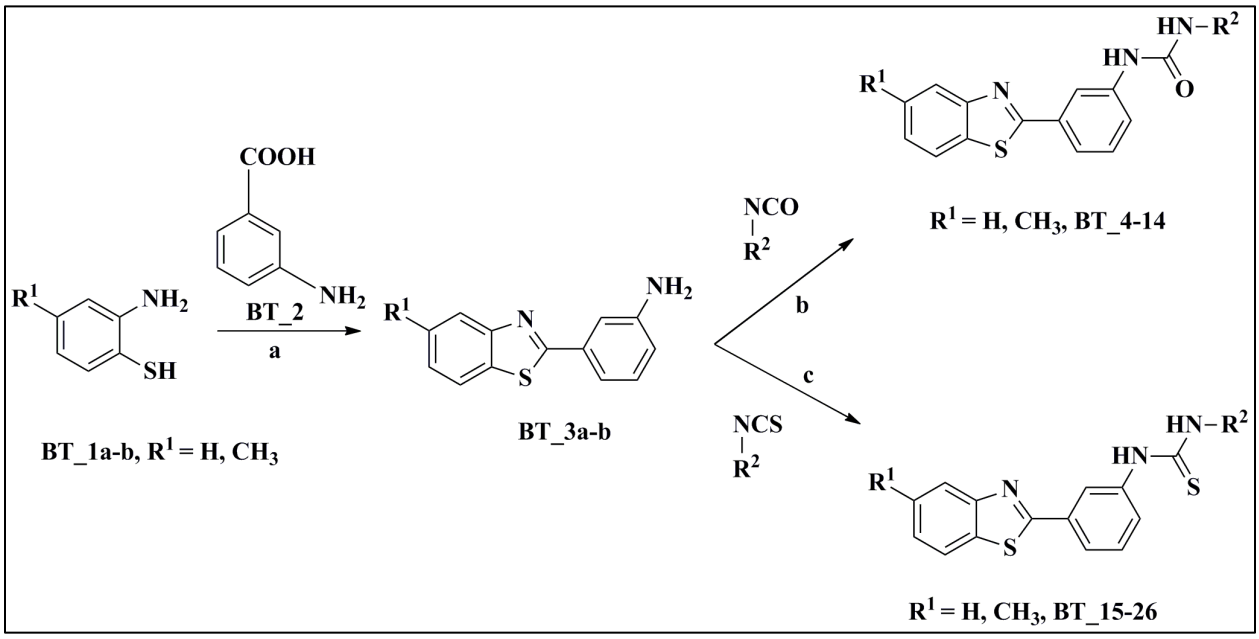

Figure 4.2: Synthetic protocol utilized for synthesis of molecules **BT_4-26**

Reagents and conditions: (a) PPA, 185°C, 6h; (b) R^2-NCO, DIPEA, DMF, rt, 2h; (c) R^2-NCS, DMF/xylene(4:1), K_2CO_3, MW, 110°C, 30min.

Synthesis of 1-(3-(benzo[*d*]oxazol-2-yl)phenyl)thiourea and urea derivatives as *M. tuberculosis* Glutamate racemase inhibitors

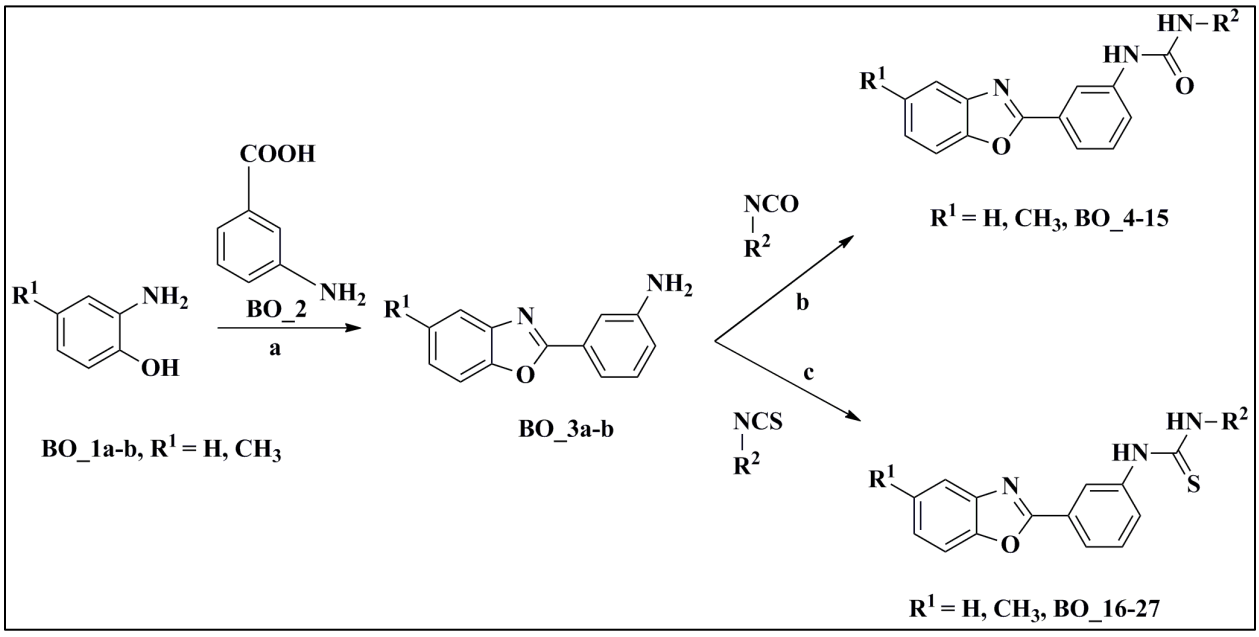

Figure 4.3: Synthetic protocol utilized for the synthesis of molecules **BO_4-27.**

Reagents and conditions: (a) PPA, 185 °C, 6h; (b) R^2-NCO, DIPEA, DMF, rt, 2h; (c) R^2-NCS, DMF/xylene(4:1), K_2CO_3, MW, 110 °C, 30 minutes.

Synthesis of 4-(4-fluoro-2-(4-methylpiperazin-1-yl)thiazol-5-yl)-amide derivatives as potent *M. tuberculosis* Glutamate racemase inhibitors

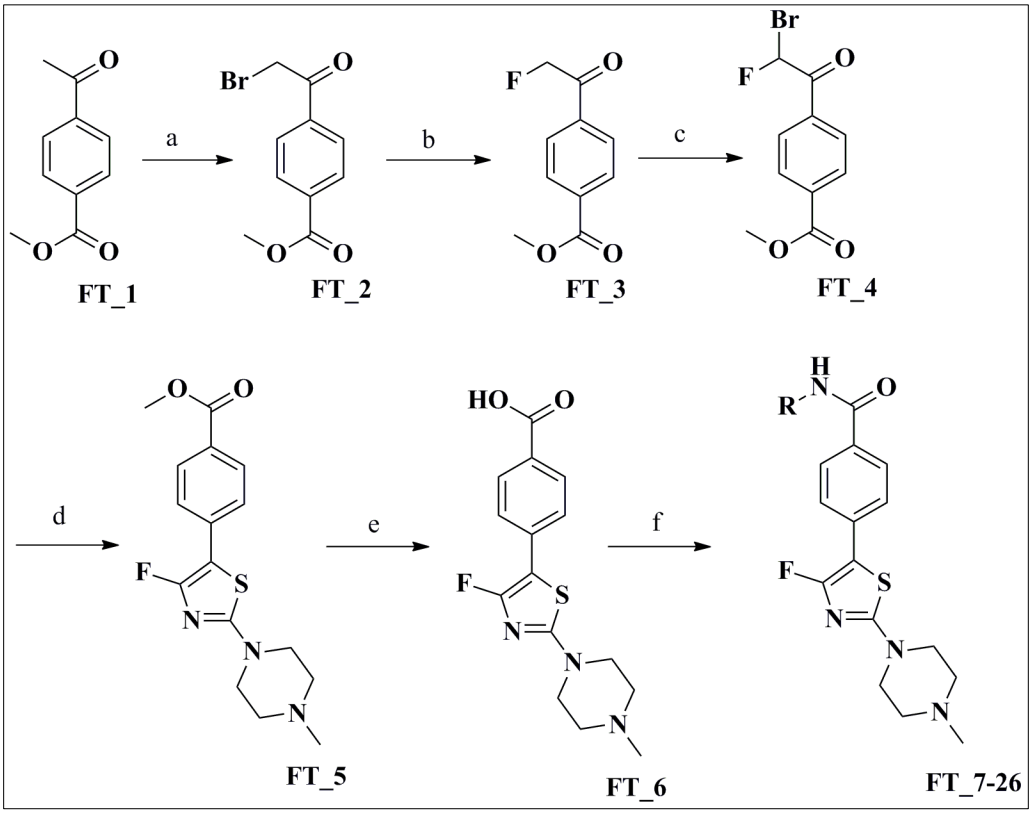

Figure 4.4: Synthetic protocol utilized for the synthesis of molecules **FT_7-26**.

Reagents and conditions: a) Br_2, 2-pyrolidinone,THF, 65 ^oC, 2 h b) KF, 18-crown ether, ACN, reflux, 16 h c) Br_2/ACOH, 45 ^oC d) 4-methylpiperazine-1-carbothioamide, toulene, reflux, 6 h e) LiOH, THF/H_2O, rt, 5 h f) RNH_2, TEA, T_3P, MDC,14 h.

Synthesis of *N*-methyl-2-(4-oxoquinazolin-3(4*H*)-yl)acetamide and *N*-methyl-2-(2-methyl-4-oxoquinazolin-3(4*H*)-yl)acetamide derivatives as potent *M. tuberculosis* Glutamate racemase inhibitors

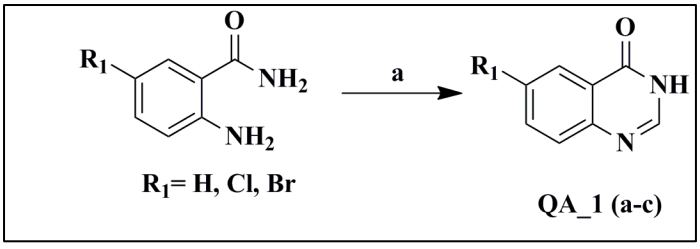

Figure 4.5: Synthetic protocol utilized for the synthesis of molecules **QA_1 (a-c).** Reagents and Conditions- a)Formamidine acetate, C_2H_5OH, reflux.

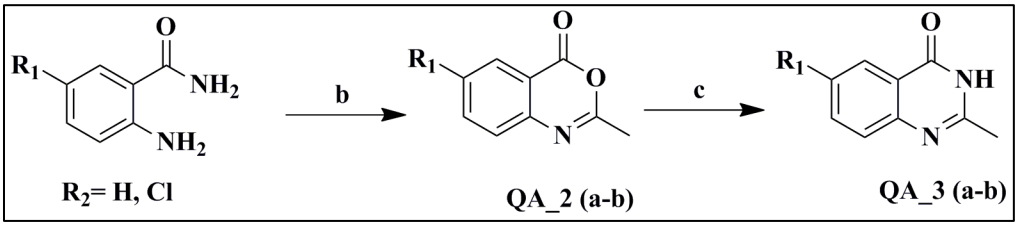

Figure 4.6: Synthetic protocol utilized for the synthesis of molecules **QA_3 (a-b).** Reagents and Conditions- b) acetic anhydride, reflux c) $HCONH_2$, 130 ^oC.

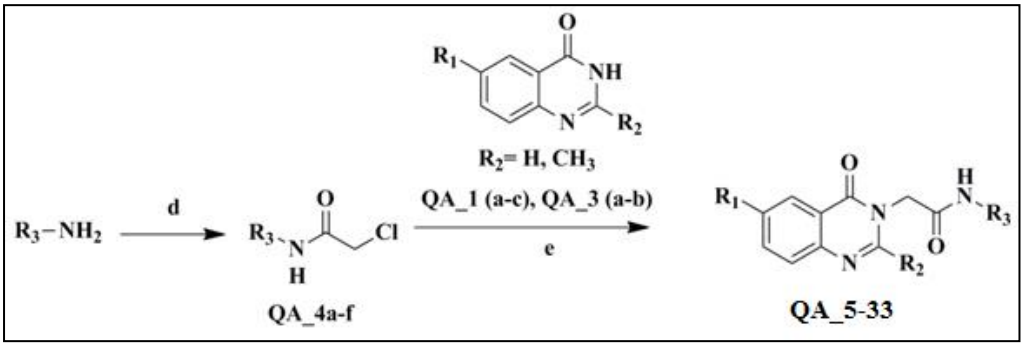

Figure 4.7: Synthetic protocol utilized for synthesis of molecules **QA_5-33.** Reagents and Conditions- d) Chloroacetyl chloride, TEA, DMF, 0 ^oC-rt e) Cs_2CO_3, DMF, 60 ^oC

Synthesis of 5-bromo-1*H*-indazole-3-carboxamide derivatives as potent *M. tuberculosis* Glutamate racemase inhibitors

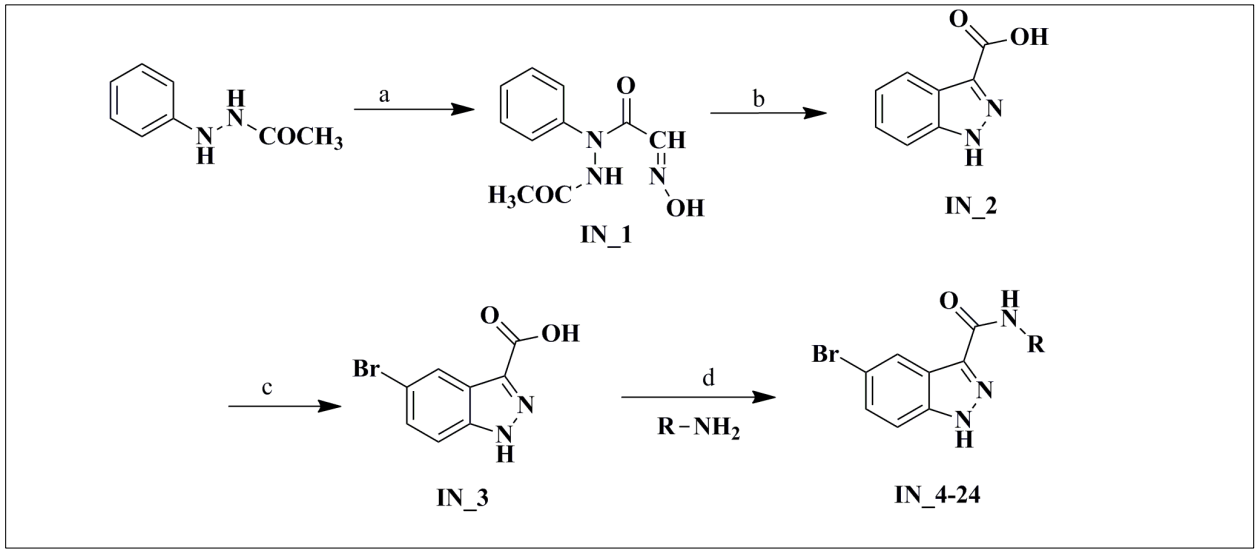

Figure 4.8: Synthetic scheme utilized for the synthesis of molecules **IN_5-26**. Reagents and conditions: a) $Cl_3CCH(OH)_2$, $NH_2OH.HCl$, Na_2SO_4, HCl, 3h, 100 °C b) H_2SO_4, 30minutes, 85 °C, 85°C to 4 °C, refluxed, 3h c) Br_2,16 h 90 °C; 90 °C to 5 °C d) DMF, EDCI, HOBt, rt, 8h

4.2.4. Molecular dynamics simulation

Molecular dynamics (MD) simulation was performed on a time scale ranging10-20 ns for the top active inhibitors against respective target proteins in order to analyze the consistency of molecular interactions between ligand and receptor employing Newton's Laws of Motions. All the MD simulations and calculations were done using Desmond employing OPLS-AA force field [Jorgenson, W.L., *et al*., 1996; Desmond v3.1, D.E. Shaw Research, NY 2012]. The prime objective of this MD study is to understand the macroscopic properties like temperature, a pressure in presence of solvent system based on its microscopic properties (bonded and non-bonded properties). For comparison studies, a 10 ns MD was also run for the crystal structure of Mtb glutamine synthetase without ligand in its ATP site (PDB ID – 4ACF (ligand was removed)). TIP3P water model was used to setup the solvent system in orthorhombic solvent box, keeping a cut-off of 10 Å from any solute atom in all directions [Jorgenson, W.L., *et al*., 1983]. Counter ions were added to neutralize the system. A cut-off of 14 Å was maintained for calculating the non-bonded interactions. Initially, the system was minimized maintaining the

convergence threshold criteria of 1 kcal.mol^{-1}.Å^{-1}. Further, a system was minimized using Berendsen thermostat applying with and without restraints on solute atoms at 10 K temperature for a time period of 12 ps. The temperature of the system was further raised to 300 K for 24 ps at a pressure of 1 atm. M-SHAKE algorithm was used with an integration time step of 2 fs for rearranging the hydrogen bonds in the simulation [Kräutler, V., *et al*., 2001]. The MD simulation was run for 10 ns recording the trajectory frames at an interval of every 4.8 ps.

RMSD analysis

The root mean square deviation (RMSD) is used to measure the average change in displacement of a selection of atoms for a particular frame with respect to a reference frame. It is calculated for all frames in the trajectory. Protein RMSD plot shows the RMSD evolution of a protein (left Y-axis). All protein frames are first aligned on the reference frame backbone, and then the RMSD is calculated based on the atom selection. Monitoring the RMSD of the protein can give insights into its structural conformation throughout the simulation. RMSD analysis can indicate if the simulation has equilibrated – its fluctuations towards the end of the simulation are around some thermal average structure. Changes of the order of 1-3 Å are perfectly acceptable for small, globular proteins. Changes much larger than that, however, indicate that the protein is undergoing a large conformational change during the simulation. Ligand RMSD (right *Y*-axis) indicates how stable the ligand is with respect to the protein and its binding pocket. The RMSD plot for ligand shows the RMSD of a ligand that is aligned and measured just on its reference conformation. This RMSD value measures the internal fluctuations of the ligand atoms.

RMSF analysis

The Root Mean Square Fluctuation (RMSF) is useful for characterizing local changes along the protein chain. In the RMSF plot, peaks indicate areas of the protein that fluctuate the most during the simulation. The ligand root mean square fluctuation (L-RMSF) is useful for characterizing changes in the ligand atom positions. Ligand RMSF shows the ligand fluctuations broken down by atom, corresponding to the 2D structure in the top panel. The ligand RMSF may give the insights on how ligand fragments interact with the protein and their entropic role in the binding event.

4.2.5. Minimum inhibitory concentration (MIC) determination

Bacterial inoculums of *M. tuberculosis* H37Rv were re-suspended in Middlebrook 7H9 broth (HiMedia) supplemented with 10% OADC (HiMedia Laboratories). This culture was grown at 37 ^{o}C until the reading A_{600} is 1. The culture was diluted to 1:25 with media and 100 µL was used as an inoculum. Each drug stock solution was diluted in Middlebrook 7H9-OADC at four-fold the final highest concentration tested. Serial two-fold dilutions of each drug were prepared directly in a sterile 96-well plate using 100 µL Middlebrook 7H9-OADC. Each has wells containing *M. tuberculosis* cultures without the addition of the tested compounds as positive controls and wells with only sterile medium as controls. Sterile water was added to all outer wells to avoid evaporation and maintain humidity during incubation. The plate was covered, sealed in plastic bags and incubated at 37 °C. MIC values were determined using the Alamar Blue assay [Collins, *et. al.,* 1997, Franzblau, *et. al.,* 1998]. After 5 days of incubation, 50 µL of 1:1 mixture of alamar blue solution (Sigma Aldrich) and sterile 10% tween 80 (Nice chemicals) were added to each well and the plate was re-incubated overnight (readings taken on the 7th day). A change in color from blue (oxidized state) to pink (reduced) indicated growth of bacteria and the minimum inhibitory concentration (MIC) was defined as the lowest concentration of the compound that prevented the change in color.

4.2.6. Nutrient starvation model

M. tuberculosis was deprived of nutrients as described in a reported procedure [Betts, *et. al.* 2002]. A culture of *M. tuberculosis* H37Rv grown (A_{600} 0.6-1.0) in Middlebrook 7H9 broth (HiMedia) supplemented with OADC was centrifuged and obtained pellet washed twice with 1XPBS (Phosphate Buffer Saline, obtained from HiMedia). The pellet was re-suspended in PBS with out tween in sealed bottles and incubated at 37 °C for 6 weeks. Tween was avoided as ***M. tuberculosis*** has lipase enzyme which hydrolyzes tween to oleic acid, which can serve as the source of energy or can cause toxicity [Dubos, R. J., *et al.,* 1946, Lyon, R. H., *et al.,* 1963]. Aliquots of these cultures were then treated with standard drugs like Isoniazid, Rifampicin and Moxifloxacin and lead compounds for 7 days at a concentration of 10 µg/mL. For the determination of CFU the cell suspensions were then diluted 10-fold to 10^{-6} using Middlebrook 7H9 medium supplemented with OADC and 50 µL of each dilution was plated in 48 well plates in triplicates along with 450 µL of Middlebrook 7H9 medium supplemented with OADC

(HiMedia Laboratories). The plates were incubated at 37 °C for 3 weeks, after which the wells were examined for visible bacterial growth. The bacterial count was evaluated using standard statistical methods [de Man, J. C., 1975].

4.2.7. Kill kinetics under nutrient-starved condition

M. tuberculosis culture (5 mL) with an A_{600} between 0.6-1.0 was centrifuged for 15 minutes at 2,500 rpm. The supernatant was discarded and the pellet was resuspended in 1mL of PBS-Tyloxapol (5 mL of 10 % Tyloxapol in 995 mL of PBS). The culture was diluted with PBS-Tyloxapol till the culture was diluted to an A_{600} of 0.1 and it was kept for starvation for about 2 weeks prior to the study.

For each compound to be tested 4 tubes were labeled as concentrations (5, 10, 20 µg/mL) and one served as DMSO control. To each tube, 5 mL of PBS-Tyloxapol and 50 µL of starved culture were added. To compound tubes, 100 µL of stock solution (50x) of the compound was added to attain desired concentration. To tube labeled as control 100 µL of DMSO was added. The contents of tubes were mixed and incubated at 37 ^{o}C. The treated cell suspensions were tested at 0, 7, 14, 21 days intervals. The bacterial suspension was diluted 10-fold up to 10^{-6} using Middlebrook 7H9 broth supplemented with OADC and 50 µL of each dilution were plated in 48 well plates in triplicates along with 450 µL of Middlebrook 7H9 broth (HiMedia) supplemented with OADC (HiMedia). The plates were incubated at 37 °C for 3-4 weeks, bacterial count was calculated down by using standard statistical methods using MPN assay [Parish, T., *et al*., 1998].

4.2.8. Inhibitory potency against biofilm forming *M. tuberculosis*

4.5 mL of sautons media inoculated with *M. tuberculosis* (1:100 dilution) was added to each well of sterile 12 well plate. Plates were sealed with several layers of parafilm and were incubated undisturbed in the humidified atmosphere at 37 ^{o}C with 5% CO_2 for 5 weeks to aid formation of biofilm. To the matured biofilm, the test compound was injected at desired concentration into media and swirled. For statistically significant results, the standard was injected in four wells. In parallel, the same volume of solvent in which the antibiotic was dissolved was injected in other four wells, and the last four wells of the plate were left untouched. The plates were incubated in an incubator for 7 days after sealing with parafilm.

At the end of the incubation, Tween-80 (0.1% volume/volume) was added to the plate, swirled and incubated at 25 ^{o}C for 15 minutes. The content of each well was mixed with pipette several times and transferred to a 15 mL conical tube. The contents of the tube were centrifuged at 4000 rpm for 10 minutes at 25 ^{o}C. The cell pellet was resuspended in 5 mL of wash buffer (PBS with 10% glycerol and 0.05% Tween-80). Washing was done for three times and the pellet was resuspended in 5 mL of wash buffer. The tubes were kept on a rocker for overnight at 25 ^{o}C. Pass the whole contents of the tube through a syringe fitted with sterile microtip (2-200 µL) for 5-6 times to attain fairly homogenous suspension. The cell suspensions were diluted 10-fold up to 10^{-6} using OADC supplemented Middlebrook 7H9 broth and 50 µL of each dilution were plated in 48 well plates in triplicates along with 450 µL of Middlebrook 7H9 medium supplemented with OADC. The plates were incubated at 37 °C for 3-4 weeks the wells with visible bacterial growth were counted as positive. The frequency of persisters in the biofilm population was determined by comparing standard treated plates to test compound treated plates [Kulka, K., *et al*., 2012, Wang, F., *et a*l., 2013].

4.2.9. Anti-mycobacterial screening using adult zebrafish

The most potent compound was further evaluated for its *in vivo* activity using adult zebrafish model established by us in a laboratory setup [Sridevi, J. P., *et al*., 2014]. We used *Mycobacterium marinum* strain (ATCC BAA-535) (genetically relative of *M. tuberculosis*) grown at 30 °C in Middlebrook 7H9 broth. Fish were initially weighed and monitored for its locomotor activities and were divided into control and treatment groups (n=6). All the fish were injected by intraperitonial injection with 20 µL of thawed bacterial stocks (around 0.75 million bacteria) [De Man, J. C., *et al*., 1975]. They were observed for lesions, reduction in swimming activities and squamous eruptions in the initial 7-day infection stage which was followed by treatment stage. The drug solutions were prepared based on the fish's body weight and the oral dosing amount of 5 µL. Fish were then administered drug orally using the micropipette, on each day during the treatment phase and were noted for their recovery symptoms. They were allowed to swim in 1.5 mg/mL solution of kanamycin sulphate to kill the external bacteria before proceeding for sacrifice at the end of study i.e., 14th day. Finally, all of them were sacrificed using homogenization technique and the sample was prepared in Middlebrook 7H9 broth [Salina, E., *et al*., 2014]. The collected homogenate was serially diluted to 10^{-6} times and plated into 48-

well plates, incubated at 30 °C for 24 h. The plates were checked for the bacterial counts using graph pad prism software 6.0.

4.2.10. Cytotoxicity studies

The synthesized compounds were further examined for its safety by determining its cytotoxicity in mouse macrophage cell line (RAW 264.7) at 50 µg/mL concentration. After 48 h of exposure, viability was assessed on the basis of cellular conversion of MTT into a formazan product using the cell proliferation assay. Cells were grown in RPMI medium supplemented with 10% fetal bovine serum (FBS), 10,000 units penicillin and 10 mg streptomycin per mL in T25 flasks to attain 80-90% confluency. Cells were scraped and seeded into wells approx 5,000 cells per well in poly-L-lysine coated plates. The microtiter plates were incubated at 37 ^{o}C, 5% CO_2 and 100% relative humidity for 24 h prior to addition of experimental drugs. The test compounds at 50 µg/mL concentrations were then added to cells and incubated at 37 °C for 48 h; later 10 µL of 0.5 mg/mL concentration of MTT was added and incubated for 3 h at 37 ^{o}C and the final product formazan crystals were measured at 595nm and 625nm. Ciprofloxacin (3% inhibition) and Novobiocin (9.8% inhibition) were used as a standard in this assay [Gerlier D., *et al*., 1986 and Scudiero D.A., *et al*., 1988].

Results and discussion Chapter 5

5.1. Design and development of *M. tuberculosis* Pantothenate kinase inhibitors

5.1.1. Design of Pantothenate kinase inhibitors using structure based drug design

Selection of PanK crystal structure and its binding site analysis

Many crystal structures of PanK were available till date co-crystallized with substrates and inhibitors. Among them, crystal structure of PanK co-crystallized with 2-((4'-cyano-2-((4-(pyridin-2-yl)piperazin-1-yl)methyl)-[1,1'-biphenyl]-4-yl)oxy)acetic acid with PDB code 4BFY was utilized in the present study for the development of e-pharmacophore. The structure was found with 2.3 Å resolution and the IC_{50} of the ligand was reported to be 0.12 µM [Björkelid C., *et al*., 2013]. The binding site analysis of crystal structure revealed the presence of a large druggable cavity which endogenously in organism accommodates ATP and pantothenate. The active site pocket was observed to be spacious, solvent exposed and highly hydrophobic as it is lined by residues Tyr182, Val99, Tyr177, Tyr153, Leu132, Leu203, Ile276, Tyr235, Phe239, Met242, Phe247, Phe254, Tyr257 and Ile272. The crystal ligand was found to be involved in hydrogen bonding with residues Arg238 and Tyr182 and also in strong hydrophobic interactions with other active site residues as shown in **Figure 5.1**. Hence, targeting PanK would be much appreciative with hydrophobic compounds which in turn can result in strong non-polar interactions.

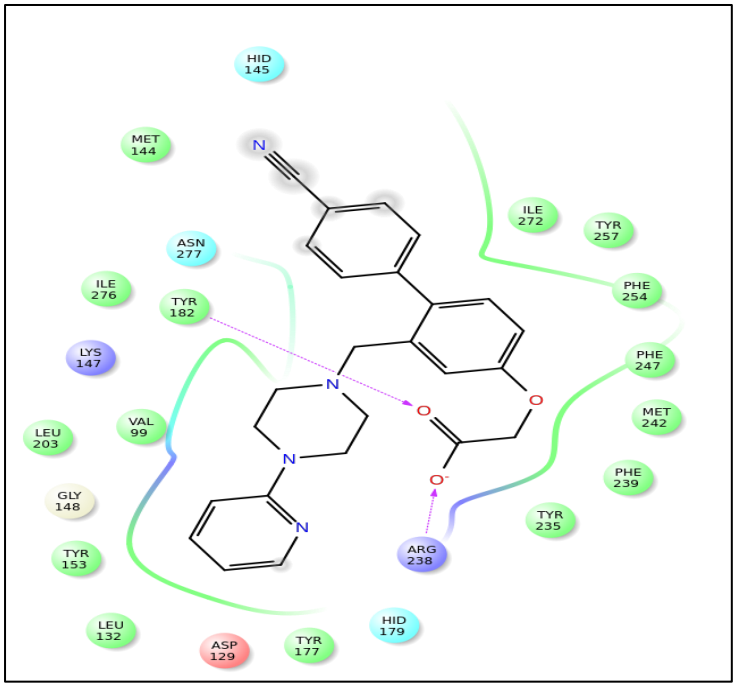

Figure 5.1: Interaction profile of the crystal ligand at the active site of Pantothenate kinase (PDB code – 4BFY)

Protein active site validation and e-pharmacophore generation

In order to validate the docking program utilized for e-pharmacophore generation, the crystal ligand was prepared and redocked on to the grid of the active site. The crystal ligand was found to be oriented in the similar manner as if in the crystal structure with an rmsd of 0.328 Å. The ligand was found to be retaining the active site interactions as of crystal structure with XP glide score of -9.172 kcal.mol^{-1}.

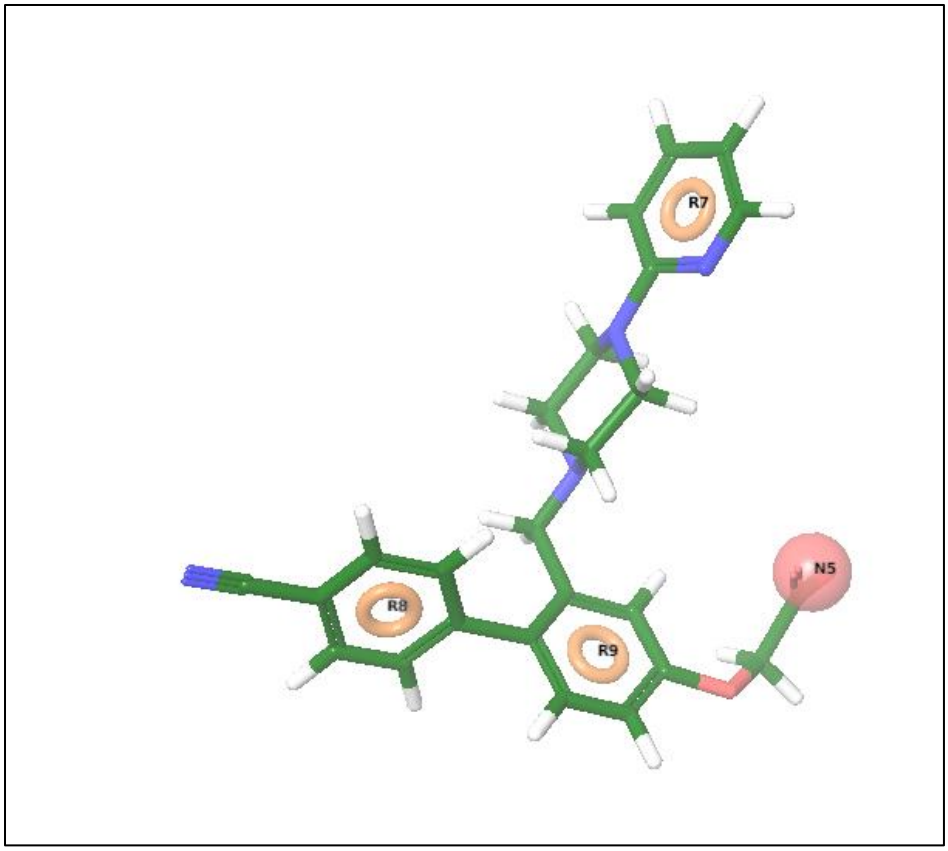

Figure 5.2: e-Pharmacophore generated for the crystal ligand from *M. tuberculosis* PanK crystal structure (PDB code – 4BFY)

Pharmacophore hypothesis was generated using the Glide descriptors which consist of polar, non-polar, van der Waals and electrostatic binding energies of the ligand with the protein which were mapped for the identification of pharmacophoric features. The pharmacophore generation protocol applied for the ligand yielded a hypothesis with four features as shown in **Figure 5.2**. Each feature was assigned a score which accounts for the energy contribution of that particular site interacting at the binding pocket of protein which is given in **Table 5.1**. The four features of the generated hypothesis are three aromatic ring features (R7, R8 and R9) and one negative-ionizable feature (N5). The N5 feature corresponds to the acid group of ligand which is involved in H-bond with Arg238 and Tyr182. The three aromatic ring features were surrounded by the hydrophobic residues.

Table 5.1: Energy scores of each feature in the generated e-pharmacophore

Rank	Feature	Label	Score Type
1	R9	-1.45	Aromatic Ring
2	N5	-1.25	Negative ionisable
3	R7	-0.91	Aromatic Ring
4	R8	-0.49	Aromatic Ring

E-pharmacophore based screening of chemical databases

The four-point e-pharmacophore was employed for screening in-house database in search of compounds with similar pharmacophore features. The search criterion was put to match 3 to 4 features of the pharmacophore. The aim of virtual screening workflow operated in this work is to reduce the enormous chemical library into a manageable number of compounds which would be comfortable for identification of inhibitors thereby increasing the chances of identification of drug candidate. The pharmacophore based screening of in-house database resulted in compounds with significant fitness value, which is a measure of how well the compound fits the pharmacophore. In the present study compounds with fitness above 1.00 were selected and carried forward for virtual screening.

Molecular docking studies of the selected compounds

The virtual screening involved high throughput virtual screening (HTVS), standard precision (SP) and extra precision (XP) docking. A cut-off of -6.0 kcal.mol^{-1} docking score was defined for the compounds to be selected from HTVS which resulted in 110 compounds which were further subjected to SP and XP docking. The final selection of compounds was done based on the XP glide score and glide energy. Further selection process of compounds fitting in the above range was done using fitness value (above 1) and their interactions at the active site. A total of 87 compounds were selected after SP docking with the docking scores ranging between -10.0 kcal.mol^{-1} and -7.0 kcal.mol^{-1}. These compounds were further subjected to XP docking and were selected considering XP glide score (above -6.0 kcal.mol^{-1}), glide energy (above -35.00 kcal.mol^{-1}), and their binding pattern at the active site.

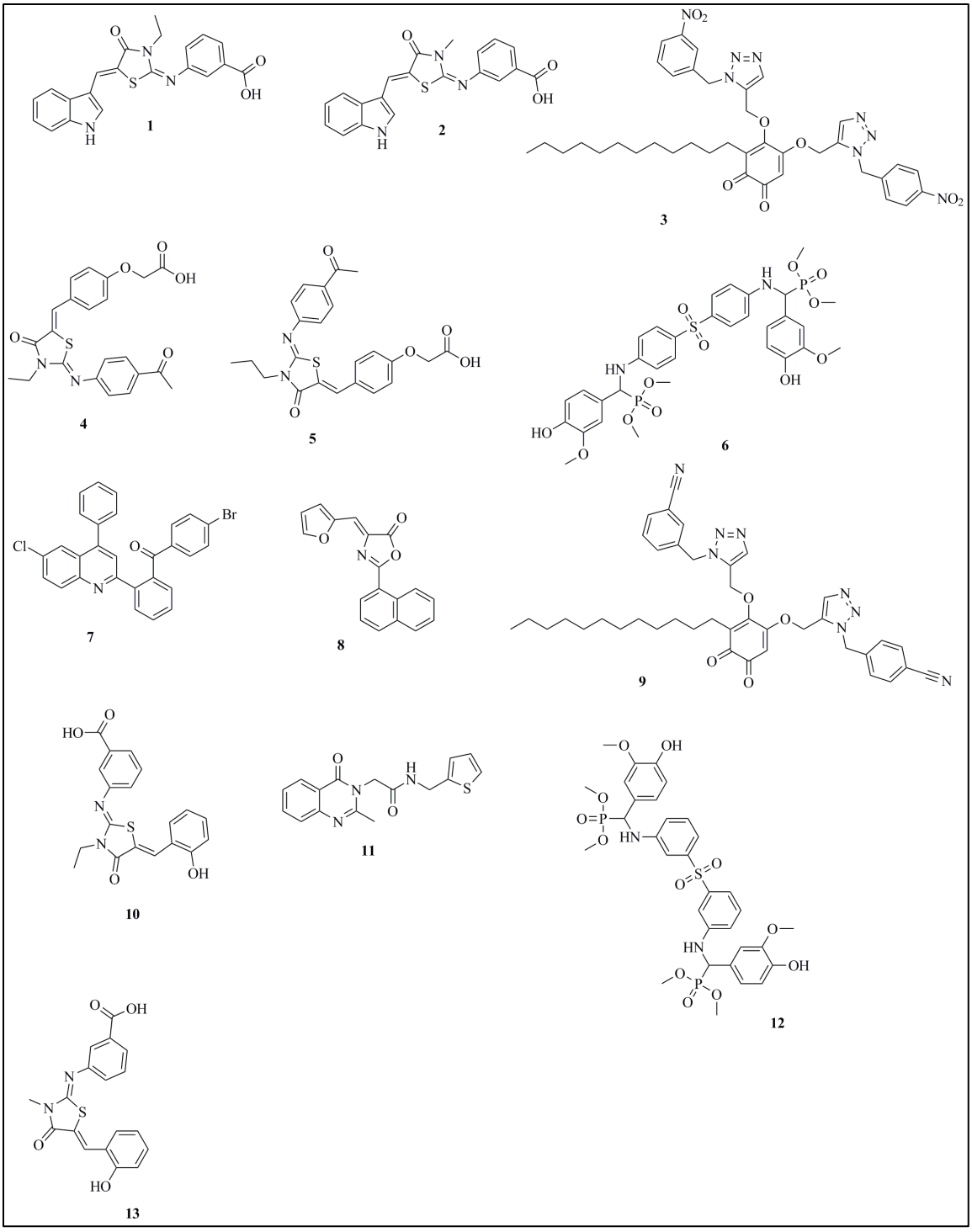

Figure 5.3: Structures of the selected 13 compounds from in-house database against *M. tuberculosis* PanK

These short listing criteria resulted in selection of 13 compounds which were further subjected to *in vitro M. tuberculosis* PanK enzymatic assay. All the 13 compounds were found to retain key

interactions at the active site like hydrogen bonding with Glu214, Asn359, Lys361, Arg364 and hydrophobic interactions with residues Tyr129, Phe232, Trp282 and Ala362. The XP glide score of the selected compounds ranged between -7.2 kcal.mol^{-1} and -9.97 kcal.mol^{-1} which are listed in **Table 5.2**. The chemical structures of the selected 13 compounds are shown in **Figure 5.3**. The selected 13 compounds fit best at the binding pocket of *M. tuberculosis* PanK. The interactions of these compounds with the active site residues are given in table **5.3**.

Table 5.2: Glide score, glide energy and fitness score for the selected 13 compounds

Compound	Glide XP gscore	Fitness	Glide energy
Crystal ligand	-9.172	2.92	-87.953
1	-9.96	1.669	-76.826
2	-9.861	1.681	-75.952
3	-9.596	1.495	-59.475
4	-9.317	1.404	-64.120
5	-9.307	1.406	-65.110
6	-9.445	1.237	-93.061
7	-8.965	1.567	-75.492
8	-8.439	1.477	-52.150
9	-8.317	1.431	-68.573
10	-7.952	1.611	-67.124
11	-7.829	1.373	-61.694
12	-9.58	1.173	-89.985
13	-7.58	1.63	-64.882

The 13 compounds selected from the molecular docking studies were observed with different scaffolds such as thiophene, triazole, thiazole and oxazole which offer a diverse set of compounds to study. The main implication of selection of compounds with diverse structural features is to evaluate their *M. tuberculosis* PanK inhibitory activity and further structural optimization of the active compounds based on their synthetic feasibility. The binding energies

of the selected 13 compounds towards *M. tuberculosis* PanK were also determined in order to assess their binding capacity towards the protein.

Table 5.3: Interactions of the selected 13 compounds at *M. tuberculosis* PanK ligand binding site

Compound	**H-bond Interactions**	**Cation-π Interactions**	**π -π Interactions**
Crystal ligand	Arg238, Tyr182	-	-
1	Lys147, Arg238	-	-
2	Arg238, Lys147, Tyr257	-	-
3	Tyr257, Tyr177, Lys147, Hid253	-	Phe254, Tyr182
4	Arg238, Tyr182	-	Tyr182
5	Arg238, Tyr182	-	Tyr182
6	Arg238, Tyr235, Tyr182, Tyr177, Tyr257, Thr275	-	-
7	Tyr177	Lys147	Hid179, Tyr182
8	Arg238, Tyr182	-	Hid179, Tyr182
9	Tyr257, Tyr177, Lys147, Hid253	-	Phe254, Tyr182
10	Asn277, Arg238	Lys147	-
11	Asn277	-	Phe254
12	Hid179, Met144, Tyr182, Tyr235, Tyr177	Arg238	Hid179
13	Tyr235, Asn277, Lys147	Arg238	-

ADMET analysis of the selected compounds

Pharmacokinetic properties analysis helps us to identify suitable compounds with pharmaceutical importance which can be further developed in to a drug candidate. All the selected compounds were subjected to *in silico* ADMET analysis using QikProp module of Schrödinger 2012. All the

compounds were found to be in accordance with Lipinski's rule of five which is the basic criteria of drug-likeliness. Various properties like SASA (Predicted Solvent Accessible Surface Area in Å2), QPlogBB (Predicted brain/blood partition coefficient), QPlogHERG (Predicted IC_{50} value for HERG K+ channels), QPPCaco (Predicted apparent Caco-2 cell permeability in nm/s) were determined for the compounds and were checked for any deviations. All the properties determined are listed out in **Table 5.4**. Almost all compounds are found to be showing good blood brain barrier permeability which indicates the compounds to be CNS (Central Nervous System) active. All the 13 compounds were found to obey Lipinski rule of five, showing good percentage oral absorption thereby reflecting the drug likeliness of the compounds.

Table 5.4: *In silico* pharmacokinetic profile for the selected 13 compounds

Compound	SASA	QPlogBB	QPlogHERG	QPPCaco	QPPMDCK	% Human Oral Absorption	QPlogKp
1	686.28	-1.621	-4.806	54.25	32.20	80.86	-1.621
2	657.18	-1.650	-4.639	40.95	23.40	76.19	-3.226
3	765.33	-2.288	-4.761	25.66	0.57	37.15	-5.653
4	741.25	-2.12	-4.517	31.57	18.42	73.1	-3.422
5	774.88	-2.25	-4.692	31.29	18.22	75.27	-3.33
6	876.92	-3.186	-3.762	60.47	24.11	45.81	-3.051
7	692.02	-0.250	-3.69	3861.5	10000	100	-0.139
8	539.53	-0.237	-4.195	2016.7	1055.9	100	-1.077
9	452.16	-2.179	-3.982	26.60	28.17	33.98	-4.27
10	648.56	-1.67	-4.396	49.58	28.50	75.4	-3.019
11	579.10	-0.313	-4.363	1210.9	1713.1	94.86	-1.491
12	524.09	-2.963	-7.020	98.06	40.97	52.6	-2.511
13	621.58	-1.701	-4.278	38.244	21.05	70.9	-3.33

Properties and Ranges: **SASA** – Predicted Solvent Accessible Surface Area in $Å_2$ (300-1000). **QPlogBB** – Predicted brain/blood partition coefficient (-3.000 to 1.200). **QPlogHERG** – Predicted IC_{50} value for HERG K+ channels (concern below -5). **QPPCaco** – Predicted apparent Caco-2 cell (model for gut-blood barrier) permeability in nm/s (<25 – poor, >500 – great). **QPPMDCK** - Predicted apparent MDCK cell (model for blood-brain barrier) permeability in nm/s (<25 – poor, >500 – great). **QPlogKp** – Predicted skin permeability (-8.000 to -1.000).

5.1.2. *In vitro* Pantothenate kinase assay for the selected compounds

The finalized 13 compounds were evaluated for their *M. tuberculosis* PanK inhibitory activity. The detailed enzymatic assay procedure is discussed in the materials and methods section. In the initial screening at 25 µM, none of the compounds have shown good inhibition towards the protein. The percentage inhibitions of all 13 compounds were calculated and they were <20% (given in **table 5.5**). We have also tried testing for the inhibitory activity using fluorescent based assay like thermal shift assay (TSA) where no change in melting temperature (T_m) with respect to unbound protein and protein bound to substrate which indicates there wasn't any inhibition of the protein. The reason for not a success of selected compounds to inhibit was assumed due to failure of screening model. Hence we have not taken this study further.

Table 5.5: Activity table showing the percentage inhibition at 25 µM for the selected 13 compounds

Compound	Percentage inhibition at 25 µM
1	16.7
2	18
3	5
4	15
5	10.3
6	12.9
7	10.8
8	7.3
9	5.1
10	18.5
11	10.2
12	4.9
13	5.2

5.2. Results and discussion for development of *Mycobacterium tuberculosis* Glutamate racemase inhibitors

5.2.1. Identification, synthesis and evaluation of *Mycobacterium tuberculosis* Glutamate racemase inhibitors

5.2.1.1. Lead identification by thermal shift assay

Drug screening to identify the protein stabilizing ligands using fluorescence technique like thermal shift assay has been very helpful for drug discovery research. The theory is based on thermodynamic stabilization of protein upon ligand binding by estimating melting temperature (T_m), which can further be used for inferring thermodynamic properties such as binding free energies [Bittker, J. A., *et al*., 2016]. In the present study, we have done a virtual screening of our in-house database of 650 compounds with chemically diverse structures employing thermal shift assay using Differential Scanning fluorimeter (DSF) to identify the leads inhibiting *M. tuberculosis* GR. We performed the assay with purified *M. tuberculosis* GR in the presence of D-glutamate and database compounds. A comparison study of T_m revealed that native protein in the absence of D-glutamate and ligand showed a melt temperature approximately of 43.4 ^oC, whereas with D-glutamate showed a temperature shift of 2.4 ^oC approximately. Screened compounds showed a varied range of positive and negative shifts in T_m. Of the entire compound library **lead 1**showed a significant shift in melt temperature. When performed along with D-glutamate, **lead 1** showed a significant difference in T_m with native protein by 3.3 ^oC inferring that its stabilizing capability and interactions with protein are much better than D-glutamate alone as well as than rest of the compound library.

We have tried purifying *M. tuberculosis* recombinant GR using the various purification protocols but wasn't successful in obtaining the catalytically active enzyme to carry out activity assay. Recent reports have discussed this point stating that homodimer interface is essential for enzyme catalytic activity [Poen, S., *et al*., 2016]. Hence we have followed the recent literature and performed *in vitro* enzyme assay using purified recombinant Glutamate racemase from Bacillus subtilis (*B. subtilis*) which are known to have 40% and 56% of respective sequence identity and similarity with M. *tuberculosis*[10]. **Lead 1** which has shown good stability data in above study has also shown good inhibitory activity on GR of *B. subtilis* with an IC_{50} of 19.47±0.81 µM (**Figure**

5.4). Hence we considered **lead 1** to optimize further through synthetic strategies and test for inhibitory activity.

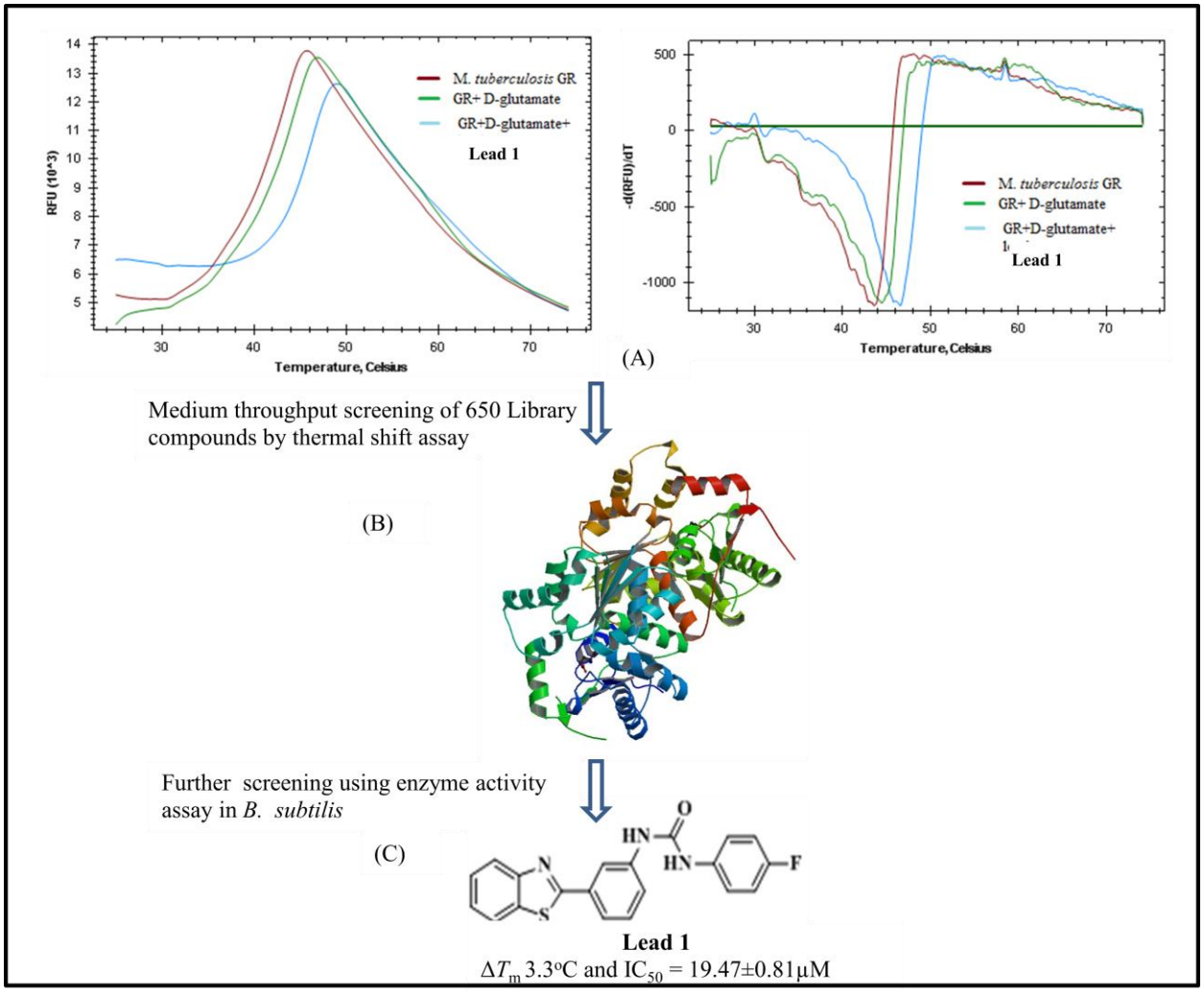

Figure 5.4: (A) (Left): DSF plots of a *M. tuberculosis* GR native, with D-glutamate and **lead 1**. (Right) represents the plot of derivative fluorescent based signal against temperature; T_m and ΔT_m (shift) can be measured from the minimum of the plot. (B) Representation of *B. subtilis* GR protein with identified lead compound using *in vitro* assay. (C) Structure of identified **lead 1** with T_m and IC_{50} value in *B. subtilis*.

5.2.1.2. Chemical synthesis and characterization

To optimize the lead we have synthesized a series of twenty three compounds (**Table 5.6**). The synthetic protocol utilized was described in **Scheme 5.1**. 2-aminobenzenethiol (**BT_1a**) and 2-amino-4-(trifluoromethyl)benzenethiol (**BT_1b**) were taken as two separate reactants and

coupled each with 3-amiobenzoicacid (**BT_2**) in polyphosphoric acid (PPA) followed by heating resulting in the clear precipitate of corresponding substituted benzthiazol derivatives (**BT_a-b**). The benzthiazol (**BT_3a-b**) derivatives were carried to next step by reacting with two different reactants as separate reactions namely substituted arylisocyanates and arylisothiocyanates. Firstly, substituted **BT_3a-b** derivatives were coupled with the corresponding arylisocyanate in the presence of a base in DMF to get the corresponding *N,N*-substituted urea derivatives **BT_4-14**. Secondly, synthesized **BT_3a-b** molecules were reacted with respective arylisthiocyanates by heating with a base (K_2CO_3) in DMF followed by purification to obtain compounds **BT_16-26** (similar conditions were used for the preparation of *N,N*-substituted thiourea derivatives but was unsuccessful). All the final compounds obtained in good yield and purity. An overview of the all the various substitutions employed in synthesis has been depicted in **Table 5.6**. All the analytical data (^{1}H NMR, ^{13}C NMR, and mass spectra) of synthesized compounds (both intermediates and finals) were on par with projected structures.

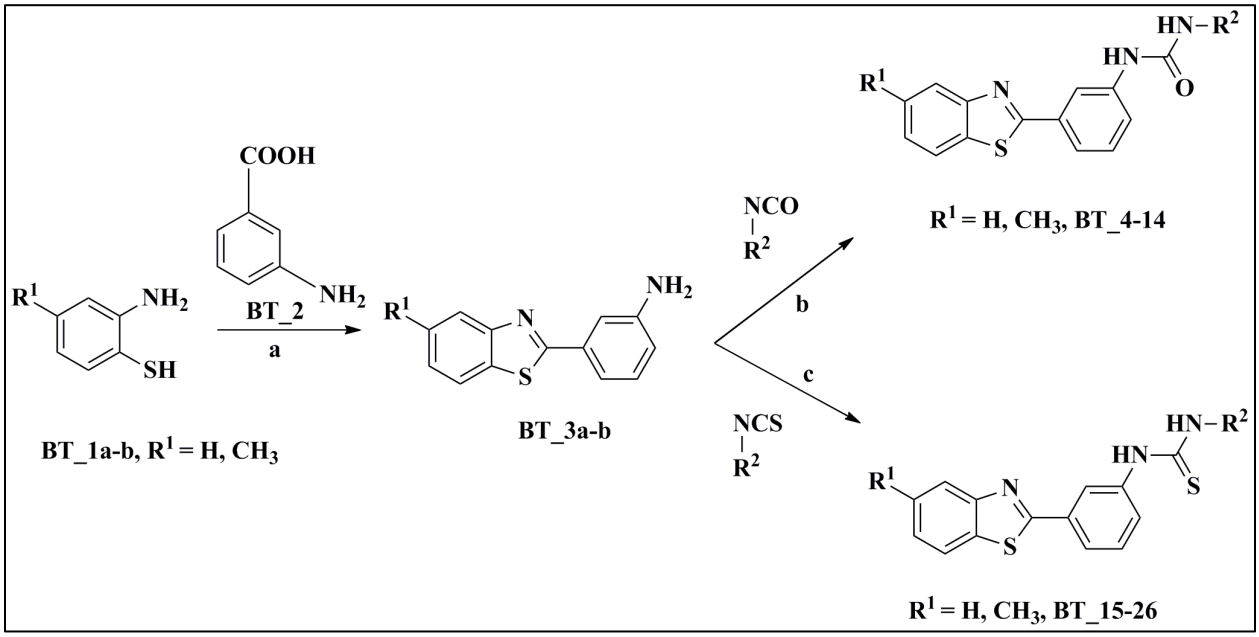

Scheme 5.1: Synthetic scheme utilized for the synthesis of molecules. Reagents and conditions: (a) PPA, 185 °C, 6h; (b) R^2-NCO, DIPEA, DMF, rt, 2h; (c) R^2-NCS, DMF/xylene(4:1), K_2CO_3, MW, 110 °C, 30min.

5.2.1.3. Synthetic protocol used for synthesis

General procedure for the preparation of BT_3a-b derivatives: To the mixture of compound **BT_1a/b** (1.1 equiv) and 3-amiobenzoicacid (**BT_2**) (1.0 equiv) PPA (10 mL) was added and allowed to the reaction mixture to stir at 185 °C for 6 hours. The reaction mixture was cooled to room temperature and added cold 6N NaOH solution dropwise. The precipitate obtained was filtered and dissolved in DMF and heated to 60°C for 15 minutes, and was poured into crushed ice. The solid obtained was filtered and washed with cold ethanol and diethyl ether to afford the corresponding compound **BT_3a-b** respectively.

General procedure for the preparation of compounds (BT_4-14): DIPEA (2.0 equiv) was added to the stirred solution of compounds **BT_3a/b** (1.0 equiv) and the corresponding arylisocyanate (1.25 equiv) in DMF. The reaction mixture was diluted with EtOAc and washed with H_2O, Brine solution and evaporated to dryness. The crude residue was purified by column chromatography using EtOAc/hexane as eluent to afford pure compounds **BT_4-l4**.

General procedure for the preparation of compounds (BT_15-26): K_2CO_3 (2.0 equiv) was added to the stirred solution of compounds **BT_3a/3b** (1.0 equiv) in DMF:xylene (4:1) and the corresponding arylisothiocyanate (1.2 equiv). The reaction mixture was subjected to microwave irradiation conditions (temperature 110 °C) for 30 minutes. The contents of microwave flask were poured into the crushed ice; the precipitate obtained was filtered and washed with ethanol. The crude residue was purified by column chromatography using EtOAc/hexanes as eluent to afford corresponding pure compounds **BT_15-26**. The physicochemical properties of synthesized derivatives are shown in **Table 5.6**.

Table 5.6: Physicochemical properties of synthesized compounds **BT_4-26**

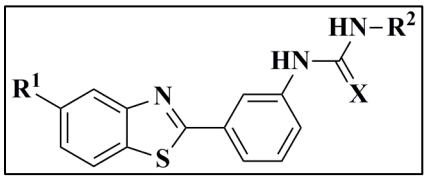

BT_4-26

Compound	R_1	R_2	X	Yield (%)	Melting point (^oC)	Molecular formula	Molecular weight
BT_4	H	4-Methoxyphenyl	O	58.3	195-197	$C_{21}H_{17}N_3O_2S$	375.1
BT_5	H	4-Chlorophenyl	O	62.6	190-192	$C_{20}H_{14}ClN_3OS$	370.62
BT _6	CF_3	1-Phenyl	O	65.8	252-254	$C_{21}H_{14}F_3N_3OS$	413.12
BT _7	CF_3	4-Methoxyphenyl	O	75.4	160-162	$C_{22}H_{16}F_3N_3O_2S$	443.34
BT _8	H	4-Tolyl	O	75.3	114-116	$C_{21}H_{17}N_3OS$	359.27
BT _9	H	Phenyl	O	78.1	196-198	$C_{20}H_{15}N_3OS$	345.19
BT _10	H	4-Nitrophenyl	O	80.2	270-272	$C_{20}H_{14}N_4O_3S$	390.33
BT _11	CF_3	4-Fluorophenyl	O	75.6	232-234	$C_{21}H_{13}F_4N_3OS$	431.31
BT _12	CF_3	4-Tolyl	O	69.7	263-265	$C_{22}H_{16}F_3N_3OS$	427.19
BT _13	CF_3	4-Chlorophenyl	O	78.3	243-245	$C_{21}H_{13}ClF_3N_3OS$	447.09
BT _14	CF_3	4-Nitrophenyl	O	80.3	259-261	$C_{21}H_{13}F_3N_4O_3S$	458.33
BT _15	CF_3	4-Nitrophenyl	S	72.2	246-248	$C_{21}H_{13}F_3N_4O_2S_2$	474.49
BT _16	H	Phenyl	S	74.6	182-184	$C_{20}H_{15}N_3S_2$	361.21
BT _17	CF_3	4-Tolyl	S	80.8	179-181	$C_{22}H_{16}F_3N_3S_2$	443.42
BT _18	H	4-Nitrophenyl	S	73.4	236-238	$C_{20}H_{14}N_4O_2S_2$	406.39
BT _19	CF_3	4-Chlorophenyl	S	81.7	211-213	$C_{21}H_{13}ClF_3N_3S_2$	463.27

BT _20	H	Benzyl	S	78.6	210-212	$C_{21}H_{17}N_3S_2$	375.11
BT _21	H	4-Chlorophenyl	S	75.9	235-237	$C_{20}H_{14}ClN_3S_2$	395.19
BT _22	CF_3	1-Phenyl	S	72.3	192-194	$C_{21}H_{14}F_3N_3S_2$	429.52
BT _23	CF_3	4-Fluorophenyl	S	83.2	218-220	$C_{21}H_{13}F_4N_3S_2$	447.41
BT _24	CF_3	1-Benzyl	S	77.4	254-256	$C_{22}H_{16}F_3N_3S_2$	443.14
BT _25	H	4-Tolyl	S	80.5	178-180	$C_{21}H_{17}N_3S_2$	375.08
BT _26	H	4-Fluorophenyl	S	78.6	240-242	$C_{20}H_{14}FN_3S_2$	379.14

5.2.1.4. Characterization of synthesized compounds

3-(Benzo[*d*]thiazol-2-yl)benzenamine (BT_3a): The compound was synthesized according to above general procedure using 2-aminobenzenethiol (1 g**,** 7.98 mmol), 3-amiobenzoicacid (0.9 g, 6.84 mmol) and PPA (10 mL) to obtain 3-(benzo[*d*]thiazol-2-yl)benzenamine (1.7 g,70%) as white solid. ^{1}H NMR (400 MHz, DMSO-d_6): δ 8.31(s, 1H), 8.10-7.87 (m, 3H), 7.47-7.23 (m, 4H), 6.74 (s, 2H). ^{13}C NMR (100 MHz, DMSO-d_6): δ 170.2, 158.9, 152.7, 135.5 (2C), 132.1, 124.7 (2C), 122.3 (3C), 118.7, 116.7. MS (ESI) *m/z* 227.5 $[M+H]^+$. Anal calcd for $C_{13}H_{10}N_2O$: C, 69.00; H, 4.45; N, 12.38; Found: C, 69.23; H, 4.46; N, 12.41.

3-(5-(Trifluoromethyl)benzo[*d*]thiazol-2-yl)benzenamine (BT_3b): The compound was synthesized according to above general procedure using 2-amino-4-(trifluoromethyl)benzenethiol (1 g, 5.17 mmol), 3-aminobenzoicacid (0.9 g, 6.84 mmol) and PPA (10 mL) to obtain 3-(5-(trifluoromethyl)benzo[*d*]thiazol-2-yl)benzenamine (1.5 g,75%) as creamy white solid. ^{1}H NMR (400 MHz, DMSO-d_6): δ 8.34 (s, 1H), 8.12 (s, 1H), 7.98-7.64 (m, 5H), 6.89 (s, 2H). ^{13}C NMR (100 MHz, DMSO-d_6): δ 168.9, 155.8, 149.7, 138.3, 136.3, 129.7, 128.2, 125.3 (2C), 121.6 (2C), 120.4, 118.3, 113.9. MS(ESI) *m/z* 295.4 $[M+H]^+$. Anal calcd for $C_{14}H_9F_3N_2O$: C, 57.14; H, 3.08; N, 9.52; Found: C, 57.25; H, 3.10; N, 9.55.

1-(3-(Benzo[*d*]thiazol-2-yl)phenyl)-3-(4-methoxyphenyl)urea (BT_4): The compound was synthesized according to above general procedure using 3-(benzo[*d*]thiazol-2-yl)benzenamine (1.5 g, 6.19 mmol), DIPEA (1.8 g, 12.62 mmol) and 1-isocyanato-4-methoxybenzene (1.5 g, 10.05 mmol) to yield 1-(3-(benzo[*d*]thiazol-2-yl)phenyl)-3-(4-methoxyphenyl)urea (2.1 g, 58.3%) as grey solid. M.p: 195-197 ^{o}C. ^{1}H NMR (400 MHz, DMSO-d_6): δ 10.17 (s, 1H), 10.03

(s, 1H), 8.27 (s, 1H), 8.16 (d, *J* = 8.0 Hz, 1H), 8.02 (d, *J* = 8.0 Hz, 1H), 7.78 (d, *J* = 8.0 Hz, 1H), 7.67 (d, *J* = 7.6 Hz, 1H), 7.49–7.33 (m, 5H), 7.29 (d, *J* = 7.6 Hz, 2H), 3.94 (s, 3H); ^{13}C NMR (100 MHz, DMSO-d_6): δ 171.9, 164.3, 160.8, 154.5, 136.9, 135.4, 134.8, 133.2, 132.6, 132.2 (2C), 128.4, 127.3, 126.7 (2C), 125.3, 125.0, 122.4, 120.4, 119.7, 61.5. MS(ESI) *m/z* 376.3 $[M+H]^+$. Anal calcd for $C_{21}H_{17}N_3O_2S$: C, 67.18; H, 4.56; N, 11.19 Found C, 67.26; H, 4.57; N, 11.17.

1-(3-(Benzo[*d*]thiazol-2-yl)phenyl)-3-(4-chlorophenyl)urea (BT_5): The compound was synthesized according to above general procedure using 3-(benzo[*d*]thiazol-2-yl)benzenamine (1.5 g, 6.61 mmol), DIPEA (1.8 g, 12.62 mmol) and 1-chloro-4-isocyanatobenzene (1.5 g, 9.76 mmol) to yield 1-(3-(benzo[*d*]thiazol-2-yl)phenyl)-3-(4-chlorophenyl)urea (2.2 g, 62.6%) as cream white solid. M.p: 190-192 ^{o}C. ^{1}H NMR (400 MHz, DMSO-d_6): δ 10.11 (s, 1H), 9.97 (s, 1H), 8.34 (d, *J* = 8.4 Hz, 1H), 8.17 (d, *J* = 8.0 Hz, 1H), 8.08 (t, *J* = 8.0 Hz, 1H), 7.83 (d, *J* = 8.0 Hz, 1H), 7.72 (d, *J* = 8.4 Hz, 1H), 7.63–7.36 (m, 7H); ^{13}C NMR (100 MHz, DMSO-d_6): δ 182.3, 166.5, 155.2, 152.4, 137.6, 136.9, 135.3, 133.9 (2C), 133.2, 132.7, 132.0 (2C), 130.4, 128.7 (2C), 127.3, 126.2, 124.3, 122.1. MS(ESI) *m/z* 380.6 $[M+H]^+$. Anal calcd for $C_{20}H_{14}ClN_3OS$: C, 63.24; H, 3.71; N, 11.06 Found C, 63.29; H, 3.72; N, 11.04.

1-Phenyl-3-(3-(5-(trifluoromethyl)benzo[*d*]thiazol-2-yl)phenyl)urea (BT_6): The compound was synthesized according to above general procedure using 3-(5-(trifluoromethyl)benzo[*d*]thiazol-2-yl)benzenamine (1.5 g, 6.12 mmol), DIPEA (1.8 g, 12.62 mmol) and 1-isocyanatobenzene (1.5 g, 9.76 mmol) to yield 1-phenyl-3-(3-(5-(trifluoromethyl)benzo[*d*]thiazol-2-yl)phenyl)urea (1.8 g, 65.8%) as pale brown solid. M.p: 252-254 ^{o}C. ^{1}H NMR (400 MHz, DMSO-d_6): δ 9.96 (s, 1H), 9.88 (s, 1H), 8.45 (s, 1H), 8.31 (s, 1H), 8.16 (d, *J* = 8.0 Hz, 1H), 7.96 (d, *J* = 7.6 Hz, 1H), 7.74–7.63 (m, 4H), 7.56–7.47 (m, 4H); ^{13}C NMR (100 MHz, DMSO-d_6): δ 180.4, 164.3, 156.8, 138.6, 136.9, 136.3, 135.2, 134.4, 133.9, 133.0 (2C), 131.4 (2C), 127.6, 126.9 (2C), 125.1, 124.8, 120.0, 119.4, 118.1. MS(ESI) *m/z* 414.1$[M+H]^+$. Anal calcd for $C_{21}H_{14}F_3N_3OS$: C, 61.01; H, 3.41; N, 10.16 Found C, 61.10; H, 3.40; N, 10.18.

1-(4-Methoxyphenyl)-3-(3-(5-(trifluoromethyl)benzo[*d*]thiazol-2-yl)phenyl)urea (BT_7): The compound was synthesized according to above general procedure using 3-(5-(trifluoromethyl)benzo[*d*]thiazol-2-yl)benzenamine (1.5 g, 6.12 mmol), DIPEA (1.8 g, 12.62 mmol) and 1-isocyanato-4-methoxybenzene (1.3 g, 8.7 mmol) to obtain 1-(4-methoxyphenyl)-

3-(3-(5-(trifluoromethyl)benzo[*d*]thiazol-2-yl)phenyl)urea (2 g, 75.4%) as cream white solid. M.p: 160-162 ^{o}C. ^{1}H NMR (400 MHz, DMSO-d_6): δ 10.06 (s, 1H), 9.92 (s, 1H), 8.40 (s, 1H), 8.26 (s, 1H), 8.04–7.92 (m, 2H), 7.84 (d, J = 8.4 Hz, 1H), 7.72–7.60 (m, 4H), 7.26 (d, J = 8.0 Hz, 2H), 3.90 (s, 3H); ^{13}C NMR (100 MHz, DMSO-d_6): δ 180.3, 164.8, 158.4, 144.3, 135.8, 135.3, 134.7, 134.2, 133.8, 132.9 (2C), 130.5 (2C), 127.0, 126.3 (2C), 124.3, 122.4, 121.3, 118.4, 118.0, 58.3. MS(ESI) *m/z* 444.2 $[M+H]^+$. Anal calcd for $C_{22}H_{16}F_3N_3O_2S$: C, 59.59; H, 3.64; N, 9.48 Found C, 59.62; H, 3.65; N, 9.46.

1-(3-(Benzo[*d*]thiazol-2-yl)phenyl)-3-(p-tolyl)urea (BT_8): The compound was synthesized according to above general procedure using 3-(benzo[*d*]thiazol-2-yl)benzenamine (1.5 g, 6.61 mmol), DIPEA (1.8 g, 12.62 mmol) and 1-isocyanato-4-methylbenzene (1.2 g, 9.01 mmol) to yield 1-(3-(benzo[*d*]thiazol-2-yl)phenyl)-3-(p-tolyl)urea (1.8 g, 75.3%) as grey colour solid. M.p: 114-116 ^{o}C. ^{1}H NMR (400 MHz, DMSO-d_6): δ 10.27 (s, 1H), 10.11 (s, 1H), 8.30 (s, 1H), 8.11 (d, J = 8.0 Hz, 1H), 7.84 (d, J = 8.0 Hz, 1H), 7.77–7.64 (m, 3H), 7.60–7.48 (m, 4H), 7.20 (d, J = 8.0 Hz, 2H), 2.43 (s, 3H); ^{13}C NMR (100 MHz, DMSO-d_6): δ 179.3, 165.3, 156.1, 138.6, 137.0, 135.2, 134.6, 133.5, 133.0, 132.2 (2C), 130.4, 129.6, 128.9 (2C), 127.1 (2C), 124.5, 119.2, 117.0, 22.4. MS(ESI) *m/z* 360.7 $[M+H]^+$. Anal calcd for $C_{21}H_{17}N_3OS$: C, 70.17; H, 4.77; N, 11.69 Found C, 70.23; H, 4.76; N, 11.67.

1-(3-(Benzo[*d*]thiazol-2-yl)phenyl)-3-phenylurea (BT_9): The compound was synthesized according to above general procedure using 3-(benzo[*d*]thiazol-2-yl)benzenamine (1.5 g, 6.61 mmol), DIPEA (1.8 g, 12.62 mmol) and 1-isocyanatobenzene (1.5 g, 9.76 mmol) to yield 1-(3-(benzo[*d*]thiazol-2-yl)phenyl)-3-phenylurea (1.8 g, 78.1%) as a white solid. M.p: 196-198 ^{o}C. ^{1}H NMR (400 MHz, DMSO-d_6): δ 10.12 (s, 2H), 8.26 (s, 1H), 8.04 (d, J = 8.0 Hz, 1H), 7.87 (d, J = 8.4 Hz, 1H), 7.77–7.63 (m, 3H), 7.54–7.45 (m, 2H), 7.33–7.21 (m, 5H); ^{13}C NMR (100 MHz, DMSO-d_6): δ 180.1, 167.6, 154.3, 141.3, 136.9, 135.3, 134.8, 133.0 (2C), 131.8, 128.2 (2C), 127.3, 126.4 (2C), 125.6, 124.0, 122.8, 120.3, 119.1. MS(ESI) *m/z* 346.3 $[M+H]^+$. Anal calcd for $C_{20}H_{15}N_3OS$: C, 69.54; H, 4.38; N, 12.17 Found C, 69.51; H, 4.39; N, 12.15.

1-(3-(Benzo[*d*]thiazol-2-yl)phenyl)-3-(4-nitrophenyl)urea (BT_10): The compound was synthesized according to above general procedure using 3-(benzo[*d*]thiazol-2-yl)benzenamine (1.5 g, 6.61 mmol), DIPEA (1.8 g, 12.62 mmol) and 1-isocyanato-4-nitrobenzene (1.3 g, 8.1 mmol) to get 1-(3-(benzo[*d*]thiazol-2-yl)phenyl)-3-(4-nitrophenyl)urea (2.1 g, 80.2%) as a yellow solid. M.p: 270-272 ^{o}C. ^{1}H NMR (400 MHz, DMSO-d_6): δ 9.45 (s, 1H), 9.34 (s, 1H),

8.35 (s, 1H), 8.19 (t, *J* = 8.0 Hz, 1H), 7.96 (d, *J* = 7.6 Hz, 2H), 7.78–7.64 (m, 3H), 7.56 (d, *J* = 7.6 Hz, 2H), 7.48–7.39 (m, 3H); ^{13}C NMR (100 MHz, DMSO-d_6): δ 182.1, 165.5, 155.3, 141.6, 137.4, 136.0, 135.1, 133.4, 131.4 (2C), 129.2, 128.2 (2C), 127.6 (2C), 126.0, 124.9, 123.6, 122.4, 120.0. MS(ESI) *m/z* 391.6 $[M+H]^+$.Anal calcd for $C_{20}H_{14}N_4O_3S$: C, 61.53; H, 3.61; N, 14.35 Found C, 61.60; H, 3.62; N, 14.33.

1-(4-Fluorophenyl)-3-(3-(5-(trifluoromethyl)benzo[*d*]thiazol-2-yl)phenyl)urea (BT_11): The compound was synthesized according to above general procedure using 3-(5-(trifluoromethyl)benzo[*d*]thiazol-2-yl)benzenamine (1.5 g, 6.12 mmol), DIPEA (1.8 g, 12.62 mmol) and 1-fluoro-4-isocyanatobenzene (1.2 g, 9.1 mmol) to obtain 1-(4-fluorophenyl)-3-(3-(5-(trifluoromethyl)benzo[*d*]thiazol-2-yl)phenyl)urea (2 g, 75.6%) as a cream white solid. M.p: 232-243 ^{o}C. ^{1}H NMR (400 MHz, DMSO-d_6): δ 10.06 (s, 1H), 9.81 (s, 1H), 8.46 (s, 1H), 8.25 (s, 1H), 8.04 (d, *J* = 8.4 Hz, 1H), 7.84–7.76 (m, 3H), 7.64 (d, *J* = 8.4 Hz, 2H), 7.56 (d, *J* = 7.6 Hz, 1H), 7.36 (d, *J* = 8.0 Hz, 2H); ^{13}C NMR (100 MHz, DMSO-d_6): δ 181.2, 165.7, 157.3, 141.6, 137.3, 136.0, 135.3, 134.6, 133.8 (2C), 132.8, 129.2, 128.4, 127.3, 126.9 (2C), 125.3, 124.2, 123.5, 122.8, 121.6. MS(ESI) *m/z* 432.2 $[M+H]^+$. Anal calcd for $C_{21}H_{13}F_4N_3OS$: C, 58.47; H, 3.04; N, 9.74 Found C, 58.53; H, 3.05; N, 9.76.

1-(*p*-Tolyl)-3-(3-(5-(trifluoromethyl)benzo[*d*]thiazol-2-yl)phenyl)urea (BT_12): The compound was synthesized according to above general procedure using 3-(5-(trifluoromethyl)benzo[*d*]thiazol-2-yl)benzenamine (1.5 g, 6.12 mmol), DIPEA (1.8 g, 12.62 mmol) and 1-isocyanato-4-methylbenzene (1.2 g, 9.01 mmol) to yield 1-(*p*-tolyl)-3-(3-(5-(trifluoromethyl)benzo[*d*]thiazol-2-yl)phenyl)urea (1.8 g, 69.7%) as a grey solid. M.p: 263-265 ^{o}C. ^{1}H NMR (400 MHz, $CDCl_3$): δ 10.27 (s, 2H), 8.36 (d, *J* = 8.4 Hz, 1H), 8.11 (s, 1H), 7.90 (d, *J* = 7.6 Hz, 1H), 7.81–7.68 (m, 3H), 7.54–7.38 (m, 3H), 7.33 (d, *J* = 8.0 Hz, 2H), 2.39 (s, 3H); ^{13}C NMR (100 MHz, $CDCl_3$): δ 178.3, 167.0, 154.6, 140.3, 136.2, 135.8, 135.2, 134.7, 133.1 (2C), 132.8, 130.4, 129.1 (2C), 127.9, 126.6, 126.1, 125.2, 124.6, 122.2, 119.7, 22.5. MS(ESI) *m/z* 428.7 $[M+H]^+$. Anal calcd for $C_{22}H_{16}F_3N_3OS$: C, 61.82; H, 3.77; N, 9.83 Found C, 61.75; H, 3.76; N, 9.81.

1-(4-Chlorophenyl)-3-(3-(5-(trifluoromethyl)benzo[*d*]thiazol-2-yl)phenyl)urea (BT_13): The compound was synthesized according to above general procedure using 3-(5-(trifluoromethyl)benzo[*d*]thiazol-2-yl)benzenamine (1.5 g, 6.12 mmol), DIPEA (1.8 g, 12.62 mmol) and 1-chloro-4-isocyanatobenzene (1.5 g, 9.76 mmol) to yield 1-(4-chlorophenyl)-3-(3-

(5-(trifluoromethyl)benzo[*d*]thiazol-2-yl)phenyl)urea (2.2 g, 78.3%) as a white solid. M.p: 243-245 ^{o}C. ^{1}H NMR (400 MHz, DMSO-d_6): δ 10.12 (s, 1H), 10.03 (s, 1H), 8.43 (s, 1H), 8.36 (d, *J* = 8.0 Hz, 1H), 7.94 (d, *J* = 7.6 Hz, 2H), 7.78–7.63 (m, 4H), 7.58 (d, *J* = 8.0 Hz, 1H), 7.46 (d, *J* = 8.0 Hz, 2H); ^{13}C NMR (100 MHz, DMSO-d_6): δ 179.7, 164.5, 156.0, 146.5, 142.4, 140.1, 137.4, 136.0, 135.2, 133.6 (2C), 132.9, 131.4, 130.1 (2C), 128.3, 127.8, 126.8, 125.3, 122.2, 120.3. MS(ESI) *m/z* 448.3 $[M+H]^+$. Anal calcd for $C_{21}H_{13}ClF_3N_3OS$: C, 56.32; H, 2.93; N, 9.38 Found C, 56.40; H, 2.92; N, 9.35.

1-(4-Nitrophenyl)-3-(3-(5-(trifluoromethyl)benzo[*d*]thiazol-2-yl)phenyl)urea (BT_14): The compound was synthesized according to above general procedure using 3-(5-(trifluoromethyl)benzo[*d*]thiazol-2-yl)benzenamine (1.5 g, 6.12 mmol), DIPEA (1.8 g, 12.62 mmol) and 1-isocyanato-4-nitrobenzene (1.3 g, 8.1 mmol) to get 1-(4-nitrophenyl)-3-(3-(5-(trifluoromethyl)benzo[*d*]thiazol-2-yl)phenyl)urea (2.3 g, 80.3%) as a yellow solid. M.p: 259-261 ^{o}C. ^{1}H NMR (400 MHz, DMSO-d_6): δ 10.11 (s, 1H), 8.44 (s, 1H), 8.32 (s, 1H), 8.12 (d, *J* = 8.4 Hz, 2H), 8.04 (d, *J* = 8.0 Hz, 1H), 7.81 (d, *J* = 8.0 Hz, 2H), 7.72–7.60 (m, 5H); ^{13}C NMR (100 MHz, DMSO-d_6): δ 169.6, 162.3, 160.0, 144.8, 143.2, 139.4, 138.0, 137.1, 136.6, 134.4, 133.0 (2C), 130.2, 129.7, 128.3, 127.2 (2C), 126.3, 125.1, 124.4, 120.6. MS (ESI) *m/z* 459.1 $[M+H]^+$. Anal calcd for $C_{21}H_{13}F_3N_4O_3S$: C, 55.02; H, 2.86; N, 12.22 Found C, 55.10; H, 2.85; N, 12.25.

1-(4-Nitrophenyl)-3-(3-(5-(trifluoromethyl)benzo[*d*]thiazol-2-yl)phenyl)thiourea (BT_15): The compound was synthesized according to above general procedure using K_2CO_3 (1.9 g, 13.7 mmol), 3-(5-(trifluoromethyl)benzo[*d*]thiazol-2-yl)benzenamine (1.5 g, 6.12 mmol), and 1-isothiocyanato-4-nitrobenzene (1.7 g, 9.4 mmol) in DMF: xylene (4:1) to get 1-(4-nitrophenyl)-3-(3-(5-(trifluoromethyl)benzo[*d*]thiazol-2-yl)phenyl)thiourea (2.1 g, 72.2%) as a yellow solid. M.p: 246-248 ^{o}C. ^{1}H NMR (400 MHz, DMSO-d_6): δ 10.11 (s, 2H), 8.37 (s, 1H), 8.03 (s, 1H), 7.92 (d, *J* = 8.0 Hz, 2H), 7.81 (t, *J* = 7.6 Hz, 1H), 7.69–7.56 (m, 3H), 7.42–7.33 (m. 3H); ^{13}C NMR (100 MHz, DMSO-d_6): δ 179.4, 166.4, 155.4, 142.3, 138.3, 137.1, 136.6, 134.8, 133.9, 131.5 (2C), 130.1, 129.3, 128.3, 127.2 (2C), 126.0, 124.2, 123.9, 121.5, 118.2. MS(ESI) *m/z* 475.5 $[M+H]^+$. Anal calcd for $C_{21}H_{13}F_3N_4O_2S_2$: C, 53.16; H, 2.76; N, 11.81 Found C, 53.23; H, 2.77; N, 11.83.

1-(3-(Benzo[*d*]thiazol-2-yl)phenyl)-3-phenylthiourea (BT_16): The compound was synthesized according to above general procedure using K_2CO_3 (1.9g, 13.7 mmol), 3-

(benzo[*d*]thiazol-2-yl)benzenamine (1.5 g, 6.61 mmol) and1-isothiocyanatobenzene (1.3 g, 9.6 mmol) in DMF: xylene (4:1) to obtain 1-(3-(benzo[*d*]thiazol-2-yl)phenyl)-3-phenylthiourea (1.8 g, 74.6%) as a white solid. M.p: 182-184 ^{o}C. ^{1}H NMR (400 MHz, $CDCl_3$): δ 9.97 (s, 2H), 8.28 (d, J = 8.0 Hz, 1H), 8.19 (s, 1H), 7.92 (d, J = 8.0 Hz, 1H), 7.72–7.64 (m, 3H), 7.56–7.36 (m, 6H), 7.28 (t, J = 7.6 Hz, 1H); ^{13}C NMR (100 MHz, $CDCl_3$): δ 179.4, 165.4, 156.2, 142.8, 138.3, 137.2, 135.3, 134.8, 133.9, 133.1 (2C), 132.2, 131.6, 128.5 (2C), 126.4, 125.1, 123.6, 120.4, 118.6. MS(ESI) *m/z* 362.3 $[M+H]^+$. Anal calcd for $C_{20}H_{15}N_3S_2$: C, 66.45; H, 4.18; N, 11.62 Found C, 66.58; H, 4.17; N, 11.64.

1-(*p*-Tolyl)-3-(3-(5-(trifluoromethyl)benzo[*d*]thiazol-2-yl)phenyl)thiourea (BT_17): The compound was synthesized according to above general procedure using K_2CO_3 (1.9 g, 13.7 mmol), 3-(5-(trifluoromethyl)benzo[*d*]thiazol-2-yl)benzenamine (1.5 g, 6.12 mmol) and 1-isocyanato-4-methylbenzene (1.3 g, 8.7 mmol) to yield 1-(*p*-tolyl)-3-(3-(5-(trifluoromethyl)benzo[*d*]thiazol-2-yl)phenyl)thiourea (2.2 g, 80.8%) as a cream white solid. M.p: 179-181 ^{o}C. ^{1}H NMR (400 MHz, DMSO-d_6): δ 10.18 (s, 2H), 8.35 (s, 1H), 8.22 (s, 1H), 7.94 (d, J = 8.0 Hz, 1H), 7.78 (d, J = 7.6 Hz, 1H), 7.54–7.33 (m, 5H), 7.20 (d, J = 8.4 Hz, 2H), 2.42 (s, 3H); ^{13}C NMR (100 MHz, DMSO-d_6): δ 179.4, 163.3, 156.3, 138.6, 136.7, 136.3, 135.4, 133.8 (2C), 133.2, 132.3, 130.6, 129.2, 127.4 (2C), 126.3, 125.2, 124.4, 123.7, 120.6, 118.3, 22.6. MS(ESI) *m/z* 444.6 $[M+H]^+$. Anal calcd for $C_{22}H_{16}F_3N_3S_2$: C, 59.58; H, 3.64; N, 9.47 Found C, 59.65; H, 3.63; N, 9.49.

1-(3-(Benzo[*d*]thiazol-2-yl)phenyl)-3-(4-nitrophenyl)thiourea (BT_18): The compound was synthesized according to above general procedure using K_2CO_3 (1.9 g, 13.7 mmol), 3-(benzo[*d*]thiazol-2-yl)benzenamine (1.5 g, 6.61 mmol) and 1-isothiocyanato-4-nitrobenzene (1.5, 8.3 mmol) to yield 1-(3-(benzo[*d*]thiazol-2-yl)phenyl)-3-(4-nitrophenyl)thiourea (2 g, 73.4%) as a yellow solid. M.p: 236-238 ^{o}C. ^{1}H NMR (400 MHz, $CDCl_3$): δ 9.47 (s, 1H), 8.18 (s, 1H), 7.99 (d, J = 8.0 Hz, 1H), 7.90 (d, J = 8.0 Hz, 2H), 7.83 (d, J = 7.6 Hz, 1H), 7.74–7.63 (m, 3H), 7.56–7.42 (m, 3H), 7.18 (d, J = 8.0 Hz, 2H); ^{13}C NMR (100 MHz, $CDCl_3$): δ 181.9, 166.3, 154.3, 140.1, 138.4, 137.9, 135.3, 134.9, 133.6 (2C), 132.5, 130.3, 129.5, 127.5, 126.2 (2C), 125.6, 124.4, 122.4, 120.4. MS(ESI) *m/z* 407.5 $[M+H]^+$. Anal calcd for $C_{20}H_{14}N_4O_2S_2$: C, 59.10; H, 3.47; N, 13.78 Found C, 59.18; H, 3.48; N, 13.80.

1-(4-Chlorophenyl)-3-(3-(5-(trifluoromethyl)benzo[*d*]thiazol-2-yl)phenyl)thiourea (BT_19): The compound was synthesized according to above general procedure using K_2CO_3 (1.9 g, 13.7

mmol), 3-(5-(trifluoromethyl)benzo[*d*]thiazol-2-yl)benzenamine (1.5 g, 6.12 mmol) and 1-chloro-4-isothiocyanatobenzene (1.5 g, 8.4 mmol) to yield 1-(4-chlorophenyl)-3-(3-(5-(trifluoromethyl)benzo[*d*]thiazol-2-yl)phenyl)thiourea (2.3 g, 81.7%) as a white solid. M.p: 211-213 ^{o}C. ^{1}H NMR (400 MHz, DMSO-d_6): δ 10.15 (s, 2H), 8.34 (s, 1H), 8.01 (d, J = 8.0 Hz, 1H), 7.90 (s, 1H), 7.78 (d, J = 8.4 Hz, 1H), 7.72 (d, J = 8.0 Hz, 1H), 7.67–7.53 (m, 4H), 7.33 (d, J = 7.6 Hz, 2H); ^{13}C NMR (100 MHz, DMSO-d_6): δ 179.3, 165.2, 156.4, 142.4, 138.4, 137.3, 136.4, 135.7, 134.3, 133.2 (2C), 131.8, 130.4, 129.4, 128.9, 127.4, 126.4 (2C), 125.5, 124.4, 123.8. MS(ESI) *m/z* 464.4 $[M+H]^+$. Anal calcd for $C_{21}H_{13}ClF_3N_3S_2$: C, 54.37; H, 2.82; N, 9.06 Found C, 54.44; H, 2.81; N, 9.08.

1-(3-(Benzo[*d*]thiazol-2-yl)phenyl)-3-benzylthiourea (BT_20): The compound was synthesized according to above general procedure using K_2CO_3 (1.9 g, 13.7 mmol), 3-(benzo[*d*]thiazol-2-yl)benzenamine (1.5 g, 6.61 mmol) and 1-(isothiocyanatomethyl)benzene (1.4 g, 9.7 mmol) to yield 1-(3-(benzo[*d*]thiazol-2-yl)phenyl)-3-benzylthiourea (1.8 g, 78.6%) as a pale brown solid. M.p: 210-212 ^{o}C. ^{1}H NMR (400 MHz, $CDCl_3$): δ 9.79 (s, 1H), 8.26 (d, J = 7.6 Hz, 1H), 7.94 (s, 1H), 7.81–7.72 (m, 3H), 7.68–7.56 (m, 4H), 7.49–7.36 (m, 5H), 5.12 (d, J = 8.4 Hz, 2H); ^{13}C NMR (100 MHz, $CDCl_3$): δ 180.4, 164.5, 153.4, 140.4, 138.1, 136.6, 135.3, 134.8, 134.0, 133.6 (2C), 132.5, 129.3 (2C), 128.2, 127.4, 126.8, 125.4, 124.0, 121.5, 119.0. MS(ESI) *m/z* 376.4 $[M+H]^+$. Anal calcd for $C_{21}H_{17}N_3S_2$: C, 67.17; H, 4.56; N, 11.19 Found C, 67.28; H, 4.55; N, 11.21.

1-(3-(Benzo[*d*]thiazol-2-yl)phenyl)-3-(4-chlorophenyl)thiourea (BT_21): The compound was synthesized according to above general procedure using K_2CO_3 (1.9 g, 13.7 mmol), 3-(benzo[*d*]thiazol-2-yl)benzenamine (1.5 g, 6.61 mmol) and 1-chloro-4-isothiocyanatobenzene (1.4 g, 8.2 mmol) to yield 1-(3-(benzo[*d*]thiazol-2-yl)phenyl)-3-(4-chlorophenyl)thiourea (2 g, 75.9%) as a cream white solid. M.p: 235-237 ^{o}C. ^{1}H NMR (400 MHz, DMSO-d_6): δ 10.05 (s, 1H), 10.03 (s, 1H), 8.31 (s, 1H), 8.16 (d, J = 8.0 Hz, 1H), 8.05 (d, J = 8.0 Hz, 1H), 7.85 (d, J = 7.6 Hz, 1H), 7.69 (d, J = 7.6 Hz, 1H), 7.58–7.36 (m, 7H); ^{13}C NMR (100 MHz, DMSO-d_6): δ 180.3, 167.4, 154.0, 140.9, 138.7, 135.0, 133.5, 130.0, 129.1 (5C), 127.2, 126.8, 126.2, 123.5, 123.4, 122.9, 122.4. MS(ESI) *m/z* 396.1 $[M+H]^+$. Anal calcd for $C_{20}H_{14}ClN_3S_2$: C, 60.67; H, 3.56; N, 10.61 Found C, 60.75; H, 3.55; N, 10.63.

1-Phenyl-3-(3-(5-(trifluoromethyl)benzo[*d*]thiazol-2-yl)phenyl)thiourea (BT_22): The compound was synthesized according to above general procedure using K_2CO_3 (1.9 g, 13.7

mmol), 3-(5-(trifluoromethyl)benzo[*d*]thiazol-2-yl)benzenamine (1.5 g, 6.12 mmol) and 1-isothiocyanatobenzene (1.3g, 9.6 mmol) to yield 1-phenyl-3-(3-(5-(trifluoromethyl)benzo[*d*]thiazol-2-yl)phenyl)thiourea (1.9 g, 72.3%) as a brown solid. M.p: 192-194 ^{o}C. ^{1}H NMR (400 MHz, DMSO-d_6): δ 10.06 (s, 1H), 8.34 (s, 1H), 8.16 (d, J = 8.0 Hz, 1H), 7.92 (d, J = 8.0 Hz, 1H), 7.81 (d, J = 7.6 Hz, 1H), 7.74–7.62 (m, 4H), 7.54–7.38 (m, 5H); ^{13}C NMR (100 MHz, DMSO-d_6): δ 180.1, 167.6, 154.2, 142.4, 139.2, 138.1, 136.8, 135.3, 134.8, 133.4 (2C), 131.4, 129.4 (5C), 126.6, 125.1, 120.3, 118.4. MS(ESI) *m/z* 430.3 $[M+H]^+$. Anal calcd for $C_{21}H_{14}F_3N_3S_2$: C, 58.73; H, 3.29; N, 9.78 Found C, 58.82; H, 3.28; N, 9.80.

1-(4-Fluorophenyl)-3-(3-(5-(trifluoromethyl)benzo[*d*]thiazol-2-yl)phenyl)thiourea (BT_23): The compound was synthesized according to above general procedure using K_2CO_3 (1.9 g, 13.7 mmol), 3-(5-(trifluoromethyl)benzo[*d*]thiazol-2-yl)benzenamine (1.5 g, 6.12 mmol) and 1-fluoro-4-isothiocyanatobenzene (1.3 g, 9.6 mmol) to yield 1-(4-fluorophenyl)-3-(3-(5-(trifluoromethyl)benzo[*d*]thiazol-2-yl)phenyl)thiourea (2.3 g, 83.2%) as a grey solid. M.p: 218-220 ^{o}C. ^{1}H NMR (400 MHz, $CDCl_3$): δ 9.93 (s, 2H), 8.39 (s, 1H), 8.12 (s, 1H), 7.92 (d, J = 8.0 Hz, 1H), 7.82 (d, J = 8.0 Hz, 1H), 7.71–7.58 (m, 5H), 7.28 (d, J = 8.0 Hz, 2H); ^{13}C NMR (100 MHz, $CDCl_3$): δ 178.2, 163.8, 156.8, 143.3, 138.3, 137.2, 136.3, 135.1, 133.2 (2C), 131.9, 129.4, 128.2, 127.3, 126.1 (2C), 125.4, 124.4, 123.9, 122.4, 120.6. MS(ESI) *m/z* 448.6 $[M+H]^+$. Anal calcd for $C_{21}H_{13}F_4N_3S_2$: C, 56.37; H, 2.93; N, 9.39 Found C, 56.48; H, 2.92; N, 9.37.

1-Benzyl-3-(3-(5-(trifluoromethyl)benzo[*d*]thiazol-2-yl)phenyl)thiourea (BT_24): The compound was synthesized according to above general procedure using K_2CO_3 (1.9 g, 13.7 mmol), 3-(5-(trifluoromethyl)benzo[*d*]thiazol-2-yl)benzenamine (1.5 g, 6.12 mmol) and 1-(isothiocyanatomethyl)benzene (1.4 g, 9.7 mmol) to yield 1-benzyl-3-(3-(5-(trifluoromethyl)benzo[*d*]thiazol-2-yl)phenyl)thiourea (2.1 g, 77.4%) as a white solid. M.p: 254-256 ^{o}C. ^{1}H NMR (400 MHz, $CDCl_3$): δ 9.56 (s, 1H), 8.43 (s, 1H), 8.18 (s, 1H), 7.89 (d, J = 8.0 Hz, 1H), 7.81 (s, 1H), 7.78 (d, J = 8.0 Hz, 1H), 7.74–7.66 (m, 2H), 7.58–7.39 (m, 6H), 5.04 (s, 2H); ^{13}C NMR (100 MHz, $CDCl_3$): δ 178.6, 163.4, 154.3, 141.3, 137.6, 136.4, 135.5, 134.3, 133.6, 133.2 (2C), 132.4, 131.4, 129.9, 129.1, 127.3, 126.7 (2C), 124.6, 122.4, 119.5, 61.8. MS(ESI) *m/z* 444.3 $[M+H]^+$. Anal calcd for $C_{22}H_{16}F_3N_3S_2$: C, 59.58; H, 3.64; N, 9.47 Found C, 59.64; H, 3.63; N, 9.49.

1-(3-(Benzo[*d*]thiazol-2-yl)phenyl)-3-(*p*-tolyl)thiourea (BT_25): The compound was synthesized according to above general procedure using K_2CO_3 (1.9 g, 13.7 mmol), 3-

(benzo[*d*]thiazol-2-yl)benzenamine (1.5 g, 6.61 mmol) and 1-isothiocyanato-4-methylbenzene (1.4 g, 9.3 mmol) to yield 1-(3-(benzo[*d*]thiazol-2-yl)phenyl)-3-(*p*-tolyl)thiourea (2 g, 80.5%) as a white solid. M.p: 178-180 ^{o}C. ^{1}H NMR (400 MHz, DMSO-d_6): δ 10.08 (s, 2H), 8.17 (d, J = 8.0 Hz, 1H), 7.99 (s, 1H), 7.89 (d, J = 8.0 Hz, 1H), 7.81–7.72 (m, 3H), 7.68–7.54 (m, 4H), 7.33 (d, J = 8.4 Hz, 2H), 2.44 (s, 3H); ^{13}C NMR (100 MHz, DMSO-d_6): δ 182.5, 165.2, 154.4, 141.3, 137.8, 137.3, 136.4, 135.3, 134.7, 133.9 (2C), 131.8, 130.4, 128.1 (2C), 126.8, 126.0, 125.4, 121.7, 119.8, 23.2. MS(ESI) *m/z* 376.4 $[M+H]^+$. Anal calcd for $C_{21}H_{17}N_3S_2$: C, 67.17; H, 4.56; N, 11.19 Found C, 67.26; H, 4.57; N, 11.21.

1-(3-(Benzo[*d*]thiazol-2-yl)phenyl)-3-(4-fluorophenyl)thiourea (BT_26): The compound was synthesized according to above general procedure using K_2CO_3 (1.9 g, 13.7 mmol), 3-(benzo[*d*]thiazol-2-yl)benzenamine (1.5 g, 6.61 mmol) and 1-fluoro-4-isothiocyanatobenzene (1.3 g, 9.6 mmol) to yield 1-(3-(benzo[*d*]thiazol-2-yl)phenyl)-3-(4-fluorophenyl)thiourea (1.9 g, 78.6%) as a grey solid. M.p: 240-242 ^{o}C. ^{1}H NMR (400 MHz, DMSO-d_6): δ 9.87 (s, 1H), 8.22 (d, J = 8.0 Hz, 1H), 8.16 (s, 1H), 7.84 (d, J = 8.0 Hz, 1H), 7.78–7.69 (m, 3H), 7.58 (d, J = 7.6 Hz, 1H), 7.54–7.45 (m, 4H), 7.29 (d, J = 8.0 Hz, 2H); ^{13}C NMR (100 MHz, DMSO-d_6): δ 179.8, 163.3, 152.6, 142.4, 138.3, 137.1, 135.8, 135.1, 134.2, 132.6 (2C), 131.5, 130.4, 129.6, 128.6 (2C), 127.3, 125.2, 124.1, 119.4. MS(ESI) *m/z* 380.1 $[M+H]^+$. Anal calcd for $C_{20}H_{14}FN_3S_2$: C, 63.30; H, 3.72; N, 11.07 Found C, 63.39; H, 3.71; N, 11.09.

5.2.1.5. Identification and characterization of inhibitors using enzyme inhibitory assay, molecular docking and protein thermal stability assay

We have performed the inhibitory enzyme assay for all the synthesized compounds using GR of B. s*ubtilis*. The enzyme was over expressed in *B. subtilis* using plasmid pET28a+and expression vector BL21 cells followed by purification as described in experimental section. The enzyme inhibitory activity was assessed through a coupled assay by monitoring NADH at A_{340}. Initially, GR was incubated with D-glutamate and test compound. Corresponding L-glutamate formation by racemization activity was measured by adding L-Glutamate dehydrogenase (GDH) and NAD^+. GDH mediates the reduction of NAD^+ to NADH which results from specific conversion from L-glutamate to α-ketoglutarate. The inhibitory results of compounds were listed in **Table 5.7**. Eight compounds have shown inhibitory activity at less than 10 µM which is better than a lead molecule, of which compounds **BT_8** and **BT_10** belong to urea substituted molecules. Most of the compounds showing IC_{50}<10 µM have the thiourea substitution. Compound **BT_25**

is showing IC_{50} of 1.32±0.43 µM inferring to be most potent than lead compound (IC_{50} of 19.47±0.81 µM) by seventeen times (**Figure 5.5**).

Table 5.7: Synthesized compounds represented with substitutions along with their biological activities

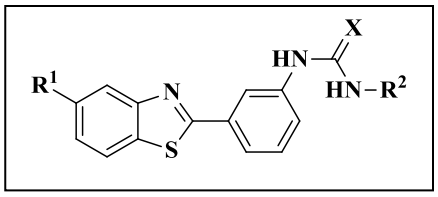

BT_4-26

Compound	X	R^1	R^2	IC_{50} (µM)	MIC (µM)			Cytotoxicity at 25 µM (% Inhib.)
					Actual MIC	MIC in the presence of Verapamil	MIC in the presence of Piperine	
BT_4	O	H	4-Methoxyphenyl	>25	33.31	ND	ND	56.12
BT_5	O	H	4-Chlorophenyl	>25	65.89	ND	ND	30.09
BT _6	O	CF_3	1-Phenyl	>25	3.76	ND	ND	40.01
BT _7	O	CF_3	4-Methoxyphenyl	>25	56.43	ND	ND	59.14
BT _8	O	H	4-Tolyl	5.92±0.25	69.67	2.17	69.67	31.18
BT _9	O	H	Phenyl	>25	72.87	ND	ND	97.15
BT _10	O	H	4-Nitrophenyl	3.56±0.34	8.09	2.04	8.09	42.10
BT _11	O	CF_3	4-Fluorophenyl	>25	57.92	ND	ND	97.67
BT _12	O	CF_3	4-Tolyl	>25	58.56	ND	ND	22.54
BT _13	O	CF_3	4-Chlorophenyl	>25	55.89	ND	ND	45.72
BT _14	O	CF_3	4-Nitrophenyl	>25	54.67	ND	ND	99.16
BT _15	S	CF_3	4-Nitrophenyl	4.18±0.66	52.73	3.34	52.73	18.45
BT _16	S	H	Phenyl	>25	69.25	ND	ND	2.35
BT _17	S	CF_3	4-Tolyl	>25	28.26	ND	ND	97.11
BT _18	S	H	4-Nitrophenyl	>25	61.59	ND	ND	98.23

BT _19	S	CF_3	4-Chlorophenyl	>25	53.90	ND	ND	97.31
BT _20	S	H	Benzyl	4.39±0.57	66.63	2.12	66.63	32.16
BT _21	S	H	4-Chlorophenyl	>25	2.09	ND	ND	58.42
BT _22	S	CF_3	1-Phenyl	8.21±0.28	14.67	1.84	14.62	28.11
BT _23	S	CF_3	4-Fluorophenyl	2.13±0.54	27.95	7.01	27.95	76.34
BT _24	S	CF_3	1-Benzyl	>25	14.69	ND	ND	96.12
BT _25	S	H	4-Tolyl	1.32±0.43	16.62	8.29	16.62	17.51
BT_26	S	H	4-Fluorophenyl	2.14±0.67	2.15	2.15	2.15	98.21
Isoniazid				>25	0.72	0.72	0.72	ND
Ethambutol				>25	7.64	3.82	3.82	ND
Rifampicin				>25	0.15	0.15	0.15	ND

ND: Not determined

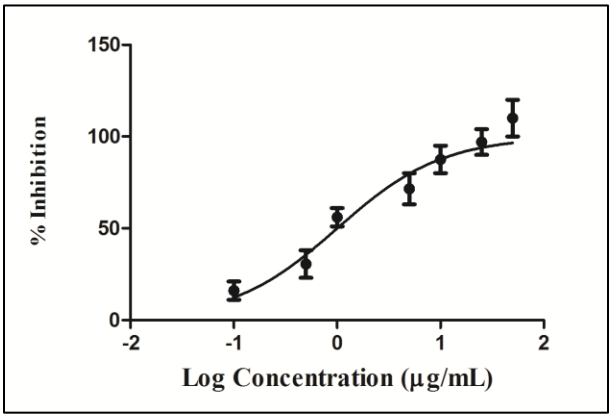

Figure 5.5: Log dose-response curve of compound **BT_25** with different log concentrations (X-axis) vs percentage inhibition (Y-axis).

Further, we analyzed the reliability of activity data of compounds obtained in *B. subtilis* with the support of molecular docking. We performed docking of active and inactive molecules (picked based on IC_{50} values) in the crystal structures of *M. tuberculosis* and *B. subtilis* GR in complex with D-glutamate (PDB ID: 5HJ7, 1ZUW respectively) using Glide XP docking (Schrodinger). The protein alignment of both crystal structures had a root mean square deviation (rmsd) 1.33 Å. The inhibitors were not docked properly on the substrate binding site (D-glutamate) in both proteins indicating binding possibility in allosteric site. To prove this concept, a putative binding

site has been identified by computational or experimental means. Even when a site for a given target is known, it may be desirable to find additional sites whose targeting could produce a desired biological response. A new program, called SiteMap, is utilized for identifying and analyzing binding sites and for predicting target druggability. In addition, a modified version of the score employed for binding-site identification allows SiteMap to accurately classify the druggability of proteins as measured by their ability to bind passively absorbed small molecules tightly. In the present study, five sites were identified in each crystal structures of proteins. Based on site-scores **site 1** in both the proteins was selected for further docking studies.

All the molecules were docked in both allosteric sites to see the binding pattern in both enzymes. We have superimposed compound **BT_25** in its binding mode and proteins using superimposition module in Schrodinger. This resulted in a superimposition can be seen in **Figure 5.6**. Here we represent the active (**BT_25**) molecule from the series in both the crystal structures. The binding orientation of one of the compounds within the *M. tuberculosis* GR binding pocket is represented in **Figure 5.7**.The predicted bound conformation of the active compound showed that the NH atom formed two hydrogen bonding interactions with the side chain of the Glu153. Apart from this the compound further stabilized through various hydrophobic and few polar amino acid residue interactions. The compound was very well fit into the active site cavity of the protein with a docking score of-5.52 kcal/mol. The binding pose of compound **BT_25** in *B. subtilis* is shown in **Figure 5.7** shows that similar kind of interaction with Glu 153 and surrounded by hydrophobic residues with a docking score of-5.11 kcal/mol. Thus molecular docking was a great help in supporting the confirmation of inhibitory activity in both the organisms.

Figure 5.6: Docking pose of active molecule **BT_25** in **site 1** of *M. tuberculosis* (5HJ7) and *B. subtilis* (1ZUW) in a superimposed view. Orange color represents protein and ligand in 5HJ7 whereas blue represents 1ZUW.

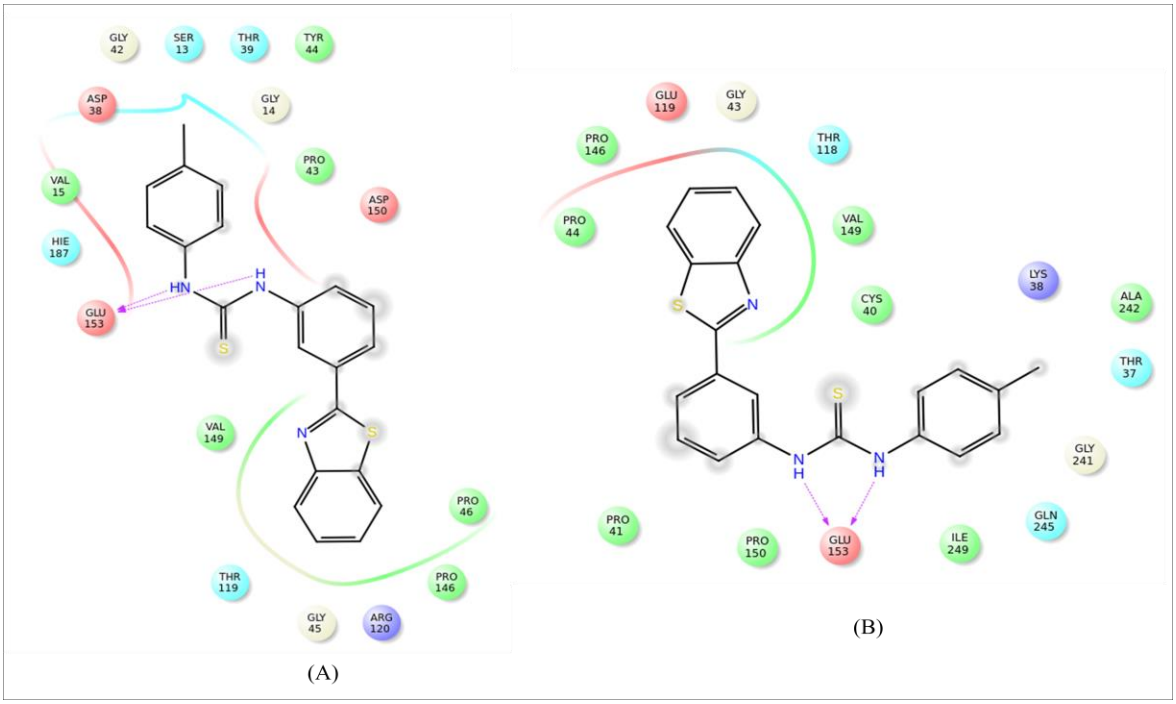

Figure 5.7: Binding pose and the interaction pattern of the compound **BT_25** in A) *M. tuberculosis* and B) *B. subtilis*.

Molecular dynamics is a great tool to generate further theoretical information to support their activity by studying the protein-ligand interaction stability in dynamic conditions (simulating body conditions). Compound **BT_25** in 5HJ7 and 1ZUW protein complexes was subjected to a 10 ns simulation using Desmond. The rmsd analysis plots for the protein-ligand complexes have been carried out so as to measure the distance between atoms during simulation (**Figure 5.8**).Rmsd for 1ZUW, C_{α} and ligand were within the average of ~2 Å and ~1.25 Å and for 5HJ7 both C_{α} and ligand were within ~1.9-1.98 Å respectively during 10 ns simulation trajectory. The root mean square fluctuation (rmsf) analysis shows the fluctuation range undergone by every residue in the protein during simulation. Rmsf plot for compound **BT_25** in both protein complexes were shown in (**Figure 5.9**). The figure shows least fluctuations of the ligand binding site residues with rmsf values in an average of ~1.05 Å and 0.51 Å respectively for 5HJ7 and 1ZUW.

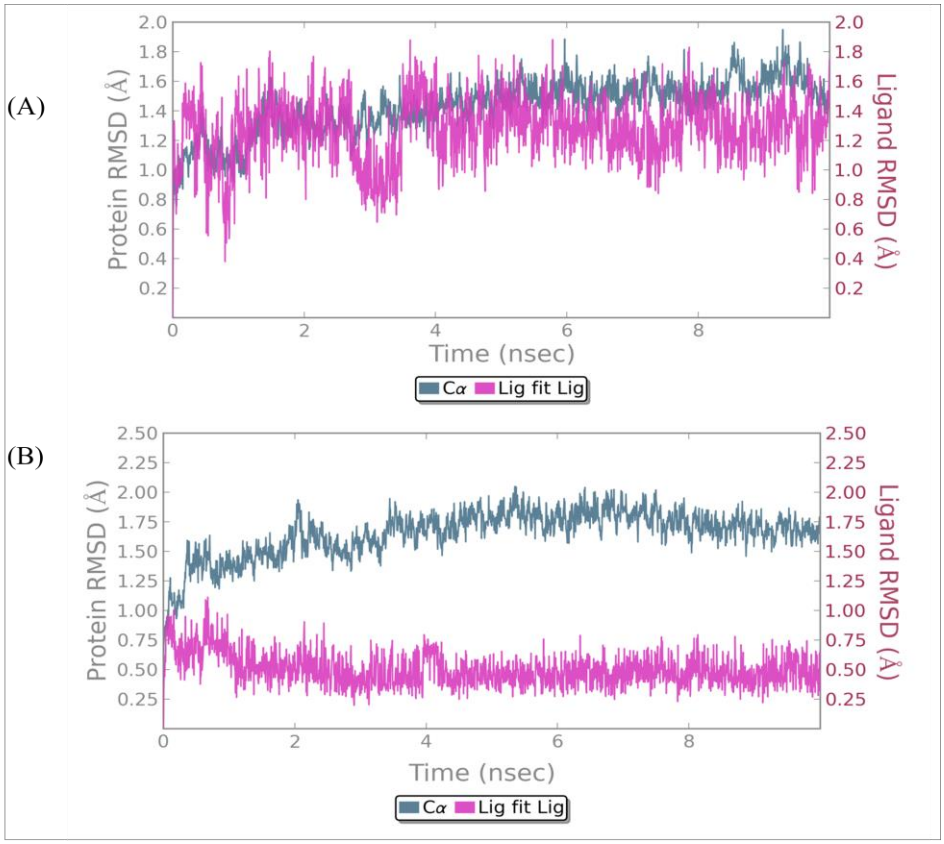

Figure 5.8: Rmsd plots of Glutamate racemase in a bound state with compounds **BT_25** as a function of time in *M. tuberculosis* (A) and *B. subtilis* (B).

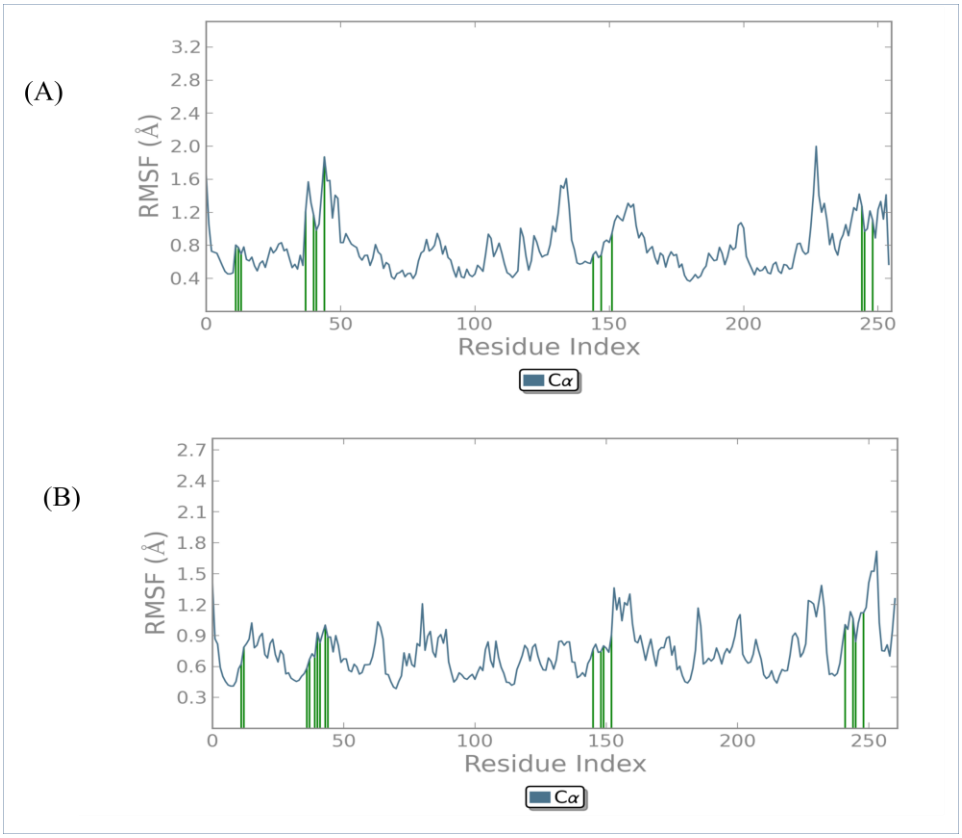

Figure 5.9: Rmsf plot for all atoms of Glutamate racemase in complex with compound **BT_25** resulted from 10 ns simulation trajectory (A) *M. tuberculosis* and (B) *B. subtilis.*

Characterization of identified inhibitors is also very important in drug discovery research. The changes in thermal stability of an enzyme can be used to determine the mode of inhibition of a compound. Usually, a positive shift in (T_m) indicates the stability enhancement of protein, can be either in presence of a substrate or a ligand where the magnitude of shift can be modulated by the second ligand. Based on this principle, mode of inhibition can be categorized into three [Venkataraman, J., *et al*., 2012].

a) Competitive: The magnitude of inhibitor-induced T_m shift will be lesser when than that of the enzyme-substrate complex shift.
b) Uncompetitive: The change in T_m by inhibitor can only be seen in the presence of substrate-bound enzyme.
c) Non-competitive: Change in T_m due to inhibitor will be seen irrespective of the presence or absence of a substrate in the enzyme.

The thermal shift analysis of active molecule **BT_25** indicated that it follows the non-competitive mode of inhibition with an approximate shift in ΔT_m by 3.9 ^oC with native protein and when tested with protein-substrate complex there was a shift by 4.7 ^oC with native protein (**Figure 5.10**). This indicates that the protein and protein-substrate complex were more stabilized in the presence of compound **BT_25** when compared to **lead 1**.

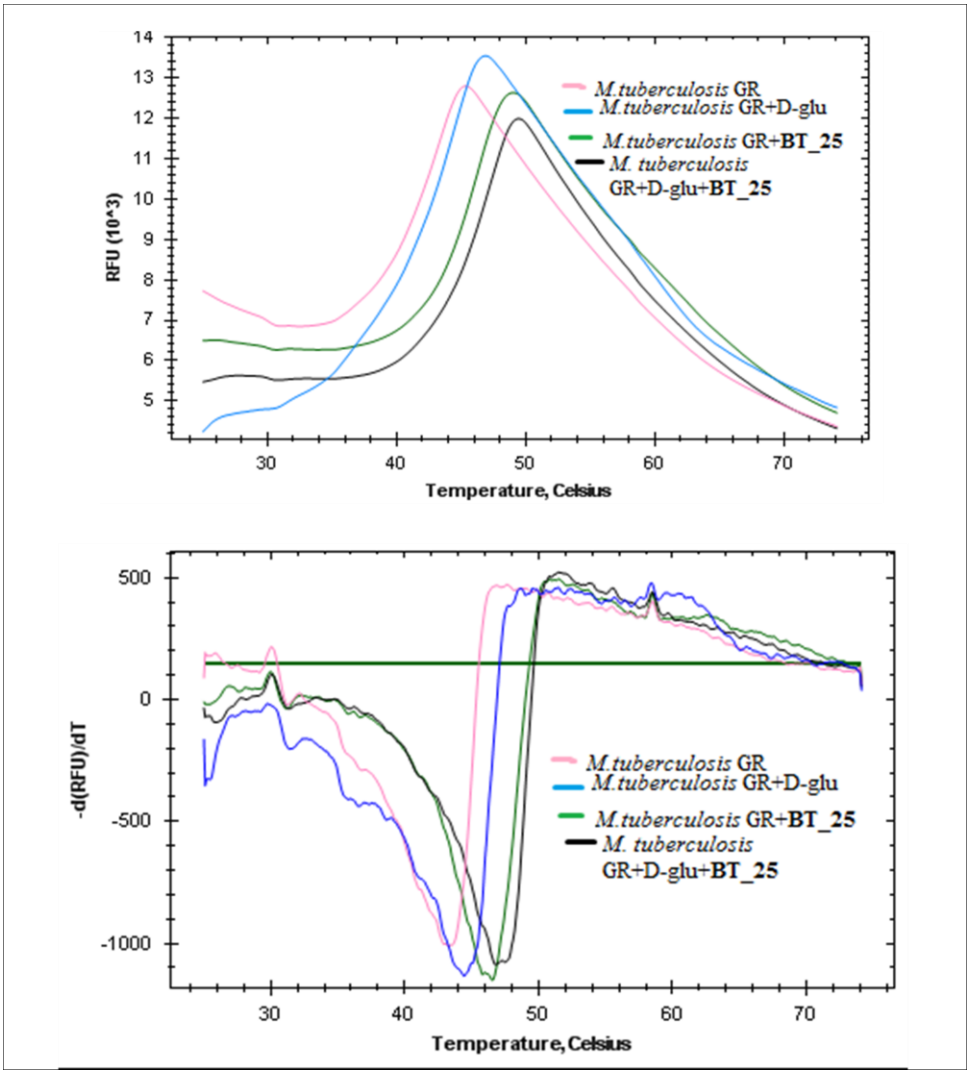

Figure 5.10: Thermal stability curves of *M. tuberculosis* GR depicting the non-competitive inhibition by compound **BT_25.**

5.2.1.6. *In vitro* active *M. tuberculosis* assay model

All the synthesized molecules were screened *in vitro* for their activity against replicating *M. tuberculosis* using microplate alamar blue assay (MABA) with drug concentrations from 50

μg/mL to 0.78 μg/mL. The minimum inhibitory concentration (MIC) was determined for each compound as the minimum concentration of compound required to completely inhibit the bacterial growth. MIC values of the synthesized compounds and the standard drugs (Isoniazid, Ethambutol and Rifampicin) for comparison were represented in **Table 5.7**. All synthesized compounds showed a varied range of activity against *M. tuberculosis*. Five compounds (**BT_10, BT_22, BT_23, BT_25** and **BT_26**) have shown inhibition in the range of 30 μM to 2 μM. Compound **BT_25** with IC_{50} of 1.32±0.43 μM in the *B. subtilis* enzyme inhibition activity, showed MIC of 16.62 μM. Compound **6** which was not active in enzyme assay but showed a good MIC of 3.76 μM, indicating that the compound is targeting a different pathway for inhibition. Compounds **BT_6, BT_21, BT_26** have shown better inhibitions than Ethambutol (MIC 7.64 μM). Some of the compounds were unsuccessful to inhibit the whole organism despite their good activity in the enzyme inhibition study. One of the major reasons can be the efflux of the drug by the organism.

5.2.1.7. *In vitro* non-replicating, *M. tuberculosis* nutrient starved assay

Persistent or latent form of TB is considered to be one of the major hurdles in the treatment of tuberculosis. It's evident that TB bacteria can survive in nutrient and oxygen-deprived conditions. First line drugs like Isoniazid, Rifampicin failed in inhibiting the bacteria. Nutrient starvation triggers latent condition in bacilli that transforms it to the non-replicating stage that replicates *M. tuberculosis* during various stages of persistent conditions. In this model, *M. tuberculosis* cultures were nutrient starved in phosphate buffer saline (PBS) for 6 weeks. After 6 weeks, the culture was treated with the synthesized test compounds and standard drugs at a concentration of 10 μg/mL [Salina, E., 2014]. Considering the IC_{50} and MIC values of the synthesized compounds we have selected compounds **BT_10, BT_23, BT_24** and **BT_25** for non replicating *M. tuberculosis* assays. It's noteworthy that the compounds **BT_10, BT_23, BT_25** which have shown activity on GR which is an important enzyme in replicating bacteria have also shown inhibition against dormant bacteria. The rest of the compounds didn't show significant inhibition (**Figure 5.11**). Compound **BT_24** was active in replicating bacteria (MIC) had also shown activity against latent form. Compounds **BT_10, BT_23, BT_24** and **BT_25** showed almost similar bacterial log reduction of 2.1 to control (Ctrl) and were more active than

Isoniazid (INH) by 1.1 log reduction and Rifampicin (RIF) by 0.5 logs. None of the compounds have significant activity when compared with Moxifloxacin (MOXI).

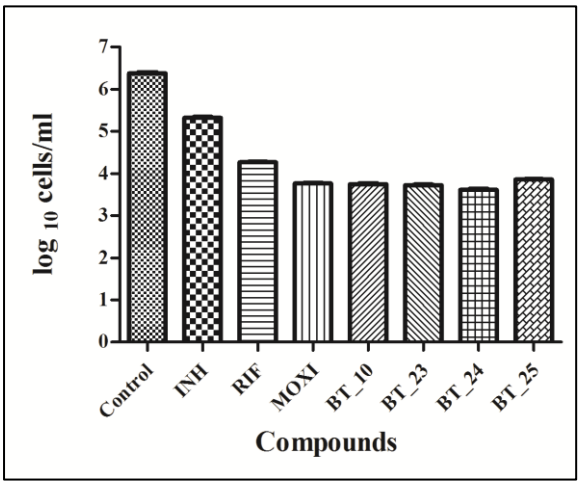

Figure 5.11: Activity profile of compounds in the nutrient starvation model. Bacterial count (Mean ± S.E., n=3) for control and treated groups was estimated through MPN (most probable number) assay.

5.2.1.8. Determination of kill kinetics in *M. tuberculosis*

For the compounds that are determined for activity against bacteria, the next step will be the analyzing nature of inhibition if they are bactericidal or bacteriostatic which will be helpful in designing a therapy. For that minimum bactericidal concentration (MBC) has to be determined, it is defined as the concentration of which there is three log inhibition of bacteria in three weeks of incubation. A compound is said to be bactericidal if MBC is not more than 4 fold of its MIC and bacteriostatic if it's more than four folds [Parish, T., *et al*., 1998]. Bactericidal compounds exhibit two kinds of kill namely time dependant and concentration dependant. We have evaluated compounds at different concentrations on bacteria obtained after 2 weeks of nutrient starvation at 0, 7, 14, 21 days after drug treatment. Compounds **BT_23, BT_24, BT_25** showing good inhibition in above study on nutrient starved culture, have shown MBC more than fourfold of their MIC values indicating that they are bacteriostatic. Compound **BT_10** has shown more than threefold reduction at concentration 10 µg/mL (25 µM) which is less than four folds of MIC (8.09 µM). The observation of kill kinetics of compound **BT_10** reveals that there was an increase in kill (**Figure 5.12**) with respect to increase in the concentration of compound (at 20 µg/mL) stating that it shows concentration dependant bactericidal activity.

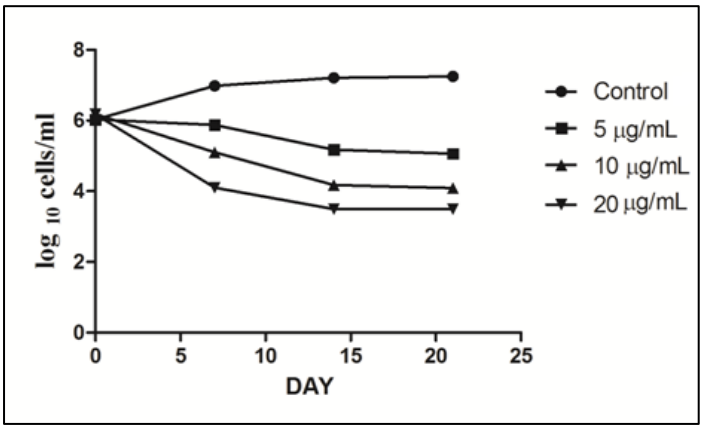

Figure 5.12: Kill kinetic curve of compound **BT_10** depicting concentration dependant kill.

5.2.1.9. Inhibitory activity testing on persistent biofilm forming *M. tuberculosis*

M. tuberculosis has developed adaptability to survive against environmental stresses as well as to antibiotics. This kind of resistance is possible through the formation of highly organized complex cellular structures named biofilm. These are capable to survive against potent first-line drugs like INH and RIF even at higher drug concentrations [kulka, K., *et al*., 2012]. There is need to develop drugs that act on this kind of persistence conditions which will help in improving the treatment regimen. Compounds **BT_10, BT_24** and **BT_25** were tested for their activity on biofilm at concentration of10 µg/mL. Standards INH, RIF and MOXI have shown a log reduction of 1, 1.2 and 1.8 respectively compared to control. Test compounds **BT_10, BT_24** and **BT_25** have shown log reduction of 0.7, 1.8 and 2 respectively as shown in **Figure 5.13**.

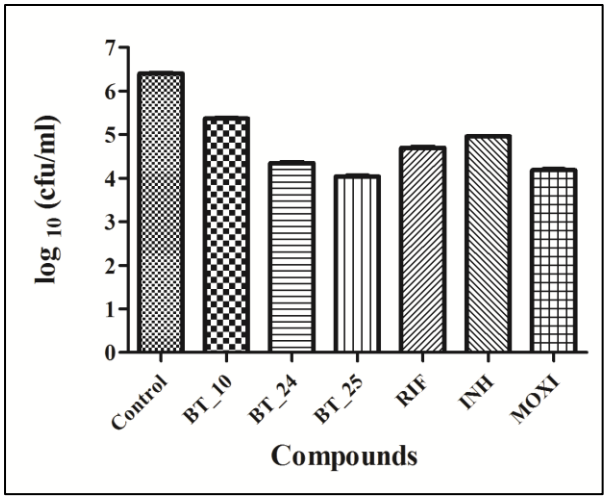

Figure 5.13: Comparative biofilm inhibitory activity plots of compounds **BT_10, BT_24** and **BT_25** against *M. tuberculosis* along with standards. Bacterial count estimation (Mean ± S.D., n = 4) for control and treated groups was conducted by using the MPN assay.

5.2.1.10. *In vivo* activity testing assay on *Mycobacterium marinum* infected zebrafish

Even with the extensive study of novel *M. tuberculosis* drugs *in vitro,* there is a requirement for the validation of bacterial genes and drugs in animal models. Of the many animal models developed for *M. tuberculosis* infection. The most versatile model known has been mouse infection model. It has limitations like failure to produce caseating granulomas unlike in humans. The same is the barrier with rabbit and guinea pigs models. The other reliable model is primate infection, but the cost and time considerations of this model force to use in a limited fashion. Under these conditions the emergence of zebrafish infection model, using *M. marinum*, a genetic relative of *M. tuberculosis* complements above models [Cronan, M. R., *et al*., 2014]. Mimicking many aspects of host infection conditions, cost-effectiveness is considered as the major advantages. The most active molecule at enzyme level compound **BT_25** was tested for *in vivo* inhibitory potency using zebra fish model. INH and MOXI were taken as standard drugs, showed a log reduction of 2.6 and 2.5 respectively against control. Our test compound has shown a good activity with a log reduction of 3.5 with control (**Figure 5.14**).

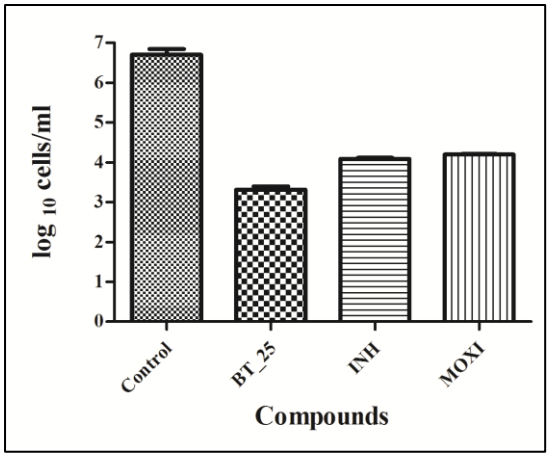

Figure 5.14: Bacterial count estimation (Mean ± S.E.M., n = 6) for control and treated groups by zebrafish model conducted by using MPN assay. Statistical significance has been analyzed by Two-way ANOVA using GraphPad Prism Software.

5.2.1.11. Cytotoxicity determination

To know the toxic effect of synthesized compounds on host cells (macrophages) we have used MTT (3-(4,5-Dimethylthiazol-2-yl)-2,5-Diphenyltetrazolium Bromide) assay. RAW 246.7 cell lines were used for experimental studies [Reck, F., *et al*., 2011]. All the compounds were tested at a concentration of 25 µM and the percentage inhibition was found to be in varied ranges. However, most of the compounds were not toxic at 25 µM (**Table 5.7**). Hence most of the compounds are devoid of effects on metabolism.

5.2.1.12. Highlights of the study

We report novel inhibitors of Glutamate racemase in bacteria. In-house compound library screening with fluorescence thermal shift assay resulted in **lead 1**. Hit expansion by medicinal chemistry efforts, identified compound **BT_25** as the most potent inhibitor with IC_{50} of 1.32 ± 0.43 µM in *B. subtilis*, further supported by molecular docking. Analysis of protein-ligand binding interaction profile using thermal shift assay showed that the compound **BT_25** was exhibiting a non-competitive mode of inhibition. The molecules exhibited promising antimicrobial potency against replicative and non-replicative forms of *M. tuberculosis* H37Rv. *In vivo* studies showed compound **BT_25** has a good drug-like activity in all synthesized molecules (**Figure 5.15**).

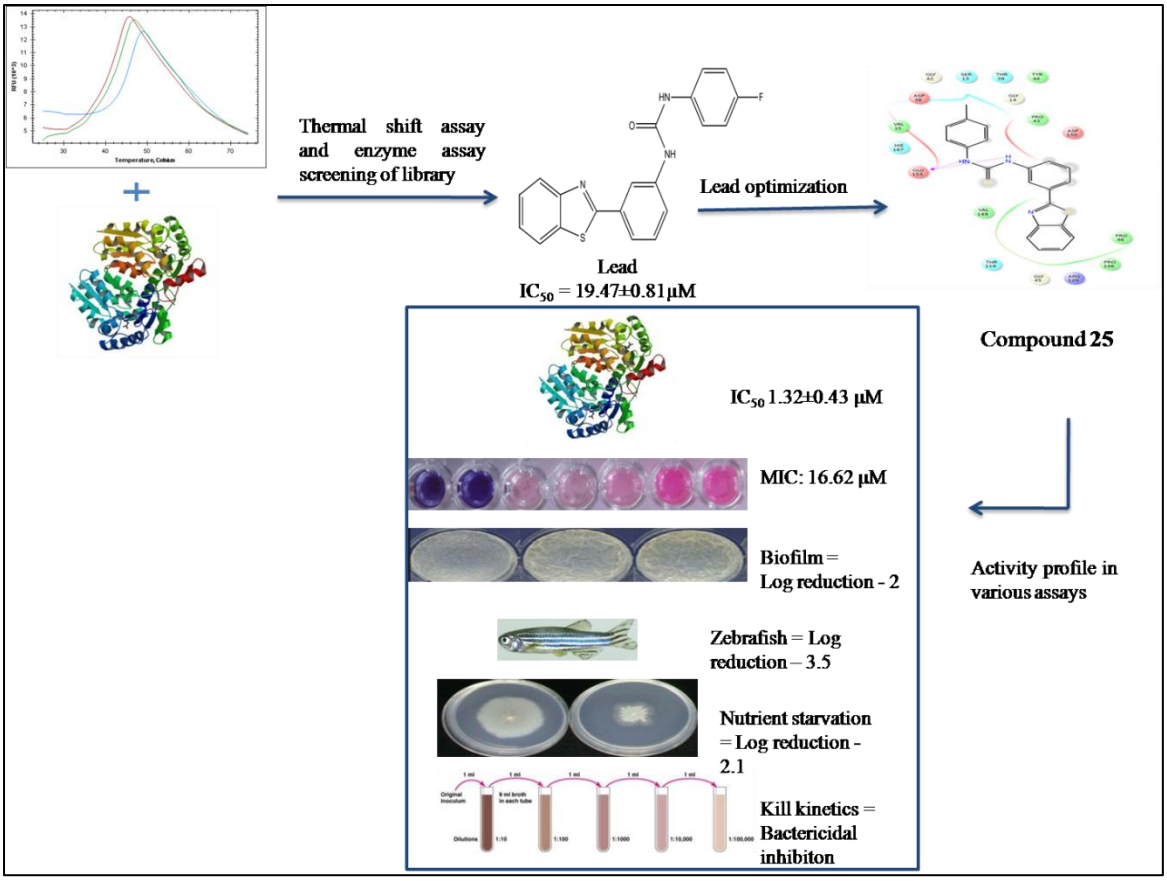

Figure 5.15: Flow of the study from identification of lead to hit optimization with chemical and biological data.

5.2.2. Identification and development of Benzoxazole derivatives as *Mycobacterium tuberculosis* Glutamate racemase inhibitors

5.2.2.1. Lead identification by fluorescence thermal shift screening

We conducted the assay with purified *M. tuberculosis* Glutamate racemase enzyme with substrate D-glu in bound and free forms against test compounds. Melt curve of protein in its free state has shown T_m at ~43.6 ^oC and in complex with D-glu at ~44.8 ^oC. Screened compounds showed a varied range ΔT_m of which **lead 2** has shown T_m at ~46.8 ^oC, which is showing a Δ3.2 ^oC with unbound protein and Δ2.0 ^oC with protein bound to D-glu. This result shows the competence of compound **lead 2** in stabilizing the protein from rest of the library and showing more chances for considering it as a lead compound.

Compound **Lead 2** has shown an IC_{50} of 20.7 ± 0.29 µM against *B. subtilis* Glutamate racemase (**Figure 5.16**). In both FTS and inhibitory assay compound **Lead 2** has shown good activity, hence it was taken as a lead molecule and further optimized through structural modifications using chemical procedures.

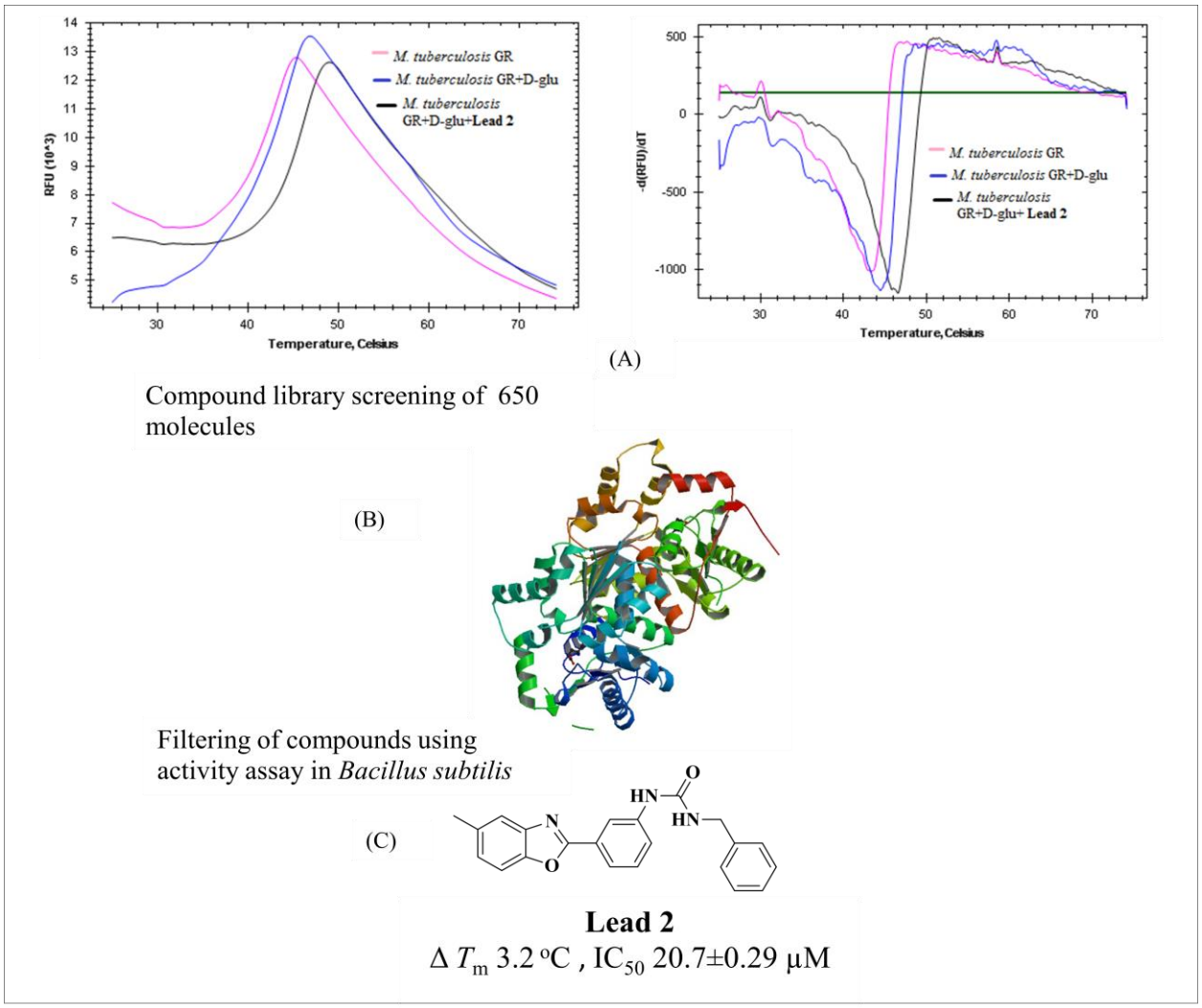

Figure 5.16: (A) (Left): Melt curves of *M. tuberculosis* in its free state, bound with substrate and ligand. (Right) represents the melt temperature plotting derivative fluorescent (Y-axis) and temperature (X-axis). T_m can be measured from the minimum of the plot. (B) 3D representation of *B. subtilis* Glutamate racemase crystal structure, employed for *in vitro* activity assay. (C) Structure of identified **lead 2** with melt temperature and IC_{50} value.

5.2.2.2. Chemical synthesis and characterization

The target molecules were synthesized by two-step synthetic protocol (**Scheme 5.2**); in first step 4-substituted-2-aminophenols (**BO_1a-b**) were treated with 3-amiobenzoicacid (**BO_2**) to produce corresponding substituted cyclized compounds **BO_3a-b** (3-(benzo[d]oxazol-2-yl)aniline). In next step, the primary amine group of phenyl ring was reacted with variously substituted arylisocyanates using ethanol as solvent to produce *N*, *N*-substituted urea derivatives (**BO_4-16**); but using similar conditions for the preparation of *N*, *N*-substituted thiourea derivatives, the reactions were not successful, then we employed K_2CO_3 as base and DMF/xylene as solvents to produce *N*, *N*-substituted thiourea derivatives (**BO_17-28**). All the analytical data (^{1}H NMR, ^{13}C NMR, and mass spectra) of synthesized compounds (both intermediates and finals) were on par with projected structures. A total twenty four compounds were synthesized as represented in (**Table 5.8**).

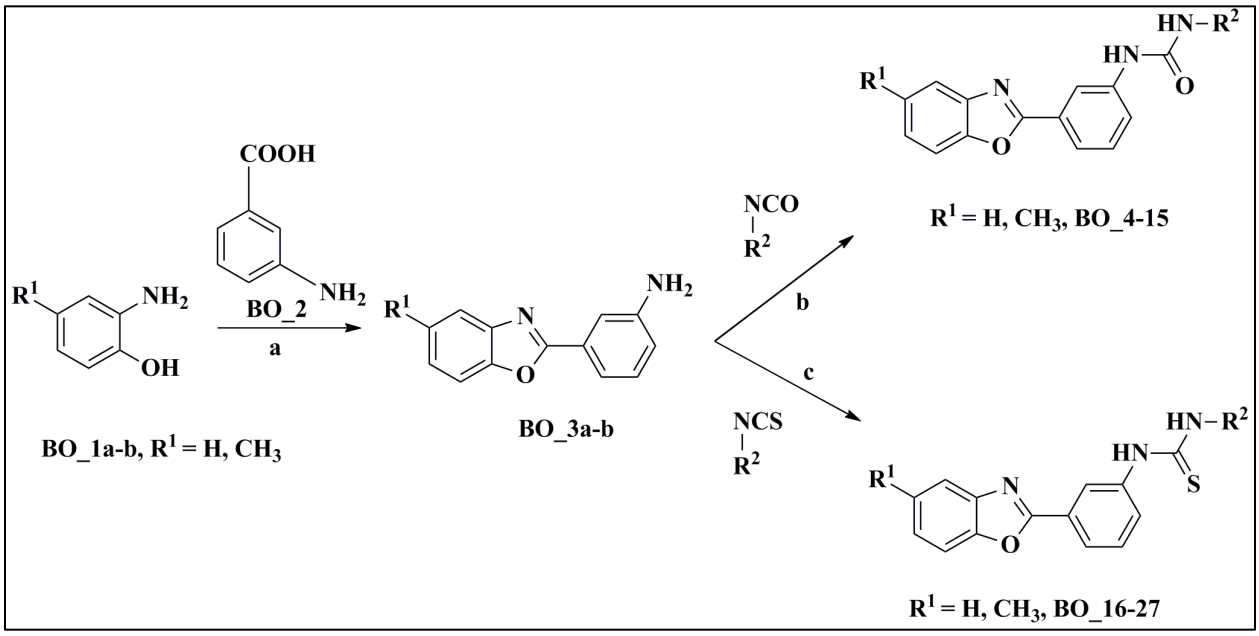

Scheme 5.2: Synthetic scheme utilized for the synthesis of target molecules. Reagents and conditions: (a) PPA, 185 °C, 6h; (b) R^2-NCO, DIPEA, DMF, rt, 2h; (c) R^2-NCS, DMF/xylene(4:1), K_2CO_3, MW, 110 °C, 30 minutes.

5.2.2.3. Synthetic protocol used for synthesis

General procedure for the preparation of BO_3a-b: 3-amiobenzoicacid (**BO_2**) (1.0 equiv), compound **BO_1a-b** (1.1 equiv) and PPA (10 volumes) mixture was allowed to reflux at 185 °C

for 6 hours. After the completion of the reaction, the contents were cooled and neutralized with cold 6N NaOH solution. The precipitate formed was filtered and further continued for heating in DMF at 60 °C for 15 minutes, and contents were transferred into crushed ice. The solid was filtered and washed with cold ethanol and diethyl ether to get the corresponding recrystallized compound **BO_3a-b** respectively.

General procedure for the preparation of compounds BO_4-15: To the mixture of compounds **BO_3a-b** (1.0 equiv), DIPEA (2.0 equiv) was added with the corresponding arylisocyanate (1.25 equiv) in DMF. After the reaction has completed, the mixture was added to EtOAc followed by washing with water, Brine solution and distilled under reduced pressure to obtain the product. The crude product was purified by column chromatography using EtOAc/hexane as eluent to obtain pure compounds **BO_4-15**.

General procedure for the preparation of compounds BO_16-27: To a solution of compounds **BO_3a-b** (1.0 equiv) and the corresponding arylisothiocyanate (1.3 equiv) in DMF: xylene (4:1), potassium carbonate (2.0 equiv) was added with stirring. The whole reaction was carried out under microwave irradiation conditions (temperature 110 °C) for about 30 minutes. The contents of the flask were poured into the crushed ice for cooling and the resulted precipitate was filtered and washed twice with ethanol. The crude residue was further purified by column chromatography using ethylacetate/hexane as eluent to get the corresponding pure compounds **BO_16-27**. The structures of synthesized compounds with their physiochemical properties were listed in **Table 5.8**.

Table 5.8: Physicochemical properties of synthesized compounds **BO_4-27**

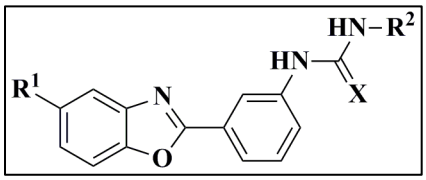

BO_4-27

Compound	R_1	R_2	X	Yield (%)	Melting point (^oC)	Molecular formula	Molecular weight
BO_4	CH_3	Phenyl	O	77.1	240-242	$C_{21}H_{17}N_3O_2$	343.12
BO_5	CH_3	4-Chlorophenyl	O	73.7	181-183	$C_{21}H_{16}ClN_3O_2$	378.33
BO _6	H	4-Methoxyphenyl	O	86.4	228-230	$C_{21}H_{17}N_3O_3$	359.17
BO _7	H	4-Nitrophenyl	O	84.1	250-252	$C_{20}H_{14}N_4O_4$	374.29
BO _8	H	Benzyl	O	88.5	243-245	$C_{21}H_{17}N_3O_2$	359.33
BO _9	CH_3	4-Methoxyphenyl	O	87.2	228-230	$C_{22}H_{19}N_3O_3$	373.41
BO _10	H	4-Chlorophenyl	O	85.1	175-177	$C_{20}H_{14}ClN_3O_2$	363.12
BO _11	CH_3	4-Fluorophenyl	O	88.2	169-171	$C_{21}H_{16}FN_3O_2$	361.49
BO _12	H	Phenyl	O	83.2	210-212	$C_{20}H_{15}N_3O_2$	329.61
BO _13	H	4-Fluorophenyl	O	81.3	180-182	$C_{20}H_{14}FN_3O_2$	347.07
BO _14	H	4-Tolyl	O	88.5	164-166	$C_{21}H_{17}N_3O_2$	343.65
BO _15	H	Isopropyl	O	78.5	174-176	$C_{17}H_{17}N_3O_2$	296.03
BO _16	H	Benzyl	S	84.6	210-212	$C_{21}H_{17}N_3OS$	359.17
BO _17	CH_3	4-Fluorophenyl	S	81.8	235-237	$C_{21}H_{16}FN_3OS$	377.35
BO _18	H	4-Nitrophenyl	S	85.2	236-238	$C_{20}H_{14}N_4O_3S$	390.11

BO _19	H	4-Fluorophenyl	S	84.8	235-237	$C_{20}H_{14}FN_3OS$	363.71
BO _20	CH_3	4-Nitrophenyl	S	81.1	241-243	$C_{21}H_{16}N_4O_3S$	404.18
BO _21	CH_3	Phenyl	S	79.9	155-157	$C_{21}H_{17}N_3OS$	359.42
BO _22	CH_3	4-Chlorophenyl	S	80.3	190-192	$C_{21}H_{16}ClN_3OS$	393.29
BO _23	CH_3	Benzyl	S	79.6	209-211	$C_{22}H_{19}N_3OS$	373.35
BO _24	CH_3	4-Tolyl	S	83.6	231-233	$C_{22}H_{19}N_3OS$	373.35
BO_25	H	4-Chlorophenyl	S	81.1	230-232	$C_{20}H_{14}ClN_3OS$	379.81
BO _26	H	Phenyl	S	82.3	182-184	$C_{20}H_{15}N_3OS$	345.37
BO _27	H	4-Tolyl	S	81.7	221-223	$C_{21}H_{17}N_3OS$	359.05

5.2.2.4. Characterization of synthesized compounds

3-(Benzo[*d*]oxazol-2-yl)aniline (BO_3a): The compound was synthesized according to above general procedure using 2-aminophenol (1 g**,** 9.17 mmol), 3-amiobenzoicacid (0.9 g, 6.84 mmol) and PPA (10 mL) to obtain 3-(benzo[*d*]oxazol-2-yl)aniline (1.6 g,73%) as pale yellow solid. ^{1}H NMR (400 MHz, $CDCl_3$): δ 8.29 (s, 1H), 8.11-7.89 (m, 3H), 7.58-7.39 (m, 4H), 6.87 (s, 2H). ^{13}C NMR (100 MHz, $CDCl_3$): δ 163.3, 151.3 (2C), 143.6, 132.7, 128.6, 124.9 (2C), 119.5 (3C), 116.3, 109.9. MS(ESI) *m/z* 211 $[M+H]^+$. Anal calcd for $C_{13}H_{10}N_2O$: C, 74.27; H, 4.79; N, 13.33; Found: C, 74.34; H, 4.78; N, 13.35.

3-(5-Methylbenzo[*d*]oxazol-2-yl)aniline (BO_3b): The compound was synthesized according to above general procedure using 2-amino-4-methylphenol (1g**,** 8.13mmol), 3-amiobenzoicacid (0.9 g, 6.84 mmol) and PPA (10 mL) to obtain 3-(5-methylbenzo[*d*]oxazol-2-yl)aniline (1.8 g,71%) as white solid. ^{1}H NMR (400 MHz, $CDCl_3$): δ 8.42 (s, 1H), 8.22 (s, 1H), 7.92-7.52 (m, 5H), 6.94 (s, 2H), 2.45 (s, 3H). ^{13}C NMR (100 MHz, $CDCl_3$): δ 162.9, 149.2, 145.6, 140.8, 135.2, 132.7, 127.6 (2C), 118.5 (3C), 113.8, 108.7, 22.3. MS(ESI) *m/z* 225 $[M+H]^+$. Anal calcd for $C_{14}H_{12}N_2O$: C, 74.98; H, 5.39; N, 12.49; Found: C, 74.82; H, 5.38; N, 12.47.

1-(3-(5-Methylbenzo[*d*]oxazol-2-yl)phenyl)-3-phenylurea (BO_4): The compound was synthesized according to above general procedure using 3-(5-methylbenzo[*d*]oxazol-2-yl)aniline (1.5 g, 6.69 mmol), DIPEA (1. 8 g, 12.62 mmol) and isocyanatobenzene (1.2 g, 10.05 mmol) to

yield 1-(3-(5-methylbenzo[*d*]xazol-2-yl)phenyl)-3-phenylurea (1.8 g, 77.1%) as grey solid. Mp: 240-242 ^{o}C. ^{1}H NMR (400 MHz, $CDCl_3$): δ 10.87 (s, 2H), 8.31 (s, 1H), 7.92 (d, J = 7.6 Hz, 1H), 7.84–7.72 (m, 4H), 7.63 (d, J = 7.2 Hz, 2H), 7.58–7.49 (m, 4H), 2.39 (s, 3H); ^{13}C NMR (100 MHz, $CDCl_3$): δ 174.6, 160.2, 144.9, 141.4, 140.6, 135.2, 135.0, 133.3, 132.4 (2C), 130.8, 129.4, 127.8 (2C), 125.9, 125.6, 125.2, 124.6, 120.3, 116.3, 22.9. MS(ESI) *m/z* 344.2 $[M+H]^+$. Anal calcd for $C_{21}H_{17}N_3O_2$: C, 73.45; H, 4.99; N, 12.24% Found C, 73.58; H, 4.98; N, 12.26%.

1-(4-Chlorophenyl)-3-(3-(5-methylbenzo[*d*]oxazol-2-yl)phenyl)urea (BO_5)*:* The compound was synthesized according to above general procedure using 3-(5-methylbenzo[*d*]oxazol-2-yl)aniline (1.5 g, 6.69 mmol), DIPEA (1.8 g, 12.62 mmol) and 1-chloro-4-isocyanatobenzene (1.3 g, 8.51 mmol) to yield 1-(4-chlorophenyl)-3-(3-(5-methylbenzo[*d*]oxazol-2-yl)phenyl)urea (1.9 g, 73.7%) as white solid. M.p:181-183 ^{o}C. ^{1}H NMR (400 MHz, DMSO-d_6): δ 9.34 (s, 2H), 8.52 (s, 1H), 7.85 (d, J = 8.0 Hz, 1H), 7.8 (d, J = 8.4 Hz, 1H), 7.75 (t, J = 8.0 Hz, 1H), 7.71–7.62 (m, 5H), 7.43 (d, J = 8.0 Hz, 2H), 3.82 (s, 3H); ^{13}C NMR (100 MHz, DMSO-d_6): δ 176.3, 163.3, 154.3, 146.4, 139.6, 137.5, 135.6, 134.8, 133.2, 132.0 (2C), 131.8, 131.3, 129.9 (2C), 128.6, 127.4, 126.0, 120.4, 113.8, 60.4, 23.2. MS(ESI) *m/z* 379.6 $[M+H]^+$. Anal calcd for $C_{21}H_{16}ClN_3O_2$: C, 70.76; H, 5.13; N, 11.25 Found C, 70.88; H, 5.14; N, 11.23.

1-(3-(Benzo[*d*]oxazol-2-yl)phenyl)-3-(4-methoxyphenyl)urea (**BO_6):** The compound was synthesized according to above general procedure using 3-(benzo[*d*]oxazol-2-yl)aniline (1.3 g, 6.19 mmol), DIPEA (1.8 g, 12.62 mmol) and 1-isocyanato-4-methoxybenzene (1.2 g, 8.02 mmol) to yield 1-(3-(benzo[*d*]oxazol-2-yl)phenyl)-3-(4-methoxyphenyl)urea (1.9 g, 86.4%) as grey solid. M.p:228-230 ^{o}C. ^{1}H NMR (400 MHz, DMSO-d_6): δ 10.25 (s, 2H), 8.40 (s, 1H), 7.89 (d, J = 8.0 Hz, 2H), 7.76–7.63 (m, 3H), 7.56–7.48 (m, 4H), 7.18 (t, J = 7.6 Hz, 2H), 3.96 (s, 3H); ^{13}C NMR (100 MHz, DMSO-d_6): δ 172.4, 162.4, 150.2, 145.8, 141.3, 138.2, 136.4, 135.1, 134.6, 134.1 (2C), 133.2, 131.4, 128.2 (2C), 126.4 (2C), 125.3, 124.2, 119.4, 114.6. MS(ESI) *m/z* 360.2 $[M+H]^+$. Anal calcd for $C_{21}H_{17}N_3O_3$: C, 70.18; H, 4.77; N, 11.69 Found C, 70.28; H, 4.76; N, 11.66.

1-(3-(Benzo[*d*]oxazol-2-yl)phenyl)-3-(4-nitrophenyl)urea (BO_7): The compound was synthesized according to above general procedure using 3-(benzo[*d*]oxazol-2-yl)aniline (1.3 g, 6.19 mmol), DIPEA (1.8 g, 12.62 mmol) and 1-isocyanato-4-nitrobenzene (1.3 g, 7.98 mmol) to yield 1-(3-(benzo[*d*]oxazol-2-yl)phenyl)-3-(4-nitrophenyl)urea (1.9 g, 84.1%) as yellow solid. M.p:250-252 ^{o}C. ^{1}H NMR (400 MHz, DMSO-d_6): δ 10.08 (s, 2H), 8.45 (s, 1H), 8.19 (d, J = 8.4

Hz, 2H), 7.94 (d, *J* = 8.0 Hz, 2H), 7.88 (d, *J* = 7.6 Hz, 1H), 7.82 (d, *J* = 8.0 Hz, 2H), 7.78–7.71 (m, 3H), 7.69 (t, *J* = 7.6 Hz, 1H); ^{13}C NMR (100 MHz, DMSO-d_6): δ 167.4, 156.3, 152.3, 146.6, 143.5, 139.3, 136.4, 134.8 (2C), 133.2, 132.8 (2C), 131.2, 130.5, 130.0, 128.4, 126.2, 125.9, 120.9, 116.7. MS(ESI) *m/z* 375.3 $[M+H]^+$. Anal calcd for $C_{20}H_{14}N_4O_4$: C, 64.17; H, 3.77; N, 14.97 Found C, 64.28; H, 3.78; N, 14.95.

1-(3-(Benzo[*d*]oxazol-2-yl)phenyl)-3-benzylurea (BO_8): The compound was synthesized according to above general procedure using 3-(benzo[*d*]oxazol-2-yl)aniline (1.3 g, 6.19 mmol), DIPEA (1.8 g, 12.62 mmol) and (isocyanatomethyl)benzene (1.1 g, 9.6 mmol) to yield 1-(3-(benzo[*d*]oxazol-2-yl)phenyl)-3-benzylurea (2.0 g, 88.5%) as brown solid. M.p:243-245 ^{o}C. ^{1}H NMR (400 MHz, $CDCl_3$): δ 10.27 (s, 2H), 8.48 (s, 1H), 7.94 (d, *J* = 8.0 Hz, 1H), 7.88 (t, *J* = 7.6 Hz, 2H), 7.72 (d, *J* = 7.6 Hz, 1H), 7.68–7.56 (m, 3H), 7.42–7.26 (m, 5H), 5.08 (s, 2H); ^{13}C NMR (100 MHz, $CDCl_3$): δ 183.9, 163.4, 154.3, 144.3, 142.4, 137.9, 135.6, 135.1, 134.3 (2C), 129.4, 128.7 (2C), 127.1, 126.2, 125.4, 125.0, 124.3, 120.4, 113.8, 62.6. MS(ESI) *m/z* 360.4 $[M+H]^+$. Anal calcd for $C_{21}H_{17}N_3O_2$: C, 73.45; H, 4.99; N, 12.24 Found C, 73.52; H, 4.98; N, 12.21.

1-(4-Methoxyphenyl)-3-(3-(5-methylbenzo[*d*]oxazol-2-yl)phenyl)urea (BO_9): The compound was synthesized according to above general procedure using 3-(5-methylbenzo[*d*]oxazol-2-yl)aniline (1.5 g, 6.69 mmol), DIPEA (1.8 g, 12.62 mmol) and 1-isocyanato-4-methoxybenzene (1.5 g, 9.1 mmol) to yield 1-(4-methoxyphenyl)-3-(3-(5-methylbenzo[*d*]oxazol-2-yl)phenyl)urea (2.1 g, 87.2%) as grey solid. M.p:228-230 ^{o}C. ^{1}H NMR (400 MHz, DMSO-d_6): δ 9.25 (s, 2H), 8.44 (s, 1H), 7.81 (d, *J* = 8.0 Hz, 1H), 7.77 (d, *J* = 8.4 Hz, 1H), 7.72 (t, *J* = 8.0 Hz, 1H), 7.67–7.60 (m, 5H), 7.21 (d, *J* = 7.6 Hz, 2H), 3.94 (s, 3H), 2.46 (s, 3H); ^{13}C NMR (100 MHz, DMSO-d_6): δ 176.3, 163.3, 154.3, 146.4, 139.6, 137.5, 135.6, 134.8, 133.2, 132.0 (2C), 131.8, 131.3, 129.9 (2C), 128.6, 127.4, 126.0, 120.4, 113.8, 60.4, 23.2. MS(ESI) *m/z* 374.5 $[M+H]^+$. Anal calcd for $C_{22}H_{19}N_3O_3$: C, 70.76; H, 5.13; N, 11.25 Found C, 70.88; H, 5.14; N, 11.28.

1-(3-(Benzo[*d*]oxazol-2-yl)phenyl)-3-(4-chlorophenyl)urea (**BO_10**): The compound was synthesized according to above general procedure using 3-(benzo[*d*]oxazol-2-yl)aniline (1.3 g, 6.19 mmol), DIPEA (1.8 g, 12.62 mmol) and 1-chloro-4-isocyanatobenzene (1.3 g, 8.51 mmol) to yield 1-(3-(benzo[*d*]oxazol-2-yl)phenyl)-3-(4-chlorophenyl)urea (1.9 g, 85.1%) as white solid. M.p:175-177 ^{o}C. ^{1}H NMR (400 MHz, $CDCl_3$): δ 10.29 (s, 2H), 8.46 (s, 1H), 7.94 (t, *J* = 8.0 Hz, 2H), 7.82 (d, *J* = 7.6 Hz, 1H), 7.76 (t, *J* = 8.0 Hz, 1H), 7.69–7.60 (m, 3H), 7.56 (d, *J* = 7.6 Hz,

2H), 7.44 (d, *J* = 8.0 Hz, 2H); ^{13}C NMR (100 MHz, $CDCl_3$): *δ* 174.4, 160.5, 148.7, 144.9, 137.5, 136.4, 135.3, 134.9, 134.3, 133.2(2C), 132.7, 131.6, 130.2 (2C), 127.3, 125.2 (2C), 120.6, 117.0. MS(ESI) *m/z* 364.1 $[M+H]^+$. Anal calcd for $C_{20}H_{14}ClN_3O_2$: C, 66.03; H, 3.88; N, 11.55 Found C, 66.18; H, 3.89; N, 11.53.

1-(4-Fluorophenyl)-3-(3-(5-methylbenzo[*d*]oxazol-2-yl)phenyl)urea (BO_11): The compound was synthesized according to above general procedure using 3-(5-methylbenzo[*d*]oxazol-2-yl)aniline (1.5 g, 6.69 mmol), DIPEA (1.8 g, 12.62 mmol) and 1-fluoro-4-isocyanatobenzene (1.2g, 9.2 mmol) to yield 1-(4-fluorophenyl)-3-(3-(5-methylbenzo[*d*]oxazol-2-yl)phenyl)urea (2.0 g, 88.2%) as pale brown solid. M.p:169-171 ^{o}C. ^{1}H NMR (400 MHz, DMSO-d_6): *δ* 10.71 (s, 2H), 8.46 (s, 1H), 7.87 (d, *J* = 8.0 Hz, 1H), 7.74–7.62 (m, 3H), 7.56 (d, *J* = 7.6 Hz, 1H), 7.54–7.46 (m, 3H), 7.36 (d, *J* = 8.0 Hz, 2H), 2.43 (s, 3H); ^{13}C NMR (100 MHz, DMSO-d_6): *δ* 174.3, 160.4, 144.7, 143.4, 139.6, 137.3, 136.2, 134.6, 133.0, 132.6 (2C), 131.8, 128.5, 127.4 (2C), 126.8, 125.2, 123.9, 120.8, 116.9, 22.4. MS(ESI) *m/z* 362.3 $[M+H]^+$. Anal calcd for $C_{21}H_{16}FN_3O_2$: C, 69.80; H, 4.46; N, 11.63 Found C, 69.88; H, 4.45; N, 11.65.

1-(3-(Benzo[*d*]oxazol-2-yl)phenyl)-3-phenylurea (BO_12): The compound was synthesized according to above general procedure using 3-(benzo[*d*]oxazol-2-yl)aniline (1.3 g, 6.19 mmol), DIPEA (1.8 g, 12.62 mmol) and isocyanatobenzene (1.2 g, 10.05 mmol) to yield 1-(3-(benzo[*d*]oxazol-2-yl)phenyl)-3-phenylurea (1.7 g, 83.2%) as grey solid. M.p:210-212 ^{o}C. ^{1}H NMR (400 MHz, DMSO-d_6): *δ* 10.26 (s, 2H), 8.46 (s, 1H), 7.96 (d, *J* = 8.0 Hz, 1H), 7.84 (t, *J* = 8.0 Hz, 2H), 7.72 (d, *J* = 7.6 Hz, 1H), 7.63–7.56 (m, 3H), 7.48–7.36 (m, 4H), 7.22 (t, *J* = 8.0 Hz, 1H); ^{13}C NMR (100 MHz, DMSO-d_6): *δ* 176.4, 162.9, 154.2, 144.7, 142.6, 142.4, 138.5, 137.6, 136.0, 133.9(2C), 133.0, 130.6, 128.3, 127.8(2C), 126.3, 120.3, 119.3, 115.9. MS(ESI) *m/z* 330.1 $[M+H]^+$. Anal calcd for $C_{20}H_{15}N_3O_2$: C, 72.94; H, 4.59; N, 12.76 Found C, 72.81; H, 4.58; N, 12.78.

1-(3-(Benzo[*d*]oxazol-2-yl)phenyl)-3-(4-fluorophenyl)urea (BO_13): The compound was synthesized according to above general procedure using 3-(benzo[*d*]oxazol-2-yl)aniline (1.3 g, 6.19 mmol), DIPEA (1.8 g, 12.62 mmol) and fluoro-4-isocyanatobenzene (1.0 g, 8.7 mmol) to yield 1-(3-(benzo[*d*]oxazol-2-yl)phenyl)-3-(4-fluorophenyl)urea (1.8 g, 81.3%) as grey solid. M.p:180-182 ^{o}C. ^{1}H NMR (400 MHz, DMSO-d_6): *δ* 9.00 (s, 1H), 8.73 (s, 1H), 8.12 (s, 1H), 8.84–8.73 (m, 3H), 7.54–7.36 (m, 6H), 7.12 (t, *J* = 8.0 Hz, 2H); ^{13}C NMR (100 MHz, DMSO-

d_6): δ 178.6,156.8, 152.1, 144.2, 143.1, 136.5, 131.2, 127.9, 127.4, 126.1, 123.1, 122.7, 122.4 (3C), 120.5, 115.4, 113.2 (3C), 111.2 . MS(ESI) *m/z* 348.7 $[M+H]^+$. Anal calcd for $C_{20}H_{14}FN_3O_2$: C, 69.16; H, 4.06; N, 12.10 Found C, 69.24; H, 4.07; N, 12.08.

1-(3-(Benzo[*d*]oxazol-2-yl)phenyl)-3-(*p*-tolyl)urea (BO_14): The compound was synthesized according to above general procedure using 3-(benzo[*d*]oxazol-2-yl)aniline (1.3 g, 6.19 mmol), DIPEA (1.8 g, 12.62 mmol) and 1-isocyanato-4-methylbenzene (1.2 g, 9.0 mmol) to yield 1-(3-(benzo[*d*]oxazol-2-yl)phenyl)-3-(*p*-tolyl)urea (1.9 g, 88.5%) as white solid. M.p:164-166 ^oC. ^1H NMR (400 MHz, DMSO-d_6): δ 9.21 (s, 2H), 8.41 (s, 1H), 7.89 (d, *J* = 8.0 Hz, 1H), 7.81–7.72 (m, 2H), 7.67–7.56 (m, 3H), 7.54–7.45 (m, 3H), 7.33 (t, *J* = 8.0 Hz, 2H), 2.46 (s, 3H); ^{13}C NMR (100 MHz, DMSO-d_6): δ 174.6, 162.6, 154.0, 146.5, 136.4, 135.3, 134.8, 134.0, 133.4, 132.3 (2C), 130.5, 129.4, 128.2 (2C), 126.8, 126.4, 124.5, 121.3, 117.4, 22.6. MS(ESI) *m/z* 344.2 $[M+H]^+$. Anal calcd for $C_{21}H_{17}N_3O_2$: C, 73.45; H, 4.99; N, 12.24 Found C, 73.56; H, 4.98; N, 12.26.

1-(3-(Benzo[*d*]oxazol-2-yl)phenyl)-3-isopropylurea (BO_15): The compound was synthesized according to above general procedure using 3-(benzo[*d*]oxazol-2-yl)aniline (1.3 g, 6.19 mmol), DIPEA (1.8 g, 12.62 mmol) and 2-isocyanatopropane (0.7 g, 8.2 mmol) to yield 1-(3-(benzo[*d*]oxazol-2-yl)phenyl)-3-isopropylurea (1.5 g, 78.5%) as pale red solid. M.p:174-176 ^oC. ^1H NMR (400 MHz, DMSO-d_6): δ 10.17 (s, 1H), 9.43 (s, 1H), 8.36 (s, 1H), 7.84 (d, *J* = 8.0 Hz, 1H), 7.74 (d, *J* = 8.4 Hz, 2H), 7.67–7.56 (m, 3H), 7.36 (t, *J* = 8.0 Hz, 1H), 3.85–3.81 (m, 1H), 1.33 (d, *J* = 8.8 Hz, 6H); ^{13}C NMR (100 MHz, DMSO-d_6): δ 171.9, 160.2, 154.4, 143.4, 136.4, 135.3, 135.0, 133.3, 129.3, 127.6, 126.1, 125.4, 118.6, 115.3, 54.6, 24.6 (2C). MS(ESI) *m/z* 296.7 $[M+H]^+$. Anal calcd for $C_{17}H_{17}N_3O_2$: C, 69.14; H, 5.80; N, 14.23 Found C, 69.26; H, 5.81; N, 14.25.

1-(3-(Benzo[*d*]oxazol-2-yl)phenyl)-3-benzylthiourea (BO_16): The compound was synthesized according to above general procedure using 3-(benzo[*d*]oxazol-2-yl)aniline (1.3 g, 6.19 mmol), K_2CO_3 (2.0 g, 14.1 mmol) and (isothiocyanatomethyl)benzene (1.2 g, 8.0 mmol) in DMF: xylene (4:1) to get 1-(3-(Benzo[*d*]oxazol-2-yl)phenyl)-3-benzylthiourea (1.9 g, 84.6%) as pale grey solid. M.p:210-212 ^oC. ^1H NMR (400 MHz, DMSO-d_6): δ 9.27 (s, 1H), 9.01 (s, 1H), 8.44 (s, 1H), 7.92 (d, *J* = 8.0 Hz, 1H), 7.82 (t, *J* = 7.6 Hz, 2H), 7.68 (d, *J* = 8.0 Hz, 1H), 7.62 (t, *J* = 7.6 Hz, 1H), 7.58 (d, *J* = 8.4 Hz, 2H), 7.42–7.31 (m, 4H), 7.12 (t, *J* = 7.2 Hz, 1H), 5.04 (s, 2H); ^{13}C NMR (100 MHz, DMSO-d_6): δ 180.9, 166.8, 156.1, 144.3, 138.3, 136.2,

134.5, 134.0, 133.2 (2C), 128.3, 127.4 (2C), 125.3 (2C), 125.1, 124.7, 123.6, 117.3, 112.5, 62.4. MS(ESI) *m/z* 360.5 $[M+H]^+$. Anal calcd for $C_{21}H_{17}N_3OS$: C, 70.17; H, 4.77; N, 11.69%Found C, 70.28; H, 4.76; N, 11.71.

1-(4-Fluorophenyl)-3-(3-(5-methylbenzo[*d*]oxazol-2-yl)phenyl)thiourea (BO_17): The compound was synthesized according to above general procedure using 3-(5-methylbenzo[*d*]oxazol-2-yl)aniline (1.5 g, 6.69 mmol), K_2CO_3 (2.0 g, 14.1 mmol) and 1-fluoro-4-isothiocyanatobenzene (1.2 g, 7.8 mmol) in DMF: xylene (4:1) to get 1-(4-Fluorophenyl)-3-(3-(5-methylbenzo[*d*]oxazol-2-yl)phenyl)thiourea (2.1 g, 81.8%) as white solid. M.p:235-237 ^oC. ^1H NMR (400 MHz, DMSO-d_6): δ 10.27 (s, 2H), 8.49 (s, 1H), 7.84–7.74 (m, 3H), 7.62–7.44 (m, 5H), 7.09 (t, *J* = 7.6 Hz, 2H), 2.42 (s, 3H); ^{13}C NMR (100 MHz, DMSO-d_6): δ 182.4, 164.5, 160.2, 146.1, 142.3, 138.5, 135.6, 133.2, 131.4 (2C), 130.9, 130.2, 128.2, 126.9, 125.6 (2C), 124.3, 123.1, 118.4, 113.6, 22.5. MS(ESI) m/z 378.4 $[M+H]^+$. Anal calcd for $C_{21}H_{16}FN_3OS$: C, 66.83; H, 4.27; F, 5.03; N, 11.13 Found C, 66.90; H, 4.28; N, 11.15.

1-(3-(Benzo[*d*]oxazol-2-yl)phenyl)-3-(4-nitrophenyl)thiourea (BO_18): The compound was synthesized according to above general procedure using 3-(5-methylbenzo[*d*]oxazol-2-yl)aniline (1.5 g, 6.69 mmol), K_2CO_3 (2.0 g, 14.1 mmol) and 1-isothiocyanato-4-nitrobenzene (1.2 g, 8.0 mmol) in DMF: xylene (4:1) to get 1-(3-(benzo[*d*]oxazol-2-yl)phenyl)-3-(4-nitrophenyl)thiourea (2.1 g, 85.2%) as yellow solid. M.p:236-238 ^oC. ^1H NMR (400 MHz, DMSO-d_6): δ 10.07 (s, 2H), 8.48 (s, 1H), 8.05 (d, *J* = 8.0 Hz, 2H), 7.92 (d, *J* = 7.6 Hz, 1H), 7.84 (t, *J* = 7.6 Hz, 2H), 7.65–7.58 (m, 3H), 7.48 (d, *J* = 8.0 Hz, 2H), 7.12 (t, *J* = 8.0 Hz, 1H); ^{13}C NMR (100 MHz, DMSO-d_6): δ 181.6, 163.4, 153.4, 143.8, 141.3, 139.3, 136.3, 134.5, 133.2, 132.9 (2C), 130.4, 129.4, 128.6 (2C), 127.2 (2C), 125.3, 118.6, 116.1. MS(ESI) *m/z* 391.1$[M+H]^+$. Anal calcd for $C_{20}H_{14}N_4O_3S$: C, 61.53; H, 3.61; N, 14.35 Found C, 61.58; H, 3.60; N, 14.37.

1-(3-(Benzo[*d*]oxazol-2-yl)phenyl)-3-(4-fluorophenyl)thiourea (BO_19): The compound was synthesized according to above general procedure using 3-(benzo[*d*]oxazol-2-yl)aniline (1.3 g, 6.19 mmol), K_2CO_3 (2.0 g, 14.1 mmol) and 1-fluoro-4-isothiocyanatobenzene (1.2 g, 7.6 mmol) in DMF: xylene (4:1) to get 1-(3-(benzo[*d*]oxazol-2-yl)phenyl)-3-(4-fluorophenyl)thiourea (1.9 g, 84.8%) as pale red solid. M.p:235-237 ^oC. ^1H NMR (400 MHz, DMSO-d_6): δ 9.67 (s, 1H), 9.21 (s, 1H), 8.46 (s, 1H), 7.94 (d, *J* = 8.0 Hz, 2H), 7.89 (d, *J* = 7.6 Hz, 1H), 7.72–7.58 (m, 4H), 7.24 (d, *J* = 8.0 Hz, 2H), 7.12 (d, *J* = 7.6 Hz, 2H); ^{13}C NMR (100

MHz, DMSO-d_6): δ 182.8, 164.2, 156.8, 144.4, 140.4, 138.2, 135.6, 133.9, 133.3, 132.3 (2C), 130.2, 129.4, 128.2, 127.3 (2C), 125.5, 124.2, 119.3, 115.2. MS(ESI) *m/z* 364.8 $[M+H]^+$. Anal calcd for $C_{20}H_{14}FN_3OS$: C, 66.10; H, 3.88; N, 11.56 Found C, 66.18; H, 3.87; N, 11.59.

1-(3-(5-Methylbenzo[*d*]oxazol-2-yl)phenyl)-3-(4-nitrophenyl)thiourea (BO_20): The compound was synthesized according to above general procedure using 3-(5-methylbenzo[*d*]oxazol-2-yl)aniline (1.5 g, 6.69 mmol), K_2CO_3 (2.0 g, 14.1 mmol) and 1-isothiocyanato-4-nitrobenzene (1.1 g, 7.5 mmol) in DMF: xylene (4:1) to get 1-(3-(5-methylbenzo[*d*]oxazol-2-yl)phenyl)-3-(4-nitrophenyl)thiourea (2.2 g, 81.1%) as pale yellow solid. M.p:241-243 ^oC. ^1H NMR (400 MHz, DMSO-d_6): δ 9.47 (s, 1H), 9.03 (s, 1H), 8.41 (s, 1H), 8.09 (d, *J* = 8.0 Hz, 2H), 7.89 (d, *J* = 7.6 Hz, 1H), 7.87–7.74 (m, 3H), 7.69–7.56 (m, 2H), 7.36 (d, *J* = 8.0 Hz, 2H), 2.40 (s, 3H); ^{13}C NMR (100 MHz, DMSO-d_6): δ 182.9, 161.9, 150.3, 144.6, 142.0, 138.4, 136.0, 133.9, 133.2, 132.6(2C), 131.4, 128.9, 128.2(2C), 127.6, 126.5, 124.1, 117.9, 114.3, 21.9. MS(ESI) *m/z* 405.4 $[M+H]^+$. Anal calcd for $C_{21}H_{16}N_4O_3S$: C, 62.36; H, 3.99; N, 13.85 Found C, 62.48; H, 3.98; N, 13.87.

1-(3-(5-Methylbenzo[*d*]oxazol-2-yl)phenyl)-3-phenylthiourea (BO_21): The compound was synthesized according to above general procedure using 3-(5-methylbenzo[*d*]oxazol-2-yl)aniline (1.5 g, 6.69 mmol), K_2CO_3 (2.0 g, 14.1 mmol) and isothiocyanatobenzene (1.0 g, 7.4 mmol) in DMF: xylene (4:1) to get 1-(3-(5-methylbenzo[*d*]oxazol-2-yl)phenyl)-3-phenylthiourea (1.9 g, 79.9%) as grey solid. M.p:155-157 ^oC. ^1H NMR (400 MHz, DMSO-d_6): δ 10.26 (s, 2H), 8.41 (s, 1H), 7.94 (d, *J* = 8.0 Hz, 1H), 7.84–7.76 (m, 3H), 7.62 (d, *J* = 7.2 Hz, 2H), 7.46–7.35 (m, 3H), 7.22 (d, *J* = 7.6 Hz, 2H), 2.44 (s, 3H); ^{13}C NMR (100 MHz, DMSO-d_6): δ 183.5, 164.6, 148.3, 143.2, 137.4, 135.9, 135.0, 134.2, 133.8 (2C), 130.4, 128.6, 128.2, 126.2 (2C), 125.4, 124.3, 123.9, 118.2, 113.7, 22.3. MS(ESI) *m/z* 360.2 $[M+H]^+$. Anal calcd for $C_{21}H_{17}N_3OS$: C, 70.17; H, 4.77; N, 11.69% Found C, 70.28; H, 4.76; N, 11.67%.

1-(4-Chlorophenyl)-3-(3-(5-methylbenzo[*d*]oxazol-2-yl)phenyl)thiourea (BO_22): The compound was synthesized according to above general procedure using 3-(5-methylbenzo[*d*]oxazol-2-yl)aniline (1.5 g, 6.69 mmol), K_2CO_3 (2.0 g, 14.1 mmol) and 1-chloro-4-isothiocyanatobenzene (1.3 g, 7.6 mmol) in DMF: xylene (4:1) to get 1-(4-chlorophenyl)-3-(3-(5-methylbenzo[*d*]oxazol-2-yl)phenyl)thiourea (2.1 g, 80.3%) as white solid. M.p:190-192 ^oC. ^1H NMR (400 MHz, DMSO-d_6): δ 10.45 (s, 2H), 8.48 (s, 1H), 7.96 (s, 1H), 7.89 (t, *J* = 8.0 Hz, 1H), 7.76 (d, *J* = 7.6 Hz, 1H), 7.56–7.48 (m, 4H), 7.26 (d, *J* = 7.6 Hz,

2H), 7.18 (t, *J* = 7.6 Hz, 1H), 2.41 (s, 3H); ^{13}C NMR (100 MHz, DMSO-d_6): δ 182.9, 163.9, 149.2, 143.6, 136.8, 135.4, 134.5, 133.2, 132.4 (2C), 129.5, 127.8 (2C), 127.2, 126.5, 125.3, 124.6, 124.2, 120.3, 116.4, 22.6. MS(ESI) *m/z* 394.2 $[M+H]^+$. Anal calcd for $C_{21}H_{16}ClN_3OS$: C, 64.03; H, 4.09; N, 10.67 Found C, 64.11; H, 4.10; N, 10.65.

1-Benzyl-3-(3-(5-methylbenzo[*d*]oxazol-2-yl)phenyl)thiourea (BO_23): The compound was synthesized according to above general procedure using 3-(5-methylbenzo[*d*]oxazol-2-yl)aniline (1.5 g, 6.69 mmol), K_2CO_3 (2.0 g, 14.1 mmol) and (isothiocyanatomethyl)benzene (1.2 g, 7.9 mmol) in DMF: xylene (4:1) to get 1-benzyl-3-(3-(5-methylbenzo[*d*]oxazol-2-yl)phenyl)thiourea (2.0 g, 79.6%) as grey solid. M.p:209-211 ^{o}C. ^{1}H NMR (400 MHz, DMSO-d_6): δ 9.46 (s, 1H), 9.21 (s, 1H), 8.34 (s, 1H), 8.21 (s, 1H), 7.83–7.74 (m, 3H), 7.63–7.48 (m, 2H), 7.31–7.24 (m, 5H), 5.01 (s, 2H), 2.43 (s, 3H); ^{13}C NMR (100 MHz, DMSO-d_6): δ 180.2, 163.7, 146.9, 142.3, 138.6, 134.7, 134.4, 133.8, 133.2(2C), 131.4, 127.6, 126.4, 125.9(2C), 125.3, 124.5, 123.6, 123.0, 119.6, 54.6, 23.1. MS(ESI) *m/z* 374.5 $[M+H]^+$. Anal calcd for $C_{22}H_{19}N_3OS$: C, 70.75; H, 5.13; N, 11.25 Found C, 70.88; H, 5.12; N, 11.27.

1-(3-(5-Methylbenzo[*d*]oxazol-2-yl)phenyl)-3-(*p*-tolyl)thiourea (BO_24): The compound was synthesized according to above general procedure using 3-(5-methylbenzo[*d*]oxazol-2-yl)aniline (1.5 g, 6.69 mmol), K_2CO_3 (2.0 g, 14.1 mmol) and 1-isothiocyanato-4-methylbenzene (1.2 g, 7.9 mmol) in DMF: xylene (4:1) to get 1-(3-(5-methylbenzo[*d*]oxazol-2-yl)phenyl)-3-(*p*-tolyl)thiourea (2.1 g, 83.6%) as pale brown solid. M.p:231-233 ^{o}C. ^{1}H NMR (400 MHz, DMSO-d_6): δ 9.63 (s, 2H), 8.36 (s, 1H), 7.96 (d, *J* = 8.0 Hz, 1H), 7.89 (d, *J* = 7.6 Hz, 2H), 7.76 (d, *J* = 8.0 Hz, 1H), 7.64–7.56 (m, 3H), 7.26 (d, *J* = 8.0 Hz, 2H), 7.18 (d, *J* = 8.0 Hz, 1H), 2.44 (s, 3H), 2.41 (s, 3H); ^{13}C NMR (100 MHz, DMSO-d_6): δ 179.7, 162.4, 146.4, 144.4, 140.8, 138.6, 135.7, 135.3, 134.0, 133.9 (2C), 131.4, 130.5, 129.3 (2C), 127.5 (2C), 124.8, 117.4, 115.2, 23.4, 22.5. MS(ESI) *m/z* 374.8 $[M+H]^+$. Anal calcd for $C_{22}H_{19}N_3OS$: C, 70.75; H, 5.13; N, 11.25 Found C, 70.83; H, 5.12; N, 11.23.

1-(3-(Benzo[*d*]oxazol-2-yl)phenyl)-3-(4-chlorophenyl)thiourea (BO_25): The compound was synthesized according to above general procedure using 3-(benzo[*d*]oxazol-2-yl)aniline (1.3 g, 6.19 mmol), K_2CO_3 (2.0 g, 14.1 mmol) and 1-chloro-4-isothiocyanatobenzene (1.3 g, 7.7 mmol) in DMF: xylene (4:1) to get 1-(3-(benzo[*d*]oxazol-2-yl)phenyl)-3-(4-chlorophenyl)thiourea (1.9 g, 81.1%) as white solid. M.p:230-232 ^{o}C. ^{1}H NMR (400 MHz, DMSO-d_6): δ 10.23 (s, 2H), 8.39 (s, 1H), 7.90 (t, *J* = 8.0 Hz, 2H), 7.81 (d, *J* = 7.6 Hz, 2H), 7.56

(d, *J* = 8.0 Hz, 1H), 7.48 (d, *J* = 7.6 Hz, 1H), 7.36 (d, *J* = 8.0 Hz, 2H), 7.21–7.12 (m, 3H); ^{13}C NMR (100 MHz, DMSO-d_6): δ 182.7, 163.5, 144.7, 142.5, 139.8, 137.5, 134.8, 134.3, 134.1, 133.4 (2C), 132.2, 131.4, 129.6 (2C), 128.1, 126.4 (2C), 118.6, 116.4. MS(ESI) *m/z* 380.8 $[M+H]^+$. Anal calcd for $C_{20}H_{14}ClN_3OS$: C, 63.24; H, 3.71; N, 11.06 Found C, 63.32; H, 3.70; N, 11.08.

1-(3-(Benzo[*d*]oxazol-2-yl)phenyl)-3-phenylthiourea (BO_26): The compound was synthesized according to above general procedure using 3-(benzo[*d*]oxazol-2-yl)aniline (1.3 g, 6.19 mmol), K_2CO_3 (2.0 g, 14.1 mmol) and isothiocyanatobenzene (1.1 g, 8.1 mmol) in DMF: xylene (4:1) to get 1-(3-(benzo[*d*]oxazol-2-yl)phenyl)-3-phenylthiourea (1.7 g, 82.3%) as white solid. M.p:182-184 ^{o}C. ^{1}H NMR (400 MHz, DMSO-d_6): δ 10.01 (s, 2H), 8.43 (s, 1H), 7.93 (d, *J* = 8.0 Hz, 1H), 7.81 (t, *J* = 7.6 Hz, 2H), 7.20 (d, *J* = 7.6 Hz, 1H), 7.54 (t, *J* = 8.0 Hz, 1H), 7.49 (d, *J* = 8.0 Hz, 2H), 7.45–7.30 (m, 4H), 7.15 (t, *J* = 8.0 Hz, 1H); ^{13}C NMR (100 MHz, DMSO-d_6): δ 179.8, 164.6, 152.3, 146.4, 143.4, 140.3, 131.2, 129.2 (2C), 128.3, 127.1, 126.3, 125.1, 124.6, 124.2 (2C), 123.8, 123.2, 120.4, 112.7. MS(ESI) *m/z* 346.4 $[M+H]^+$. Anal calcd for $C_{20}H_{15}N_3OS$: C, 69.54; H, 4.38; N, 12.17 Found C, 69.63; H, 4.37; N, 12.19.

1-(3-(Benzo[*d*]oxazol-2-yl)phenyl)-3-(*p*-tolyl)thiourea (BO_27): The compound was synthesized according to above general procedure using 3-(benzo[*d*]oxazol-2-yl)aniline (1.3 g, 6.19 mmol), K_2CO_3 (2.0 g, 14.1 mmol) and 1-isothiocyanato-4-methylbenzene (1.2 g, 7.9 mmol) in DMF: xylene (4:1) to get 1-(3-(benzo[*d*]oxazol-2-yl)phenyl)-3-(*p*-tolyl)thiourea (1.9 g, 81.7%) as pale brown solid. M.p:221-223 ^{o}C. ^{1}H NMR (400 MHz, DMSO-d_6): δ 10.21 (s, 2H), 8.37 (s, 1H), 7.87 (d, *J* = 8.0 Hz, 1H), 7.78–7.64 (m, 3H), 7.60–7.47 (m, 5H), 7.27 (t, *J* = 7.6 Hz, 2H), 2.43 (s, 3H); ^{13}C NMR (100 MHz, DMSO-d_6): δ 176.4, 163.3, 152.1, 144.7, 138.3, 138.0, 136.7, 136.1, 135.3, 133.3 (2C), 132.6, 132.0, 129.3 (2C), 127.2, 126.6, 125.3, 120.4, 116.8, 22.3. MS(ESI) *m/z* 360.1 $[M+H]^+$. Anal calcd for $C_{21}H_{17}N_3OS$: C, 70.17; H, 4.77; N, 11.69 Found C, 70.26; H, 4.76; N, 11.71.

5.2.2.5. Determination and classification of inhibitors by means of enzyme activity assay, molecular docking simulations and thermal shift analysis

A total of thirteen compounds have shown activity less than 25 µM, of which except two compounds rest were active below 10 µM concentration. The IC_{50} values of compounds were shown in **Table 5.9**. Compounds **BO_16, BO_19, BO_21** and **BO_22** have shown activity <5

μM. Most of the compounds showing good activity have thiourea substitution, out of twelve compounds belonging to thiourea group, nine have shown good activity. Most potent of the series, compound **BO_22** showed an IC_{50} of 1.1±0.52 μM which is less inhibitory concentration than lead compound (IC_{50} of 20.7±0.29 μM) by twenty times. The log dose response curve of most potent compound **BO_22** of series was shown in (**Figure 5.17**).

Table 5.9: Synthesized compounds represented with substitutions along with their biological activities

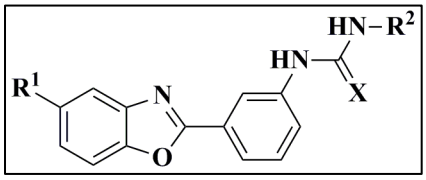

BO_4-27

Compound	X	R^1	R^2	GR IC_{50} (μM)	MIC (μM)			Cytotoxicity at 25μM (% Inhib.)
					Actual MIC	MIC in the presence of Verapamil	MIC in the presence of Piperine	
BO_4	O	CH_3	Phenyl	6.25±0.14	72.90	72.90	72.90	10.15
BO_5	O	CH_3	4-Chlorophenyl	>25	66.34	ND	ND	1.09
BO _6	O	H	4-Methoxyphenyl	7±0.46	69.35	69.35	69.35	17.26
BO _7	O	H	4-Nitrophenyl	>25	66.98	ND	ND	95.11
BO _8	O	H	Benzyl	>25	72.76	ND	ND	2.12
BO _9	O	CH_3	4-Methoxyphenyl	>25	67.89	ND	ND	11.09
BO _10	O	H	4-Chlorophenyl	>25	68.32	ND	ND	38.91
BO _11	O	CH_3	4-Fluorophenyl	>25	69.32	ND	ND	3.17
BO _12	O	H	Phenyl	>25	75.08	ND	ND	48.38
BO _13	O	H	4-Fluorophenyl	11.5±0.72	72.14	72.14	72.14	2.98
BO _14	O	H	4-Tolyl	8.5±0.83	36.24	36.24	36.24	1.09
BO _15	O	H	Isopropyl	>25	81.18	ND	ND	3.52
BO _16	S	H	Benzyl	1.82±0.52	69.24	2.21	2.21	47.21
BO _17	S	CH_3	4-Fluorophenyl	8.35±0.24	2.16	ND	ND	81.92
BO _18	S	H	4-Nitrophenyl	7.12±0.71	2.09	ND	ND	88.12

BO _19	S	H	4-Fluorophenyl	1.3±0.34	4.37	ND	ND	96.02
BO _20	S	CH_3	4-Nitrophenyl	22.8±0.42	61.89	1.91	1.91	98.1
BO _21	S	CH_3	Phenyl	4.4±0.21	69.61	8.69	8.69	87.32
BO _22	S	CH_3	4-Chlorophenyl	1.1±0.52	8.72	2.01	2.01	55.82
BO _23	S	CH_3	Benzyl	6.8±0.62	2.05	ND	ND	38.91
BO _24	S	CH_3	4-Tolyl	8.8±0.47	76.98	76.98	76.98	2.12
BO_25	S	H	4-Chlorophenyl	>25	63.89	ND	ND	22.81
BO _26	S	H	Phenyl	>25	19.32	ND	ND	96.23
BO _27	S	H	4-Tolyl	>25	69.51	ND	ND	99.14
Isoniazid				>25	0.78	0.78	0.78	ND
Ethambutol				>25	7.89	3.82	3.82	ND
Rifampicin				>25	0.21	0.21	0.21	ND

ND: Not determined

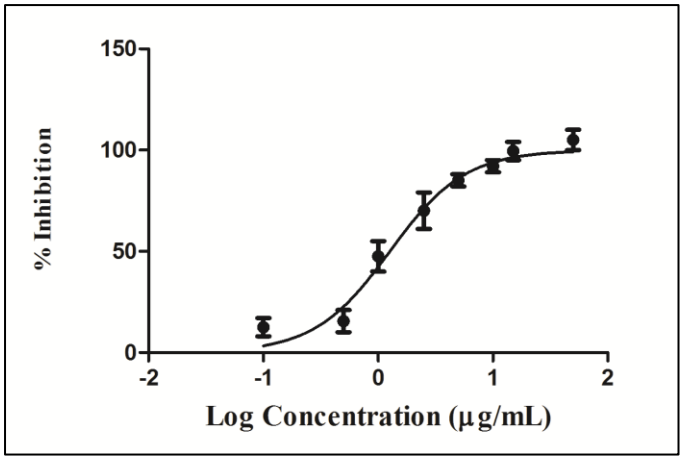

Figure 5.17: Log dose-response curve of compound **BO_22**

Although we have performed the inhibitory activity on Glutamate racemase of *B. subtilis* there is a requirement of further validation of results. Molecular docking is one technique which gives the all the possible interactions of the ligand with the protein and suggests the possibility of a compound to accept as an inhibitor. We performed docking analysis using Schrodinger software. We have selected substrate (D-glu) bound Glutamate racemase crystal structures of both organisms from protein data bank namely PDB ID: 5HJ7 (*M. tuberculosis*) and 1ZUW (*B. subtilis*), the protein alignment of both proteins has a root mean square deviation (rmsd) 1.33 Å.

We tried docking of energy minimized ligands into substrate binding site but was unsuccessful, hence we have tried docking in allosteric sites (assuming the inhibitors act through the allosteric site) generated using an in-built program called SiteMap. In the present study, five sites were identified in each crystal structures of proteins. Based on site-scores **site 1** in both the proteins was selected for further docking studies.

Compounds were docked into allosteric sites of both the crystal structures. We have superimposed both the proteins bound with ligand **BO_22** using superimposition module in Schrodinger shown in **Figure 5.18**. In this study, we have studied the docking orientation of most active compound **BO_22** in both the crystal structures. The binding orientation showed two H-bond interactions with allosteric residue Glu153 in both the crystal structures with NH moiety of compound (**Figure 5.19).** Along with previous interactions, the orientation was stabilized by hydrophobic and polar interactions. The compound was very well fit into the cavity of both proteins retaining similar kind of interaction with docking scores of -5.075 kcal/mol and -3.457 kcal/mol respectively in *B. subtilis* and *M. tuberculosis*. Hence we infer that there established a correlation of inhibitory activity of compound **BO_22** in both the organisms.

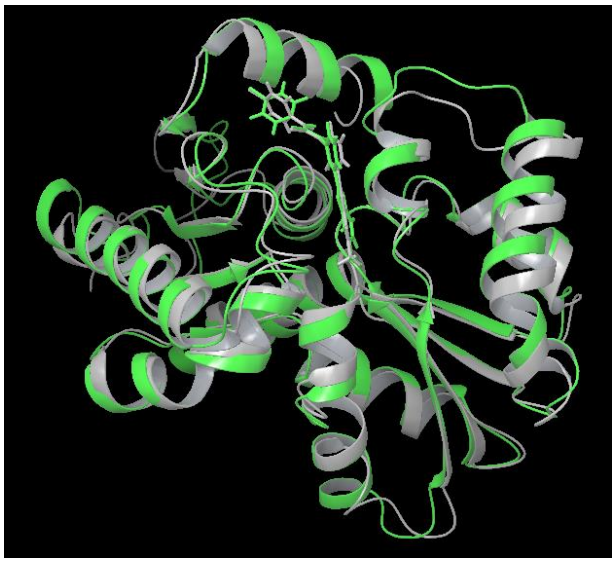

Figure 5.18: Docking pose of active molecule **BO_ 22** in **site 1** of *M. tuberculosis* (5HJ7) and *B. subtilis* (1ZUW) in superimposed view. Grey color represents protein and ligand in 5HJ7 whereas green represents 1ZUW.

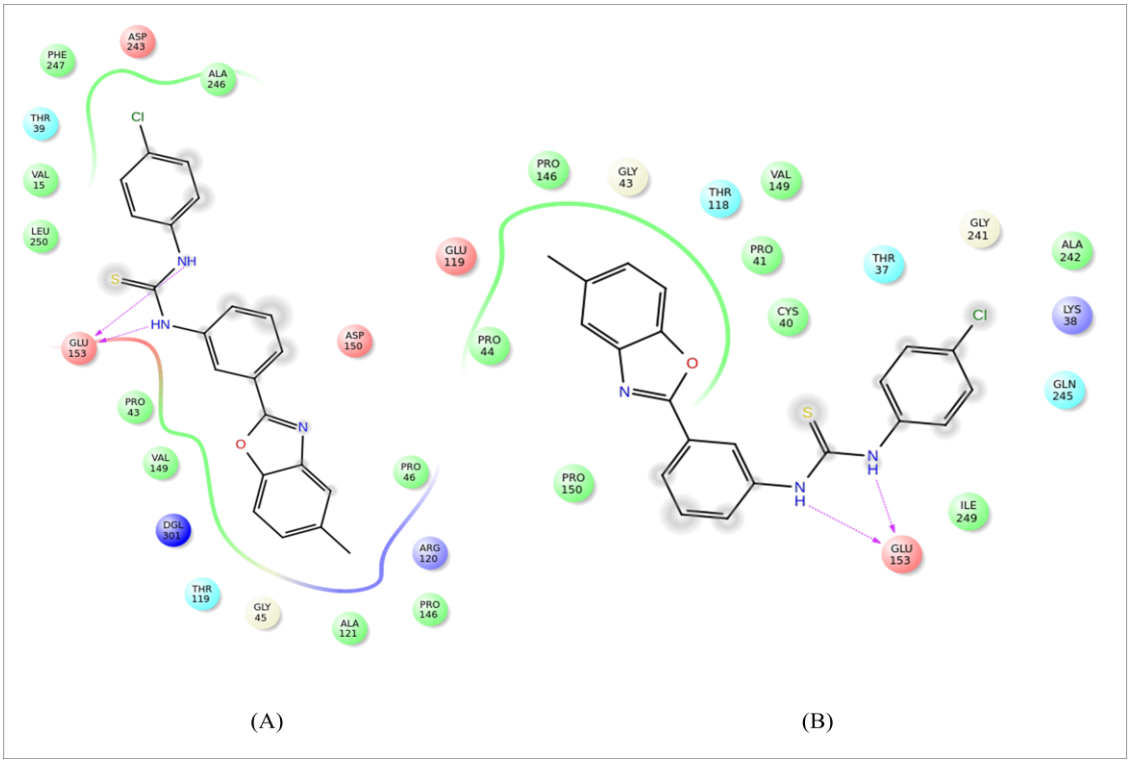

Figure 5.19: Binding pose and the interaction pattern of the compound **BO_22** in A) *M. tuberculosis* and B) *B. subtilis*.

Molecular dynamics simulations help in understanding the structure and function of macromolecules at a basic level. Simulations provide every minute detail about every particle/atom movement with respect to time. This will help in answering the questions arising on deviation and fluctuation pattern of protein. [We have subjected the Compound **22** bound in 5HJ7 and 1ZUW protein complexes to a 10 ns simulation using Desmond. The deviation and fluctuation patterns were measured in terms of rmsd and rmsf (root mean square fluctuation). Rmsd of protein (C_α) and ligand obtained during 10 ns simulation for the 1ZUW crystal structure were within the average of ~1.21 Å and ~0.9 Å and for 5HJ7 both C_α and ligand were within an average of ~1.35 Å and ~0.82 Å respectively (**Figure 5.20)**. Rmsf analysis inferred that proteins and ligand at their binding site have shown negligible fluctuations with ~1.36 Å and 1.41 Å respectively for 5HJ7 and 1ZUW (**Figure 5.21**).

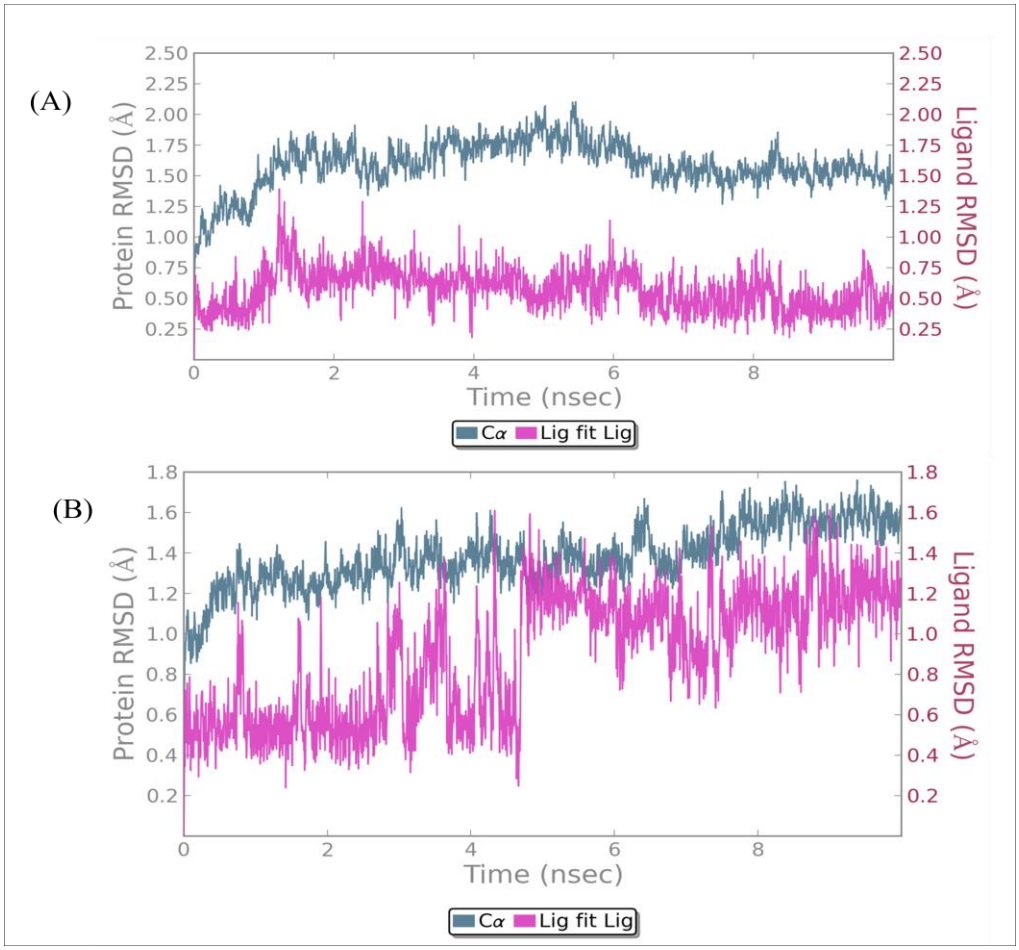

Figure 5.20: Rmsd plots of Glutamate racemase in a bound state with compounds **BO_22** as a function of time in *M. tuberculosis* (A) and (B) *B. subtilis.*

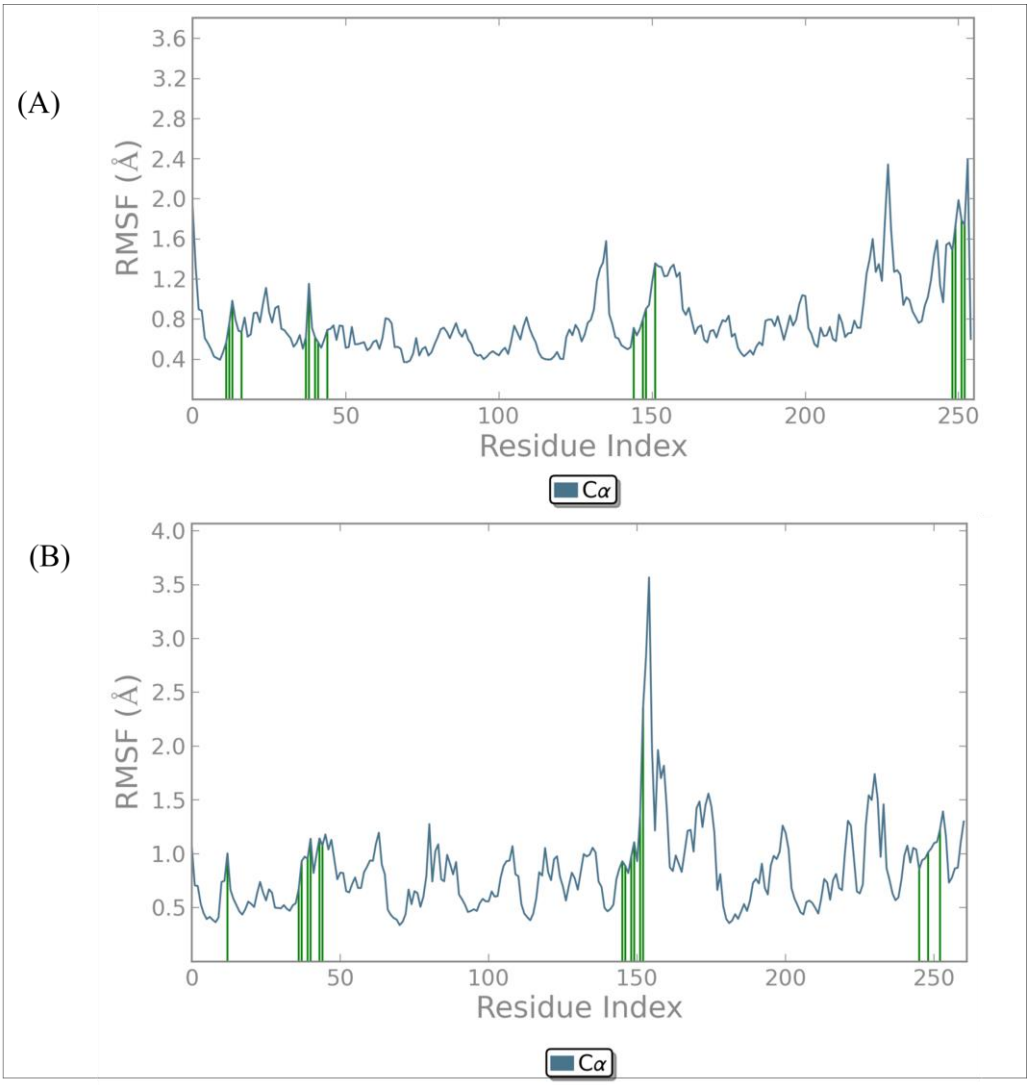

Figure 5.21: Rmsf plot for all atoms of Glutamate racemase in complex with compound **BO_22** resulted from 10 ns simulation trajectory (A) *M. tuberculosis* and (B) *B. subtilis.*

We have analyzed inhibitor characterization in *M. tuberculosis* Glutamate racemase. The thermal shift analysis of active compound **BO_22** shows a clear non-competitive mode of inhibition. The protein unbound form showed T_m ~43.7 ^oC and bound form at ~45.1 ^oC respectively. The compound **BO_22** showed T_m ~49.8 ^oC with unbound protein and T_m ~51.9 ^oC with protein bound with the substrate (**Figure 5.22**). These melt temperature shifts (ΔT_m) were higher compared to that of **lead 2** (reported above). This infers that the protein and protein-substrate complex were more stabilized in the presence of compound **BO_22** when compared to **lead 2**.

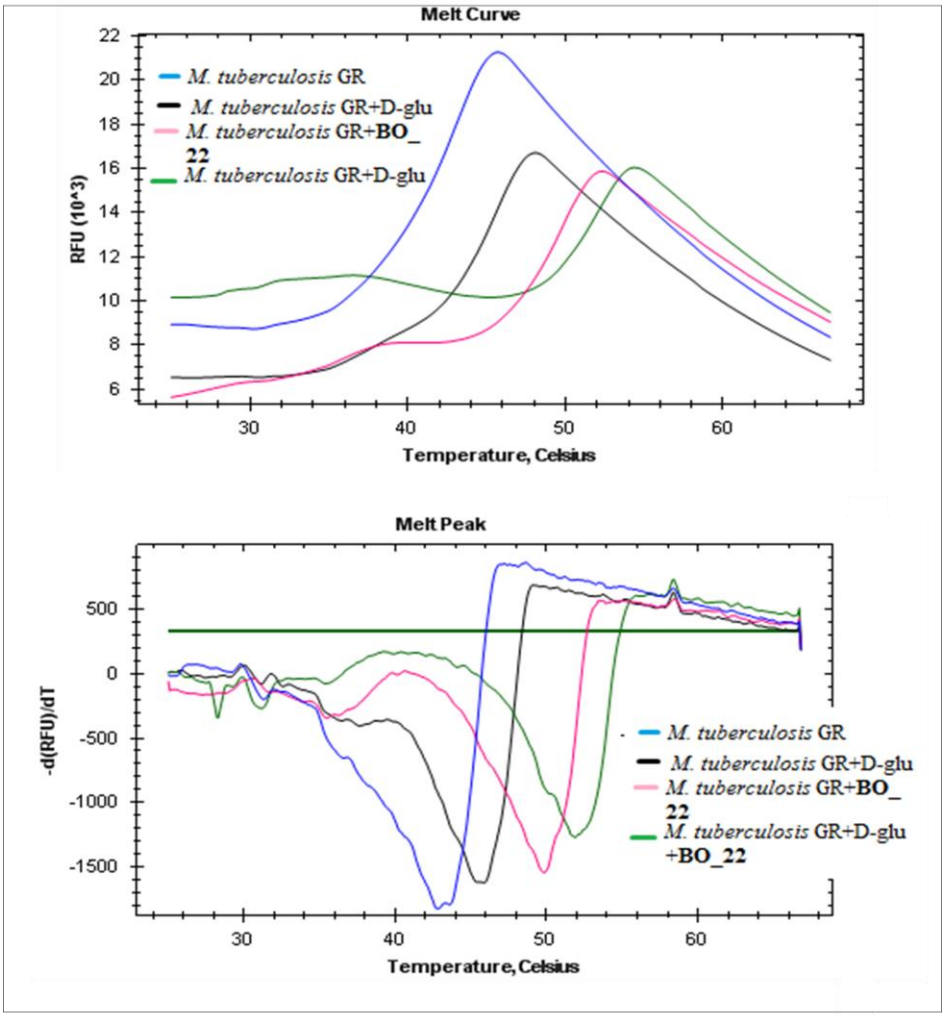

Figure 5.22: Thermal stability curves of *M. tuberculosis* GR depicting the non-competitive inhibition by compound **BO_22.**

Susceptibility testing

Determining whole cell activity against *M. tuberculosis* is an important factor in drug development research against tuberculosis. MABA assay was performed for all the synthesized compounds to determine the minimum inhibitory concentration (MIC) of each compound when tested at concentrations varying from 50 µg/mL to 0.78 µg/mL. MIC values of the test compounds and the standard drugs (Isoniazid, Ethambutol and Rifampicin) were represented in **Table 5.9**. Compounds **BO_17, BO_18, BO_19, BO_22** and **BO_23** having thiourea substitution, have shown inhibition below 10 µM. Of which four compounds (**BO_17, BO_18,**

BO_19 and **BO_23**) were more active than standard drug Ethambutol (MIC 7.89 μM). Compounds **BO_17, BO_18, BO_23** have shown a whole cell inhibition compared to that of enzyme inhibition. To our assumption, this conjugate effect might be due to an additional pathway inhibition. Few compounds in spite of having good activity profile in enzyme assay failed to inhibit the whole organism, where the reason could be the efflux of the compound by the complex cell wall of bacteria. Assuming that the failure of compounds in replicating bacteria might be due to efflux of the drug, the compounds **BO_4, BO_6**, **BO_13**, **BO_14**, **BO_16**, **BO_20**, **BO_21**, **BO_22** and **BO_24** active in enzyme assay were tested for their susceptibility in the presence of verapamil and piperine. Compounds **BO_16**, **BO_20**, **BO_21** and **BO_22** have shown a drastic increase in activity against *M. tuberculosis* than as individual drugs (**Table 5.9**). The remaining compounds haven't shown any difference in their activities. The most active molecule in an enzyme assay, compound **BO_22** (IC_{50} of 1.1±0.52 μM) has shown a MIC of 8.72 μM in the absence of efflux pump inhibitors and 2.01 μM with a difference of four times in the presence of efflux pump inhibitors.

5.2.2.7. *M. tuberculosis* nutrient starved dormancy model

M. tuberculosis attains dormancy and phenotypically develop drug resistance when it undergoes stress within the host. Nutrient starvation is one such model which creates the dormancy in bacteria by starving culture in phosphate buffer saline (PBS) for 6 weeks. The dormant culture was tested with selected compounds at a concentration of 10 μg/mL. Based on enzyme and MABA assay activities, compounds **BO_17**, **BO_18**, **BO_19** and **BO_22** were selected to test against dormant assays. Rifampicin (RIF), Isoniazid (INH) and Moxifloxacin (MOXI) were used as reference compounds. The comparative inhibitory activity plots in the nutrient starvation model were shown in **Figure 5.23**. Compounds **BO_17, BO_18** and **BO_22** have shown a similar inhibition with a log reduction of 2.5 (with control), 1.4 (with INH), 0.8 (with RIF) and 0.3 with (MOXI). Compound **BO_19** has shown a difference of 0.2 log reduction when compared to other test compounds. Test compounds have shown similar inhibition with less variation with good activities in the active and dormant model.

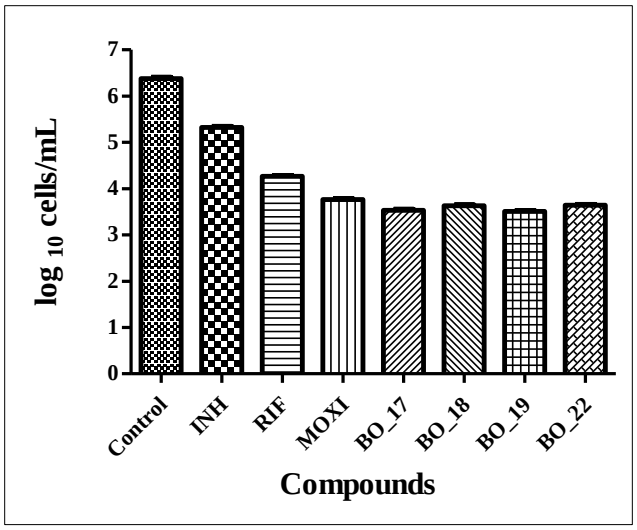

Figure 5.23: Activity profile of compounds in the nutrient starvation model. Bacterial count (Mean ± S.E., n=3) for control and treated groups was estimated through MPN (most probable number) assay.

5.2.2.8. Time-kill kinetics determination

It's essential to study the pharmacodynamics of novel drug molecules by analyzing the kill of drug molecule at different concentrations against time. This aids in determining the concentration-dependent and time-dependent bactericidal activities of drug molecules. Minimum bactericidal concentration (MBC) is defined as the concentration at which inhibitor shows three fold inhibition of bacteria, incubated for 21 days. To determine MBC, the compound at different concentrations (decided according to MIC value) was incubated for 21 days and recorded the readings at different time points (0, 7, 15 and 21 days). A compound is said to be bactericidal if MBC is within 4 folds of its MIC and bacteriostatic if it's more than four folds. Bactericidal compounds exhibit two types of kill namely time dependent and concentration dependent. We have used starved culture (depleted of nutrients for 2 weeks) for assay. Compounds **BO_17, BO_18, BO_19** and **BO_22** were tested for determining their kill kinetics. Compounds **BO_19** and **BO_22** have shown the bactericidal mode of inhibition with their MBC values 27.47 µM and 25.38 µM respectively. We have represented the kinetics study of compound **BO_22** in **Figure 5.24.** It shows a time dependent kill, where one can observe the kill increased with time irrespective of concentration.

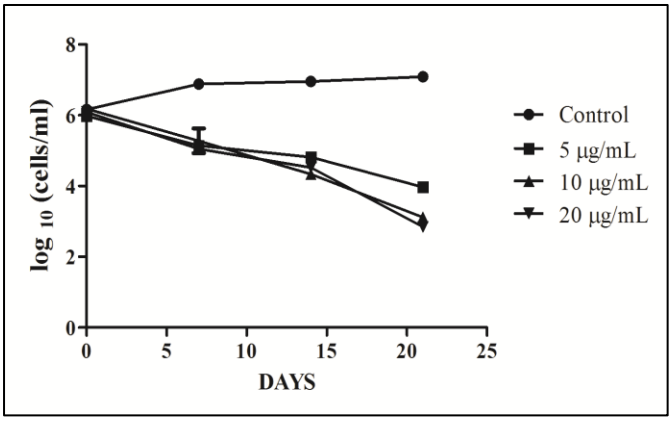

Figure 5.24: Kill kinetic curve of compound **BO_22** depicting time dependant kill kinetics.

5.2.2.9. Biofilm assay

M. tuberculosis forms organized biofilm containing mycolic-acid-rich extracellular matrix which are drug tolerant. Compounds **BO_17, BO_18, BO_19** and **BO_22** were tested for their activity on biofilm at concentration of10 µg/mL. Reference drugs INH, RIF and MOXI have shown a log reduction of 1.2, 1.5 and 2.0 respectively compared to control. Test compounds **BO_17, BO_18** have shown 0.8 and compounds **BO_19** and **BO_22** have shown log reduction of 0.4 and 2.4 respectively (**Figure 5.25**). These values infer that compound **BO_22** is active in both active and dormant forms of bacteria.

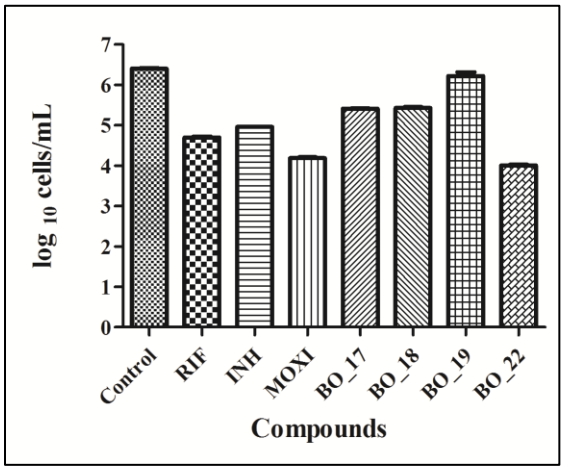

Figure 5.25: Comparative biofilm inhibitory activity plots of compounds **BO_17, BO_18, BO_19**, **BO_25** and standard drugs against *M. tuberculosis*. Bacterial count estimation (Mean ± S.D., n = 4) for control and treated groups was conducted by using the MPN assay.

5.2.2.10. *In vivo* activity testing assay by *M. marinum* infected adult zebrafish and cytotoxicity determination

In this study, zebrafish is infected with *Mycobacterium marinum* (belong to the same family genetically. Active molecule **BO_22** at *in vitro* level was tested for *in vivo* inhibitory activity using adult zebrafish model. Standard compounds INH and MOXI have shown reductions of 2.5 and 2.4 in log scale and test compound **BO_22** has shown 3.4 log reduction with control, which is more than standards (**Figure 5.26**). Toxicity testing of new compounds is very much essential for drug development process, can be observed by *in vivo* and *in vitro* models. In this study, we have tested toxicity using *in vitro* technique employing cell lines by MTT (3-(4,5-Dimethylthiazol-2-yl)-2,5-Diphenyltetrazolium Bromide) assay. RAW 246.7 cell lines were used for experimental studies. All the compounds were tested at a concentration of 25 µM and the percentage inhibition was found to be in different ranges as shown in **Table 5.9**. Hence most of the compounds are devoid of effects on metabolism.

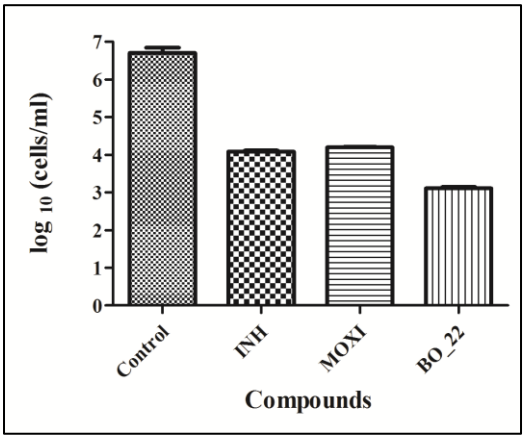

Figure 5.26: Bacterial count estimation (Mean ± S.E.M., n = 6) for control and treated groups by zebrafish model conducted by using MPN assay. Statistical significance has been analyzed by Two-way ANOVA using GraphPad Prism Software.

5.2.2.11. Highlights of the study

In the current scenario persistence, resistance and co-infection are the foremost drawbacks that hinder the tuberculosis treatment regimen. In present work, we have focused on combating persistence and resistance by targeting a novel enzyme vital for the bacterial survival. We have we have identified and optimized through hit expansion. Compounds which showed good *in*

vitro and *in vivo* activities belong to thiourea family. Compound **BO_22** (1-(4-chlorophenyl)-3-(3-(5-methylbenzo[*d*]oxazol-2-yl)phenyl)thiourea) was proven to be the most potent molecule of series in both *in vitro* and *in vivo* evaluation studies. This data was supported by molecular docking and simulation studies, both the compounds retained similar kind of interactions with amino acid residues. There were some compounds which are active in vitro but were unsuccessful on whole cell organism, one of the drawbacks can be the strong efflux nature of cell wall. Further, there were few compounds showing very food whole organism inhibition than enzyme inhibition, these might be targeting an additional pathway for inhibition. These compounds need further studies to answer all questions in drug discovery. Further optimization of compounds can results in still better compounds for treating tuberculosis (**Figure 5.27**).

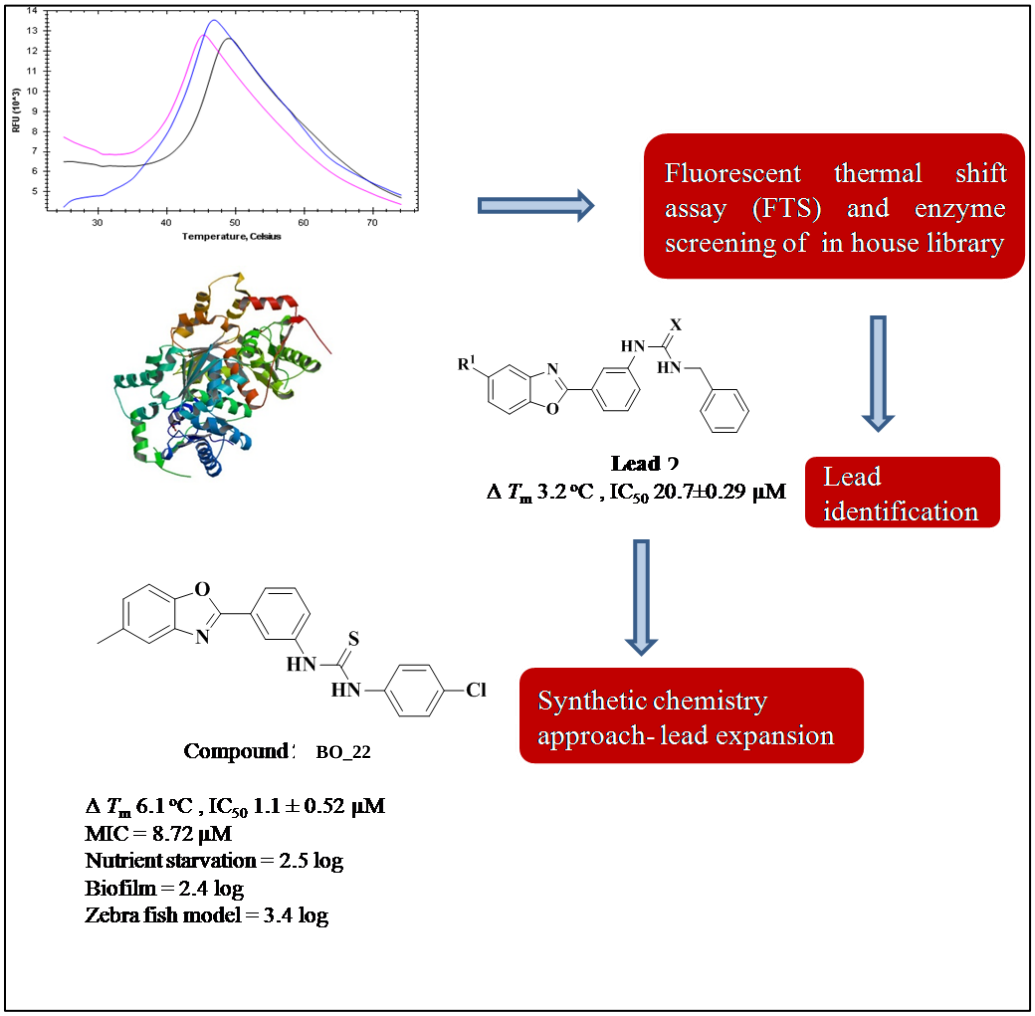

Figure 5.27: Flow of the study from identification of lead to hit optimization with chemical and biological data**.**

5.2.3. Development of novel flourothiazole derivatives targeting *Mycobacterium tuberculosis* Glutamate racemase

5.2.3.1. Screening, identification of lead using thermal shift and enzyme inhibitory assay

We have performed a medium-throughput screening of our in-house compound library of 650 compounds having diverse structures. The compound screening was done using purified *M. tuberculosis* GR enzyme with its substrate D-glu in bound and free forms against library molecules. Melt curve of protein in its unbound state (native) has shown T_m at ~43.1 ^oC and ~44.2 ^oC when bound with D-glu (**Figure 5.28**). Library compounds showed a wide-ranging ΔT_m (thermal shift). Among all molecules **lead 3** has shown T_m at ~46.4 ^oC when added to the unbound protein. There was a shift of 3.2 ^oC with unbound protein and 2.0 ^oC with protein bound to D-glu on comparison to melting temperatures. This result shows the ability of compound **lead 3** in stabilizing the protein against thermal denaturation from rest of the library.

We have tried purifying recombinant *M. tuberculosis* GR enzyme with good catalytic activity and failed, this is in accordance with the recent literature. Therefore we have opted for carrying out activity assay using GR of bacteria having genetic similarities with *M. tuberculosis*. Following the recent literature *Bacillus subtilis* (*B. subtilis*) was considered having 40% and 56% of respective genetic sequence identity and similarity with *M. tuberculosis*. The compounds filtered through TSA method were assayed for inhibitory activity. Compound **lead 3** among all have shown an IC_{50} of 21.6±0.24 µM against *B. subtilis* GR (**Figure 5.28**). In both the screening processes (TSA and inhibitory assays) compound **lead 3** has shown reliable activity, hence it was considered as a lead molecule and further optimized through structural modifications using medicinal chemistry approach.

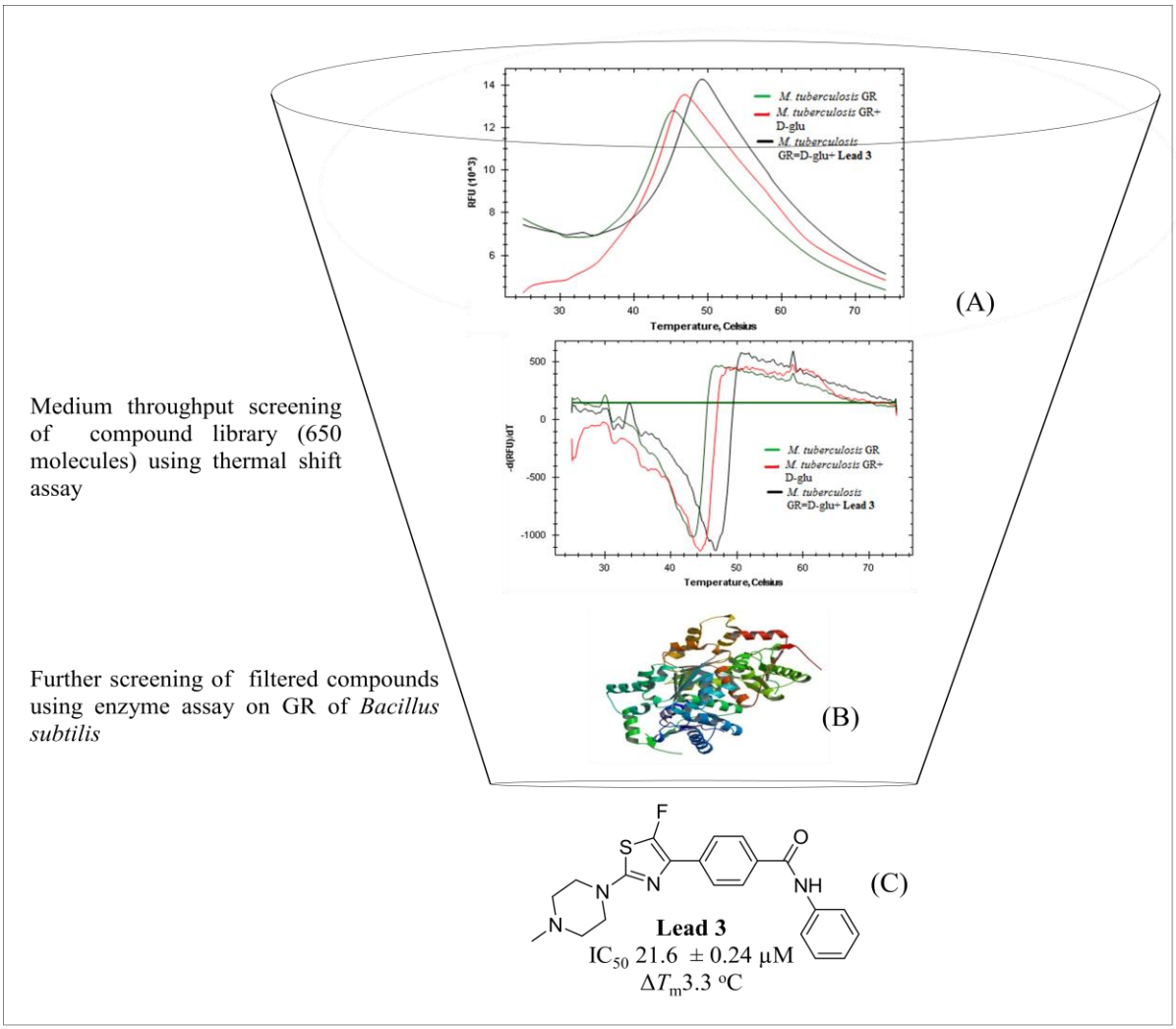

Figure.5.28: (A) Melt curves of *M. tuberculosis* in its free state, bound with substrate and ligand with melt temperature plotting derivative fluorescent (Y-axis) and temperature (X-axis), T_m can be measured from the minimum of the plot. (B) 3D representation of *B. subtilis* GR crystal structure, employed for *in vitro* activity assay. (C) Structure of identified **lead 3** with ΔT_m and IC_{50} value.

5.2.3.2. Chemical synthesis and characterization

To expand and optimize the hit, we further synthesized 18 compounds and assayed them for *M. tuberculosis* GR inhibition. The synthetic pathway employed to achieve the target compounds has been delineated in **Scheme 5.3**. The final compounds were synthesized in following steps: In the First step, compound **FT_1**, bromine and 2-pyrrolidinone were heated to get compound

FT_2. Compound **FT_2** was reacted with potassium fluoride and 18-crown-6 and refluxed for 16 h to obtain compound **FT_3**. Completely dried compound **FT_3** was added to a mixture of acetic acid and Bromine with heating to get compound **FT_4** as solid (65% yield), which was used for further reaction with 4-methylpiperazine-1-carbothioamide in toluene and refluxed to get dried form of compound **FT_5** with 70% yield. The compound **FT_5** was reacted with LiOH in THF/water (5 mL) at room temperature to obtain solid of compound **FT_6** (60% yield) which was reacted with various diverse amines to yield compounds **FT_7-26**.

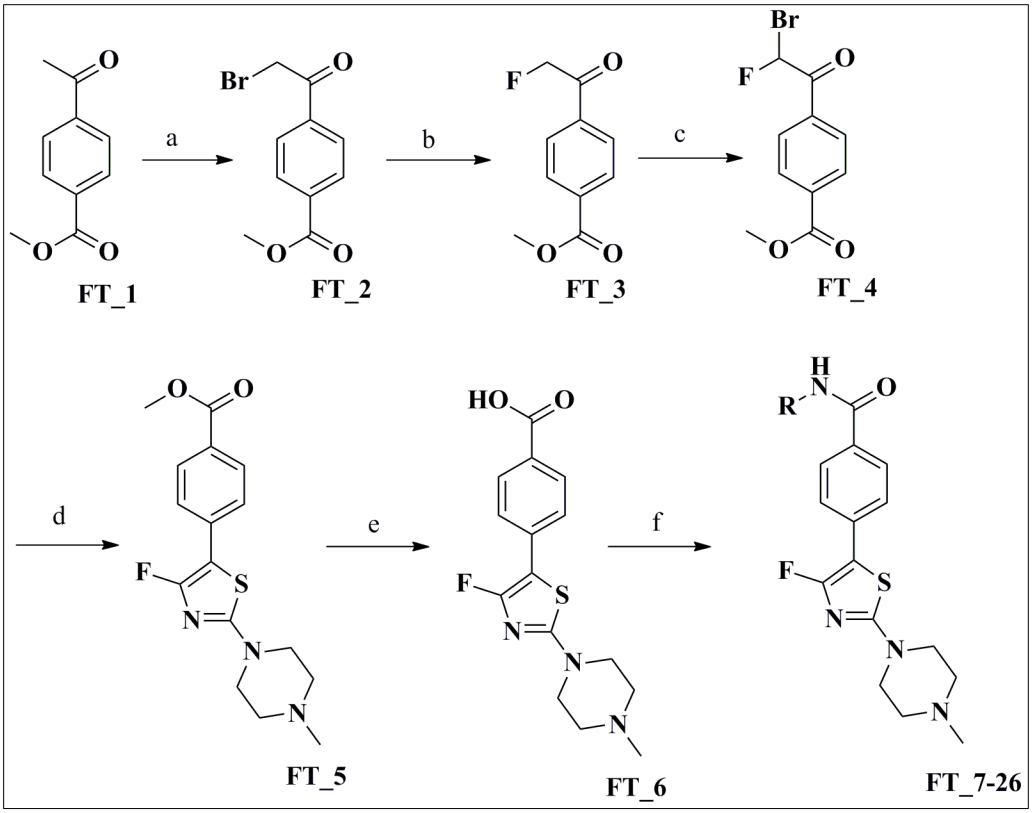

Scheme 5.3: Synthetic strategy for hit expansion Reagents and conditions **FT_7-26**. Reagents and conditions: a) Br_2, 2-pyrolidinone,THF, 65 ^oC, 2 h b) KF, 18-crown ether, ACN, reflux, 16 h c) Br_2/ACOH, 45 ^oC d) 4-methylpiperazine-1-carbothioamide, toulene, reflux, 6 h e) LiOH, THF/H_2O, rt, 5 h f) RNH_2, TEA, T_3P, MDC,14 h.

5.2.3.3. Synthetic protocol used for synthesis

Preparation of Methyl 4-(2-bromoacetyl)benzoate (FT_2): To a mixture of the methyl-4-acetylbenzoate **FT_1** (11.2 mmol) and Bromine (16.75 mmol), THF (20 mL) and 2-

pyrrolidinone (32.9 mmol) were added. After heating at 60-65 °C for 2 h, the mixture was concentrated under vacuum and then the resulting mixture was extracted thrice with ethyl acetate (15 ml each time) and the organic phases were combined, dried over Na_2SO_4, concentrated and purified by column chromatography on silica gel 60-120 grade with ethylacetate:hexane to obtain methyl 4-(2-bromoacetyl)benzoate **FT_2**.

Preparation of Methyl 4-(2-fluoroacetyl)benzoate (FT_3): The mixture of potassium fluoride (12 mmol) in acetonitrile (10 mL) was added 18-crown-6 (1.8 mmol) and the reaction was heated at 90 °C for 30 minutes. To this completely dried methyl 4-(2-bromoacetyl)benzoate **FT_2** (6.6 mmol) was added to and heated at 90 °C for 16 h. The reaction mixture was extracted with ethyl acetate (3 x 20 mL). The product was purified by column chromatography eluting with ethyl acetate: hexane to obtain methyl 4-(2-floroacetyl)benzoate **FT_3**.

Preparation of Methyl 4-(2-bromo-2-fluoroacetyl)benzoate (FT_4): The completely dried compound **FT_3** (6.1 mmol) from the previous step was added to a mixture of acetic acid (8 mL) and Bromine (11.3 mmol) and heated for 4 h at 45 °C. After the reaction has completed the solid formed was filtered and washed with waster twice and dried to yield methyl 4-(4-fluoro-2-(4-methylpiperazin-1-yl)thiazol-5-yl)benzoate **FT_4**.

Preparation of Methyl 4-(4-fluoro-2-(4-methylpiperazin-1-yl)thiazol-5-yl)benzoate (FT_5): Compound **FT_4** (4.4 mmol) was used for further reaction with 4-methylpiperazine-1 carbothioamide (4.3 mmol) in toluene and refluxed for 6 h. After the reaction has completed toluene was evaporated through vacuum and extracted with ethylacetate (20 mL twice) and water, dried with sodium sulphate and purified through column chromatography with ethylacetate: hexane to get a dried form of methyl 4-(4-fluoro-2-(4-methylpiperazin-1-yl)thiazol-5-yl)benzoate **FT_5**.

Preparation of 4-(4-fluoro-2-(4-methylpiperazin-1-yl)thiazol-5-yl)benzoic acid (FT_6): The resultant product **FT_5** (2.9 mmol) from the previous step was reacted with LiOH (4.5 mmol) in THF/water (5 mL) at room temperature for 5 h. THF was evaporated under vacuum and the mixture was neutralized with HCl to get a solid precipitate. The solid was washed and dried to get 4-(4-fluoro-2-(4-methylpiperazin-1-yl)thiazol-5-yl)benzoic acid **FT_6**.

General procedure for preparation of derivatives FT_7-26: To the mixture of Triethylamine (7.2 mmol) and T_3P (2.9 mmol) in dichloromethane (5 mL), 4-(4-fluoro-2-(4-methylpiperazin-1-

yl)thiazol-5-yl)benzoic acid **FT_6** (2.8mmol) was added along with different amines procured from commercial sources. The reaction was continued for 16 h at room temperature. After the reaction has completed the solvent was evaporated under vacuum and extracted with ethylacetate (15 mL thrice) and water, the organic layers were dried over sodium sulphate and evaporated to get solid which is purified by column chromatography using ethylacetate: hexane to yield amide derivatives **FT_7-26**. The physicochemical properties of synthesized derivatives are shown in **Table 5.10**.

Table 5.10: Physicochemical properties of synthesized compounds **FT_7-26**

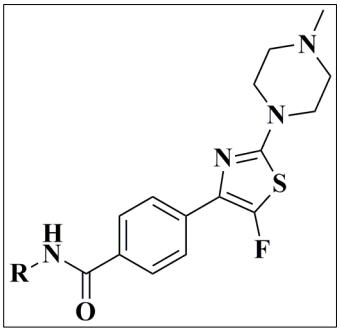

FT_7-26

Compound	R	Yield (%)	Melting point (^{o}C)	Molecular formula	Molecular weight
FT _7	Methyl	59.3	110-112	$C_{16}H_{19}FN_4OS$	334.61
FT _8	Ethyl	52.4	123-125	$C_{17}H_{21}FN_4OS$	348.7
FT _9	1-Methylpiperazinyl	56.7	198-200	$C_{20}H_{26}FN_5OS$	403.12
FT _10	Morpholinyl	58.1	183-185	$C_{19}H_{23}FN_4O_2S$	390.14
FT _11	Thiomorpholinyl	63.3	190-192	$C_{19}H_{23}FN_4OS_2$	406.35
FT 12	Benzyl	70.2	193-195	$C_{22}H_{23}FN_4OS$	410.25

FT _13	Furan-2-ylmethyl	61.9	182-184	$C_{20}H_{21}FN_4O_2S$	400.7
FT _14	1*H*-pyrrol-1-yl	64.6	188-190	$C_{19}H_{19}FN_4OS$	370.52
FT _15	Isopropyl	76.6	120-122	$C_{18}H_{23}FN_4OS$	362.13
FT _16	Cyclohexyl	70.4	180-182	$C_{21}H_{27}FN_4OS$	402.41
FT _17	Phenylpiperazin-1-yl	74.8	219-221	$C_{25}H_{28}FN_5OS$	465.11
FT _18	Methylpiperazin-1-yl	54.7	211-213	$C_{21}H_{28}FN_5OS$	417.27
FT _19	Benzyloxy	59.5	222-224	$C_{21}H_{28}FN_4OS$	426.14
FT _20	Ethoxy	61.6	250-252	$C_{17}H_{21}FN_4OS$	364.17
FT _21	Thiazol-2-yl	57.8	198-200	$C_{17}H_{21}FN_4OS$	403.29
FT _22	5-Nitrobenzo[*d*]thazol-2-yl	63.4	260-262	$C_{22}H_{19}FN_6O_3S_2$	498.19
FT _23	4-Nitrothiazol-2-yl	70.2	234-236	$C_{18}H_{17}FN_6O_3S_2$	448.31
FT_24	2-Hydroxyethyl	68.6	215-217	$C_{17}H_{21}FN_4O_2S$	364.35
FT_25	Hydryl	78.3	115-117	$C_{15}H_{17}FN_4OS$	320.23
FT_26	Thiophen-2-ylmethyl	73.2	163-165	$C_{20}H_{21}FN_4OS_2$	416.12

5.2.3.4. Characterization of synthesized compounds

Methyl 4-(2-bromoacetyl)benzoate (FT_2): The compound was prepared using methyl-4-acetylbenzoate **FT_1** (2 g, 11.2 mmol) and Bromine (1.34 g, 16.75 mmol) and 2-pyrrolidinone (2.8 g, 32.9 mmol) to obtain methyl 4-(2-bromoacetyl)benzoate **FT_2** as a Pale brown solid (3.1 g, 67%). ^{1}H NMR (400 MHz, DMSO-d_6, TMS): δ = 7.91-7.83 (m, 4H), 4.98 (s, 2H), 4.12 (s, 3H). ^{13}C NMR (400 MHz, DMSO-d_6, TMS): δ= 195.1, 166.7, 138.9, 133.9, 130.2 (4C), 52.1, 32.8. ESI-MS m/z 258.21 $(M+H)^+$. Anal calcd for $C_{10}H_9BrO_3$: C, 46.72; H, 3.53 Found: C, 46.83; H, 3.54.

Methyl 4-(2-fluoroacetyl)benzoate (FT_3): The mixture of potassium fluoride (0.69 g, 12 mmol), 18-crown-6 (0.47 g, 1.8 mmol) and methyl 4-(2-bromoacetyl)benzoate **FT_2** (1.7 g, 6.6 mmol) were used to methyl 4-(2-floroacetyl)benzoate **FT_3** as pale yellow solid (3.2 g, 78%). ^{1}H NMR (400 MHz, DMSO-d_6, TMS): δ =7.97-7.81 (m, 4H), 5.29 (s, 2H), 4.28 (s, 3H). ^{13}C NMR (100 MHz, DMSO-d_6, TMS): δ= 197.2, 166.3, 140.7, 133.6, 129.4 (4C), 93.3, 52.5. ESI-MS m/z 197.34 $(M+H)^+$. Anal calcd for $C_{10}H_9FO_3$: C, 61.22; H, 4.62 Found: C, 61.35; H, 4.61.

Methyl 4-(2-bromo-2-fluoroacetyl)benzoate (FT_4): The completely dried compound **FT_3** (1.2 g, 6.1 mmol) and a mixture of acetic acid (8 mL) and Bromine (0.9 g, 11.3 mmol) were reacted to yield methyl 4-(4-fluoro-2-(4-methylpiperazin-1-yl)thiazol-5-yl)benzoate **FT_4** as brown solid (2.7 g, 60%). ^{1}H NMR (400 MHz, DMSO-d_6, TMS): δ = 8.01-7.93 (m, 4H), 6.93 (s, 1H), 4.39 (s, 3H). ^{13}C NMR (100 MHz, DMSO-d_6, TMS): δ= 195.3, 173.2, 138.9, 135.3, 127.9 (4C), 106.2, 50.9. ESI-MS m/z 276.19 $(M+H)^+$. Anal calcd for $C_{10}H_8BrFO_3$: C, 43.66; H, 2.93 Found: C, 43.76; H, 2.94.

Methyl 4-(4-fluoro-2-(4-methylpiperazin-1-yl)thiazol-5-yl)benzoate (FT_5): Compound **FT_4** (1.2 g, 4.4 mmol) was used for further reaction with 4-methylpiperazine-1 carbothioamide (0.7 g, 4.3 mmol) to get dried form of methyl 4-(4-fluoro-2-(4-methylpiperazin-1-yl)thiazol-5-yl)benzoate **FT_5** as white solid (3.4 g, 75%). ^{1}H NMR (400 MHz, DMSO-d_6, TMS): δ = 7.95-7.81 (m, 4H), 4.43 (s, 3H), 2.89-2.43 (m, 8H), 2.34 (s, 3H). ^{13}C NMR (100 MHz, DMSO-d_6, TMS): δ= 172.5, 156.2, 141.6 (2C), 130.5, 126.3 (4C), 120.9, 58.5 (2C), 52.3 (3C), 45.1. ESI-MS m/z 336.20 $(M+H)^+$. Anal calcd for $C_{16}H_{18}FN_3O_2S$: C, 57.30; H, 5.41; N, 12.53 Found: C, 57.42; H, 5.42; N, 12.57.

4-(4-Fluoro-2-(4-methylpiperazin-1-yl)thiazol-5-yl)benzoic acid (FT_6): The resultant product **FT_5** (1 g, 2.9 mmol) from the previous step was reacted with LiOH (1 g, 4.5 mmol) to get 4-(4-fluoro-2-(4-methylpiperazin-1-yl)thiazol-5-yl)benzoic acid **FT_6** as pale yellow solid (3.1 g, 82%). ^{1}H NMR (400 MHz, DMSO-d_6, TMS): δ = 11.43 (s, 1H), 8.09-7.89 (m, 4H), 2.53-2.44 (m, 8H), 2.23 (s, 3H). ^{13}C NMR (100 MHz, DMSO-d_6, TMS): δ= 171.3, 157.9, 141.5 (2C), 131.4, 128.5 (4C), 121.7, 63.2, 50.9 (2C), 44.8. ESI-MS m/z 322.43 $(M+H)^+$. Anal calcd for $C_{15}H_{16}FN_3O_2S$: C, 56.06; H, 5.02; N, 13.08 Found: C, 56.17; H, 5.01; N, 13.06.

4-(5-Fluoro-2-(4-methylpiperazin-1-yl)thiazol-4-yl)-*N*-methylbenzamide (FT_7): The compound was synthesized according to the above general procedure using triethylamine (0.7 g, 7.2 mmol) and T_3P (0.9 g, 2.9 mmol) in dichloromethane (5 mL), 4-(4-fluoro-2-(4-

methylpiperazin-1-yl)thiazol-5-yl)benzoic acid **FT_6** (0.9 g, 2.8mmol) and methanamine (0.9 g, 29.1 mmol) to afford **FT_7** as brown solid (1.2 g, 59.3%). M.p: 110-112 ^{o}C. ^{1}H NMR (400 MHz, DMSO-d_6, TMS):δ =8.24 (m, 1H), 7.95-7.8 (m, 4H), 3.21 (d, *J*=4Hz, 3H), 2.43-2.37 (m, 8H), 2. 25(s, 3H). ^{13}C NMR (100 MHz, DMSO-d_6, TMS): δ= 170.2, 156.9, 150.9, 138.2, 133.5, 131.3 (2C), 130.5 (2C), 105.8, 55.2 (2C), 50.8 (2C), 47.2, 28.4. ESI-MS m/z 335.61 $(M+H)^{+}$. Anal calcd for $C_{16}H_{19}FN_4OS$: C, 61.79; H, 6.71; N, 16.95 Found: C, 61.87; H, 6.73; N, 16.92.

***N*-Ethyl-4-(5-fluoro-2-(4-methylpiperazin-1-yl)thiazol-4-yl)benzamide (FT_8):** The compound was synthesized according to the above general procedure using triethylamine (0.7 g, 7.2 mmol) and T_3P (0.9 g, 2.9 mmol) in dichloromethane (5 mL), 4-(4-fluoro-2-(4-methylpiperazin-1-yl)thiazol-5-yl)benzoic acid **FT_6** (0.9 g, 2.8mmol) and ethanamine (1 g, 22.2 mmol) to afford **FT_8** as brown solid (0.9g, 52.4%). M.p: 123-125 ^{o}C. ^{1}H NMR (400 MHz, DMSO-d_6, TMS): δ =8.3 (m, 1H), 8.0-7.82 (m,4H), 3.23-3.09 (m, 5H), 2.38-2.33 (m,8H), 2.18 (s, 1H). ^{13}C NMR (100 MHz, DMSO-d_6, TMS): δ= 165.3, 159.4, 151.4, 137.2, 135.6, 129.4 (2C), 130.1 (2C), 104.2, 55.2 (2C), 48.5 (2C), 43.2, 36.2, 17.3. ESI-MS m/z 349.1 $(M+H)^{+}$. Anal calcd for $C_{17}H_{21}FN_4OS$: C, 61.79; H, 6.71; N, 16.95 Found: C, 61.85; H, 6.72; N, 16.95.

(4-(5-Fluoro-2-(4-methylpiperazin-1-yl)thiazol-4-yl)phenyl)(4-methylpiperazin-1-yl)methanone (FT_9): The compound was synthesized according to the above general procedure using triethylamine (0.7 g, 7.2 mmol) and T_3P (0.9 g, 2.9 mmol) in dichloromethane (5 mL), 4-(4-fluoro-2-(4-methylpiperazin-1-yl)thiazol-5-yl)benzoic acid **FT_6** (0.9 g, 2.8mmol) and 1-methylpiperazine (1 g, 10 mmol) to afford **FT_9** as white solid (1.1g, 56.7%). M.p: 198-200 ^{o}C. ^{1}H NMR (400 MHz, DMSO-d_6, TMS): δ = 7.78-7.53 (m, 4H), 3.2-3.48(m, 8H), 2.52 (s, 3H), 2.31-2.45(m, 8H), 2.26 (s, 3H). ^{13}C NMR (100 MHz, DMSO-d_6, TMS): δ= 170.2, 158.2, 152.5, 137.9, 135.6, 130.1(2C), 129.4 (2C), 105, 57.8(2C), 51.7 (2C), 49.4(2C), 46.3 (2C). ESI-MS m/z 404.3 $(M+H)^{+}$. Anal calcd for $C_{20}H_{26}FN_5OS$: C, 61.79; H, 6.71; N, 16.95 Found: C, 61.68; H, 6.72; N, 16.97.

(4-(5-Fluoro-2-(4-methylpiperazin-1-yl)thiazol-4-yl)phenyl)(morpholino)methanone (FT_10): The compound was synthesized according to the above general procedure using triethylamine (0.7 g, 7.2 mmol) and T_3P (0.9 g, 2.9 mmol) in dichloromethane (5 mL), 4-(4-fluoro-2-(4-methylpiperazin-1-yl)thiazol-5-yl)benzoic acid **FT_6** (0.9 g, 2.8 mmol) and morpholine (1.2 g, 13.1 mmol) to afford **FT_10** as grey solid (1.2 g, 58.1%). M.p: 183-185 ^{o}C.^{1}H NMR (400 MHz, DMSO-d_6, TMS):δ = 8.0-7.82 (m, 4H), 3.56-3.71 (m, 8H), 2.6-2.43 (m, 8H),

2.26 (s, 3H). ^{13}C NMR (100 MHz, DMSO-d_6, TMS): δ= 171.4, 160.8, 153.9, 137.9, 133.8, 131.3 (2C), 128.5 (2C), 105, 69.3 (2C), 57.3 (2C), 51.5 (2C), 47.8, 43.2 (2C). ESI-MS m/z 391.2 $(M+H)^+$. Anal calcd for $C_{19}H_{23}FN_4O_2S$: C, 58.44; H, 5.94; N, 14.35 Found: C, 58.51; H, 5.93; N, 14.33.

(4-(5-Fluoro-2-(4-methylpiperazin-1-yl)thiazol-4 yl)phenyl)(thiomorpholino)methanone (FT_11): The compound was synthesized according to the above general procedure using triethylamine (0.7 g, 7.2 mmol) and T_3P (0.9 g, 2.9 mmol) in dichloromethane (5 mL), 4-(4-fluoro-2-(4-methylpiperazin-1-yl)thiazol-5-yl)benzoic acid **FT_6** (0.9 g, 2.8mmol) and thiomorpholine (1.2 g, 13.5 mmol) to afford **FT_11** as light Brown solid (1.4g, 63.3%). M.p: 190-192 ^{o}C. ^{1}H NMR (400 MHz, DMSO-d_6, TMS): δ = 8.12-7.95 (m, 4H), 3.43-3.62 (m, 8H), 2.58-2.45 (m, 8H), 2.32 (s, 3H). ^{13}C NMR (100 MHz, DMSO-d_6, TMS): δ= 171.3, 159.2, 153.5, 139.6, 136.2, 131.5 (2C), 130.7 (2C), 109.7, 59.4 (2C), 52.3 (2C), 47.4 (2c), 44.4, 33.7 (2C). ESI-MS m/z 407.8 $(M+H)^+$. Anal calcd for $C_{19}H_{23}FN_4OS_2$: C, 56.13; H, 5.70; N, 13.78 Found: C, 56.25; H, 5.69; N, 13.80.

***N*-Benzyl-4-(5-fluoro-2-(4-methylpiperazin-1-yl)thiazol-4-yl)benzamide (FT_12):** The compound was synthesized according to the above general procedure using triethylamine (0.7 g, 7.2 mmol) and T_3P (0.9 g, 2.9 mmol) in dichloromethane (5 mL), 4-(4-fluoro-2-(4-methylpiperazin-1-yl)thiazol-5-yl)benzoic acid **FT_6** (0.9 g, 2.8mmol) and phenylmethanamine (0.9 g, 12.1 mmol) to afford **FT_12** as brown solid (1.8g, 70.2%). M.p: 193-195 ^{o}C. ^{1}H NMR (400 MHz, DMSO-d_6, TMS): δ = 8.39 (m, 1H), 7.83-7.78 (m, 4H), 7.63-7.58 (m, 5H), 4.67 (d, *J*= 3.8Hz, 2H), 2.54-2.48 (m, 8H), 2.35(s, 3H). ^{13}C NMR (100 MHz, DMSO-d_6, TMS): δ= 171.4, 160.3, 154.5, 141.3, 137.5, 134.3, 131.6 (2C), 130.8 (2C), 128.3 (2C), 127.5, 125.4 (2C), 109.2, 58.4 (2C), 51.6 (2C), 47.2, 45.4. ESI-MS m/z 411.1 $(M+H)^+$. Anal calcd for $C_{22}H_{23}FN_4OS$: C, 64.37; H, 5.65; N, 13.65 Found: C, 64.43; H, 5.66; N, 13.67.

4-(5-Fluoro-2-(4-methylpiperazin-1-yl)thiazol-4-yl)-*N*-(furan-2-ylmethyl)benzamide (FT_13): The compound was synthesized according to the above general procedure using triethylamine (0.7 g, 7.2 mmol) and T_3P (0.9 g, 2.9 mmol) in dichloromethane (5 mL), 4-(4-fluoro-2-(4-methylpiperazin-1-yl)thiazol-5-yl)benzoic acid **FT_6** (0.9 g, 2.8mmol) and furan-2-ylmethanamine (1.0 g, 10.8 mmol) to afford **FT_13** as brown solid (1.2 g, 61.9%). M.p: 182-184 ^{o}C. ^{1}H NMR (400 MHz, DMSO-d_6, TMS): δ = 8.42 (m, 1H), 7.92-7.86 (m, 4H), 7.43-7.32(m, 3H), 3.82(d, *J*= 4.2Hz, 2H), 2.43-2.38(m, 8H), 2.43(s, 3H).^{13}C NMR (100 MHz, DMSO-d_6,

TMS): δ= 170.6, 159.2, 153.7,150.9,148.7,137.4,136.6,132.5 (2C), 130.8 (2C), 111.3 (2C), 105.5, 59.6 (2C), 51.4 (2C), 47.8, 39.2. ESI-MS m/z 401.2 $(M+H)^+$. Anal calcd for $C_{20}H_{21}FN_4O_2S$: C, 59.98; H, 5.29; N, 13.99 Found: C, 59.81; H, 5.30; N, 13.97.

(4-(5-Fluoro-2-(4-methylpiperazin-1-yl)thiazol-4-yl)phenyl)(1*H*-pyrrol-1-yl)methanone (FT_14): The compound was synthesized according to the above general procedure using triethylamine (0.7 g, 7.2 mmol) and T_3P (0.9 g, 2.9 mmol) in dichloromethane (5 mL), 4-(4-fluoro-2-(4-methylpiperazin-1-yl)thiazol-5-yl)benzoic acid **FT_6** (0.9 g, 2.8mmol) and 1*H*-pyrrole (0.9 g, 13.4 mmol) to afford **FT_14** as grey solid(1.3 g, 64.6%). M.p: 188-190 ^oC. ^1H NMR (400 MHz, DMSO-d_6, TMS): δ = 7.85-7.76 (m, 4H), 7.21-7.17 (m, 4H), 2.52-2.44 (m, 8H), 2.4 (s, 3H). ^{13}C NMR (100 MHz, DMSO-d_6, TMS): δ= 169.2, 160.4, 152.7, 143.9, 135.4, 133.5 (2C), 131.2 (2C), 119.7 (4C), 112.4, 57.3 (2C), 51.5 (2C), 47.4. ESI-MS m/z 371.5 $(M+H)^+$. Anal calcd for $C_{19}H_{19}FN_4OS$: C, 61.60; H, 5.17; N, 15.12 Found: C, 61.51; H, 5.16; N, 15.14.

4-(5-Fluoro-2-(4-methylpiperazin-1-yl)thiazol-4-yl)-*N*-isopropylbenzamide (FT_15): The compound was synthesized according to the above general procedure using triethylamine (0.7 g, 7.2 mmol) and T_3P (0.9 g, 2.9 mmol) in dichloromethane (5 mL), 4-(4-fluoro-2-(4-methylpiperazin-1-yl)thiazol-5-yl)benzoic acid **FT_6** (0.9 g, 2.8mmol) and propan-2-amine (0.9 g, 15.1 mmol) to afford **FT_15** as grey solid (1.9 g, 76.6%). M.p: 120-122 ^oC. ^1H NMR (400 MHz, DMSO-d_6, TMS): δ = 8.45 (m, 1H), 7.97-7.91 (m, 4H), 4.5 (m, 1H), 2.32-2.22 (m, 8H), 2.52 (s, 3H), 14.2-1.33 (m, 6H).^{13}C NMR (100 MHz, DMSO-d_6, TMS): δ= 172.3, 164.2, 150.6,138.4, 133.9, 127.4 (2C), 125.9 (2C), 109.3, 57.3 (2C), 52.5 (2C), 47.2, 40.5, 37.6 (2C). ESI-MS m/z 363.4 $(M+H)^+$. Anal calcd for $C_{18}H_{23}FN_4OS$: C, 59.65; H, 6.40; N, 15.46 Found: C, 59.72; H, 6.39; N, 15.49.

***N*-Cyclohexyl-4-(5-fluoro-2-(4-methylpiperazin-1-yl)thiazol-4-yl)benzamide (FT_16):** The compound was synthesized according to the above general procedure using triethylamine (0.7 g, 7.2 mmol) and T_3P (0.9 g, 2.9 mmol) in dichloromethane (5 mL), 4-(4-fluoro-2-(4-methylpiperazin-1-yl)thiazol-5-yl)benzoic acid **FT_6** (0.9 g, 2.8mmol) and cyclohexanamine (0.9 g, 10.2 mmol) to afford **FT_16** as brown solid (1.8 g, 70.4%). M.p: 180-182 ^oC. ^1H NMR (400 MHz, DMSO-d_6, TMS): δ = 8.24 (s, 1H), 7.91-7.82 (m, 4H), 2.64 (m, 1H), 2.43-2.37 (m, 8H), 2.24 (s, 3H), 1.82-1.24 (m, 10H). ^{13}C NMR (100 MHz, DMSO-d_6, TMS): δ=170.9, 155.5, 153.8, 143.7, 133.9, 131.4 (2C), 129.5 (2C), 110.6, 57.3 (2C), 52.4 (2C), 49.8, 47.2, 35.7 (2C),

26.4, 25.7 (2C). ESI-MS m/z 403.6 $(M+H)^+$. Anal calcd for $C_{21}H_{27}FN_4OS$: C, 62.66; H, 6.76; N, 13.92 Found: C, 62.73; H, 6.75; N, 13.90.

(4-(5-Fluoro-2-(4-methylpiperazin-1-yl)thiazol-4-yl)phenyl)(4-phenylpiperazin-1-yl)methanone (FT_17): The compound was synthesized according to the above general procedure using triethylamine (0.7 g, 7.2 mmol) and T_3P (0.9 g, 2.9 mmol) in dichloromethane (5 mL), 4-(4-fluoro-2-(4-methylpiperazin-1-yl)thiazol-5-yl)benzoic acid **FT_6** (0.9 g, 2.8 mmol) and 1-phenylpiperazine (0.8 g, 4.9 mmol) to afford **FT_17** as brown solid (1.9 g, 74.8%). M.p: 219-221 ^oC. ^1H NMR (400 MHz, DMSO-d_6, TMS): δ = 7.92-7.83 (m, 4H), 7.25-7.16 (m, 5H), 3.85-3.61 (m, 8H), 2.43-4.37 (m, 8H), 2.24 (s, 3H). ^{13}C NMR (100 MHz, DMSO-d_6, TMS): δ=172.3, 159.4, 152.1, 150.9, 139.3, 135.7, 131.7 (4C), 129.4 (2C), 120.8, 117.5 (2C), 106.3, 56.3 (2C), 51.2 (2C), 48.5 (2C), 45.3 (2C), 43.4. ESI-MS m/z 466.3 $(M+H)^+$. Anal calcd for $C_{25}H_{28}FN_5OS$: C, 64.49; H, 6.06; N, 15.04 Found: C, 64.36; H, 6.05; N, 15.06.

(4-Ethylpiperazin-1-yl)(4-(5-fluoro-2-(4-methylpiperazin-1-yl)thiazol-4-yl)phenyl)methanone (FT_18): The compound was synthesized according to the above general procedure using triethylamine (0.7 g, 7.2 mmol) and T_3P (0.9 g, 2.9 mmol) in dichloromethane (5 mL), 4-(4-fluoro-2-(4-methylpiperazin-1-yl)thiazol-5-yl)benzoic acid **FT_6** (0.9 g, 2.8 mmol) and 1-methylpiperazine (0.8 g, 5.1 mmol) to afford **FT_18** as dark red solid (1.2 g, 54.7%). M.p: 211-213 ^oC. ^1H NMR (400 MHz, DMSO-d_6, TMS): δ = 7.82-7.75 (m, 4H), 3.6-3.33 (m, 8H), 2.48-2.32 (m, 8H), 2.32 (s, 3H), 1.94-1.56 (m, 5H). ^{13}C NMR (100 MHz, DMSO-d_6, TMS): δ= 169.7, 159.6, 153.8, 137.8, 135.7, 131.3 (2C), 129.6 (2C), 109.6, 57.8 (2C), 55.2 (2C), 50.8 (2C), 48.6 (2C), 46.5, 42.1, 19.2. ESI-MS m/z 418.6 $(M+H)^+$. Anal calcd for $C_{21}H_{28}FN_5OS$: C, 60.41; H, 6.76; N, 16.77 Found: C, 60.34; H, 6.77; N, 16.79.

***N*-(Benzyloxy)-4-(5-fluoro-2-(4-methylpiperazin-1-yl)thiazol-4-yl)benzamide (FT_19):** The compound was synthesized according to the above general procedure using triethylamine (0.7 g, 7.2 mmol) and T_3P (0.9 g, 2.9 mmol) in dichloromethane (5 mL), 4-(4-fluoro-2-(4-methylpiperazin-1-yl)thiazol-5-yl)benzoic acid **FT_6** (0.9 g, 2.8 mmol) and *O*-benzylhydroxylamine (0.9 g, 7.3 mmol) to afford **FT_19** as yellow solid (1.4 g, 59.5%). M.p: 222-224 ^oC. ^1H NMR (400 MHz, DMSO-d_6, TMS): δ = 8.25 (s, 1H), 7.94-7.82 (m, 4H), 7.61-7.48 (m, 5H), 5.32 (s, 2H), 2.43-2.37 (m, 8H), 2.24 (s, 3H). ^{13}C NMR (100 MHz, DMSO-d_6, TMS): δ= 166.8, 156.5, 148.9, 139.8, 133.4, 131.5 (2C), 127.5 (2C), 125.5 (2C), 123.3, 120.2,

107.2, 75.5, 55.2 (2C), 43.2, 48.7 (2C). ESI-MS m/z 427.1 $(M+H)^+$. Anal calcd for $C_{21}H_{28}FN_4OS$: C, 61.95; H, 5.44; N, 13.14 Found: C, 61.89; H, 5.43; N, 13.11.

***N*-Ethoxy-4-(5-fluoro-2-(4-methylpiperazin-1-yl)thiazol-4-yl)benzamide (FT_20):** The compound was synthesized according to the above general procedure using triethylamine (0.7 g, 7.2 mmol) and T_3P (0.9 g, 2.9 mmol) in dichloromethane (5 mL), 4-(4-fluoro-2-(4-methylpiperazin-1-yl)thiazol-5-yl)benzoic acid **FT_6** (0.9 g, 2.8 mmol) and *O*-ethylhydroxylamine (0.8 g, 13.1 mmol) to afford **FT_20** as brown solid, (1.5 g, 61.6%). M.p: 250-252 ^oC. ^1H NMR (400 MHz, DMSO-d_6, TMS):δ = 8.32 (s, 1H), 7.79-7.65 (m, 4H), 4.21 (m, 2H), 2.34-2.22 (m, 8H), 2.52 (s, 3H), 1.36 (m, 3H). ^{13}C NMR (100 MHz, DMSO-d_6, TMS): δ= 166.4, 159.8, 153.2, 138.5 (2C), 131.5, 129.5, 125.8 (2C), 123.8, 105.2, 79.8, 55.2 (2C), 53.2, 51.5, 43.7. ESI-MS m/z 365.4 $(M+H)^+$. Anal calcd for $C_{17}H_{21}FN_4OS$: C, 56.58; H, 5.11; N, 15.84 Found: C, 56.47; H, 5.10; N, 15.82.

4-(5-Fluoro-2-(4-methylpiperazin-1-yl)thiazol-4-yl)-*N*-(thiazol-2-yl)benzamide (FT_21): The compound was synthesized according to the above general procedure using triethylamine (0.7 g, 7.2 mmol) and T_3P (0.9 g, 2.9 mmol) in dichloromethane (5 mL), 4-(4-fluoro-2-(4-methylpiperazin-1-yl)thiazol-5-yl)benzoic acid **FT_6** (0.9 g, 2.8 mmol) and thiazol-2-amine (0.9 g, 10.1 mmol) to afford **FT_21** as brown solid, (1.3 g, 57.8%). M.p: 198-200 ^oC. ^1H NMR (400 MHz, DMSO-d_6, TMS): δ = 8.32 (s, 1H), 7.92-7.73 (m, 4H), 7.69 (d, *J*= 8.2Hz, 1H), 7.52 (d, *J*= 8.2Hz, 1H), 2.52-2.41 (m, 8H), 2.25 (s, 3H). ^{13}C NMR (100 MHz, DMSO-d_6, TMS): δ= 165.4, 156.9, 153.2, 139.9, 136.3, 132.5, 129.8 (2C), 126.5 (2C), 119.5, 107.7, 57.8 (2C), 51.3 (2C), 47.3. ESI-MS m/z 404.4 $(M+H)^+$. Anal calcd for $C_{17}H_{21}FN_4OS$: C, 53.58; H, 4.50; N, 17.36 Found: C, 53.65; H, 4.51; N, 17.38.

4-(5-Fluoro-2-(4-methylpiperazin-1-yl)thiazol-4-yl)-*N*-(5-nitrobenzo[*d*]thiazol-2-yl)benzamide (FT_22): The compound was synthesized according to the above general procedure using triethylamine (0.7 g, 7.2 mmol) and T_3P (0.9 g, 2.9 mmol) in dichloromethane (5 mL), 4-(4-fluoro-2-(4-methylpiperazin-1-yl)thiazol-5-yl)benzoic acid **FT_6** (0.9 g, 2.8 mmol) and 5-nitrobenzo[*d*]thiazol-2-amine (0.9 g, 4.6 mmol) to afford **FT_22** as yellow solid, (1.7 g, 63.4%). M.p: 260-262 ^oC. ^1H NMR (400 MHz, DMSO-d_6, TMS): δ = 9.31 (s, 1H), 8.31-8.2 (m, 2H), 8.12 (s, 1H), 7.91-7.79 (m, 4H), 2.54-2.27 (m, 8H), 2.17 (s, 3H). ^{13}C NMR (100 MHz, DMSO-d_6, TMS): δ= 178.2, 169.5, 159.5, 153.8, 150.1, 147.4, 138.2, 136.5, 132.7 (2C), 130.3,

128.5, 121.3, 117.7, 115.5, 105.2, 55.6 (2C), 53.7 (2C), 47.3. ESI-MS m/z 499.3 $(M+H)^+$. Anal calcd for $C_{22}H_{19}FN_6O_3S_2$: C, 53.00; H, 3.84; N, 16.86 Found: C, 53.10; H, 3.85; N, 16.84.

4-(5-Fluoro-2-(4-methylpiperazin-1-yl)thiazol-4-yl)-*N*-(4-nitrothiazol-2-yl)benzamide (FT_23): The compound was synthesized according to the above general procedure using triethylamine (0.7 g, 7.2 mmol) and T_3P (0.9 g, 2.9 mmol) in dichloromethane (5 mL), 4-(4-fluoro-2-(4-methylpiperazin-1-yl)thiazol-5-yl)benzoic acid **FT_6** (0.9 g, 2.8 mmol) and 4-nitrothiazol-2-amine (0.8 g, 5.5 mmol) to afford **FT_23** as yellow solid, (1.9 g, 70.2%). M.p: 234-236 ^oC. ^1H NMR (400 MHz, DMSO-d_6, TMS): δ = 8.41 (s, 1H), 7.93-7.79 (m, 4H), 7.54 (s, 1H), 2.53-2.38 (m, 8H), 2.24 (s, 3H). ^{13}C NMR (100 MHz, DMSO-d_6, TMS): δ= 166.1, 160.1 (2C), 159.5, 153.2, 142.3, 137.5, 133.7, 131.3 (2C), 129.8 (2C), 110.3, 108.5, 59.2 (2C), 53.6 (2C), 47.3. ESI-MS m/z 449.6 $(M+H)^+$. Anal calcd for $C_{18}H_{17}FN_6O_3S_2$: C, 48.20; H, 3.82; N, 18.74 Found: C, 48.13; H, 3.81; N, 18.77.

4-(5-Fluoro-2-(4-methylpiperazin-1-yl)thiazol-4-yl)-*N*-(2-hydroxyethyl)benzamide (FT_24): The compound was synthesized according to the above general procedure using triethylamine (0.7 g, 7.2 mmol) and T_3P (0.9 g, 2.9 mmol) in dichloromethane (5 mL), 4-(4-fluoro-2-(4-methylpiperazin-1-yl)thiazol-5-yl)benzoic acid **FT_6** (0.9 g, 2.8 mmol) and 2-aminoethanol (0.8 g, 13.1 mmol) to afford **FT_24** as white solid, (1.8 g, 68.6%). M.p: 215-217 ^oC. ^1H NMR (400 MHz, DMSO-d_6, TMS):δ = 8.42 (m, 1H), 7.95-7.83 (m, 4H), 5.23-5.11 (m, 1H), 3.52-3.21 (m, 4H), 2.43-2.37 (m, 8H), 2.24 (s, 3H). ^{13}C NMR (100 MHz, DMSO-d_6, TMS): δ= 167.5, 155.2, 150.9, 137.2, 133.9, 130.6 (2C), 125.2 (2C), 110.5, 55.9, 53.2 (2C), 47.6 (2C), 44.3, 40.9. ESI-MS m/z 365.2 $(M+H)^+$. Anal calcd for $C_{17}H_{21}FN_4O_2S$: C, 56.03; H, 5.81; N, 15.37 Found: C, 56.13; H, 5.80; N, 15.39.

4-(5-Fluoro-2-(4-methylpiperazin-1-yl)thiazol-4-yl)benzamide(FT_25): The compound was synthesized according to the above general procedure using triethylamine (0.7 g, 7.2 mmol) and T_3P (0.9 g, 2.9 mmol) in dichloromethane (5 mL), 4-(4-fluoro-2-(4-methylpiperazin-1-yl)thiazol-5-yl)benzoic acid **FT_6** (0.9 g, 2.8 mmol) and ammonia (0.5 g, 25.1 mmol) to afford **FT_25** as dark brown solid, (2.1 g, 78.3%). M.p: 115-117 ^oC. ^1H NMR (400 MHz, DMSO-d_6, TMS):δ = 8.32 (s, 2H), 7.85-7.69 (m, 4H), 2.51-2.34 (m, 8H), 2.27 (s, 3H). ^{13}C NMR (100 MHz, DMSO-d_6, TMS): δ= 171.3, 159.3, 149.2, 140.1, 137.3, 129.5 (2C), 125.5, 123.1, 110.9, 55.3 (2C), 52.1 (2C), 47.3. ESI-MS m/z 321.6 $(M+H)^+$. Anal calcd for $C_{15}H_{17}FN_4OS$: C, 56.23; H, 5.35; N, 17.49 Found: C, 56.28; H, 5.36; N, 17.47.

4-(5-Fluoro-2-(4-methylpiperazin-1-yl)thiazol-4-yl)-*N*-(thiophen-2-ylmethyl)benzamide (FT_26): The compound was synthesized according to the above general procedure using triethylamine (0.7 g, 7.2 mmol) and T_3P (0.9 g, 2.9 mmol) in dichloromethane (5 mL), 4-(4-fluoro-2-(4-methylpiperazin-1-yl)thiazol-5-yl)benzoic acid **FT_6** (0.9 g, 2.8 mmol) and thiophen-2-ylmethanamine (0.8 g, 12.5 mmol) to afford **FT_26** as white solid, (1.9 g, 73.2%). M.p: 163-165 ^{o}C. ^{1}H NMR (400 MHz, DMSO-d_6, TMS):δ = 8.45 (m, 1H), 8.12-7.92 (m, 4H), 7.68-7.53 (m, 3H), 5.23-5.16 (d, *J*=4.8Hz, 2H), 2.56-2.41 (m, 8H), 2.39 (s, 3H). ^{13}C NMR (100 MHz, DMSO-d_6, TMS): δ= 173.5, 160.8, 153.5, 143.7, 139.3, 135.3, 133.7 (2C), 130.1 (2C), 128.6 (2C), 125.3, 112.9, 55.3 (2C), 51.6 (2C), 47.8, 42.1. ESI-MS m/z 417.3 $(M+H)^+$. Anal calcd for $C_{20}H_{21}FN_4OS_2$: C, 57.67; H, 5.08; N, 13.45 Found: C, 57.73; H, 5.07; N, 13.43.

5.2.3.5. Identification and characterization of inhibitors using enzyme inhibitory assay, molecular docking and protein thermal stability assay

Enzyme inhibitory activity assay was performed for synthesized eighteen compounds. The inhibitory concentration was determined by analyzing the readings for each compound. The IC_{50} values of compounds were shown in **Table 5.11**. Six compounds have shown good inhibitory activity. Of which compounds **FT_9, FT_12, FT_18, FT_24** and **FT_25** have shown activity at less than 10 µM, further compounds **FT_18** and **FT_25** have shown activity <5 µM. Most potent of the series, compound **FT_25** showed an IC_{50} of 3.97±0.72 which indicates this compound as more potent than **lead 3** (IC_{50} of 21.6±0.24 µM) by seven times. The log dose response curve of most potent compound **FT_25** was shown in (**Figure 5.29**).

Table 5.11: Biological evaluations of synthesized analogues **FT_7–26**

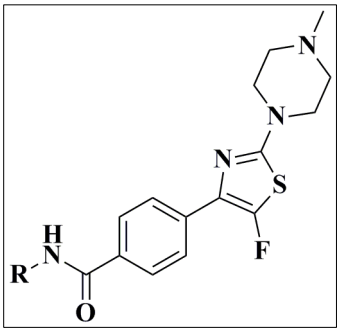

FT_7-26

Compound	R	IC_{50} (μM)[a]	*M. tuberculosis* MIC (μM) [b]	Cytotoxicity at 25 μM (% Inhib.) [c]
FT _7	Methyl	>25	74.8	5
FT _8	Ethyl	>25	35.9	3
FT _9	1-Methylpiperazinyl	9.13 ± 0.24	3.9	77
FT _10	Morpholinyl	>25	8.0	1
FT _11	Thiomorpholinyl	>25	1.9	98
FT 12	Benzyl	7.62 ± 0.45	30.4	2
FT _13	Furan-2-ylmethyl	10.09 ± 0.56	3.9	5
FT _14	1*H*-pyrrol-1-yl	>25	16.9	99
FT _15	Isopropyl	>25	34.5	1
FT _16	Cyclohexyl	>25	62.1	7
FT _17	Phenylpiperazin-1-yl	>25	53.7	10
FT _18	Methylpiperazin-1-yl	4.31 ± 0.65	3.7	12
FT _19	Benzyloxy	>25	14.7	40
FT _20	Ethoxy	>25	31.0	19
FT _21	Thiazol-2-yl	>25	50.1	6
FT _22	5-Nitrobenzo[*d*]thazol-2-yl	>25	55.1	9
FT _23	4-Nitrothiazol-2-yl	>25	13.9	23
FT_24	2-Hydroxyethyl	5.75 ± 0.61	8.6	21

FT_25	Hydryl	3.97 ± 0.72	4.9	24
FT_26	Thiophen-2-ylmethyl	>25	60.0	15
Isoniazid		>25	0.72	ND
Rifampicin		>25	7.64	ND
Ethambutol		>25	0.15	ND

[a] Against the *B. subtilis* GR enzyme. Results were given as the mean ± S from *n*=3 experiments. [b] Minimum inhibitory concentration (MIC) against *M. tuberculosis* H37Rv cells. [c] Percent inhibition of RAW 264.7 cell growth with test compounds at a concentration of 25 µM. Results were given as the mean ± SD from *n*=3 experiments; ND: not determined.

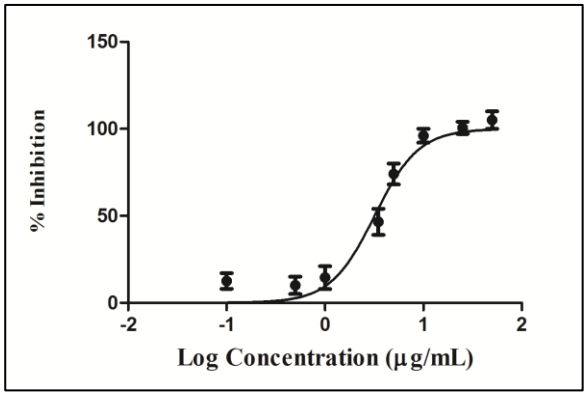

Figure 5.29: Log dose-response curve of compound **FT_25**

As the next step in our study, we have taken the aid of simulation techniques to validate the inhibitory results. All the molecules (energy minimized) were docked in to substrate binding active site but in vain. Assuming that these molecules bind to an allosteric site, we have generated different allosteric sites using an inbuilt program named SiteMap. A total of five sites were identified in each crystal structure. Based on site-scores and other parameters **site 1** in both the proteins was selected for further docking studies. Compounds were docked into allosteric sites of both the crystal structures. We have superimposed both the proteins bound with ligand **FT_24** using superimposition module in Schrodinger shown in **Figure 5.30**. In this study, we have represented the docking orientation of one of the active compounds, molecule **FT_24** in both the crystal structures. The binding orientation shows two H-bond interactions with allosteric residue Glu153 in both the crystal structures with NH and OH moieties of compounds (**Figure**

5.31). Along with H-bonds, the orientation was stabilized by hydrophobic as well as polar interactions. The compound fitted very well in the cavity of two proteins with similar kind of interactions with docking scores of -4.075 kcal/mol and -4.247 kcal/mol respectively in *B. subtilis* and *M. tuberculosis*. Hence we infer that there established a correlation of inhibitory activity of compound **FT_24** in both the organisms.

Figure 5.30: Docking pose of molecule **FT_24** in **site 1** of *M. tuberculosis* (5HJ7) and *B. subtilis* (1ZUW) in superimposed view. Grey color represents protein and ligand in 5HJ7 whereas green represents 1ZUW.

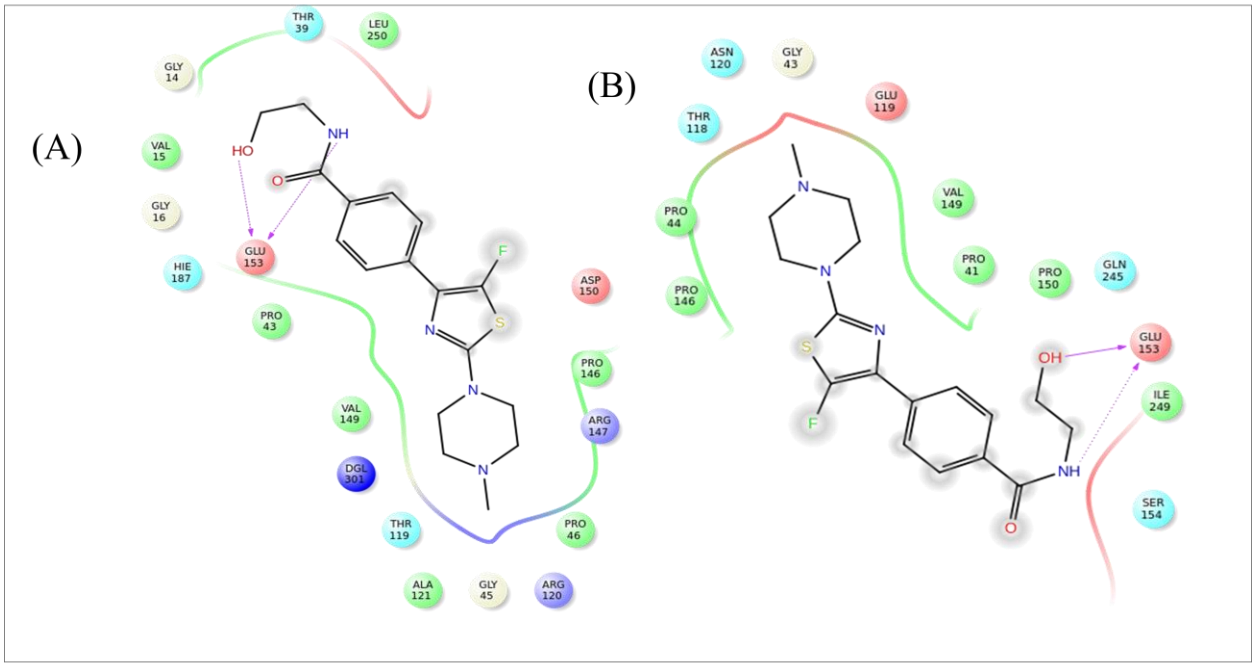

Figure 5.31: Binding pose and the interaction profile of the compound **FT_24** in A) *M. tuberculosis* and B) *B. subtilis*.

We have performed the dynamic study for 10 ns in Desmond software for compound **FT_24** in 5HJ7 and 1ZUW protein complexes. The deviation and fluctuation patterns were measured in terms of rmsd and rmsf (root mean square fluctuation). Rmsd of protein (C_α) and ligand obtained during 10 ns simulation for the 1ZUW crystal structure were within average range of ~1.19 Å and ~1.16 Å and for 5HJ7 both C_α and ligand were within an average range of ~1.44. Å and ~1.09 Å respectively **(Figure 5.32)**. Rmsf analysis inferred that proteins and ligand at their binding site have shown negligible fluctuations with ~1.79 Å and 1.06 Å respectively for 5HJ7 and 1ZUW (**Figure 5.33**).

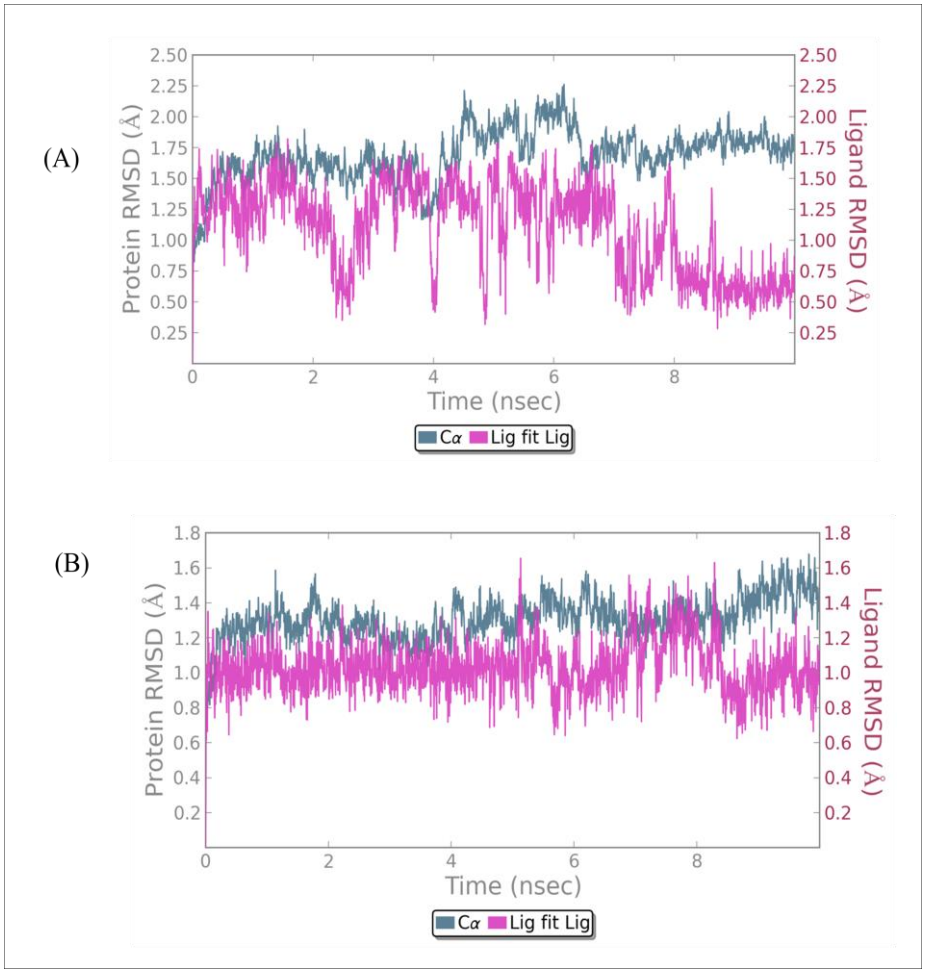

Figure 5.32: Rmsd plots of GR inbound state with compounds **FT_24** as a function of time in *M. tuberculosis* (A) and (B) *B. subtilis.*

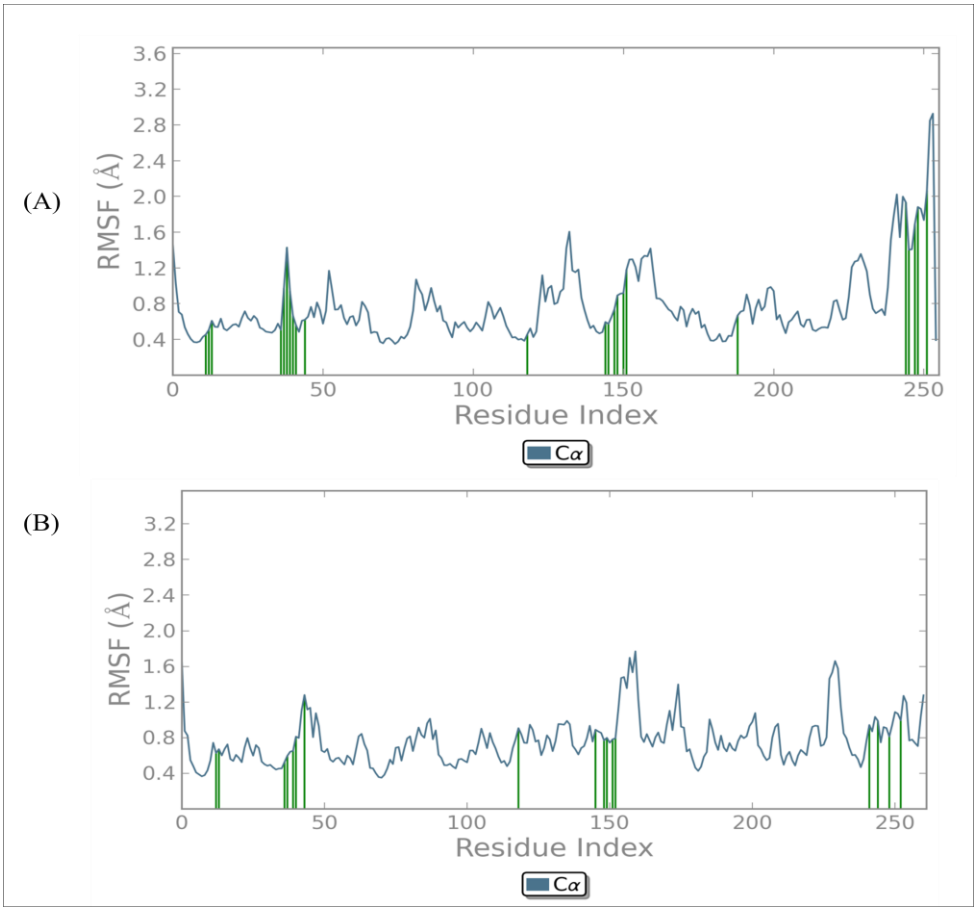

Figure 5.33: Rmsf plots for all atoms of GR in complex with compound **FT_24** resulted from 10 ns simulation trajectory (A) *M. tuberculosis* and (B) *B. subtilis.*

We have analyzed inhibitor mode of action in *M. tuberculosis* GR. The thermal shift analysis of active compound **FT_25** reveals its uncompetitive mode of inhibition. The protein unbound form showed T_m approximately at 43.5 ^oC and bound form at 44.3 ^oC respectively. The compound **FT_25** showed approximate T_m 43.6 ^oC for unbound protein and T_m 47.8 ^oC for protein bound with the substrate (D-glu) as shown in **figure 5.34**. There was a shift in melt temperature shifts (ΔT_m) only in the presence of a substrate in protein indicating its uncompetitive nature. The uncompetitive inhibitor **FT_25** melt temperatures were higher compared to that of **lead 3** (T_m 46.4 ^oC). This infers that the protein and protein-substrate complex were more stabilized in the presence of compound **FT_25** when compared to **lead 3**.

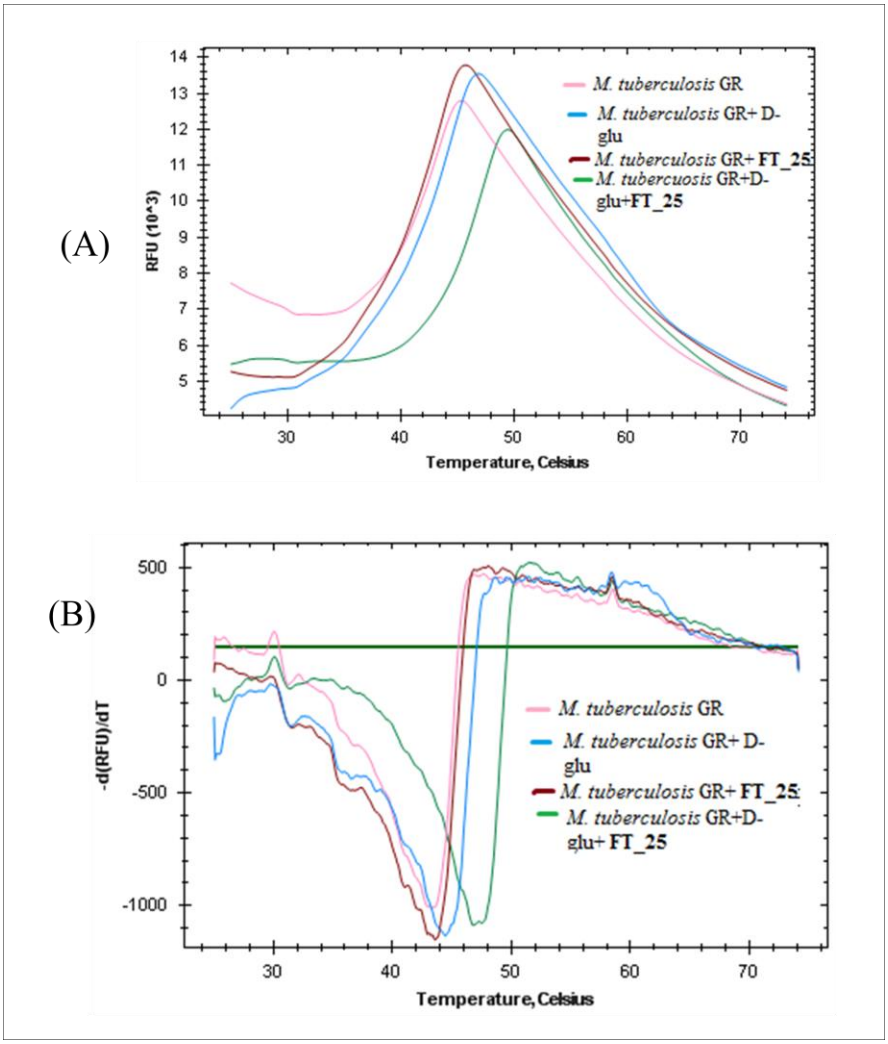

Figure 5.34: Thermal stability curves of *M. tuberculosis* GR depicting the uncompetitive inhibition by compound **FT_25**. (A) Represents the melt curve of protein with D-glu and compound **FT_25.** (B) Indicates the melt peaks where melt temperature can be determined.

5.2.3. 6. *In vitro* active and nutrient-starved dormant *M. tuberculosis* assay models

MABA assay was performed for all the synthesized compounds to determine the minimum inhibitory concentration (MIC) of each compound when tested at concentrations varying from 50 µg/mL to 0.78 µg/mL. MIC values of the test compounds and the standard drugs (Isoniazid, Ethambutol and Rifampicin) were represented in **table 5.11**. Compounds **FT_9**, **FT_10**, **FT_11**, **FT_13**, **FT_18**, **FT_24** and **FT_25** have shown MIC below 10 µM. Of which four compounds (**FT_9**, **FT_11**, **FT_13**, **FT_18** and **FT_25**) were more active than standard drug Ethambutol (MIC 7.89 µM). Compounds **FT_9**, **FT_10**, **FT_11**, **FT_13** and **FT_18** have shown better

inhibition compared to that of enzyme inhibition. To our assumption this inhibition might be their action through an alternate pathway. The most active molecule inhibiting GR, compound **FT_25** (IC_{50} of 3.97±0.72 μM) has shown a MIC of 4.9 μM.

Nutrient starvation is one such model which creates the dormancy in bacteria by starving culture in phosphate buffer saline (PBS) for 6 weeks. The dormant culture was tested with selected compounds at concentration 10 μg/mL. Based on IC_{50} and MIC data of synthesized derivatives, compounds **FT_13, FT_18, FT_24** and **FT_25** were selected to test their activities on dormant bacteria. RIF, INH and Moxifloxacin (MOXI) were used as reference compounds. The comparative inhibitory activity plots in the nutrient starvation model were shown in **Figure 5.35**. Compounds **FT_18, FT_24** and **FT_25** have shown a similar inhibition with a log reduction of 2.7 with control. Compound **FT_13** has shown a difference of 1.3 log reductions when compared to control. Standards INH, RIF and MOXI have shown a log reduction of 0.9, 2 and 2.4 respectively with control. The test compounds have shown more inhibition compared to standards.

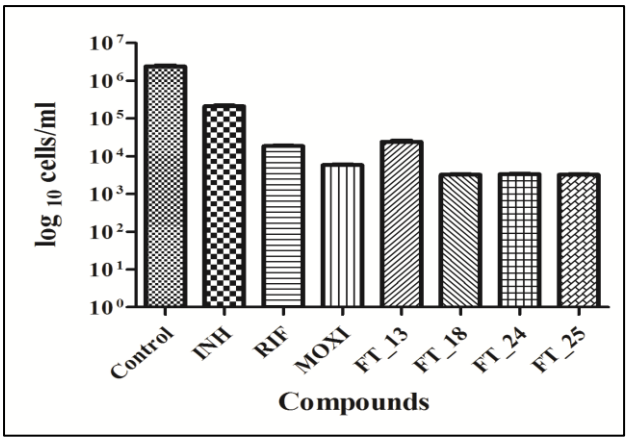

Figure 5.35: Activity profile of compounds in the nutrient starvation model. Bacterial count (Mean ± S.E., n=3) for control and treated groups was estimated through MPN (most probable number) assay.

5.2.3. 7. Determination of kill kinetics using nutrient starved culture of *M. tuberculosis*

It's essential to study and characterize the mode of inhibition of novel compounds against bacteria as a whole cell organism. This is evaluated by analyzing the kill of drug molecule at

different concentrations against time. We have used starved culture (depleted of nutrients for 2 weeks) for assay. Compounds **FT_18, FT_24** and **FT_25** were tested for determining their kill kinetics. Compounds **FT_24** and **FT_25** have shown the bactericidal mode of inhibition with their MBC values 27.39 µM and 31.15 µM respectively whereas compound **FT_18** has shown bacteriostatic inhibition. We have represented the kinetics study of compound **FT_25** in **Figure 5.36.** It shows a time dependent kill, where one can observe the kill increased with time irrespective of drug concentration change.

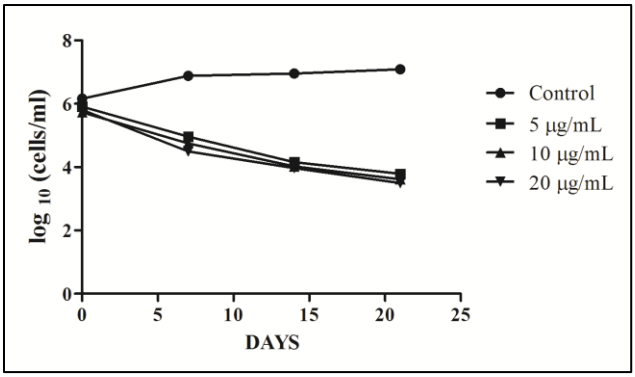

Figure 5.36: Kill kinetic curve of compound **FT_25** depicting time dependant kill kinetics

5.2.3.8. Inhibitory studies on persistent *M. tuberculosis* bacteria (biofilm) and cytotoxicity assay

M. tuberculosis is well known spontaneously grow as biofilms that harbor drug-tolerant bacilli where the existed potent drugs failed to combat against it. Compounds **FT_18, FT_24** and **FT_25** were tested for their activity on biofilm at concentration of10 µg/mL. Reference drugs RIF, INH and MOXI have shown a log reduction of 1.3, 1.2 and 2.1 respectively compared to control. Test compounds **FT_18, FT_24 and FT_25** have shown 0.9, 2.5 and 0.5 respectively (**Figure 5.37**). These values infer that test compound was active in both active and dormant forms of bacteria.

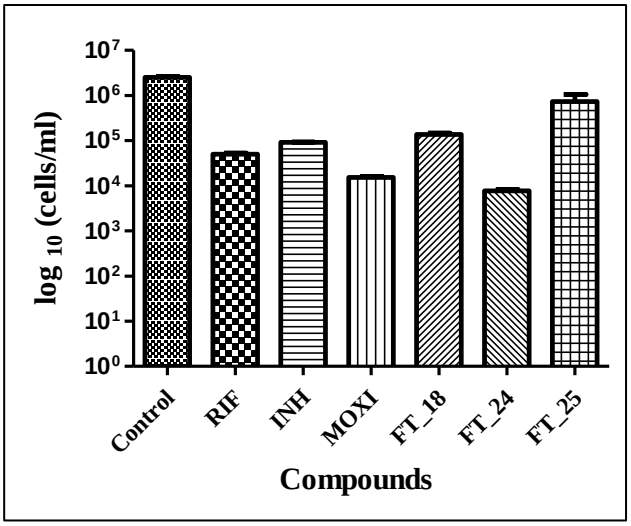

Figure 5.37: Comparative biofilm inhibitory activity plots of compounds **FT_18, FT_24, FT_25** and standard drugs against *M. tuberculosis*. Bacterial count estimation (Mean ± S.D., n = 4) for control and treated groups was conducted by using the MPN assay.

Toxicity testing of developed inhibitors is necessary for drug discovery process, can be tested using various *in vivo* and *in vitro* models. In the present study, we have tested toxicity using *in vitro* technique employing cell lines by MTT (3-(4,5-Dimethylthiazol-2-yl)-2,5-Diphenyltetrazolium Bromide) assay on RAW 246.7 cell lines. All the compounds were tested at a concentration of 25 µM and the percentage inhibition was found to be in different ranges as shown in **Table 5.11**. Hence most of the compounds are devoid of toxic effects on metabolism.

5.2.3.9. Highlights of the study

With an aim to combat the increasing resistance and persistence of *M. tuberculos*is we have chosen the essential unexploited enzyme named Glutamate racemase (GR). Screened, identified hit , further optimized to get potent derivative (compound **FT_25**) with IC_{50} value 3.97 ± 0.72 µM, MIC = 4.9 µM. In dormant *M. tuberculosis*, it showed a log reduction of 2.7 in the nutrient starvation model and 0.8 in biofilm assay respectively (**Figure 5.38**).

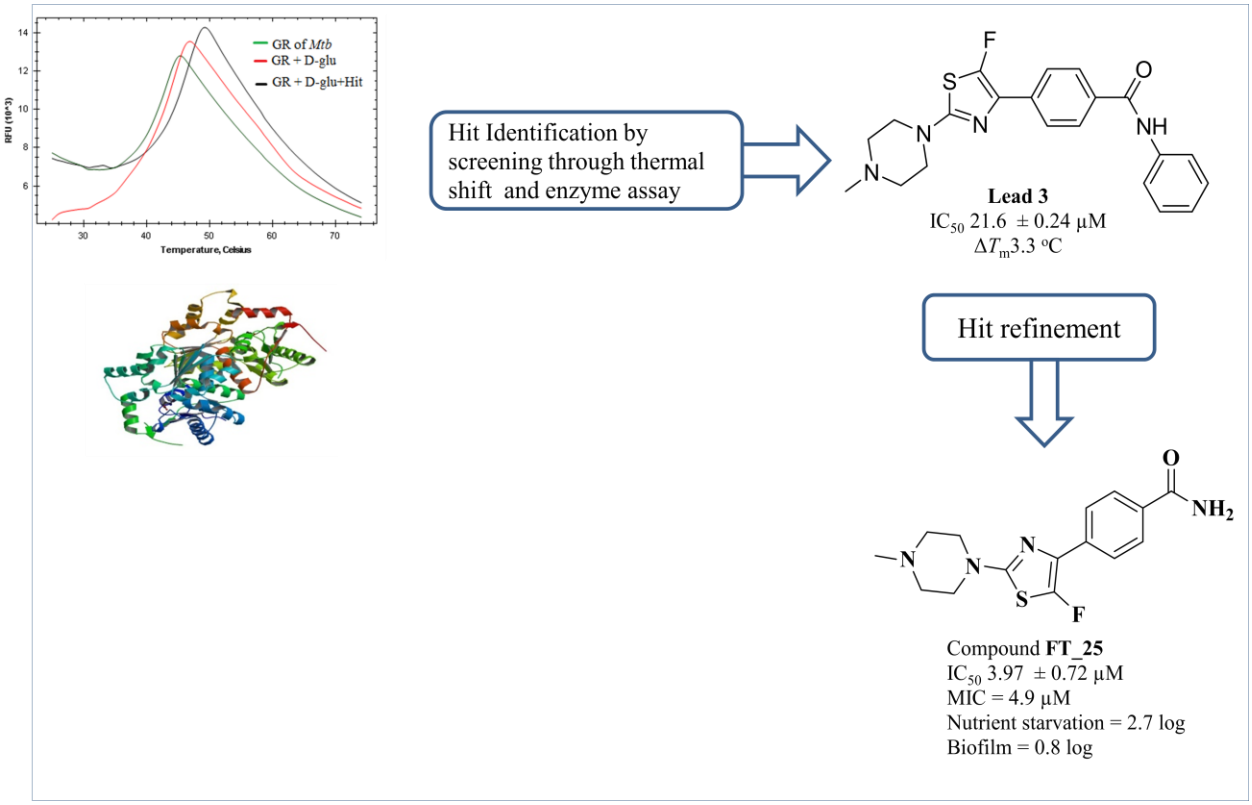

Figure 5.38: Representation of flow of study in identification and developing inhibitors with their structures

5.2.4. Identification and development of substituted oxoquinazoline derivatives as potent *Mycobacterium tuberculosis* Glutamate racemase inhibitors

5.2.4.1. Identification of lead

In the present study, we have done a virtual screening of our in-house database with chemically diverse structures using thermal shift assay to identify the lead inhibiting *M. tuberculosis* GR. A comparison study of T_m revealed that native protein in the absence of D-glu and ligand showed a melt temperature approximately of 43.1 ^oC, whereas with D-glu showed T_m at 44.3 ^oC approximately. Screened compounds showed a varied range of positive and negative shifts in T_m. Of the entire compound library **lead 4** showed a significant shift in melt temperature. When performed along with D-glu, **lead 4** showed T_m with native protein at 46.6 ^oC inferring that its stabilizing capability and interactions with protein is much better than D-glu alone as well as

than rest of the compound library. The screening by enzyme assay also showed good inhibitory activity on GR of *B. subtilis* by **lead 4** with an IC_{50} of 21.45 ±0.58 µM (**Figure 5.39**). Hence we considered **lead 4** to optimize further through synthetic strategies.

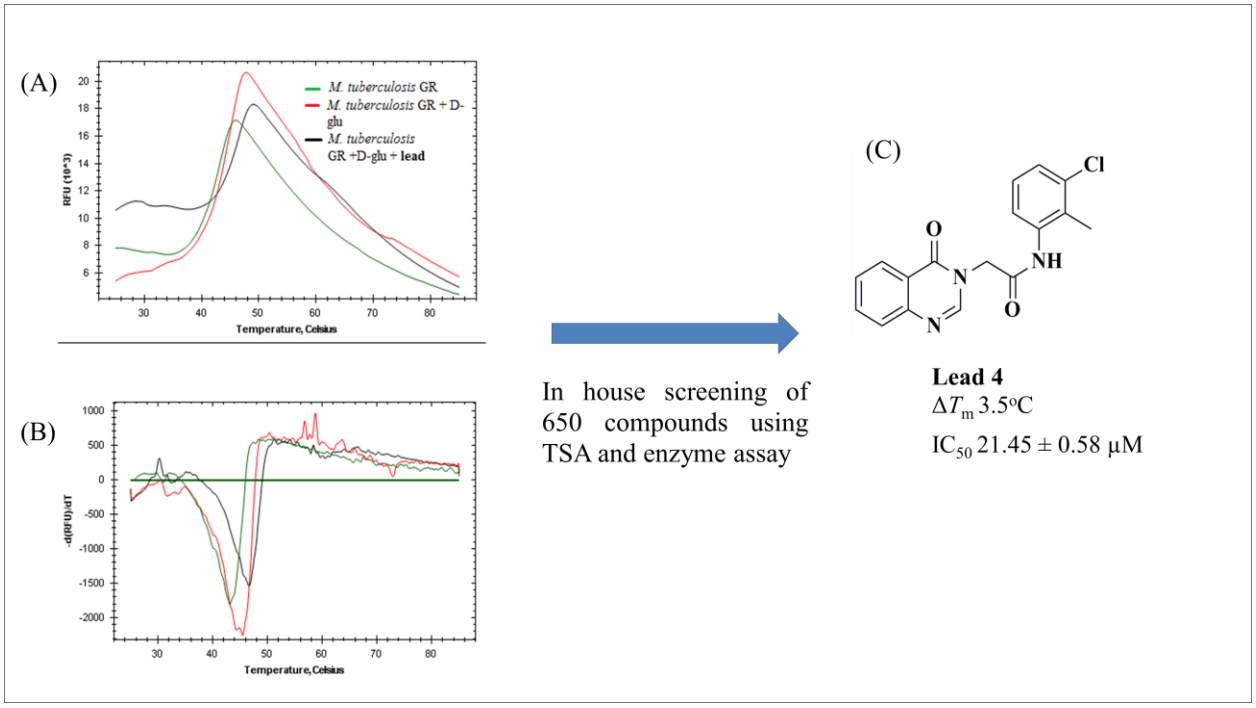

Figure 5.39 (A) DSF plots of a *M. tuberculosis* GR native, with D-glu and **lead 4** (B) represents the plot of derivative fluorescent based signal against temperature; T_m and ΔT_m (shift) can be measured from the minimum of the plot (C) Structure of identified **lead 4** with T_m and IC_{50} value in *B. subtilis*

5.2.4.2. Chemical Synthesis and characterization

The target molecules were achieved by using a simple and straightforward strategy as depicted in **Scheme 5.4-5.6**. It began by condensing commercially available anthranilamide with formamidine acetate in refluxing ethanol as reported by Li F. *et al.* [Li F. *et al.*, 2007]. The condensation reaction went smoothly resulting in the desired quinazolin-4(3*H*)-one in very good yield. 2-methylquinazolin-4(3*H*)-one was prepared by condensing corresponding anthranilic acid with acetic anhydride followed by dehydration with formamide as reported by Ning *et al.* [Ning W. *et al.*, 2013]. Acetyl link was attached to the above-prepared compounds by first treating the corresponding amine with chloroacetyl chloride in presence of triethylamine (TEA) as a base to

give the corresponding 2-chloro-*N*- (aryl)acetamide. The so formed 2-chloro-*N*-(aryl)acetamide was then introduced into the desired quinazolin-4(3*H*)-one/2-methylquinazolin-4(3*H*)-one by alkylation using cesium carbonate (Cs_2CO_3) as a base at 60 °C.

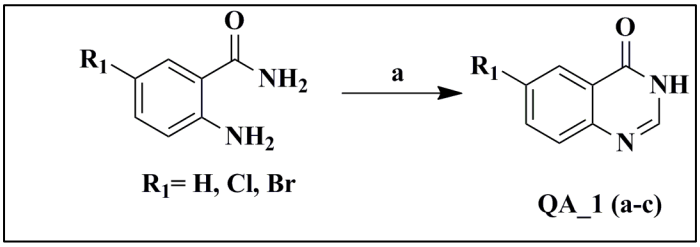

Scheme 5.4: Reagents and Conditions- a)Formamidine acetate, C_2H_5OH, reflux.

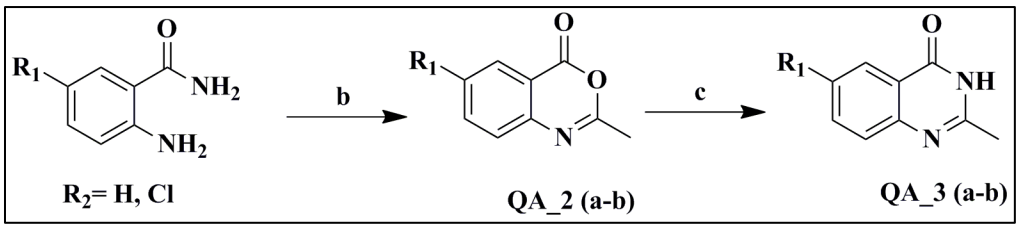

Scheme 5.5: Reagents and Conditions- b) acetic anhydride, reflux c) $HCONH_2$, 130 ^oC.

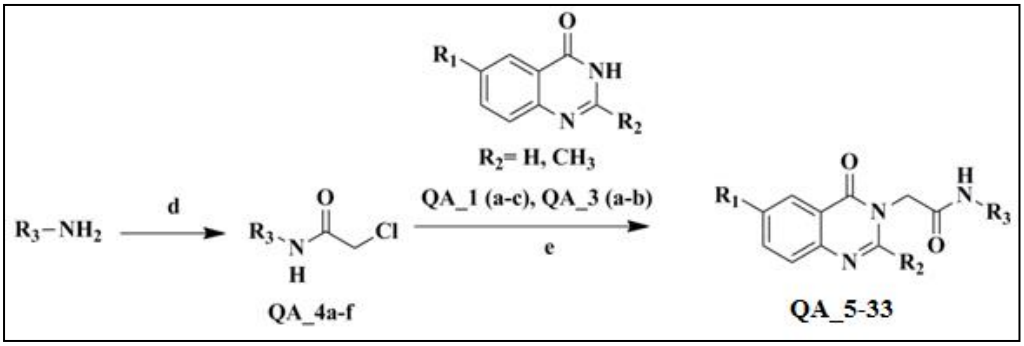

Scheme 5.6: Reagents and Conditions- d) Chloroacetyl chloride, TEA, DMF, 0 ^oC-rt e) Cs_2CO_3, DMF, 60 ^oC.

5.2.4.3. Synthetic protocol used for synthesis

Procedure for the synthesis of Quinazolin-4(3*H*)-ones (QA_1a-c):

Formamidine acetate (2 mmol) was added to a solution mixture of corresponding anthranilamide (1 mmol) in ethanol (30 mL) and refluxed for 6 h. After the reaction has completed solvent was evaporated through vacuum evaporator. The residue was diluted with ethyl acetate and (50 mL)

water (30 mL). The organic layer was collected and dried over anhydrous sodium sulphate followed by evaporation. The residue was purification by silica gel column chromatography using hexane: ethyl acetate (7:3) to give the corresponding quinazolin-4(3*H*)-one (**QA_1a-c**) in good yield.

Procedure for the synthesis of 2-Methyl-4*H*-benzo[*d*][1,3]oxazin-4-ones (QA_2a-b)

Acetic anhydride (15 mL) and corresponding anthranilic acid (1 mmol) solution were refluxed for an hour, followed by ice quenching and evaporation. The residue was washed with ethyl acetate (20 mL) and water (50 mL) and this step was repeated for three times. Organic layers were collected, dried over anhydrous sodium sulphate, filtered, and concentrated. The crude residue was purified by silica gel column chromatography using hexane: ethyl acetate (6:4) as eluent to give the corresponding 2-methyl-4*H*-benzo[*d*][1,3]oxazin-4-one (**QA_2a-b**).

Procedure for the synthesis of 2-Methylquinazolin-4(3*H*)-ones (QA_3a-b)

The mixture of corresponding 2-methyl-4*H*-benzo[*d*][1,3]oxazin-4-one (**QA_2a-b**) (1 mmol) in formamide (15 mL) solution was heated for 7 h at 130 °C. Upon cooling, the solid residue was further washed with water, and recrystallized the product using ethanol to give 2-methylquinazolin-4(3*H*)-one (**QA_3a-b**).

Procedure for the synthesis of 2-Chloro-*N*-(aryl)acetamides (QA_4a-f)

To the solution mixture of different amines (1 mmol) and TEA (3 mmol) in DMF (15 mL), chloroacetyl chloride (2 mmol) was added dropwise at 0 °C. The reaction was carried at for 3 h. Upon completion of the reaction the solvent was evaporated, the residue was further extracted with water (20 mL) and ethyl acetate (30 mL), the organic layer was washed with brine solution (20 mL), dried over anhydrous sodium sulphate and concentrated. The residue was purified by column chromatography using hexane: ethyl acetate (7:3) as eluent to give corresponding 2-chloro-*N*-(aryl)acetamides (**QA_4a-f**).

Procedure for the synthesis of substituted 2-(4-Oxoquinazolin-3(4*H*)-yl)acetamides (QA_5-33)

Anhydrous cesium carbonate (2 mmol) and respective quinazolin-4(3*H*)-one (**QA_1a-c**/ **3a-b**) (1 mmol) were added to the solution of corresponding 2-chloro-*N*-(aryl/heteroaryl)acetamides (**QA_4a-f**) (1.2 mmol) in DMF (3 mL). The reaction was carried at 60 °C for 3 h to complete. The residue was further diluted with water (10 mL) and ethyl acetate (20 mL) and the layers separated. The above extraction step was repeated thrice; the combined organic layers were

washed with brine solution (15 mL), dried over anhydrous sodium sulphate, filtered and evaporated. The residue was purified by silica column chromatography using hexane: ethyl acetate (8:2) to give substituted 2-(4-oxoquinazolin-3(4*H*)-yl)acetamides (**QA_5-33**). The physicochemical properties of synthesized derivatives are shown in **Table 5.12**

Table 5.12: Physicochemical properties of synthesized compounds **QA_5-33**

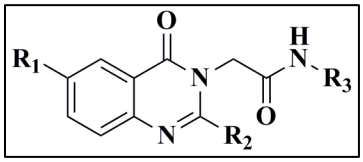

QA_5-33

Compound	R_1	R_2	R_3	Yield (%)	Melting point (^oC)	Molecular formula	Molecular weight
QA_5	Cl	H	2,6-Dimethylphenyl	71.9	239-241	$C_{18}H_{16}ClN_3O_2$	341.79
QA_6	Cl	H	3-Chloro-2-methylphenyl	72.8	212-214	$C_{17}H_{13}Cl_2N_3O_2$	362.13
QA_7	Cl	H	2-Bromophenyl	70.9	260-262	$C_{16}H_{11}BrClN_3O_2$	392.23
QA_8	Cl	H	2,6-Diethylphenyl	73.5	250-252	$C_{20}H_{20}ClN_3O_2$	369.51
QA_9	Cl	H	2-Methyl-4-nitrophenyl	70.4	282-284	$C_{17}H_{13}ClN_4O_4$	372.54
QA_10	Cl	H	4-Chlorophenyl	72.5	221-223	$C_{16}H_{11}Cl_2N_3O_2$	348.26
QA_11	Cl	CH_3	2,6-Dimethylphenyl	75.1	253-255	$C_{19}H_{18}ClN_3O_2$	355.34
QA_12	Cl	CH_3	3-Chloro-2-methylphenyl	78.2	168-170	$C_{18}H_{15}Cl_2N_3O_2$	376.45
QA_13	Cl	CH_3	2-Bromophenyl	70.8	189-191	$C_{17}H_{13}BrClN_3O_2$	406.12

QA_14	Cl	CH_3	2,6-Diethylphenyl	73.8	201-203	$C_{21}H_{22}ClN_3O_2$	383.01
QA_15	Cl	CH_3	2-Methyl-4-nitrophenyl	71.9	245-247	$C_{18}H_{15}ClN_4O_4$	386.13
QA_16	Cl	CH_3	4-Chlorophenyl	70.5	193-195	$C_{17}H_{13}Cl_2N_3O_2$	363.07
QA_17	H	H	2,6-Dimethylphenyl	74.8	212-214	$C_{18}H_{17}N_3O_2$	307.31
QA_18	H	H	2-Bromophenyl	73.6	194-196	$C_{16}H_{12}BrN_3O_2$	358.32
QA_19	H	H	2,6-Diethylphenyl	72.8	256-258	$C_{20}H_{21}N_3O_2$	333.40
QA_20	H	H	2-Methyl-4-nitrophenyl	69.8	243-245	$C_{17}H_{14}N_4O_4$	338.15
QA_21	H	H	4-Chlorophenyl	75.9	236-238	$C_{16}H_{12}ClN_3O_2$	312.53
QA_22	H	CH_3	2,6-Dimethylphenyl	80.3	210-212	$C_{19}H_{19}N_3O_2$	321.25
QA_23	H	CH_3	3-Chloro-2-methylphenyl	78.2	198-200	$C_{18}H_{16}ClN_3O_2$	342.17
QA_24	H	CH_3	2-Bromophenyl	77.9	242-244	$C_{17}H_{14}BrN_3O_2$	371.27
QA_25	H	CH_3	2,6-Diethylphenyl	73.7	235-237	$C_{21}H_{23}N_3O_2$	349.11
QA_26	H	CH_3	2-Methyl-4-nitrophenyl	76.2	270-272	$C_{18}H_{16}N_4O_4$	352.26
QA_27	H	CH_3	4-Chlorophenyl	78.6	237-239	$C_{17}H_{14}ClN_3O_2$	327.13
QA_28	Br	H	2,6-Dimethylphenyl	79.5	241-243	$C_{18}H_{16}BrN_3O_2$	386.43
QA_29	Br	H	3-Chloro-2-methylphenyl	72.1	215-217	$C_{17}H_{13}BrClN_3O_2$	406.66
QA_30	Br	H	2-Bromophenyl	78.3	280-282	$C_{16}H_{11}Br_2N_3O_2$	437.54

QA_31	Br	H	2,6-Diethylphenyl	77.4	271-273	$C_{20}H_{20}BrN_3O_2$	415.64
QA_32	Br	H	2-Methyl-4-nitrophenyl	75.4	189-191	$C_{18}H_{15}BrN_4O_4$	431.29
QA_33	Br	H	4-Chlorophenyl	73.8	178-180	$C_{17}H_{13}BrClN_3O_2$	406.48

5.2.4.4. Characterization of synthesized compounds

Both analytical and spectral data (^{1}H NMR, ^{13}C NMR, and mass spectra) of all the synthesized compounds were in full agreement with the proposed structures.

Quinazolin-4(3*H*)-one (QA_1a): The compound was synthesized according to the above general procedure using anthranilamide (2.0 g, 14.68 mmol) and formamidine acetate (3.05 g, 29.37 mmol) to afford **QA_1a** (1.95 g, 90.7 %) as white solid. ^{1}H NMR (400 MHz, DMSO-d_6): δ 9.48 (s, 1H), 8.64 (s, 1H), 8.23-8.21 (d, *J*= 8Hz, 1H), 8.03-8.00 (t, *J*= 12Hz, 1H), 7.82-7.80 (d, *J*= 8Hz, 1H), 7.61-7.58 (t, *J*= 12Hz, 1H). ^{13}C NMR (100 MHz, DMSO-d_6): δ 163.2, 152.3, 147.9, 136.1, 130.7, 127.3, 118.9. MS (ESI) *m/z* 147 $[M+H]^+$. Anal calcd for $C_8H_6N_2O$: C, 65.75; H, 4.14; N, 19.17 Found C, 65.68; H, 4.13; N, 19.15.

6-Chloroquinazolin-4(3*H*)-one (QA_1b): The compound was synthesized according to the above general procedure using 2-amino-5-chlorobenzamide (2.0 g, 11.72 mmol) and formamidine acetate (2.44 g, 23.44 mmol) to afford **QA_1b** (1.87 g, 88.6 %) as off white solid. ^{1}H NMR (400 MHz, DMSO-d_6): δ 9.62 (s, 1H), 8.72 (s, 1H), 8.32 (s, 1H), 8.10-8.02 (d, *J*= 8Hz, 1H), 7.88-7.86 (d, *J*= 8Hz, 1H). ^{13}C NMR (100 MHz, DMSO-d_6): δ163.9, 153.1, 148.5, 140.1, 132.8, 129.5, 123.1, 119.7. MS (ESI) *m/z* 181 $[M+H]^+$. Anal calcd for $C_8H_5ClN_2O$: C, 53.21; H, 2.79; N, 15.51 Found C, 53.34; H, 2.80; Cl, N, 15.53.

6-Bromoquinazolin-4(3*H*)-one (QA_1c): The compound was synthesized according to the above general procedure using 2-amino-5-bromobenzamide (2.0 g, 15.92 mmol) and formamidine acetate (2.44 g, 23.44 mmol) to afford **QA_1c** (1.89 g, 91.2%) as white solid. ^{1}H NMR (400 MHz, DMSO-d_6): δ 9.73 (s, 1H), 8.60 (s, 1H), 8.35 (s, 1H), 8.22-8.20 (d, *J*= 8Hz, 1H), 7.89-7.87 (d, *J*= 8Hz, 1H). ^{13}C NMR (100 MHz, DMSO-d_6): δ 166.9, 151.5, 147.7, 132.9,

130.7, 127.1, 124.8, 121.6. MS (ESI) *m/z* 226 $[M+H]^+$. Anal calcd for $C_8H_5BrN_2O$: C, 42.70; H, 2.24; N, 12.45 Found C, 42.79; H, 2. 23; N, 12.47.

2-Methyl-4H-benzo[*d*][1,3]oxazin-4-one (QA_2a): The compound was synthesized according to the general procedure using anthranilic acid (2.0 g, 14.58 mmol) to afford **QA_2a** (1.84 g, 78.4 %) as white solid. ^{1}H NMR (400 MHz, DMSO-d_6): δ 8.19-8.17 (d, *J*= 8Hz, 1H), 7.94- 7.91 (t, *J*= 12Hz, 1H), 7.77-7.75 (d, *J*= 8Hz, 1H), 7.58-7.55 (t, *J*= 12Hz, 1H), 2.63 (s, 3H). ^{13}C NMR (100 MHz, DMSO-d_6): δ 166.2, 161.7, 148.3, 137.1, 130.9, 129.3, 126.7, 117.8, 27.9. MS (ESI) *m/z* 162 $[M+H]^+$. Anal calcd for $C_9H_7NO_2$: C, 67.07; H, 4.38; N, 8.69 Found C, 67.18; H, 4.37; N, 8.68.

6-Chloro-2-methyl-4H-benzo[*d*][1,3]oxazin-4-one (QA_2b): The compound was synthesized according to the general procedure using 2-amino-5-chlorobenzoic acid (2.0 g, 11.65 mmol) to afford **QA_2b** (1.74 g, 76.7 %) as white solid. ^{1}H NMR (400 MHz, DMSO-d_6): δ 8.38 (s, 1H), 8.21-8.19 (d, J= 8Hz, 1H), 7.98-7.96 (d, J= 8Hz, 1H), 2.63 (s, 3H). ^{13}C NMR (100 MHz, DMSO-d_6): δ 161.2 (2C), 144.7, 137.3, 1131.9 (2C), 129.9, 115.1, 27.3. MS (ESI) *m/z* 196 $[M+H]^+$. Anal calcd for $C_9H_6ClNO_2$: C, 55.26; H, 3.09; N, 7.16 Found C, 55.82; H, 3.73; N, 7.01.

2-Methylquinazolin-4(3*H*)-one (QA_3a): The compound was synthesized according to the general procedure using 2-methyl-4*H*-benzo[*d*][1,3]oxazin-4-one (**QA_2a**) (1.6 g, 9.98 mmol) to afford **QA_13a** (1.31 g, 82.8 %) as white solid. ^{1}H NMR (400 MHz, DMSO-d_6): δ 9.49 (s, 1H), 8.23-8.21 (d, *J*= 8Hz, 1H), 8.08- 8.05 (t, *J*= 12Hz, 1H), 7.75-7.73 (d, *J*= 8Hz, 1H), 7.62-7.59 (t, *J*= 12Hz, 1H), 2.58 (s, 3H). ^{13}C NMR (100 MHz, DMSO-d_6): δ 163.7, 156.1, 147.3, 136.4, 128.5 (2C), 121.9, 23.7. MS (ESI) *m/z* 161 $[M+H]^+$. Anal calcd for $C_9H_8N_2O$: C, 67.49; H, 5.03; N, 17.49 Found C, 67.54; H, 5.02; N, 17.51.

6-Chloro-2-methylquinazolin-4(3*H*)-one (QA_3b): The compound was synthesized according to the general procedure using 6-chloro-2-methyl-4*H*-benzo[*d*][1,3]oxazin-4-one (**QA_2b**) (1.6 g, 8.22 mmol) to afford **QA_3b** (1.31 g, 82.7 %) as white solid. ^{1}H NMR (400 MHz, DMSO-d_6): δ 9.37 (s,1H), 8.42 (s, 1H), 8.25-8.23 (d, *J*= 8Hz, 1H), 7.93-7.91 (d, *J*= 8Hz, 1H), 2.49 (s, 3H). ^{13}C NMR (100 MHz, DMSO-d_6): δ 164.2, 153.9, 149.1, 133.7 (2C), 128.9 (2C), 120.7, 23.2. MS (ESI) *m/z* 195 $[M+H]^+$. Anal calcd for $C_9H_7ClN_2O$: C, 55.54; H, 3.63; N, 14.39 Found C, 55.59; H, 3.64; N, 14.37.

2-Chloro-N-(2,6-dimethylphenyl)acetamide (QA_4a): The compound was synthesized according to the general procedure using chloroacetyl chloride (1.55 g, 13.77 mmol) and 2,6-dimethylphenyl amine (1.0 g, 7.2 mmol) to afford **QA_4a** (1.08 g, 68.7 %) as white solid. ^{1}H NMR (400 MHz, DMSO-d_6): δ 2.23 (s, 6H), 4.23 (s, 2H), 9.89 (s, 1H), 7.09-6.99 (m, 3H). ^{13}C NMR (100 MHz, DMSO-d_6): δ 167.2, 142.7, 131.9 (2C), 129.3 (2C), 127.1, 45.3, 18.3 (2C). MS (ESI) *m/z* 198 $[M+H]^+$. Anal calcd for $C_{10}H_{12}NO$: C, 60.76; H, 6.12; N, 7.09 Found C, 60.69; H, 6.11; N, 7.10.

2-Chloro-N-(3-chloro-2-methylphenyl)acetamide (QA_4b): The compound was synthesized according to the general procedure using chloroacetyl chloride (1.55 g, 13.77 mmol) and 3-chloro-2-methylphenyl amine (1.2g, 6.9 mmol) to afford **QA_4b** (1.2 g, 71.2 %) as white solid. ^{1}H NMR (400 MHz, DMSO-d_6): δ 9.95 (s, 1H), 4.42 (s, 2H), 2.31 (s, 3H), 7.15-7.09 (m, 3H). ^{13}C NMR (100 MHz, DMSO-d_6): δ 167.3, 140.1, 136.2 (2C), 129.5, 125.7, 115.1, 45.4, 16.3. MS (ESI) *m/z* 219 $[M+H]^+$. Anal calcd for $C_9H_9Cl_2NO$: C, 49.57; H, 4.16; N, 6.42 Found C, 49.51; H, 4.15; N, 6.41.

N-(2-Bromophenyl)-2-chloroacetamide (QA_4c): The compound was synthesized according to the general procedure using chloroacetyl chloride (1.55 g, 13.77 mmol) and 2-bromophenyl amine (1.2g, 7.4 mmol) to afford **QA_4c** (1.15 g, 70.2 %) as white solid. ^{1}H NMR (400 MHz, DMSO-d_6): δ 9.98 (s, 1H), 4.38 (s, 2H), 8.29-8.27 (d, *J*= 8Hz, 1H), 8.15-8.13 (d, *J*=8Hz, 1H), 7.79-7.76 (t, *J*=12Hz, 1H), 7.58-7.55 (t, *J*=12Hz, 1H). ^{13}C NMR (100 MHz, DMSO-d_6): δ 167.5, 140.5, 132.7 (2C), 129.1, 127.3, 119.7, 43.5. MS (ESI) *m/z* 249 $[M+H]^+$. Anal calcd for $C_8H_7BrClNO$: C, 38.67; H, 2.84; N, 5.64 Found C, 38.64; H, 2.84; N, 5.65.

2-Chloro-N-(2,6-diethylphenyl)acetamide (QA_4d): The compound was synthesized according to the general procedure using chloroacetyl chloride (1.55 g, 13.77 mmol) and 2,6-diethylphenyl amine (1.2g, 7.8 mmol) to afford **QA_4d** (1.3 g, 71.4 %) as white solid. ^{1}H NMR (400 MHz, DMSO-d_6): δ 9.72 (s, 21H), 7.75-7.69 (m, 3H), 4.49 (s, 2H), 2.92-2.85 (m, 4H), 1.72-1.65 (m, 6H). ^{13}C NMR (100 MHz, DMSO-d_6): δ 167.3, 135.8, 131.2(2C), 125.3, 123.2, 43.9, 25.6 (2C), 14.8 (2C). MS (ESI) *m/z* 226 $[M+H]^+$. Anal calcd for $C_{12}H_{16}ClNO$: C, 63.85; H, 7.14; N, 6.21 Found C, 63.87; H, 7.13; N, 6.20.

2-Chloro-N-(2-methyl-4-nitrophenyl)acetamide (QA_4e): The compound was synthesized according to the general procedure using chloroacetyl chloride (1.55 g, 13.77 mmol) and 2-methyl-4-nitrophenyl amine (1.1g, 8.2 mmol) to afford **QA_4e** (1.4g, 75.4 %) as pale yellow

solid. ^{1}H NMR (400 MHz, DMSO-d_6): δ 9.82 (s, 1H), 8.53 (s, 1H), 8.12-8.10 (d, *J*= 8Hz, 1H), 7.96-7.94 (d, *J*= 8Hz, 1H), 4.52 (s, 2H), 2.34 (s, 3H). ^{13}C NMR (100 MHz, DMSO-d_6): δ 167.8, 145.7, 142.1, 139.4, 127.4, 123.5, 110.9, 43.1, 17.7. MS (ESI) *m/z* 229 $[M+H]^+$. Anal calcd for $C_9H_9ClN_2O_3$: C, 63.85; H, 7.14; N, 6.21 Found C, 63.79; H, 7.15; N, 6.22.

2-Chloro-N-(4-chlorophenyl)acetamide (QA_4f): The compound was synthesized according to the general procedure using chloroacetyl chloride (1.55 g, 13.77 mmol) and 4-chlorophenyl amine (1.3g, 7.8 mmol) to afford **QA_4f** (1.3g, 74.2 %) as off white solid. ^{1}H NMR (400 MHz, DMSO-d_6): δ 9.81 (s, 1H), 7.89-7.75 (m, 4H), 4.51 (s, 2H). ^{13}C NMR (100 MHz, DMSO-d_6): δ 167.1, 137.4, 134.2, 130.4 (2C), 121.7 (2C), 44.3. MS (ESI) *m/z* 205 $[M+H]^+$. Anal calcd for $C_8H_7Cl_2NO$: C, 47.09; H, 3.46; N, 6.86 Found C, 47.14; H, 3.45; N, 6.84.

2-(6-Chloro-4-oxoquinazolin-3(4*H*)-yl)-N-(2,6-dimethylphenyl)acetamide (QA_5): The compound was synthesized according to the general procedure using 2-chloro-N-(2,6-dimethylphenyl)acetamide (**QA_4a**) (0.16 g, 0.75 mmol) and 6-Chloroquinazolin-4(3*H*)-one (**QA_1b**) (0.1 g, 0.68 mmol) to afford **QA_5** (0.15 g, 71.9 %) as white solid. M.p: 239-241 ^{o}C. ^{1}H NMR (400 MHz, DMSO-d_6): δ 9.82 (s, 1H), 8.56 (s, 1H), 8.42 (s, 1H), 8.23-8.21 (d, *J*=8Hz, 1H), 8.07-8.05 (d, *J*=8Hz, 1H), 7.07-6.98 (m, 3H), 4.97 (s, 2H), 2.21 (s, 6H). ^{13}C NMR (100 MHz, DMSO-d_6): δ 169.2, 160.5, 150.1, 147.5, 138.3, 135.2(2C), 131.2(2C), 129.1(4C), 126.4, 120.8, 52.5, 19.6(2C). MS (ESI) *m/z* 343 $[M+H]^+$. Anal calcd for $C_{18}H_{16}ClN_3O_2$: C, 63.25; H, 4.72; N, 12.29; Found C, 63.22; H, 4.73; N, 12.27.

N-(3-Chloro-2-methylphenyl)-2-(6-chloro-4-oxoquinazolin-3(4*H*)-yl)acetamide (QA_6): The compound was synthesized according to the general procedure using 2-chloro-N-(3-chloro-2-methylphenyl)acetamide (**QA_4b**) (0.18 g, 0.71 mmol) and 6-Chloroquinazolin-4(3*H*)-one (**QA_1b**) (0.1 g, 0.68 mmol) to afford **QA_6** (0.15 g, 72.8 %) as white solid. M.p: 212-214 ^{o}C. ^{1}H NMR (400 MHz, DMSO-d_6): δ 9.93 (s, 1H), 8.59 (s, 1H), 8.38 (s, 1H), 8.22-8.20 (d, *J*= 8Hz, 1H), 8.03-8.01 (d, *J*= 8Hz, 1H), 7.10-7.05 (m, 3H), 4.99 (s, 2H), 2.25 (s, 3H). ^{13}C NMR (100 MHz, DMSO-d_6): δ 170.5, 160.3, 149.4, 146.4, 140.1, 137.3(2C), 134.4(2C), 129.7(3C), 124.9, 121.8, 112.5, 46.2, 14.3. MS (ESI) *m/z* 363 $[M+H]^+$. Anal calcd for $C_{17}H_{13}Cl_2N_3O_2$: C, 56.37; H, 3.62; N, 11.60 Found C, 56.41; H, 3.61; N, 11.58.

N-(2-Bromophenyl)-2-(6-chloro-4-oxoquinazolin-3(4*H*)-yl)acetamide (QA_7): The compound was synthesized according to the general procedure using 2-chloro-N-(2-bromophenyl)acetamide (**QA_4c**) (0.18 g, 0.77 mmol) and 6-Chloroquinazolin-4(3*H*)-one

(**QA_1b**) (0.1 g, 0.68 mmol) to afford **QA_7** (0.12 g, 70.9 %) as white solid. M.p: 260-262 ^{o}C. ^{1}H NMR (400 MHz, DMSO-d_6): δ 9.97 (s, 1H), 8.56 (s, 1H), 8.40 (s, 1H), 8.26-8.24 (d, *J*= 8Hz, 1H), 8.21-8.19 (d, J= 8Hz, 1H), 8.12-8.10 (d, *J*= 8Hz, 1H), 7.90-7.89 (t, *J*= 12Hz, 1H), 7.70-7.68 (d, *J*=8Hz, 1H), 7.61-7.59 (t, *J*=12Hz, 1H), 4.87 (s, 2H). ^{13}C NMR (100 MHz, DMSO-d_6): δ 170.3, 160.7, 148.2 (2C), 135.2, 131.5 (2C), 129.5 (2C), 126.9 (3C), 126.2, 123.5, 119.5, 49.2. MS (ESI) *m/z* 393 $[M+H]^+$. Anal calcd for $C_{16}H_{11}BrClN_3O_2$: C, 48.94; H, 2.82; N, 10.70 Found C, 48.99; H, 2.82; N, 10.72.

2-(6-Chloro-4-oxoquinazolin-3(4*H*)-yl)-N-(2,6-diethylphenyl)acetamide (QA_8): The compound was synthesized according to the general procedure using 2-chloro-N-(2,6-diethylphenyl)acetamide (**QA_4d**) (0.16 g, 0.72 mmol) and 6-Chloroquinazolin-4(3*H*)-one (**QA_1b**) (0.1 g, 0.68 mmol) to afford **QA_8** (0.15 g, 73.5%) as off-white solid. M.p: 250-252 ^{o}C. ^{1}H NMR (400 MHz, DMSO-d_6): δ 10.01 (s,1H), 8.61 (s, 1H), 8.19-8.17 (d, *J*= 8Hz, 1H), 8.07 (s, 1H), 7.97-9.75 (d, *J*=8Hz, 1H), 7.72-7.65 (m, 3H), 4.52 (s, 2H), 2.89-2.82 (m, 4H), 1.5-1.42 (m, 4H). ^{13}C NMR (100 MHz, DMSO-d_6): δ 170.1, 160.7, 147.3, 146.1, 135.2 (2C), 132.5, 130.3 (2C), 127.1 (2C), 123.5, 122.3 (3C), 52.7, 24.7 (2C), 15.7 (2C). MS (ESI) *m/z* 370 $[M+H]^+$. Anal calcd for $C_{20}H_{20}ClN_3O_2$: C, 64.95; H, 5.45; N, 11.36 Found C, 64.91; H, 5.44; N, 11.35.

2-(6-Chloro-4-oxoquinazolin-3(4*H*)-yl)-N-(2-methyl-4-nitrophenyl)acetamide (QA_9): The compound was synthesized according to the general procedure using 2-chloro-N-(2-methyl-4-nitrophenyl)acetamide (**QA_4e**) (0.15 g, 0.78 mmol) and 6-Chloroquinazolin-4(3*H*)-one (**QA_1b**) (0.1 g, 0.68 mmol) to afford **QA_9** (0.17 g, 70.4%) as pale yellow solid. M.p: 282-284 ^{o}C. ^{1}H NMR (400 MHz, DMSO-d_6): δ 10.03 (s, 1H), 8.53 (s, 1H), 8.34 (s, 1H), 8.33-8.31 (d, *J*=8Hz, 1H), 8.24 (s, 1H), 8.10-8.08 (d, *J*= 8Hz, 1H), 8.03-8.01 (d, *J*= 8Hz, 1H), 7.77-7.75 (d, *J*= 8Hz, 1H), 4.52 (s, 2H), 2.32 (s, 3H). ^{13}C NMR (100 MHz, DMSO-d_6): δ 169.4, 162.3, 148.9, 146.5, 144.7, 143.8, 141.6, 133.9(2C), 129.5 (2C), 125.5, 121.5 (2), 110.2, 52.3, 18.9. MS (ESI) *m/z* 373$[M+H]^+$. Anal calcd for $C_{17}H_{13}ClN_4O_4$: C, 54.78; H, 3.52; N, 15.03 Found C, 54.81; H, 3.51; N, 15.04.

2-(6-Chloro-4-oxoquinazolin-3(4*H*)-yl)-N-(4-chlorophenyl)acetamide (QA_10): The compound was synthesized according to the general procedure using 2-chloro-N-(4-chlorophenyl)acetamide (**QA_4f**) (0.16 g, 0.76 mmol) and 6-Chloroquinazolin-4(3*H*)-one (**QA_1b**) (0.1 g, 0.68 mmol) to afford **QA_10** (0.18 g, 72.5%) as off-white solid. M.p: 221-223

^{o}C. ^{1}H NMR (400 MHz, DMSO-d_6): δ 9.95 (s, 1H), 8.58 (s, 1H), 8.29 (s, 1H), 8.23-8.21 (d, *J*=8Hz, 1H), 8.06-8.04 (d, *J*=8Hz, 1H), 7.73-7.68 (m, 4H), 4.48 (s, 2H). ^{13}C NMR (100 MHz, DMSO-d_6): δ 170.7, 162.3, 149.2, 147.4, 137.2, 134.3 (2C), 129.3 (2C), 126.9 (2C), 123.5, 120.6 (2C), 52.3. MS (ESI) *m/z* 349[M+H]$^{+}$. Anal calcd for $C_{16}H_{11}Cl_2N_3O_2$: C, 55.19; H, 3.18; N, 12.07 Found C, 55.69; H, 3.90; N, 12.18.

2-(6-Chloro-2-methyl-4-oxoquinazolin-3(4*H*)-yl)-N-(2,6-dimethylphenyl)acetamide (QA_11): The compound was synthesized according to the general procedure using 2-chloro-N-(2,6-dimethylphenyl)acetamide (**QA_4a**) (0.13 g, 0.76 mmol) and 6-chloro-2-methylquinazolin-4(3*H*)-one (**QA_3b**) (0.14 g, 0.70 mmol) to afford **QA_11** (0.17 g, 75.1%) as white solid. M.p: 253-255 ^{o}C. ^{1}H NMR (400 MHz, DMSO-d_6): δ 9.69 (s, 1H), 8.41 (s, 1H), 8.25-8.23 (d, *J*= 8, 1H), 8.02-8.00 (d, *J*= 8Hz, 1H), 7.12 (m, 3H), 4.62 (s, 2H), 2.63 (s, 3H), 2.09 (s, 6H). ^{13}C NMR (100 MHz, DMSO-d_6): δ 170.3, 162.8, 155.5, 147.4, 138.3, 133.7 (2C), 131.2 (2C), 126.5 (4C), 125.1, 120.3, 52.4, 22.3, 17.9. MS (ESI) *m/z* 356[M+H]$^{+}$. Anal calcd for $C_{19}H_{18}ClN_3O_2$: C, 64.91; H, 5.10; N, 11.81 Found C, 64.97; H, 5.11; N, 11.83.

2-(6-Chloro-2-methyl-4-oxoquinazolin-3(4*H*)-yl)-N-(3-chloro-2-methylphenyl)acetamide (QA_12): The compound was synthesized according to the general procedure using 2-chloro-N-(3-chloro-2-methylphenyl)acetamide (**QA_4b**) (0.12 g, 0.79 mmol) and 6-chloro-2-methylquinazolin-4(3*H*)-one (**QA_3b**) (0.14 g, 0.70 mmol) to afford **QA_12** (0.18 g, 78.2%) as white solid. M.p: 168-170 ^{o}C. ^{1}H NMR (400 MHz, DMSO-d_6): δ 9.89 (s, 1H), 8.61 (s, 1H), 8.32-8.30 (d, *J*= 8Hz, 1H), 8.08-8.06 (d, *J*=8Hz, 1H), 7.81-7.77 (m, 3H), 4.56 (s, 2H), 2.62 (s, 3H), 2.25 (s, 3H). ^{13}C NMR (100 MHz, DMSO-d_6): δ 169.7, 162.3, 155.9, 147.2, 138.6, 135.3, 134.7 (2C), 132.3, 125.8 (3C), 124.7, 123.1, 112.9, 52.3, 20.1, 15.3. MS (ESI) *m/z* 377[M+H]$^{+}$. Anal calcd for $C_{18}H_{15}Cl_2N_3O_2$: C, 57.46; H, 4.02; N, 11.17 Found C, 57.38; H, 4.03; N, 11.15.

N-(2-Bromophenyl)-2-(6-chloro-2-methyl-4-oxoquinazolin-3(4*H*)-yl)acetamide (QA_13): The compound was synthesized according to the general procedure using 2-chloro-N-(2-bromophenyl)acetamide (**QA_4c**) (0.12 g, 0.73 mmol) and 6-chloro-2-methylquinazolin-4(3*H*)-one (**QA_3b**) (0.14 g, 0.70 mmol) to afford **QA_13** (0.13 g, 70.8%) as white solid. M.p: 189-191 ^{o}C. ^{1}H NMR (400 MHz, DMSO-d_6): δ 10.11 (s, 1H), 8.61 (s, 1H), 8.29-8.27 (d, *J*=8Hz, 1H), 7.63-7.58 (m, 4H), 4.58 (s, 2H), 2.56 (s, 3H). ^{13}C NMR (100 MHz, DMSO-d_6): δ 167.9, 161.2, 156.7, 146.3, 139.8, 133.6 (2C), 131.7 (2C), 126.9 (3C), 125.1, 121.3, 119.2, 53.2, 23.5. MS

(ESI) *m/z* 407[M+H]$^+$. Anal calcd for $C_{17}H_{13}BrClN_3O_2$: C, 50.21; H, 3.22; N, 10.33 Found C, 50.17; H, 3.21; N, 10.31.

2-(6-Chloro-2-methyl-4-oxoquinazolin-3(4*H*)-yl)-N-(2,6-diethylphenyl)acetamide (QA_14): The compound was synthesized according to the general procedure using 2-chloro-N-(2,6-diethylphenyl)acetamide (**QA_4d**) (0.13 g, 0.75 mmol) and 6-chloro-2-methylquinazolin-4(3*H*)-one (**QA_3b**) (0.14 g, 0.70 mmol) to afford **QA_14** (0.13 g, 73.8%) as white solid. M.p: 201-203 ^{o}C. ^{1}H NMR (400 MHz, DMSO-d_6): δ 10.07 (s, 1H), 8.57 (s, 1H), 8.25-8.23 (d, *J*=8Hz, 1H), 8.06-8.04 (d, J= 8Hz, 1H), 7.79-7.72 (m, 3H), 4.57 (s, 2H), 2.64 (m, 6H), 2.53 (s, 3H), 1.32 (m, 6H). ^{13}C NMR (100 MHz, DMSO-d_6): δ 169.2, 162.9, 155.5, 141.7, 135.6, 133.7 (2C), 130.2 (2C), 125.6 (2C), 123.5, 121.8 (2C), 53.8, 25.2 (2C), 21.7 17.3 (2C). MS (ESI) *m/z* 384[M+H]$^+$. Anal calcd for $C_{21}H_{22}ClN_3O_2$: C, 65.71; H, 5.78; N, 10.95 Found C, 65.66; H, 5.77; N, 10.97.

2-(6-Chloro-2-methyl-4-oxoquinazolin-3(4*H*)-yl)-N-(2-methyl-4-nitrophenyl)acetamide (QA_15): The compound was synthesized according to the general procedure using 2-chloro-N-(2-methyl-4-nitrophenyl)acetamide (**QA_4e**) (0.14 g, 0.82 mmol) and 6-chloro-2-methylquinazolin-4(3*H*)-one (**QA_3b**) (0.14 g, 0.70 mmol) to afford **QA_15** (0.13 g, 71.9 %) as yellow solid. M.p: 245-247 ^{o}C. ^{1}H NMR (400 MHz, DMSO-d_6): δ 10.07 (s,1H), 8.62 (s, 1H), 8.32 (s, 1H), 8.10-7.96 (m, 4H), 4.71(s, 2H), 2.61 (s, 3H), 2.09 (s, 3H). ^{13}C NMR (100 MHz, DMSO-d_6): δ 169.9, 160.3, 155.6, 146.2, 142.7, 141.5, 136.7, 132.4 (2C), 125.9 (2C), 124.3, 121.5 (2C), 108.5, 47.2, 23.3, 16.5. MS (ESI) *m/z* 387[M+H]$^+$. Anal calcd for $C_{18}H_{15}ClN_4O_4$: C, 55.89; H, 3.91; N, 14.49 Found C, 55.77; H, 3.90; N, 14.47.

2-(6-Chloro-2-methyl-4-oxoquinazolin-3(4*H*)-yl)-N-(4-chlorophenyl)acetamide (QA_16): The compound was synthesized according to the general procedure using 2-chloro-N-(4-chlorophenyl)acetamide (**QA_4f**) (0.14 g, 0.78 mmol) and 6-chloro-2-methylquinazolin-4(3*H*)-one (**QA_3b**) (0.14 g, 0.70 mmol) to afford **QA_16** (0.13 g, 70.5 %) as white solid. M.p: 193-195 ^{o}C. ^{1}H NMR (400 MHz, DMSO-d_6): δ 9.82 (s, 1H), 8.58 (s, 1H), 8.25-8.23 (d, *J*= 8Hz, 1H), 8.10-8.08 (d, *J*= 8Hz, 1H), 7.75-7.68 (m, 4H), 4.52 (s, 2H), 2.64 (s, 3H). ^{13}C NMR (100 MHz, DMSO-d_6): δ 169.3, 160.9, 155.5, 146.2, 137.3, 133.8 (3C), 129.7 (2C), 127.2 (2C), 122.3, 119.3 (2C), 53.5, 24.3. MS (ESI) *m/z* 363[M+H]$^+$. Anal calcd for $C_{17}H_{13}Cl_2N_3O_2$: C, 56.37; H, 3.62; N, 11.60 Found C, 56.27; H, 3.61; N, 11.62.

N-(2,6-Dimethylphenyl)-2-(4-oxoquinazolin-3(4*H*)-yl)acetamide (QA_17): The compound was synthesized according to the general procedure using 2-chloro-N-(2,6-

dimethylphenyl)acetamide (**QA_4a**) (0.13 g, 0.75 mmol) and quinazolin-4(3*H*)-one (**QA_1a**) (0.15 g, 0.67 mmol) to afford **QA_17** (0.14 g, 74.8 %) as off-white solid. M.p: 212-214 ^{o}C. ^{1}H NMR (400 MHz, DMSO-d_6): δ 10.01 (s, 1H), 8.63 (s, 1H), 8.21-8.19 (d, *J*= 8Hz, 1H), 7.89-7.86 (t, *J*=12Hz, 1H), 7.71-7.69 (d, *J*=8Hz, 1H), 7.58-7.55 (t, *J*= 12Hz, 1H), 7.009-6.95 (m, 3H), 4.51 (s, 2H), 2.13 (s, 6H). ^{13}C NMR (100 MHz, DMSO-d_6): δ 170.1, 160.8, 149.5 (2C), 138.6, 133.9, 131.3(2C), 128.4 (2C), 126.7 (4C), 121.3, 53.1, 18.5 (2C). MS (ESI) *m/z* 308[M+H]$^{+}$. Anal calcd for $C_{18}H_{17}N_3O_2$: C, 70.34; H, 5.58; N, 13.67 Found C, 70.15; H, 5.59; N, 13.69.

N-(2-Bromophenyl)-2-(4-oxoquinazolin-3(4*H*)-yl)acetamide (QA_18): The compound was synthesized according to the general procedure using 2-chloro-N-(2-bromophenyl)acetamide (**QA_4c**) (0.14 g, 0.73 mmol) and quinazolin-4(3*H*)-one (**QA_1a**) (0.15 g, 0.67 mmol) to afford **QA_18** (0.13 g, 73.6 %) as grey solid. M.p: 194-196 ^{o}C. ^{1}H NMR (400 MHz, DMSO-d_6): δ 9.98 9s, 1H), 8.61 (s, 1H), 8.23-8.09 (m, 8H), 4.51 (s, 2H). ^{13}C NMR (100 MHz, DMSO-d_6): δ 169.5, 159.9, 148.8 (2C), 140.1, 133.7, 130.7, 127.3, 126.9, 125.3 (2C), 124.8, 1221.7, 119.3, 51.8. MS (ESI) *m/z* 359[M+H]$^{+}$. Anal calcd for $C_{16}H_{12}BrN_3O_2$: C, 53.65; H, 3.38; N, 11.73 Found C, 53.71; H, 3.39; N, 11.71.

N-(2,6-Diethylphenyl)-2-(4-oxoquinazolin-3(4*H*)-yl)acetamide (QA_19): The compound was synthesized according to the general procedure using 2-chloro-N-(2,6-diethylphenyl)acetamide (**QA_4d**) (0.14 g, 0.75 mmol) and quinazolin-4(3*H*)-one (**QA_1a**) (0.15 g, 0.67 mmol) to afford **QA_19** (0.13 g, 72.8 %) as white solid. M.p: 256-258 ^{o}C. ^{1}H NMR (400 MHz, DMSO-d_6): δ 9.83 (s, 1H), 8.62 (s, 1H), 8.21-8.19 (d, *J*= 8Hz, 1H), 7.95-7.92 (t, *J*= 12Hz, 1H), 7.73-7.71 (d, *J*= 8Hz, 1H), 7.65-7.62 (t, *J*= 12Hz, 1H), 7.20-7.12 (m, 3H), 4.58 (s, 2H), 2.64 (m, 4H), 1.34(m, 6H). ^{13}C NMR (100 MHz, DMSO-d_6): δ 169.2, 160.8, 149.5 (2C), 135.2 (2C), 131.2 (2C), 128.1 (2C), 125.5, 121.5, 48.7, 21.6 (2C), 15.3 (2C). MS (ESI) *m/z* 334[M+H]$^{+}$. Anal calcd for $C_{20}H_{21}N_3O_2$: C, 71.62; H, 6.31; N, 12.53 Found C, 71.69; H, 6.32; N, 12.54.

N-(2-Methyl-4-nitrophenyl)-2-(4-oxoquinazolin-3(4*H*)-yl)acetamide (QA_20): The compound was synthesized according to the general procedure using 2-chloro-N-(2-methyl-4-nitrophenyl)acetamide (**QA_4e**) (0.15 g, 0.76 mmol) and quinazolin-4(3*H*)-one (**QA_1a**) (0.15 g, 0.67 mmol) to afford **QA_20** (0.10 g, 69.8 %) as yellow solid. M.p: 243-245 ^{o}C. ^{1}H NMR (400 MHz, DMSO-d_6): δ 9.87 (s, 1H), 8.59 (s, 1H), 8.17-8.15 (d, *J*= 8Hz, 1H), 8.10-8.08 (d, *J*=8Hz, 1H), 7.93-7.87 (m, 4H), 4.51 (s, 2H), 2.17 (s, 3H). ^{13}C NMR (100 MHz, DMSO-d_6): δ 171.0, 162.1, 149.4 (2C), 145.2, 141.9, 137.3, 132.8, 137.5, 125.9 (3C), 121.3 (2C), 110.5, 51.7,

18.5. MS (ESI) *m/z* 339[M+H]$^+$. Anal calcd for $C_{17}H_{14}N_4O_4$: C, 60.35; H, 4.17; N, 16.56 Found C, 60.43; H, 4.16; N, 16.57.

N-(4-Chlorophenyl)-2-(4-oxoquinazolin-3(4*H*)-yl)acetamide (QA_21): The compound was synthesized according to the general procedure using 2-chloro-N-(4-chlorophenyl)acetamide (**QA_4f**) (0.16 g, 0.72 mmol) and quinazolin-4(3*H*)-one (**QA_1a**) (0.15 g, 0.67 mmol) to afford **QA_21** (0.14g, 75.9 %) as white solid. M.p: 236-238 ^{o}C. ^{1}H NMR (400 MHz, DMSO-d_6): δ 9.93 (s, 1H), 8.62 (s, 1H), 8.03-7.89 (m, 8H), 4.54 (s, 2H). ^{13}C NMR (100 MHz, DMSO-d_6): δ 169.3, 159.9, 148.3 (2C), 138.1, 133,5 (2C), 129.4 (2C), 126.9 (3C), 121.5, 120.5 (2C), 48.9. MS (ESI) *m/z* 314[M+H]$^+$. Anal calcd for $C_{16}H_{12}ClN_3O_2$: C, 61.25; H, 3.86; N, 13.39 Found C, 61.16; H, 3.87; N, 13.41.

N-(2,6-Dimethylphenyl)-2-(2-methyl-4-oxoquinazolin-3(4*H*)-yl)acetamide (QA_22): The compound was synthesized according to the general procedure using 2-chloro-N-(2,6-dimethylphenyl)acetamide (**QA_4a**) (0.16 g, 0.73 mmol) and 2-methylquinazolin-4(3*H*)-one (**QA_3a**) (0.16 g, 0.77 mmol) to afford **QA_22** (0.18g, 80.3 %) as white solid. M.p: 210-212 ^{o}C. ^{1}H NMR (400 MHz, DMSO-d_6): δ 9.72 (s, 1H), 8.13-8.11 (d, *J*=8Hz, 1H), 7.82-7.79 (t, *J*=12Hz, 1H), 7.63-7.61 (d, *J*=8Hz, 1H), 7.52-7.49 (t, *J*=12Hz, 1H), 7.08 (m, 3H), 5.02 (s, 2H), 2.59 (s, 3H), 2.22 (s, 6H). ^{13}C NMR (100 MHz, DMSO-d_6): δ 170.5, 162.3, 157.3, 147.3, 138.3, 134.2, 130.9 (2C), 129.1 (3C), 128.3 (3C), 119.3, 47.3, 23.4, 18.5 (2C). MS (ESI) *m/z* 322[M+H]$^+$. Anal calcd for $C_{19}H_{19}N_3O_2$: C, 71.01; H, 5.96; N, 13.08 Found C, 71.11; H, 5.97; N, 13.10.

N-(3-Chloro-2-methylphenyl)-2-(2-methyl-4-oxoquinazolin-3(4*H*)-yl)acetamide (QA_23): The compound was synthesized according to the general procedure using 2-chloro-N-(3-chloro-2-methylphenyl)acetamide (**QA_4b**) (0.15 g, 0.71 mmol) and 2-methylquinazolin-4(3*H*)-one (**QA_3a**) (0.16 g, 0.77 mmol) to afford **QA_23** (0.17g, 78.2 %) as white solid. M.p: 198-200 ^{o}C. ^{1}H NMR (400 MHz, DMSO-d_6): δ 10.02 (s, 1H), 8.23-8.21 (d, *J*=8Hz, 1H), 8.15-8.12 (d, *J*=8Hz, 1H), 7.82-7.80 (d, *J*=8Hz, 1H), 7.68-7.65 (t, *J*=12Hz, 1H), 7.27-7.20 (m, 3H), 4.59 (s, 2H), 2.62 (s, 3H), 2.19(s, 3H). ^{13}C NMR (100 MHz, DMSO-d_6): δ 170.7, 161.5, 155.7, 147.3, 139.2, 135.1, 133.9(2C), 128.9 (2C), 126.1 (2C), 125.7, 121.7, 112.1, 51.3, 23.5, 14.3. MS (ESI) *m/z* 343[M+H]$^+$. Anal calcd for $C_{18}H_{16}ClN_3O_2$: C, 63.25; H, 4.72. N, 12.29 Found C, 63.33; H, 4.71; N, 12.27.

N-(2-Bromophenyl)-2-(2-methyl-4-oxoquinazolin-3(4*H*)-yl)acetamide (QA_24): The compound was synthesized according to the general procedure using 2-chloro-N-(2-

bromophenyl)acetamide (**QA_4b**) (0.16 g, 0.75 mmol) and 2-methylquinazolin-4(3*H*)-one (**QA_3a**) (0.16 g, 0.77 mmol) to afford **QA_24** (0.17g, 77.9 %) as white solid. M.p: 242-244 ^{o}C. ^{1}H NMR (400 MHz, DMSO-d_6): δ 10.04 (s, 1H), 8.23-8.11 (m, 8H), 4.59 (s, 2H), 2.65 (s, 3H). ^{13}C NMR (100 MHz, DMSO-d_6): δ 169.7, 161.8, 154.8, 147.1, 140.1, 133.9, 132.5 (2C), 129.3 (2C), 126.6 (2C), 121.4, 119.6, 48.3, 24.4. MS (ESI) *m/z* 372[M+H]$^{+}$. Anal calcd for $C_{17}H_{14}BrN_3O_2$: C, 54.86; H, 3.79; N, 11.29 Found C, 54.94; H, 3.80; N, 11.27.

N-(2,6-Diethylphenyl)-2-(2-methyl-4-oxoquinazolin-3(4*H*)-yl)acetamide (QA_25): The compound was synthesized according to the general procedure using 2-chloro-N-(2,6-diethylphenyl)acetamide (**QA_4c**) (0.14 g, 0.7 mmol) and 2-methylquinazolin-4(3*H*)-one (**QA_3a**) (0.16 g, 0.77 mmol) to afford **QA_25** (0.14 g, 73.7 %) as white solid. M.p: 235-237 ^{o}C. ^{1}H NMR (400 MHz, DMSO-d_6): δ 9.95 (s, 1H), 8.28-8.26 (d, *J*=8Hz, 1H), 8.18-8.15 (t, *J*=12Hz, 1H), 7.77-7.75 (d, *J*=8Hz, 1H), 7.64-7.61 (t, *J*=12Hz, 1H), 7.34-7.28 (m, 3H), 4.51 (s, 2H), 2.64 (s, 3H), 2.52 (m, 4H), 1.34 (m, 6H). ^{13}C NMR (100 MHz, DMSO-d_6): δ 170.2, 161.3, 154.9, 147.4, 135.5, 133.9, 131.4 (2C), 128.5 (2C), 125.6, 122.9 (2C), 121.7, 48.3, 24.2 (2C), 23.7, 15.5. MS (ESI) *m/z* 350[M+H]$^{+}$. Anal calcd for $C_{21}H_{23}N_3O_2$: C, 72.18; H, 6.63; N, 12.03 Found C, 72.09; H, 6.64; N, 12.02.

N-(2-Methyl-4-nitrophenyl)-2-(2-methyl-4-oxoquinazolin-3(4*H*)-yl)acetamide (QA_26): The compound was synthesized according to the general procedure using 2-chloro-N-(2-methyl-4-nitrophenyl)acetamide (**QA_4d**) (0.15 g, 0.73 mmol) and 2-methylquinazolin-4(3*H*)-one (**QA_3a**) (0.16 g, 0.77 mmol) to afford **QA_26** (0.15 g, 76.2 %) as yellow solid. M.p: 270-272 ^{o}C. ^{1}H NMR (400 MHz, DMSO-d_6): δ 10.03 (s, 1H), 8.64 (s, 1H), 8.23-8.21 (d, *J*=8Hz, 1H), 8.07-8.05 (d, *J*= 8Hz, 1H), 7.89-7.80 (m, 4H), 4.60 (s, 2H), 2.64 (s, 3H), 2.18 (s, 3H). ^{13}C NMR (100 MHz, DMSO-d_6): δ 169.3, 160.9, 154.2, 147.5, 145.6, 143.1, 135.6, 132.8, 127.3 (3C), 126.1, 122.4 (2C), 109.4, 47.3, 22.9, 18.1. MS (ESI) *m/z* 353[M+H]$^{+}$. Anal calcd for $C_{18}H_{16}N_4O_4$: C, 61.36; H, 4.58; N, 15.90 Found C, 61.27; H, 4.59; N, 15.88.

N-(4-Chlorophenyl)-2-(2-methyl-4-oxoquinazolin-3(4*H*)-yl)acetamide (QA_27): The compound was synthesized according to the general procedure using 2-chloro-N-(4-chlorophenyl)acetamide (**QA_4e**) (0.12 g, 0.71 mmol) and 2-methylquinazolin-4(3*H*)-one (**QA_3a**) (0.16 g, 0.77 mmol) to afford **QA_27** (0.18 g, 78.6 %) as white solid. M.p: 237-239 ^{o}C.^{1}H NMR (400 MHz, DMSO-d_6): δ 9.81 (s, 1H), 8.11-7.98 (m, 8H), 4.58 (s, 2H), 2.60 (s, 3H). ^{13}C NMR (100 MHz, DMSO-d_6): δ 170.3, 161.5, 154.9, 148.1, 138.3, 133.4 (2C), 130.2 (2C),

17.5 (3C), 121.3, 120.1 (2C), 52.3, 23.4. MS (ESI) *m/z* 328$[M+H]^+$. Anal calcd for $C_{17}H_{14}ClN_3O_2$: C, 62.30; H, 4.31; N, 12.82 Found C, 62.39; H, 4.30; N, 12.80.

2-(6-Bromo-4-oxoquinazolin-3(4*H*)-yl)-N-(2,6-dimethylphenyl)acetamide (QA_28): The compound was synthesized according to the general procedure using 2-chloro-N-(2,6-dimethylphenyl)acetamide (**QA_4a**) (0.13 g, 0.74 mmol) and 2-methylquinazolin-4(3*H*)-one (**QA_1c**) (0.17 g, 0.79 mmol) to afford **QA_28** (0.19 g, 79.5 %) as white solid. M.p: 241-243 ^oC. ^1H NMR (400 MHz, DMSO-d_6): δ 9.97 (s, 1H), 8.61 (s, 1H), 8.42 (s, 1H), 8.12-8.10 (d, *J*= 8Hz, 1H), 7.99-7.97 (d, *J*=8Hz, 1H), 7.53-7.48 (m, 3H), 4.57 (s, 2H), 2.21 (s, 6H). ^{13}C NMR (100 MHz, DMSO-d_6): δ 169.9, 162.3, 147.3 (2C), 138.6, 137.2, 133.4, 132.7 (2C), 129.5 (2C), 127.3, 125.2, 123.1, 121.3, 51.2, 19.3 (2C). MS (ESI) *m/z* 387$[M+H]^+$. Anal calcd for $C_{18}H_{16}BrN_3O_2$: C, 55.97; H, 4.18; N, 10.88 Found C, 55.88; H, 4.17; N, 10.90.

2-(6-Bromo-4-oxoquinazolin-3(4*H*)-yl)-N-(3-chloro-2-methylphenyl)acetamide (QA_29): The compound was synthesized according to the general procedure using 2-chloro-N-(2,6-dimethylphenyl)acetamide (**QA_4b**) (0.13 g, 0.74 mmol) and 6-bromoquinazolin-4(3*H*)-one (**QA_3a**) (0.16 g, 0.77 mmol) to afford **QA_29** (0.13 g, 72.1 %) as off-white solid. M.p: 215-217 ^oC. ^1H NMR (400 MHz, DMSO-d_6): δ 10.02 (s, 1H), 8.64 (s, 1H), 8.39 (s, 1H), 8.09-8.07 (d, *J*= 8Hz, 1H), 7.95-7.93 (d, *J*=8Hz, 1H), 7.61-7.55 (m, 3H), 4.58 (s, 2H), 2.28 (s, 3H). ^{13}C NMR (100 MHz, DMSO-d_6): δ 169.5, 162.3, 148.7 (2C), 139.2, 136.3 (2C), 134.7 (2C), 131.9, 126.9, 124.9 (2C), 123.1, 120.8, 113.5, 54.2, 16.3. MS (ESI) *m/z* 407$[M+H]^+$. Anal calcd for $C_{17}H_{13}BrClN_3O_2$: C, 50.21; H, 3.22; N, 10.33 Found C, 50.28; H, 3.21; N, 10.35.

2-(6-Bromo-4-oxoquinazolin-3(4*H*)-yl)-N-(2-bromophenyl)acetamide (QA_30): The compound was synthesized according to the general procedure using 2-chloro-N-(2-bromophenyl)acetamide (**QA_4c**) (0.14 g, 0.76 mmol) and 6-bromoquinazolin-4(3*H*)-one (**QA_3a**) (0.16 g, 0.77 mmol) to afford **QA_30** (0.16 g, 78.3 %) as off-white solid. M.p: 280-282 ^oC. ^1H NMR (400 MHz, DMSO-d_6): δ 10.09 (s, 1H), 8.53 (s, 1H), 8.43 (s, 1H), 8.27-8.25 (d, *J*=8Hz, 1H), 8.03-8.01 (d, *J*=8Hz, 1H), 7.69-7.67 (d, *J*=8Hz, 1H), 7.61-7.59 (d, *J*=8Hz, 1H), 7.39-7.36 (t, *J*=12Hz, 1H), 7.16-7.13 (t, *J*=12Hz, 1H), 4.95 (s, 2H). ^{13}C NMR (100 MHz, DMSO-d_6): δ 170.1, 163.2, 149.2 (2C), 139.3, 137.2, 133.3, 131.9 (2C), 129.1, 126.7, 125.2 (2C), 122.9, 118.2, 49.8. MS (ESI) *m/z* 438$[M+H]^+$. Anal calcd for $C_{16}H_{11}Br_2N_3O_2$: C, 43.97; H, 2.54; N, 9.61 Found C, 43.91; H, 2.54; N, 9.62.

2-(6-Bromo-4-oxoquinazolin-3(4*H*)-yl)-N-(2,6-diethylphenyl)acetamide (QA_31): The compound was synthesized according to the general procedure using 2-chloro-N-(2,6-diethylphenyl)acetamide (**QA_4d**) (0.15 g, 0.79 mmol) and 6-bromoquinazolin-4(3*H*)-one (**QA_1c**) (0.16 g, 0.77 mmol) to afford **QA_31** (0.15 g, 77.4 %) as white solid. M.p: 271-273 ^{o}C. ^{1}H NMR (400 MHz, DMSO-d_6): δ 9.97 (s, 1H), 8.58 (s, 1H), 8.31 (s, 1H), 8.13-8.11 (d, *J*=8Hz, 1H), 7.88-7.86 (d, *J*=8Hz, 1H), 7.53-7.48 (m, 4H), 4.50 (s, 2H), 2.54 (m, 4H), 1.36 (m, 6H). ^{13}C NMR (100 MHz, DMSO-d_6): δ 170.5, 162.7, 148.9 (2C), 137.2, 135.1, 132.7, 131.2 (2C), 124.3 (2C), 123.2, 121.9 (3C), 49.7, 24.2 (2C), 16.3 (2C). MS (ESI) *m/z* 415[M+H]$^{+}$. Anal calcd for $C_{20}H_{20}BrN_3O_2$: C, 57.98; H, 4.87; N, 10.14 Found C, 57.86; H, 4.88; N, 10.16.

2-(6-Bromo-2-methyl-4-oxoquinazolin-3(4*H*)-yl)-N-(2-methyl-4-nitrophenyl)acetamide (QA_32): The compound was synthesized according to the general procedure using 2-chloro-N-(2-methyl-4-nitrophenyl)acetamide (**QA_4e**) (0.14 g, 0.77 mmol) and 6-bromoquinazolin-4(3*H*)-one (**QA_1c**) (0.16 g, 0.77 mmol) to afford **QA_32** (0.14 g, 75.4 %) as pale yellow solid. M.p: 189-191 ^{o}C. ^{1}H NMR (400 MHz, DMSO-d_6): δ 9.85 (s, 1H), 8.60 (s, 1H), 8.34 (s, 1H), 8.09-7.99 (m, 4H), 4.51 (s, 2H), 2.71 (s, 3H), 2.17 (s, 3H). ^{13}C NMR (100 MHz, DMSO-d_6): δ 169.3, 161.7, 155.2, 146.3, 144.6, 143.1, 137.4, 135.8, 133.5, 124.2, 123.1 (2C), 121.9 (2C), 109.1, 47.2, 23.1, 18.5. MS (ESI) *m/z* 432[M+H]$^{+}$. Anal calcd for $C_{18}H_{15}BrN_4O_4$: C, 50.13; H, 3.51; N, 12.99 Found C, 50.21; H, 3.50; N, 12.97.

2-(6-Bromo-2-methyl-4-oxoquinazolin-3(4H)-yl)-N-(4-chlorophenyl)acetamide (QA_33): The compound was synthesized according to the general procedure using 2-chloro-N-(4-chlorophenyl)acetamide (**QA_4f**) (0.15 g, 0.79 mmol) and 6-bromoquinazolin-4(3*H*)-one (**QA_1c**) (0.16 g, 0.77 mmol) to afford **QA_33** (0.13 g, 73.8 %) as white solid. M.p: 178-180 ^{o}C. ^{1}H NMR (400 MHz, DMSO-d_6): δ 10.02 (s, 1H), 8.61 (s, 1H), 8.32-8.30 (d, *J*=8Hz, 1H), 8.07-8.05 (d, *J*=8Hz, 1H), 7.63-7.58 (m, 4H), 4.58 (s, 2H), 2.54 (s, 3H). ^{13}C NMR (100 MHz, DMSO-d_6): δ 170.2, 161.3, 156.1, 143.8, 137.2 (2C), 134.4, 132.8, 130.7 (2C), 125.3, 121.9, 121.5 (2C), 47.3, 23.7. MS (ESI) *m/z* 407 [M+H]$^{+}$. Anal calcd for $C_{17}H_{13}BrClN_3O_2$: C, 50.21; H, 3.22; N, 10.33 Found C, 50.29; H, 3.21; N, 10.35.

5.2.4.5. Identification and characterization of inhibitors using enzyme inhibitory assay, molecular docking and protein thermal stability assay

We have performed the inhibitory enzyme assay for all the synthesized compounds using GR of *B. subtilis*. The inhibitory activity results of compounds were listed in **Table 5.13**. Among all, four compounds have shown considerable inhibitory activity around 10 µM which is better than **lead 4** molecule (IC_{50} 21.45 ± 0.58 µM). Compound **QA_19** is showing IC_{50} of 5.23 ± 0.76 µM inferring to be most potent in the series than lead compound by five times. Log dose response curve of compound **QA_19** is shown in **Figure 5.40**.

Table 5.13 Synthesized compounds represented with substitutions along with their biological activities

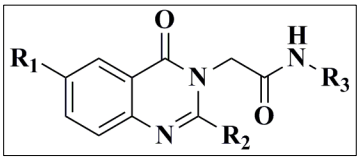

QA_5-33

Compd	R_1	R_2	R_3	IC_{50} (µM)	MIC (µM)			Cytotoxicity at 25 µM (% Inhib.)
					Actual MIC	MIC in the presence of Verapamil	MIC in the presence of Piperine	
QA_5	Cl	H	2,6-Dimethylphenyl	>25	73.31	ND	ND	30.41
QA_6	Cl	H	3-Chloro-2-methylphenyl	>25	69.79	ND	ND	58.11
QA_7	Cl	H	2-Bromophenyl	>25	63.76	ND	ND	27.98
QA_8	Cl	H	2,6-Diethylphenyl	>25	67.13	ND	ND	60.32
QA_9	Cl	H	2-Methyl-4-nitrophenyl	>25	67.17	ND	ND	20.02
QA_10	Cl	H	4-Chlorophenyl	>25	71.87	ND	ND	46.61
QA_11	Cl	CH_3	2,6-Dimethylphenyl	>25	70.32	ND	ND	40.72
QA_12	Cl	CH_3	3-Chloro-2-	>25	66.47	ND	ND	37.22

			methylphenyl					
QA_13	Cl	CH_3	2-Bromophenyl	>25	61.56	ND	ND	49.35
QA_14	Cl	CH_3	2,6-Diethylphenyl	>25	65.17	ND	ND	58.81
QA_15	Cl	CH_3	2-Methyl-4-nitrophenyl	>25	64.67	ND	ND	57.23
QA_16	Cl	CH_3	4-Chlorophenyl	10.1±0.62	69.02	8.62	69.02	79.36
QA_17	H	H	2,6-Dimethylphenyl	>25	81.35	ND	ND	37.71
QA_18	H	H	3-Chloro-2-methylphenyl	>25	69.82	ND	ND	20.98
QA_19	H	H	2,6-Diethylphenyl	5.23±0.34	73.98	37.21	73.98	50.71
QA_20	H	H	2-Bromophenyl	>25	74.58	ND	ND	31.82
QA_21	H	H	2-Methyl-4-nitrophenyl	>25	79.72	ND	ND	46.98
QA_22	H	H	4-Chlorophenyl	>25	77.81	ND	ND	64.21
QA_23	H	CH_3	2,6-Dimethylphenyl	>25	73.16	ND	ND	60.23
QA_24	H	CH_3	3-Chloro-2-methylphenyl	>25	67.23	ND	ND	36.67
QA_25	H	CH_3	2-Bromophenyl	>25	71.56	ND	ND	54.53
QA_26	H	CH_3	2,6-Diethylphenyl	>25	71.03	ND	ND	36.52
QA_27	H	CH_3	2-Methyl-4-nitrophenyl	10.3±0.51	76.37	76.37	76.37	39.81
QA_28	H	CH_3	4-Chlorophenyl	>25	64.71	ND	ND	45.17
QA_29	Br	H	2,6-Dimethylphenyl	>25	61.56	ND	ND	38.32
QA_30	Br	H	3-Chloro-2-methylphenyl	9.27±0.64	57.26	57.26	57.26	43.65
QA_31	Br	H	2-Bromophenyl	>25	60.38	ND	ND	67.43
QA_32	Br	H	2,6-Diethylphenyl	>25	59.9	ND	ND	49.73

QA_33	Br	H	2-Methyl-4-nitrophenyl	>25	63.87	ND	ND	43.98
Isoniazid				>25	0.72	0.72	0.72	ND
Ethambutol				>25	7.64	3.82	3.82	ND
Rifampicin				>25	0.15	0.15	0.15	ND

ND: Not determined

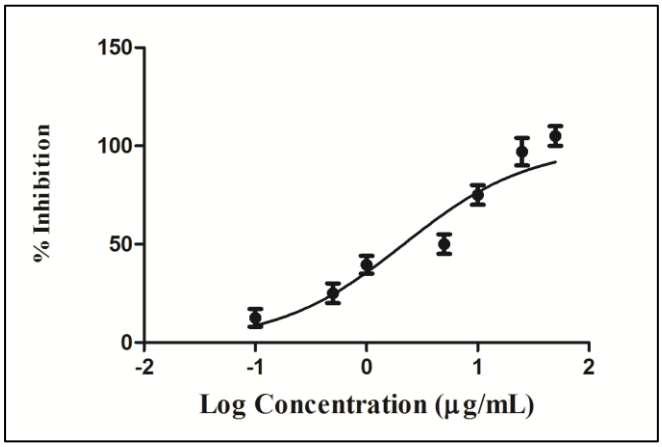

Figure 5.40: Log dose response curve of compound **QA_19** with different log concentrations (X-axis) vs percentage inhibition (Y-axis).

Further, we analyzed of the binding poses of synthesized compounds with the support of molecular docking. We performed docking and molecular dynamics of molecules (picked based on IC_{50} values) in the crystal structures of *M. tuberculosis* and *B. subtilis* GR in complex with D-glutamate (PDB ID: 5HJ7, 1ZUW respectively) using Glide XP docking and Desmond (Schrodinger). The inhibitors were not docked properly on the substrate binding site (D-glutamate) in both proteins; hence we have tried docking in allosteric sites generated by using sitemap. Based on site-scores **site 1** in both the proteins was selected for further docking studies. Here we discuss the binding pattern of one of the active compounds **QA_16**, the superimposition of both proteins and compound **QA_16** in its binding mode was shown in **Figure 5.41**. The 2D-binding orientation of compound **QA_16** within both proteins binding pocket is represented in **Figure 5.42**. The predicted bound conformation of the active compound showed interactions with the side chain of the Glu 153 in both proteins. Apart from this the compound further stabilized through various hydrophobic and few polar amino acid residue interactions. The compound was very well fit into the allosteric site cavity of the protein with a docking scores of-

2.598 kcal/mol and -4.245 kcal/mol in 5HJ7 and 1ZUW respectively. Thus molecular docking was a great help in supporting the confirmation of inhibitory activity in both the organisms.

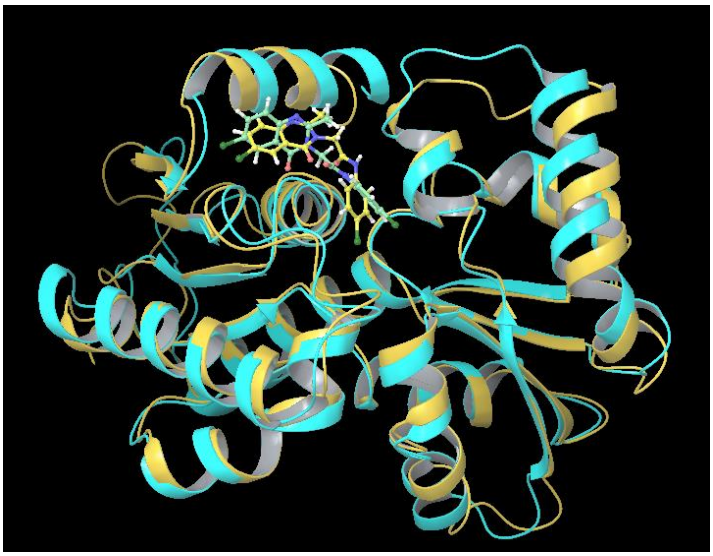

Figure 5.41: Docking pose of active molecule **QA_ 16** in **site 1** of *M. tuberculosis* (5HJ7) and *B. subtilis* (1ZUW) in superimposed view. Yellow color represents protein and ligand in 5HJ7 whereas blue represents 1ZUW.

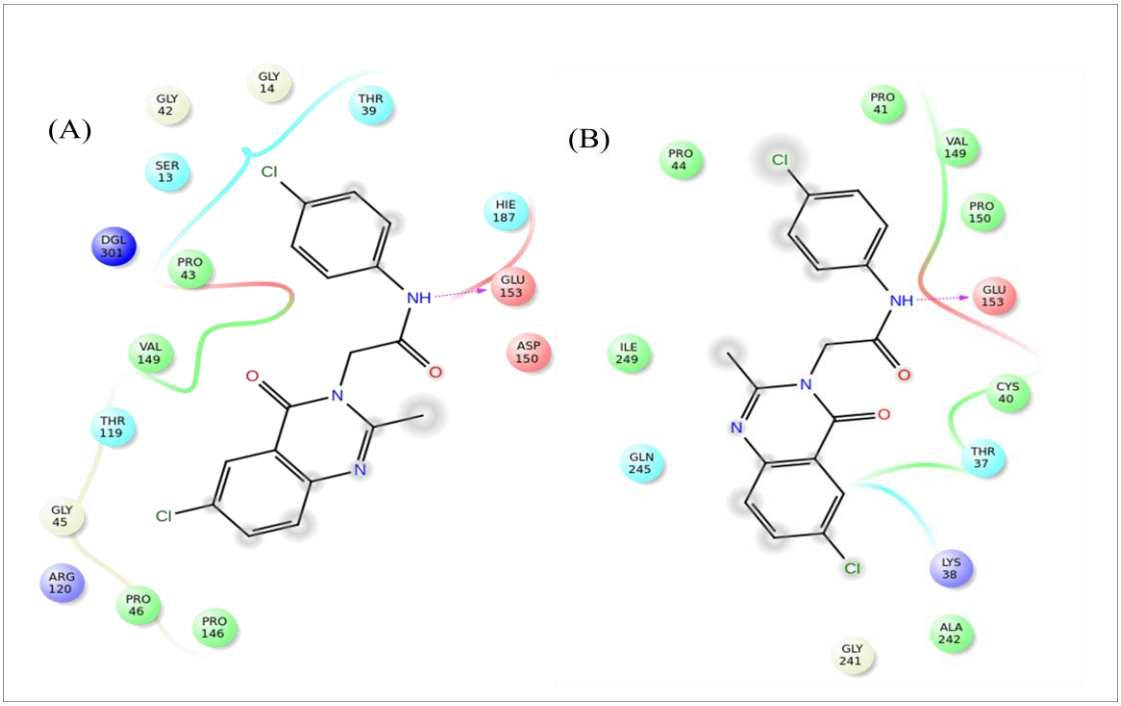

Figure 5.42: Binding pose and interaction pattern of compound **QA_16** in (A) *M. tuberculosis* and (B) *B. subtilis*

Compound **QA_16** in 5HJ7 and 1ZUW protein complexes were subjected to a 10 ns simulation. The rmsd analysis plots for the protein-ligand complexes have been carried out so as to measure the distance between atoms during simulation (**Figure 5.43**).Rmsd for 1ZUW, C_{α} and ligand were within the average of ~1.5 Å and ~0.9 Å and for 5HJ7 both C_{α} and ligand were within the average of ~1.5 Å and ~0.8 Å respectively during 10 ns simulation trajectory. The root mean square fluctuation (rmsf) analysis shows the fluctuation range undergone by every residue in the protein during simulation. Rmsf plot for compound **QA_16** in both protein complexes was shown in (**Figure 5.44**). The figure shows least fluctuations of the ligand binding site residues with rmsf values in an average of ~1.3 Å and 1.2 Å respectively for 5HJ7 and 1ZUW.

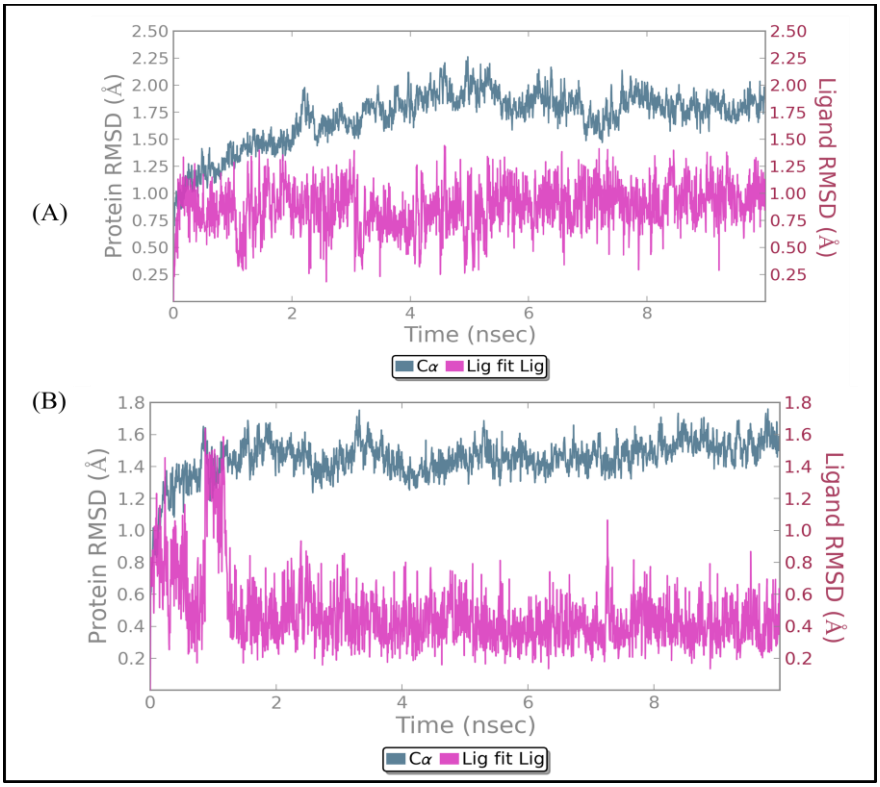

Figure 5.43: Rmsd plots of GR inbound state with compounds **QA_16** as a function of time in *M. tuberculosis* (A) and (B) *B. subtilis.*

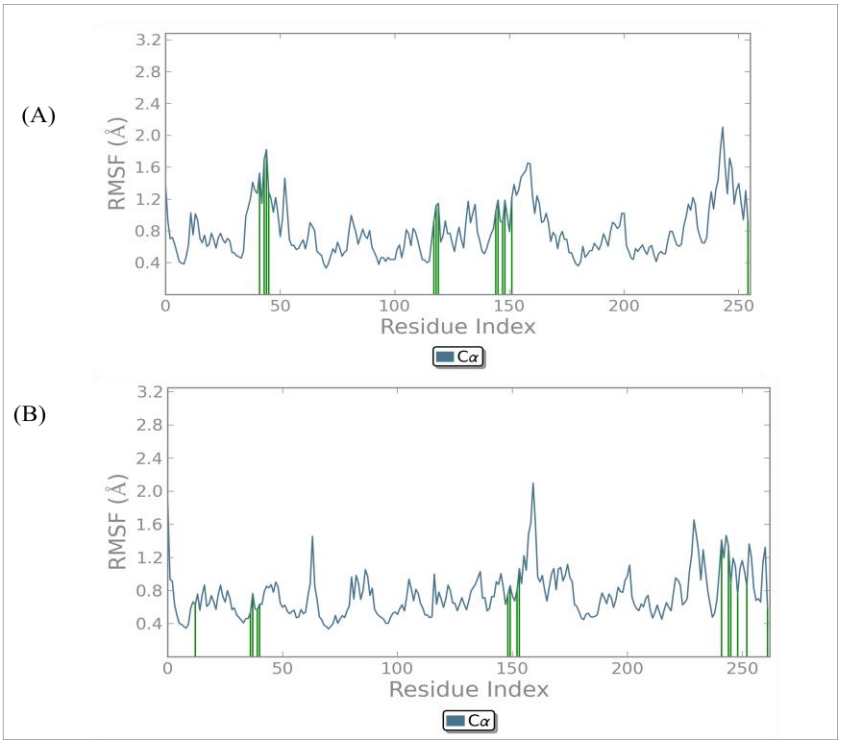

Figure 5.44: Rmsf plots of GR inbound state with compounds **QA_16** as a function of time in *M. tuberculosis* (A) and (B) *B. subtilis.*

Mode of inhibition of active compound was characterized using TSA. The thermal shift analysis of active molecule **QA_16** indicated that it follows the non-competitive mode of inhibition with an approximate shift in ΔT_m by 1.5 ^oC with native protein and when tested with protein-substrate complex there was a shift by 5.6 ^oC with native protein (**Figure 5.45**). This indicates that the protein and protein-substrate complex were more stabilized in the presence of compound **QA_16** when compared to **lead 4**.

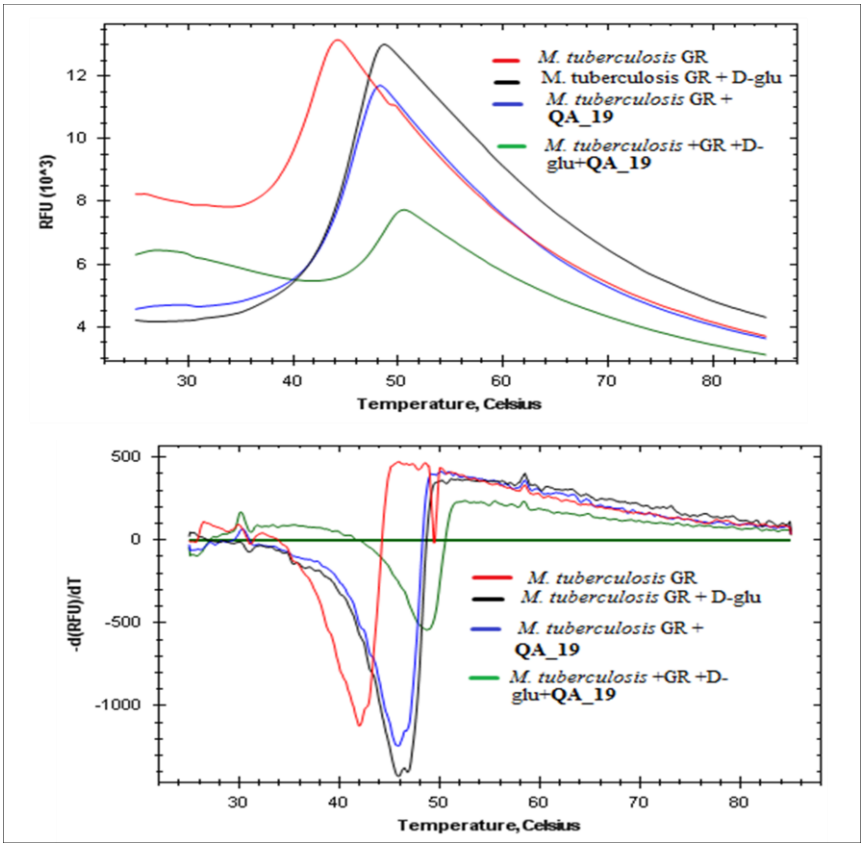

Figure 5.45: Thermal stability curves of *M. tuberculosis* GR depicting the non-competitive inhibition by compound **QA_19.**

5.2.4.6. *In vitro* active and nutrient-starved dormant *M. tuberculosis* assay models

All the synthesized molecules were screened *in vitro* for their activity against replicating *M. tuberculosis* using microplate alamar blue assay (MABA) with drug concentrations from 50 µg/mL to 0.78 µg/mL and the minimum inhibitory concentration (MIC) was determined for each compound MIC values of the synthesized compounds and the standard drugs (Isoniazid, Ethambutol and Rifampicin) for comparison were represented in **Table 5.13**. None of the compounds have shown good inhibitory activity against whole cell bacteria. Assuming efflux of the drug by bacteria as the major reason for their inactivity compounds **QA_16, QA_19, QA_27** and **QA_30** that showed activity in enzyme assay were tested for susceptibility in the presence of efflux pump inhibitors like verapamil and piperine. The compounds **QA_16** and **QA_19** have shown improvement in activity in the presence of verapamil and no change when carried out with piperine (**Table 5.13**). In this model, *M. tuberculosis* cultures were starved of nutrients in phosphate buffer saline (PBS) for 6 weeks. After 6 weeks, the culture was treated with the

synthesized test compounds and standard drugs at a concentration of 10 µg/mL. Considering the IC_{50} and MIC values of the synthesized compounds we have selected compounds QA_**16** and **QA_19** for nonreplicating *M. tuberculosis* assays. INH, RIF and MOXI were selected for standard comparison. INH, RIF and MOXI have shown an inhibition of 1, 1.8 and 2.2 log reduction respectively compared with control (**Figure 5.46**). Test compounds **QA_16** and **QA_19** have shown a log reduction of 1.7 and 1.6 respectively. This indicates that test compounds were showing better activities than INH on dormant culture.

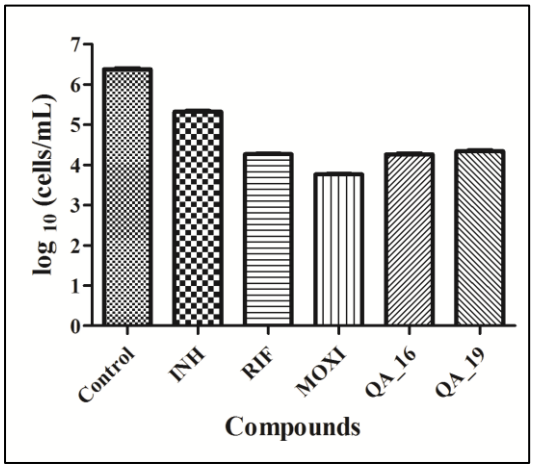

Figure 5.46: Activity profile of compounds in the nutrient starvation model. Bacterial count (Mean ± S.E., n=3) for control and treated groups was estimated through MPN (most probable number) assay.

5.2.4.7. Determination of kill kinetics using nutrient starved culture of *M. tuberculosis*

We have evaluated compounds at different concentrations on bacteria obtained after 2 weeks of nutrient starvation at 0, 7, 14, 21 days after drug treatment. Compounds **QA_16** and **QA_19** showing good inhibition in above study on nutrient starved culture have shown MBC more than fourfold of their MIC values indicating that they are bacteriostatic. The kinetic graph of compound **QA_19** was shown in **Figure 5.47**.

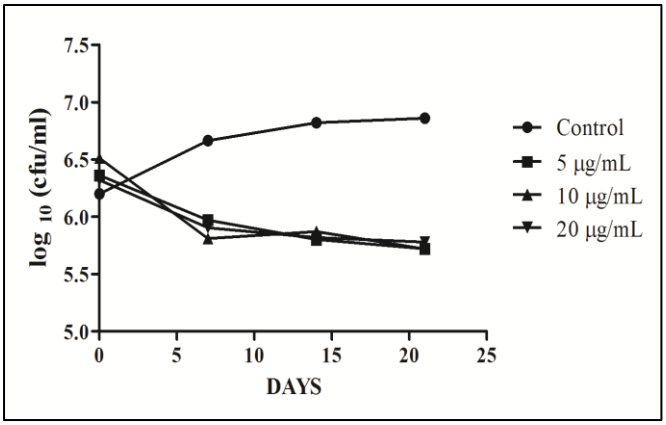

Figure 5.47: Kill kinetic curve of compound **QA_19** depicting bacteriostatic inhibition.

5.2.4.8. Inhibitory studies on persistent *M. tuberculosis* bacteria (biofilm) and cytotoxicity assay

Compounds **QA_16** and **QA_19** were tested for their activity on biofilm at concentration of10 µg/mL Standards INH, RIF and MOXI have shown a log reduction of 1, 1.2 and 1.8 respectively compared to control. Test compounds **QA_16** and **QA_19** have shown log reduction of 0.5 and 2 respectively as shown in **Figure 5.48**. All the compounds were tested at a concentration of 25 µM and the percentage inhibition was found to be in varied ranges. However, most of the compounds were not toxic at 25 µM (**Table 5.13**). Hence most of the compounds are devoid of effects on metabolism.

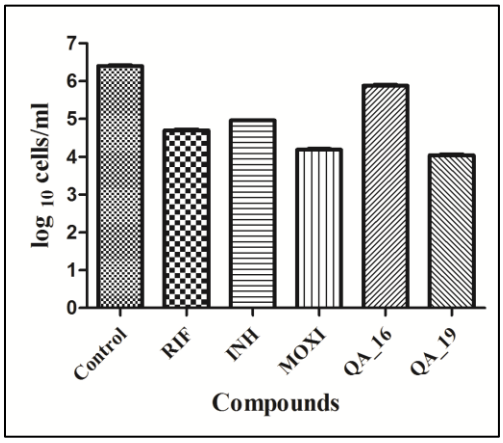

Figure 5.48: Comparative biofilm inhibitory activity plots of compounds **QA_16** and **QA_19** against *M. tuberculosis* along with standards. Bacterial count estimation (Mean ± S.D., n = 4) for control and treated groups was conducted by using the MPN assay.

5.2.4.9. Highlights of the study

In present work, we attempted to modify oxoquinazoline leads to increase efficiency against *M. tuberculosis* by targeting GR enzyme. We were able to identify compounds which have efficacy against both replicating and non-replicating stages of *M. tuberculosis*. **QA_16** and **QA_19** results show that they are equally effective as standard drugs against active stage of tuberculosis, additionally, they have the advantage of potency against the persistent phase of tuberculosis (**Figure 5.49**). As the urge for new antitubercular drugs is increasing day by day the present class of drugs would be a suitable class for further drug development studies.

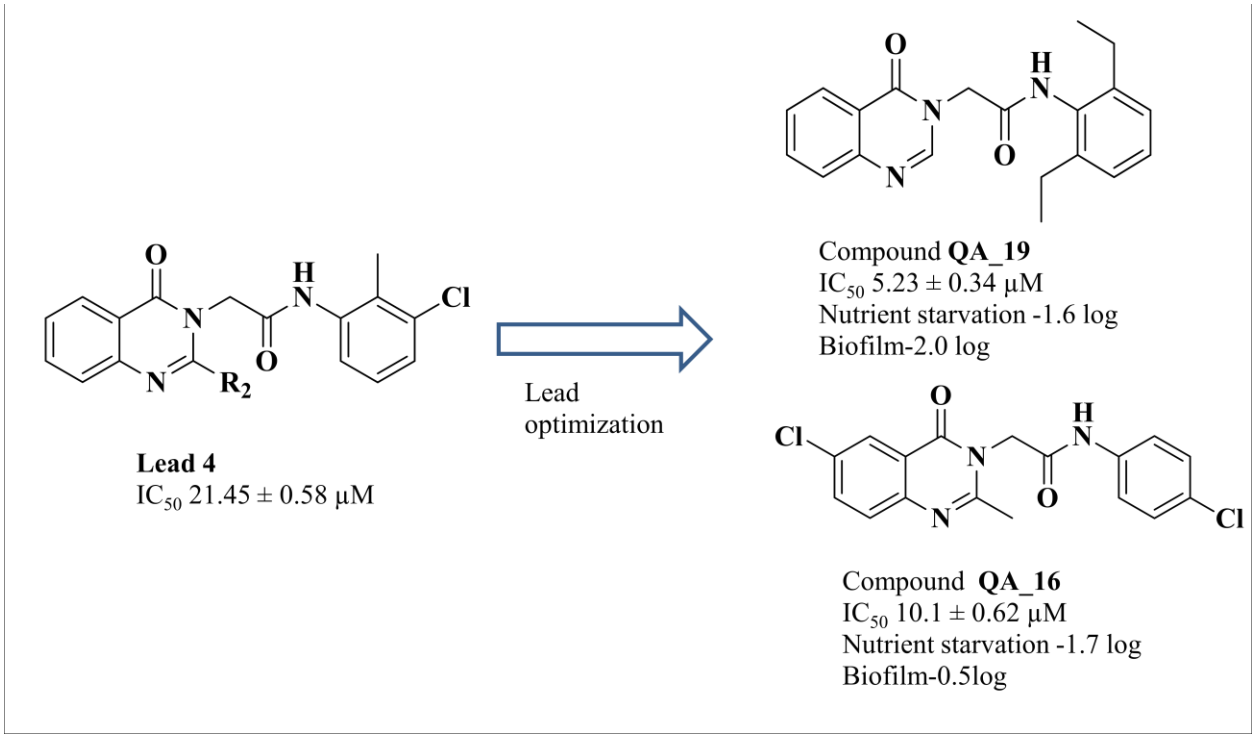

Figure 5.49: Chemical structure and biological activity of the most active compounds **QA_16** and **QA_19**

5.2.5. Identification and development of novel indazole derivatives as potent *Mycobacterium tuberculosis* Glutamate racemase inhibitors

5.2.5.1. Identification of lead

In the present study, we have done medium throughput screening of our in-house database with chemically diverse structures using thermal shift assay to identify the lead inhibiting *M.*

tuberculosis GR. A comparison study of T_m revealed that native protein in the absence of D-glu and ligand showed a melt temperature approximately of 43.1 ^oC, whereas with D-glu showed T_m at 44.3 ^oC approximately. Screened compounds showed a varied range of positive and negative shifts in T_m. Of the entire compound library **lead 5** showed a significant shift in melt temperature. When performed along with D-glu, **lead 5** showed T_m with native protein at 46.9 ^oC inferring that its stabilizing capability and interactions with protein are much better than D-glu alone as well as than rest of the compound library. The screening by enzyme assay also showed good inhibitory activity on GR of *B. subtilis* by **lead 5** with an IC_{50} of 19.73 ±0.65 µM (**Figure 5.50**). Hence we considered **lead 5** to optimize further through synthetic strategies.

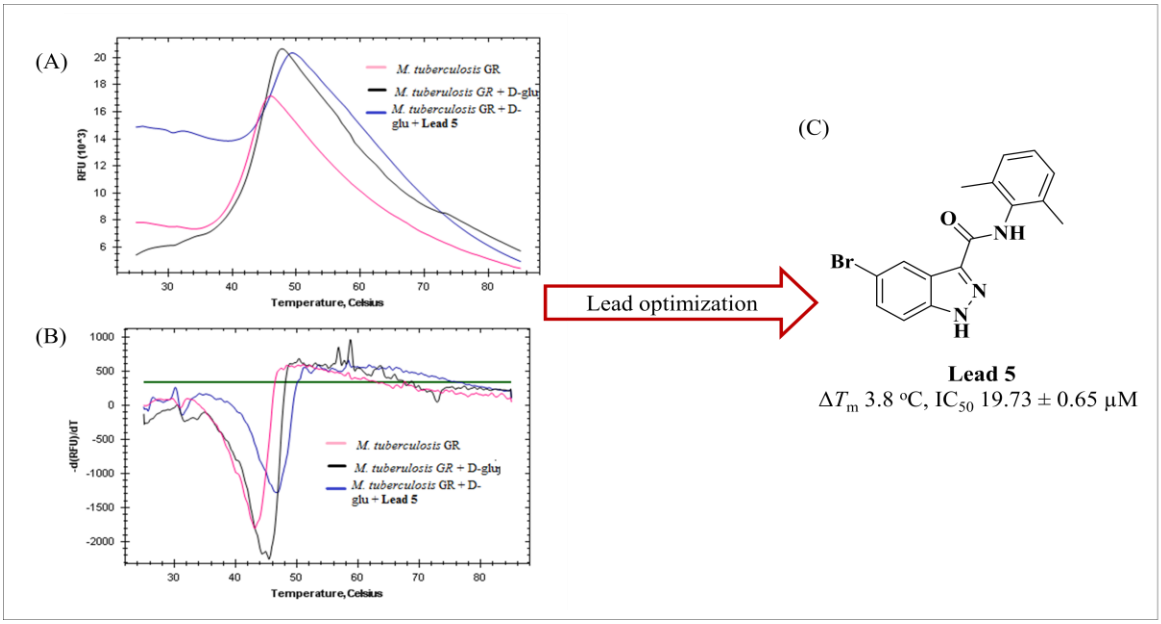

Figure 5.50: (A) DSF plots of a *M. tuberculosis* GR native, with D-glu and **lead 5** (B) represents the plot of derivative fluorescent based signal against temperature; T_m and ΔT_m (shift) can be measured from the minimum of the plot (C) Structure of identified **lead 5** with T_m and IC_{50} value in *B. subtilis*

5.2.5.2. Chemical Synthesis and characterization

The desired compounds were synthesized using the protocol mentioned in **Scheme 5.7**. β-acetylphenylhydrazine, hydroxylamine hydrochloride, hydrochloric acid and chloral hydrate to get *N*-Acetylaminoisonitrosoacetanilide with good yield. *N*-Acetylaminoisonitrosoacetanilide was further reacted with sulphuric acid to give indazole-3-carboxylic acid. The formed

compound was suspended in glacial acetic acid and bromine at cold conditions to result in 5-bromo-1H-indazole-3-carboxylic acid as yellow precipitate with good yield. 5-bromo-1H-indazole-3-carboxylic acid, 1-Ethyl-3-(3-dimethylaminopropyl)carbodiimide (EDCI) (3mmol) and Hydroxybenzotriazole (HOBt) were added along with different amines procured from commercial sources. the precipitates obtained were collected, extracted with ethylacetate (15ml thrice) and water, the organic layers were dried over sodium sulphate and evaporated to get solid which is purified by column chromatography using ethylacetate:hexane to yield respective amide derivatives **IN_4-25**.

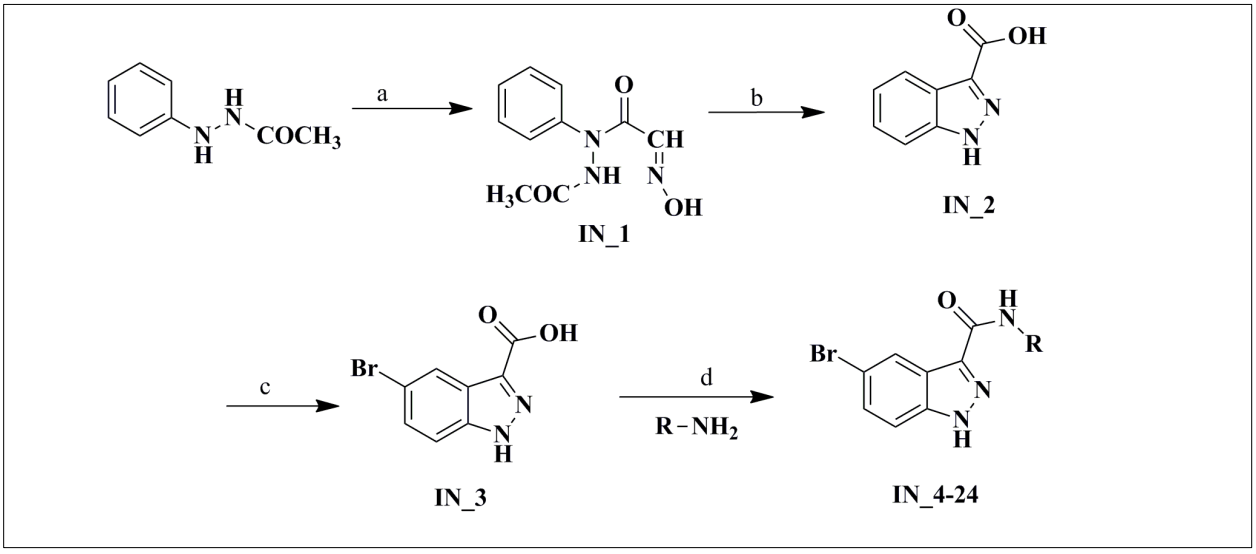

Scheme 5.7: Reagents and conditions: a) $Cl_3CCH(OH)_2$, $NH_2OH.HCl$, Na_2SO_4, HCl, 3h, 100 °C b) H_2SO_4, 30min, 85 °C c) Br_2,CH_3COOH, 16 h 90 °C; 90 °C to 5 °C d) DMF, EDCI, HOBt, rt, 8h

5.2.5.3. Synthetic protocol used for synthesis

Preparation of *N*-Acetylaminoisonitrosoacetanilide (IN_1)

A round bottom flask equipped a nitrogen inlet, was charged with β-acetylphenylhydrazine (46 mmol), hydroxylamine hydrochloride (110 mmol) and sodium sulphate (225 mmol) in 25 mL of water having 1N Hydrochloric acid (30 mL) with stirring. To this chloral hydrate (20 mmol) was slowly added at 100 °C and was stirred for 15minutes followed by cooling to 20 °C. The solvent was evaporated till the solvent reaches half its volume. The mixture is cooled to refrigerate

resulting in a precipitate which was filtered and washed with water and dried under vacuum at 70 °C overnight to give *N*-Acetylaminoisonitrosoacetanilide **(IN_1)** with good yield.

Preparation of Indazole-3-carboxylic acid (IN_2)

N-Acetylaminoisonitrosoacetanilide **(IN_1)** (45 mmol) was added slowly to sulphuric acid (30 mL) in a round bottom flask with a nitrogen inlet at 55 °C. To this mixture was heated to 85 °C for about 30 minutes. The mixture was cooled; ice was added and refluxed for 3h. After the reaction has completed the solid was filtered and washed with water and recrystallized with acetic acid to give indazole-3-carboxylic acid **(IN_2)** with good yield.

Preparation of 5-Bromo-1*H*-indazole-3-carboxylic acid (IN_3)

In a round-bottomed flask indazole-3-carboxylic acid (**IN_2)** (23.4 mmol) was suspended in glacial acetic acid (25 mL) and kept for stirring at the temperature of 90 °C. To the above mixture Bromine (52 mmol) was added in acetic acid (15 mL). The mixture was stirred for 16 h at 90 °C, later cooled to 5 °C. The yellow precipitate was filtered; washed with EtOAc and Et_2O and dried to afford a pale yellow solid 5-bromo-1H-indazole-3-carboxylic acid **(IN_3)** with a better yield.

Preparation of 5-bromo-1*H*-indazole-3-carboxamide derivatives (IN_4-24)

5-bromo-1*H*-indazole-3-carboxylic acid **(IN_3)** (2 mmol) and 10 mL of ethanol were taken in a round bottom flask inserted with a nitrogen inlet. To this mixture 1-Ethyl-3-(3-dimethylaminopropyl)carbodiimide (EDCI) (3 mmol) and Hydroxybenzotriazole (HOBt) (0.8 mmol) were added along with (2.4 mmol) of different amines procured from commercial sources. The reaction was kept for stirring for 8h at room temperature. After the reaction was completed water (20 mL) was added, the precipitates obtained were collected, extracted with ethylacetate (15 mL thrice) and water, the organic layers were dried with sodium sulphate and evaporated to get solid which is purified with column chromatography using ethylacetate: hexane to yield respective amide derivatives **IN_4-24**.

Table 5.14. Physicochemical properties of synthesized compounds **IN_4-24**

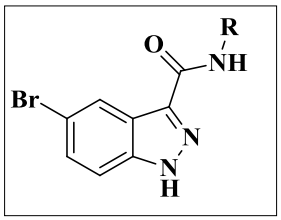

IN_4-24

Comp	R	Yield (%)	Melting point (^{o}C)	Molecular formula	Molecular weight
IN_4	4-Nitrophenyl	72.3	231-233	$C_{14}H_9BrN_4O_3$	361.15
IN_5	3-(trifluoromethyl)phenyl	69.8	190-192	$C_{15}H_9BrF_3N_3O$	384.15
IN_6	3-Chlorophenyl	71.5	210-212	$C_{14}H_9BrClN_3O$	350.62
IN_7	2,6-Diethylphenyl	74.9	242-244	$C_{18}H_{18}BrN_3O$	372.26
IN_8	2-Hydroxy-4-nitrophenyl	79.1	263-265	$C_{16}H_9BrN_4O_4$	377.15
IN_9	2-Bromophenyl	73.1	179-181	$C_{14}H_9Br_2N_3O$	395.05
IN_10	Thiazol-2-yl	76.5	219-221	$C_{11}H_7BrN_4OS$	323.17
IN_11	Benzo[d]thiazol-2-yl	77.9	235-237	$C_{15}H_9BrN_4OS$:	373.23
IN_12	Pyridin-3-yl	80.6	281-283	$C_{13}H_9BrN_4O$	317.14
IN_13	4-Fluorophenyl	75.7	270-272	$C_{14}H_9BrFN_3O$	334.14
IN_14	3-Chloro-2-methylphenyl	77.4	244-246	$C_{15}H_{11}BrClN_3O$	364.62
IN_15	Pyrimidin-2-yl	79.9	225-227	$C_{12}H_8BrN_5O$	318.13
IN_16	5-Nitrothiazol-2-yl	81.1	210-212	$C_{11}H_6BrN_5O_3S$	368.17
IN_17	3,4-Dichlorophenyl	78.5	239-241	$C_{14}H_8BrCl_2N_3O$	385.04

IN_18	5-Nitrothiazol-2-yl	71.5	251-253	$C_{11}H_6BrN_5O_3S$	368.17
IN_19	5-Chloro-2-methoxyphenyl	73.3	264-266	$C_{15}H_{11}BrClN_3O_2$	380.62
IN_20	2,4-Dimethylphenyl	76.1	277-279	$C_{16}H_{14}BrN_3O$	344.21
IN_21	2,5-Dimethylphenyl	70.9	241-243	$C_{16}H_{14}BrN_3O$	344.21
IN_22	2-Methoxy-4-nitrophenyl	71.5	197-199	$C_{15}H_{11}BrN_4O_4$	391.18
IN_23	5-Chloro-2-hydroxyphenyl	79.1	183-185	$C_{14}H_9BrClN_3O_2$	366.60
IN_24	2-Hydroxy-5-methylphenyl	70.8	209-211	$C_{15}H_{12}BrN_3O_2$	346.18

5.2.5.4. Characterization of synthesized compounds

Both analytical and spectral data (^{1}H NMR, ^{13}C NMR and mass spectra) of all the synthesized compounds were in full agreement with the proposed structures.

***N*-Acetylaminoisonitrosoacetanilide (IN_1):** The compound was synthesized according to the above general procedure using β-acetylphenylhydrazine (3 g, 20 mmol), hydroxylamine hydrochloride (3.4 g, 50 mmol) and chloral hydrate (1.65 g, 10 mmol) to afford **IN_1** (2.4 g, 90.1 %) as white solid. ^{1}H NMR (400 MHz, DMSO-d_6, TMS):δ = 11.89 (m, 1H), 10.76 (m,1H), 8.21 (m, 1H), 7.56-7.32 (m, 5H), 2.32 (s, 3H). ^{13}C NMR (100 MHz, DMSO-d_6, TMS): δ= 169.5, 155.3, 144.7, 139.4, 131.5 (2C), 124.5, 119.5 (2C), 22.5. MS (ESI) *m/z* 222.32 $(M+H)^+$. Anal calcd for $C_{10}H_{11}N_3O_3$: C, 54.05; H, 5.44; N, 18.91 Found: C, 54.10; H, 5.43; N, 18.93.

Indazole-3-carboxylic acid (IN_2): The compound was synthesized according to the above general procedure using *N*-Acetylaminoisonitrosoacetanilide (**IN_1**) (2.21 g, 10 mmol) and sulphuric acid (3 mL) to afford **IN_2** (2.6 g, 78.2 %) as white solid. ^{1}H NMR (400 MHz, DMSO-d_6, TMS):δ = 8.21(m, 1H), 7.54 (m, 1H), 7.44 (m, 1H), 7.21 (m, 1H), 2.72 (s, 1H), 10.83 (s, 1H). ^{13}C NMR (100 MHz, DMSO-d_6, TMS): δ= 161.5, 142.3, 138.2, 125.1, 120.7, 119.9, 118.5, 110.5. MS (ESI) *m/z* 164.14 $(M+H)^+$. Anal calcd for $C_8H_6N_2O_2$: C, 59.26; H, 3.73; N, 17.28 Found: C, 59.21; H, 3.72; N, 17.30.

5-Bromo-1*H*-indazole-3-carboxylic acid (IN_3): The compound was synthesized according to the above general procedure using indazole-3-carboxylic acid (**IN_2)** (1.8 g, 11.2 mmol) and bromine (1.84g, 23 mmol) to afford **IN_3** (2.5 g, 72.2 %). ^{1}H NMR (400 MHz, DMSO-d_6,

TMS):δ = 13.4 (s, 1H), 11.44 (s, 1H), 8.52 (s, 1H), 8.31-7.92 (m, 2H). ^{13}C NMR (100 MHz, DMSO-d_6, TMS): δ= 161.5, 142.9, 139.5, 131.3, 127.5, 121.9, 117.8, 112.9. MS (ESI) *m/z* 243.15 $(M+H)^+$. Anal calcd for $C_8H_5BrN_2O_2$: C, 39.86; H, 2.09; N, 11.62 Found: C, 39.89; H, 2.09; N, 11.60.

5-Bromo-*N*-(4-nitrophenyl)-1*H*-indazole-3-carboxamide (IN_4): The compound was synthesized according to the above general procedure using 5-Bromo-1*H*-indazole-3-carboxylic acid (**IN_3)** (0.72 g, 3 mmol) and 4-nitrophenylamine (0.5 g, 4 mmol) to afford **IN_4** (1.2 g, 72.3 %) as yellow solid. M.p: 231-233 ^{o}C. ^{1}H NMR (400 MHz, DMSO-d_6, TMS) δ = 13.56 (s, 1H), 9.34 (s, 1H), 8.13 (d, *J*= 8.2Hz, 1H), 8.02 (s, 1H), 7.75 (d, =8.2Hz, 1H), 7.53-7.15 (m, 4H). ^{13}C NMR (100 MHz, DMSO-d_6, TMS): δ= 163.5, 153.5, 147.2, 141.5, 135.3, 127.8, 121.3 (3C), 117.5, 112.7 (2C), 108.3 (2C). MS (ESI) *m/z* 362.23 $(M+H)^+$. Anal calcd for $C_{14}H_9BrN_4O_3$: C, 46.56; H, 2.51; N, 15.51 Found: C, 46.59; H, 2.51; N, 15.53.

5-Bromo-*N*-(3-(trifluoromethyl)phenyl)-1*H*-indazole-3-carboxamide (IN_5): The compound was synthesized according to the above general procedure using 5-Bromo-1*H*-indazole-3-carboxylic acid (**IN_3)** (0.72 g, 3 mmol) and 3-(trifluoromethyl)phenylamine (0.6 g, 4 mmol) to afford **IN_5** (1.4 g, 69.8%) as brown solid. M.p: 190-192 ^{o}C. ^{1}H NMR (400 MHz, DMSO-d_6, TMS):δ = 13.54 (s, 1H), 9.35 (s, 1H), 8.25 (d, *J*= 8.5Hz, 1H), 8.13 (s, 1H), 7.97 (s, 1H), 7.73 (d, *J*= 8.5Hz, 1H), 7.53-7.32 (m, 3H). ^{13}C NMR (100 MHz, DMSO-d_6, TMS): δ= 163.2, 143.5, 140.9 (2C), 1331.1, 131.3 (2C), 127.7 (2C), 124.3, 120.5, 118.3, 116.8, 109.5 (2C). MS (ESI) *m/z* 385.13 $(M+H)^+$. Anal calcd for $C_{15}H_9BrF_3N_3O$: C, 46.90; H, 2.36; N, 10.94 Found: C, 46.97; H, 2.36; N, 10.96.

5-Bromo-*N*-(3-chlorophenyl)-1*H*-indazole-3-carboxamide (IN_6): The compound was synthesized according to the above general procedure using 5-Bromo-1*H*-indazole-3-carboxylic acid (**IN_3)** (0.72 g, 3 mmol) and 3-chlorophenylamine (0.7 g, 4 mmol) to afford **IN_6** (1.4 g, 71.5%) as white solid. M.p: 210-212 ^{o}C. ^{1}H NMR (400 MHz, DMSO-d_6, TMS): δ = 13.67 (s, 1H), 9.63 (s, 1H), 8.39 (d, *J*= 8.1Hz, 1H), 8.02 (s, 2H), 7.89 (d, *J*= 8.1Hz, 1H), 7.73-7.51 (m, 3H). ^{13}C NMR (100 MHz, DMSO-d_6, TMS): δ= 163.4, 142.1, 138.3, 136.4 (2C), 132.3 (2C), 129.2, 125.5, 121.7 (2C), 118.7, 113.1, 109.5. MS (ESI) *m/z* 351.6 $(M+H)^+$. Anal calcd for $C_{14}H_9BrClN_3O$: C, 47.96; H, 2.59; Br, 22.79; Cl, 10.11; N, 11.99; O, 4.56%; Found: C, 47.08; H, 2.12; Br, 22.98; Cl, 10.01; N, 11.56; O, 4.67%.

5-Bromo-*N*-(2,6-diethylphenyl)-1*H*-indazole-3-carboxamide (IN_7): The compound was synthesized according to the above general procedure using 5-Bromo-1*H*-indazole-3-carboxylic acid (**IN_3)** (0.72 g, 3 mmol) and 2,6-diethylphenylamine (0.5 g, 4 mmol) to afford **IN_7** (2.5 g, 74.9%) as white solid. M.p: 242-244 ^{o}C. ^{1}H NMR (400 MHz, DMSO-d_6, TMS): δ = 13.23 (s, 1H), 9.81 (s, 1H), 8.44 (d, *J*= 8.4Hz, 1H), 8.12 (s, 1H), 7.8 (d, *J*= 8.4Hz, 1H), 7.23-7.09 (m, 3H), 2.77-2.63 (m, 4H), 1.42-1.23 (m, 6H). ^{13}C NMR (100 MHz, DMSO-d_6, TMS): δ= 166.2, 143.5, 139.5, 135.3, 132.4 (2C), 130.1, 127.2 (2C), 124.3 (3C), 119.3, 115.8, 38.3(2C), 17.9 (2C). MS (ESI) *m/z* 373.45 $(M+H)^{+}$. Anal calcd for $C_{18}H_{18}BrN_3O$: C, 58.08; H, 4.87; N, 11.29 Found: C, 58.16; H, 4.88; N, 11.27.

5-Bromo-*N*-(2-hydroxy-4-nitrophenyl)-1*H*-indazole-3-carboxamide (IN_8): The compound was synthesized according to the above general procedure using 5-Bromo-1*H*-indazole-3-carboxylic acid (**IN_3)** (0.72 g, 3 mmol) and 2-hydroxy-4-nitrophenylamine (0.6 g, 4 mmol) to afford **IN_8** (1.6 g, 79.1%) as yellow solid. M.p: 183-185 ^{o}C. ^{1}H NMR (400 MHz, DMSO-d_6, TMS): δ = 13.3 (s, 1H), 9.7 (s, 1H), 9.3 (s, 1H), 8.4 (s, 1H), 8.2-7.81 (m, 4H), 7.55 (s, 1H). ^{13}C NMR (100 MHz, DMSO-d_6, TMS): δ= 169.5, 155.5, 153.4, 143.5, 140.1, 135.3, 132.7, 127.9 (2C), 119.3 (3C), 110.8, 108.3. MS (ESI) *m/z* 378.26 $(M+H)^{+}$. Anal calcd for $C_{16}H_9BrN_4O_4$: C, 44.58; H, 2.41; N, 14.86 Found: C, 44.63; H, 2.41; N, 14.85.

5-Bromo-*N*-(2-bromophenyl)-1*H*-indazole-3-carboxamide (IN_9): The compound was synthesized according to the above general procedure using 5-Bromo-1*H*-indazole-3-carboxylic acid (**IN_3)** (0.72 g, 3 mmol) and 2-bromophenylamine (0.7 g, 4 mmol) to afford **IN_9** (1.3 g, 73.1%) as white solid. M.p: 179-181 ^{o}C. ^{1}H NMR (400 MHz, DMSO-d_6, TMS):δ = 13.7 (s, 1H), 10.1 (s, 1H), 8.13 (d, *J*= 8.7Hz, 1H), 7.9 (s, 1H), 7.83-7.54 (m, 4H), 7.43 (d, *J*= 8.7Hz, 1H). ^{13}C NMR (100 MHz, DMSO-d_6, TMS): δ= 165.3, 145.3, 141.3 (2C), 135.5(2C), 131.3, 128.6, 125.7, 121.3(2C), 115.2, 113.1, 110.9. MS (ESI) *m/z* 396.13 $(M+H)^{+}$. Anal calcd for $C_{14}H_9Br_2N_3O$: C, 42.56; H, 2.30; N, 10.64 Found: C, 42.51; H, 2.30; N, 10.66.

5-Bromo-*N*-(thiazol-2-yl)-1*H*-indazole-3-carboxamide (IN_10): The compound was synthesized according to the above general procedure using 5-Bromo-1*H*-indazole-3-carboxylic acid (**IN_3)** (0.72 g, 3 mmol) and thiazol-2-ylamine (0.6 g, 4 mmol) to afford **IN_10** (1.3 g, 76.5%) as brown solid. M.p: 219-221 ^{o}C. ^{1}H NMR (400 MHz, DMSO-d_6, TMS): δ = 13.9 (s, 1H), 8.31 (d, *J*= 8.4Hz, 1H), 8.12 (s, 1H), 7.73 (d, *J*=2.5Hz, 1H), 7.51 (d, *J*=8.4Hz, 1H), 7.34 (d, *J*=2.5Hz, 1H). ^{13}C NMR (100 MHz, DMSO-d_6, TMS): δ= 164.3, 144.5, 140.8, 138.9, 135.3,

125.3 (2C), 117.4, 114.3, 109.8, 105.7. MS (ESI) *m/z* 334.16 $(M+H)^+$. Anal calcd for $C_{11}H_7BrN_4OS$: C, 40.88; H, 2.18; N, 17.34 Found: C, 40.76; H, 2.18; N, 17.37.

***N*-(Benzo[*d*]thiazol-2-yl)-5-bromo-1*H*-indazole-3-carboxamide (IN_11):** The compound was synthesized according to the above general procedure using 5-Bromo-1*H*-indazole-3-carboxylic acid (**IN_3)** (0.72 g, 3 mmol) and benzo[*d*]thiazol-2-ylamine (0.7 g, 4 mmol) to afford **IN_11** (1.5 g, 77.9%) as white solid. M.p: 235-237 ^oC.^1H NMR (400 MHz, DMSO-d_6, TMS): δ = 13.5 (s, 1H), 12.9 (s, 1H), 8.23 (s, 1H0, 8.09-7.75 (m, 6H). ^{13}C NMR (100 MHz, DMSO-d_6, TMS): δ= 175.6, 161.3, 158.5, 143.7, 140.9, 138.5, 133.8 (2C), 127.4, 125.2 (2C), 121.1, 119.4, 116.3, 112.5. MS (ESI) *m/z* 373.92 $(M+H)^+$. Anal calcd for $C_{15}H_9BrN_4OS$: C, 48.27; H, 2.43; N, 15.01 Found: C, 48.21; H, 2.43; N, 15.03.

5-Bromo-*N*-(pyridin-3-yl)-1*H*-indazole-3-carboxamide (IN_12): The compound was synthesized according to the above general procedure using 5-Bromo-1*H*-indazole-3-carboxylic acid (**IN_3)** (0.72 g, 3 mmol) and pyridin-3-ylamine (0.8 g, 4 mmol) to afford **IN_12** (1.7 g, 80.6%) as brown solid. M.p: 281-283 ^oC. ^1H NMR (400 MHz, DMSO-d_6, TMS): δ = 13.7 (s, 1H), 9.97 (s, 1H), 9.2 (s, 1H), 8.4-8.13 (m, 5H), 8.1 (s, 1H). ^{13}C NMR (100 MHz, DMSO-d_6, TMS): δ= 164.2, 148.3 (2C), 142.5, 139.3 (2C), 132.1, 129.5, 126.3, 121.3 (2C), 117.3, 114.3. MS (ESI) *m/z* 316.12 $(M-H)^+$. Anal calcd for $C_{13}H_9BrN_4O$: C, 49.23; H, 2.86; N, 17.67 Found: C, 49.29; H, 2.86; N, 17.66.

5-Bromo-*N*-(4-fluorophenyl)-1*H*-indazole-3-carboxamide (IN_13): The compound was synthesized according to the above general procedure using 5-Bromo-1*H*-indazole-3-carboxylic acid (**IN_3)** (0.72 g, 3 mmol) and 4-fluorophenylamine (0.7 g, 4 mmol) to afford **IN_13** (1.5 g, 75.7%) as grey solid. M.p: 270-272 ^oC.^1H NMR (400 MHz, DMSO-d_6, TMS): δ = 13.52 (s, 1H), 9.73 (s, 1H), 8.31 (d, *J*=7.9Hz, 1H), 8.03 (s, 1H), 7.88 (d, *J*= 7.9Hz, 1H), 7.63-7.45 (m, 4H). ^{13}C NMR (100 MHz, DMSO-d_6, TMS): δ= 165.4, 160.8, 143.2, 139.7, 135.2, 132.4, 129.5 (2C), 125.7 (2C), 119.7 (2C), 110.7. MS (ESI) *m/z* 335.13 $(M+H)^+$. Anal calcd for $C_{14}H_9BrFN_3O$: C, 50.32; H, 2.71; N, 12.58 Found: C, 50.38; H, 2.71; N, 12.56.

5-Bromo-*N*-(3-chloro-2-methylphenyl)-1*H*-indazole-3-carboxamide (IN_14): The compound was synthesized according to the above general procedure using 5-Bromo-1*H*-indazole-3-carboxylic acid (**IN_3)** (0.72 g, 3 mmol) and 3-chloro-2-methylphenylamine (0.6 g, 4 mmol) to afford **IN_14** (1.4 g, 77.4%) as white solid. M.p: 244-246 ^oC. ^1H NMR (400 MHz, DMSO-d_6, TMS): δ = 13.1 (s, 1H), 10.93 (s, 1H), 8.42 (d, *J*= 8.2Hz, 1H), 8.13 (s, 1H), 7.64 (d, *J*=8.2Hz,

1H), 7.42-7.29 (m, 3H), 2.32 (s, 3H). ^{13}C NMR (100 MHz, DMSO-d_6, TMS): δ= 165.3, 142.7, 135.3 (2C), 132.7 (2C), 127.5, 123.8, 121.5, 119.9, 117.7, 112.5 (2C), 18.2. MS (ESI) *m/z* 365.14 $(M+H)^+$. Anal calcd for $C_{15}H_{11}BrClN_3O$: C, 49.41; H, 3.04; N, 11.52 Found: C, 49.51; H, 3.05; N, 11.54.

5-Bromo-*N*-(pyrazin-2-yl)-1*H*-indazole-3-carboxamide (IN_15): The compound was synthesized according to the above general procedure using 5-Bromo-1*H*-indazole-3-carboxylic acid (**IN_3)** (0.72 g, 3 mmol) and pyrazin-2-ylamine (0.7 g, 4 mmol) to afford **IN_15** (1.8 g, 79.4%) as brown solid. M.p: 225-227 ^{o}C. ^{1}H NMR (400 MHz, DMSO-d_6, TMS): δ = 13.53 (s, 1H), 10.23 (s, 1H), 9.3 (s, 1H), 8.53 (d, *J*= 6.6Hz, 1H), 8.42 (d, *J*=6.6Hz, 1H), 8.31(d, *J*=8.4Hz, 1H), 8.11 (s, 1H), 7.66 (d, *J*= 8.4Hz, 1H). ^{13}C NMR (100 MHz, DMSO-d_6, TMS): δ= 165.3, 151.2, 141.3 (2C), 139.6 (2C), 136.3, 131.4, 125.6, 121.9, 117.3, 115.2. MS (ESI) *m/z* 316.89 $(M-H)^+$. Anal calcd for $C_{12}H_8BrN_5O$: C, 45.31; H, 2.53; N, 22.01 Found: C, 45.40; H, 2.53; N, 22.04.

5-Bromo-*N*-(pyrimidin-2-yl)-1*H*-indazole-3-carboxamide (IN_16): The compound was synthesized according to the above general procedure using 5-Bromo-1*H*-indazole-3-carboxylic acid (**IN_3)** (0.72 g, 3 mmol) and pyrimidin-2-ylamine (0.5 g, 4 mmol) to afford **IN_16** (1.8 g, 81.1%) as brown solid. M.p: 210-212 ^{o}C. ^{1}H NMR (400 MHz, DMSO-d_6, TMS): δ = 13.5 (s, 1H), 9.21 (s, 1H), 8.32-8.11 (m, 3H), 8.41(d, *J*= 8.9Hz, 1H), 7.83 (s, 1H), 7.53 (d, *J*= 8.9Hz, 1H). ^{13}C NMR (100 MHz, DMSO-d_6, TMS): δ= 171.3, 161.5 (3C), 143.7, 139.5, 130.1, 125.7 (2C), 119.7 (2C), 115.6. MS (ESI) *m/z* 316.93 $(M-H)^+$. Anal calcd for $C_{12}H_8BrN_5O$: C, 45.31; H, 2.53; N, 22.01 Found: C, 45.39; H, 2.53; N, 22.04.

5-Bromo-*N*-(3,4-dichlorophenyl)-1*H*-indazole-3-carboxamide (IN_17): The compound was synthesized according to the above general procedure using 5-Bromo-1*H*-indazole-3-carboxylic acid (**IN_3)** (0.72 g, 3 mmol) and 3,4-dichlorophenylamine (0.6 g, 4 mmol) to afford **IN_17** (1.5 g, 78.5%) as white solid. M.p: 239-241 ^{o}C. ^{1}H NMR (400 MHz, DMSO-d_6, TMS):δ = 13.73 (s, 1H), 9.53 (s, 1H), 8.34 (d, *J*= 8.5Hz,1H), 8.13 (s,2H), 7.85 (d, *J*= 8.5Hz, 1H), 7.57 (d, *J*= 7.9Hz, 1H), 7.32 (d, *J*= 7.9Hz, 1H). ^{13}C NMR (100 MHz, DMSO-d_6, TMS): δ= 163.2, 143.5, 139.2 (2C), 132.5 (2C), 128.8 (2C), 121.7 (2C), 119.3117.2, 114.2, 110.9. MS (ESI) *m/z* 386.24 $(M+H)^+$. Anal calcd for $C_{14}H_8BrCl_2N_3O$: C, 43.67; H, 2.09; N, 10.91 Found: C, 43.59; H, 2.09; N, 10.89.

5-Bromo-*N*-(5-nitrothiazol-2-yl)-1*H*-indazole-3-carboxamide (IN_18): The compound was synthesized according to the above general procedure using 5-Bromo-1*H*-indazole-3-carboxylic acid (**IN_3)** (0.72 g, 3 mmol) and 5-nitrothiazol-2-ylamine (0.7 g, 4 mmol) to afford **IN_18** (1.2 g, 71.5%) as yellow solid. M.p: 251-253 ^{o}C. ^{1}H NMR (400 MHz, DMSO-d$_6$, TMS): δ = 13.2 (s, 1H), 8.8 (s, 1H), 8.34 (d, *J*= 8.3Hz, 1H), 8.12 (s, 1H), 7.77 (d, *J*= 8.3Hz, 1H). ^{13}C NMR (100 MHz, DMSO-d$_6$, TMS): δ= 171.3 (2C), 152.1, 142.1, 138.3, 135.1, 130.8, 121.5 (2C), 117.3, 113.4. MS (ESI) *m/z* 369.14 $(M+H)^+$. Anal calcd for $C_{11}H_6BrN_5O_3S$: C, 35.89; H, 1.64; N, 19.02 Found: C, 35.81; H, 1.64; N, 19.04.

5-Bromo-*N*-(5-chloro-2-methoxyphenyl)-1*H*-indazole-3-carboxamide (IN_19): The compound was synthesized according to the above general procedure using 5-Bromo-1*H*-indazole-3-carboxylic acid (**IN_3)** (0.72 g, 3 mmol) and 5-chloro-2-methoxyphenylamine (0.6 g, 4 mmol) to afford **IN_19** (1.3 g, 73.3%) as grey solid. M.p: 264-266 ^{o}C. ^{1}H NMR (400 MHz, DMSO-d$_6$, TMS): δ = 13.3 (s, 1H), 9.89 (s, 1H), 8.31 (d, *J*=8.7Hz, 1H), 8.09 (s, 2H), 7.7 (d, *J*= 8.7Hz, 1H), 7.62 (d, *J*= 8.2Hz, 1H), 7.43 (d, *J*= 8.2Hz, 1H), 4.2 (s, 3H). ^{13}C NMR (100 MHz, DMSO-d$_6$, TMS): δ= 163.5, 152.7, 143.2, 139.6, 132.9, 129.3 (2C), 125.3, 121.9 (2C), 117.3, 115.5, 112.7, 110.9, 64.3. MS (ESI) *m/z* 381.23 $(M+H)^+$. Anal calcd for $C_{15}H_{11}BrClN_3O_2$: C, 47.54; H, 2.23; N, 11.04 Found: C, 47.48; H, 2.23; N, 11.06.

5-Bromo-*N*-(2,4-dimethylphenyl)-1*H*-indazole-3-carboxamide (IN_20): The compound was synthesized according to the above general procedure using 5-Bromo-1*H*-indazole-3-carboxylic acid (**IN_3)** (0.72 g, 3 mmol) and 2,4-dimethylphenylamine (0.7 g, 4 mmol) to afford **IN_20** (1.5 g, 76.1%) as white solid. M.p: 277-279 ^{o}C. ^{1}H NMR (400 MHz, DMSO-d$_6$, TMS): δ = 13.72 (s, 1H), 9.97 (s, 1H), 8.31 (d, *J*= 8.7Hz, 1H), 8.11 (s, 1H), 7.81 (d, *J*= 8.7Hz, 1H), 7.2-7.03 (m, 3H), 2.42 (s, 3H), 2.12 (s, 3H). ^{13}C NMR (100 MHz, DMSO-d$_6$, TMS): δ= 163.2, 141.3, 140.1, 138.3, 135.3, 130.7 (2C), 128.6, 126.3, 124.3 (2C), 117.2 (2C), 111.2, 33.7, 11.5. MS (ESI) *m/z* 345.12 $(M+H)^+$. Anal calcd for $C_{16}H_{14}BrN_3O$: C, 55.83; H, 4.10; N, 12.21 Found: C, 55.90; H, 4.11; N, 12.23.

5-Bromo-*N*-(2,5-dimethylphenyl)-1*H*-indazole-3-carboxamide (IN_21): The compound was synthesized according to the above general procedure using 5-Bromo-1*H*-indazole-3-carboxylic acid (**IN_3)** (0.72 g, 3 mmol) and 2,5-dimethylphenylamine (0.8 g, 4 mmol) to afford **IN_21** (1.1 g, 70.9%) as white solid. M.p: 241-243 ^{o}C. ^{1}H NMR (400 MHz, DMSO-d$_6$, TMS): δ = 13.34 (s, 1H), 9.72 (s, 1H), 8.41 (d, *J*= 8.3Hz, 1H), 7.9 (s, 1H), 7.81 (d, *J*= 8.3Hz, 1H), 7.23-7.09

(m, 3H), 2.32(s, 6H).). ^{13}C NMR (100 MHz, DMSO-d_6, TMS): δ= 166.7, 143.5, 139.5, 135.2 (2C), 130.5 (2C), 125.3, 123.2, 121.9, 117.5, 112.5, 111.8, 23.5. MS (ESI) *m/z* 345.32 $(M+H)^+$. Anal calcd for $C_{16}H_{14}BrN_3O$: C, 55.83; H, 4.10; N, 12.21 Found: C, 55.77; H, 4.11; N, 12.23.

5-Bromo-*N*-(2-methoxy-4-nitrophenyl)-1*H*-indazole-3-carboxamide (IN_22): The compound was synthesized according to the above general procedure using 5-Bromo-1*H*-indazole-3-carboxylic acid (**IN_3)** (0.72 g, 3 mmol) and 2-methoxy-4-nitrophenylamine (0.7 g, 4 mmol) to afford **IN_22** (1.2 g, 71.5%) as yellow solid. M.p: 197-199 ^{o}C. ^{1}H NMR (400 MHz, DMSO-d_6, TMS): δ = 13.56 (s, 1H), 9.85 (s, 1H), 8.13 (s, 1H), 7.97-7.46 (m, 5H), 4.2 (s, 3H). ^{13}C NMR (100 MHz, DMSO-d_6, TMS): δ= 163.4, 158.3, 147.3, 141.3, 138.4, 131.7 (2C), 125.9, 122.5, 119.5 (2C), 114.7 (2C), 103.7, 57.3. MS (ESI) *m/z* 392.16 $(M+H)^+$. Anal calcd for $C_{15}H_{11}BrN_4O_4$: C, 46.06; H, 2.83; N, 14.32 Found: C, 46.12; H, 2.83; N, 14.34.

5-Bromo-*N*-(5-chloro-2-hydroxyphenyl)-1*H*-indazole-3-carboxamide (IN_23): The compound was synthesized according to the above general procedure using 5-Bromo-1*H*-indazole-3-carboxylic acid (**IN_3)** (0.72 g, 3 mmol) and 5-chloro-2-hydroxyphenylamine (0.8 g, 4 mmol) to afford **IN_23** (1.9 g, 79.1%) as white solid. M.p: 183-185 ^{o}C. ^{1}H NMR (400 MHz, DMSO-d_6, TMS): δ = 13.94 (s, 1H), 9.75 (s, 1H), 9.2 (s, 1H), 8.34 (s, 1H), 7.77-7.57 (m, 3H), 7.05 (d, *J*= 7.9Hz, 1H), 6.96 (d, *J*= 7.9Hz, 1H). ^{13}C NMR (100 MHz, DMSO-d_6, TMS): δ= 157.2, 138.2, 135.8, 130.9, 128.1, 125.3, 122.4 (2C), 123.5, 121.4, 112.5, 110.7, 97.3, 94.6. MS (ESI) *m/z* 367.45 $(M+H)^+$. Anal calcd for $C_{14}H_9BrClN_3O_2$: C, 45.87; H, 2.47; N, 11.46 Found: C, 45.76; H, 2.47; N, 11.44.

5-Bromo-*N*-(2-hydroxy-5-methylphenyl)-1*H*-indazole-3-carboxamide (IN_24): The compound was synthesized according to the above general procedure using 5-Bromo-1*H*-indazole-3-carboxylic acid (**IN_3)** (0.72 g, 3 mmol) and 2-hydroxy-5-methylphenylamine (0.9 g, 4 mmol) to afford **IN_24** (1.2 g, 7970.8%) as white solid. M.p: 209-211 ^{o}C. ^{1}H NMR (400 MHz, DMSO-d_6, TMS): δ = 13.62 (s, 1H), 9.89 (s, 1H), 9.53 (s, 1H), 8.43 (d, *J*= 8.9Hz, 1H), 8.21 (s, 1H), 8.01 (s, 1H), 7.75 (d, *J*= 8.9Hz, 1H), 6.93 (d, *J*= 7.9Hz, 1H), 6.79 (d, *J*= 7.9Hz, 1H), 2.27 (s, 3H). ^{13}C NMR (100 MHz, DMSO-d_6, TMS): δ= 165.3, 152.7, 143.7, 139.9, 131.5, 129.7, 125.3 (2C), 123.21, 121.5 (2C), 118.7, 111.5 (2C), 25.7. MS (ESI) *m/z* 347.21 $(M+H)^+$. C, 52.04; H, 3.49; N, 12.14 Found: C, 52.12; H, 3.50; N, 12.16.

5.2.5.5. Identification and characterization of inhibitors using enzyme inhibitory assay, molecular docking and protein thermal stability assay

We have performed the inhibitory enzyme assay for all the synthesized compounds using GR of *B. subtilis*. The inhibitory activity results of compounds were listed in **Table 5.15**. Among all, five compounds have shown considerable inhibitory activity better than **lead 5** (IC_{50} 19.73 ± 0.65 µM). Compounds **IN_11**, **IN_13** and **IN_22** have shown activity less than 10 µM. Compound **IN_22** has shown the highest activity among the group with IC_{50} of 6.11 ± 0.51µM. In comparison with **lead 5,** compound **IN_22** has shown better activity by three times. Log dose-response curve of compound **IN_22** is shown in **Figure 5.51**.

Table 5.15 Synthesized compounds represented with substitutions along with their biological activities

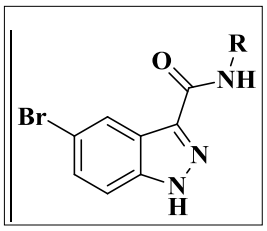

IN_4-24

Compound	R	IC_{50} (µM)	MIC (µM)			Cytotoxicity at 25 µM (% Inhib.)
			Actual MIC	MIC in the presence of Verapamil	MIC in the presence of Piperine	
IN_4	4-Nitrophenyl	>25	69.31	ND	ND	30.41
IN_5	3-(trifluoromethyl)phenyl	11.91±0.24	65.15	2.05	16.23	58.11
IN_6	3-Chlorophenyl	>25	71.45	ND	ND	27.98
IN_7	2,6-Diethylphenyl	>25	67.24	ND	ND	60.32
IN_8	2-Hydroxy-4-nitrophenyl	>25	66.39	ND	ND	20.02
IN_9	2-Bromophenyl	>25	31.67	ND	ND	46.61
IN_10	Thiazol-2-yl	>25	77.41	ND	ND	40.72

IN_11	Benzo[d]thiazol-2-yl	6.32±0.35	67.09	67.09	67.09	37.22
IN_12	Pyridin-3-yl	>25	78.93	ND	ND	49.35
IN_13	4-Fluorophenyl	8.11±0.76	74.92	ND	ND	58.81
IN_14	3-Chloro-2-methylphenyl	>25	68.79	ND	ND	57.23
IN_15	Pyrimidin-2-yl	>25	39.37	ND	ND	79.36
IN_16	5-Nitrothiazol-2-yl	10.96±0.13	78.62	78.62	78.62	37.71
IN_17	3,4-Dichlorophenyl	>25	64.98	ND	ND	20.98
IN_18	5-Nitrothiazol-2-yl	>25	67.82	ND	ND	31.82
IN_19	5-Chloro-2-methoxyphenyl	>25	65.23	ND	ND	50.71
IN_20	2,4-Dimethylphenyl	>25	72.78	ND	ND	46.98
IN_21	2,5-Dimethylphenyl	>25	72.78	ND	ND	64.21
IN_22	2-Methoxy-4-nitrophenyl	6.11±0.51	63.93	63.93	63.93	60.23
IN_23	5-Chloro-2-hydroxyphenyl	>25	68.26	ND	ND	36.67
IN_24	2-Hydroxy-5-methylphenyl	>25	72.38	ND	ND	54.53
Isoniazid		>25	0.72	0.72	0.72	ND
Ethambutol		>25	7.64	3.82	3.82	ND
Rifampicin		>25	0.15	0.15	0.15	ND

ND: Not determined

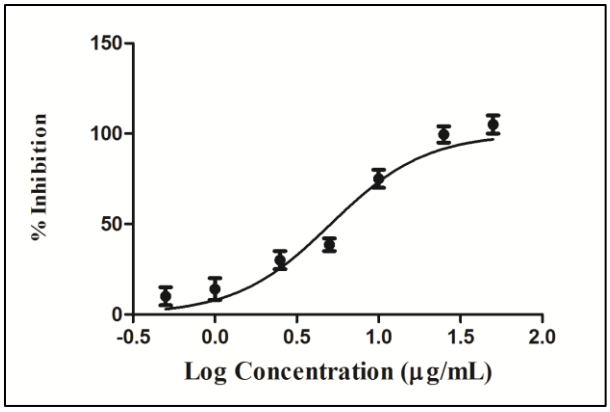

Figure 5.51: Log dose response curve of compound **IN_22** with different log concentrations (X-axis) vs percentage inhibition (Y-axis).

Further, we analyzed of the binding poses of synthesized compounds with the support of molecular docking. We performed docking and molecular dynamics of molecules (picked based on IC_{50} values) in the crystal structures of *M. tuberculosis* and *B. subtilis* GR in complex with D-glutamate (PDB ID: 5HJ7, 1ZUW respectively) using Glide XP docking and Desmond (Schrodinger). The inhibitors were not docked properly on the substrate binding site (D-glutamate) in both proteins; hence we have tried docking in allosteric sites generated by using site map. Based on site-scores **site 1** in both the proteins was selected for further docking studies.

Here we discuss the binding pattern of one of the active compounds **IN_11** (IC_{50} 6.32 ± 0.35 µM), the superimposition of both proteins and compound **IN_11** in its binding mode was shown in **Figure 5.52**. The 2D-binding orientation of compound **IN_11** within the two proteins binding allosteric sites were represented in **Figure 5.53**. The predicted bound conformation of the active compound showed interactions with the side chain of the Glu 153 in both proteins. Apart from this the compound further stabilized through various hydrophobic and few polar amino acid residue interactions. The compound was very well fit into the allosteric site cavity of the protein with a docking scores of-3.578 kcal/mol and -4.892 kcal/mol in 5HJ7 and 1ZUW respectively. Thus molecular docking was a great help in supporting the confirmation of inhibitory activity in both the organisms.

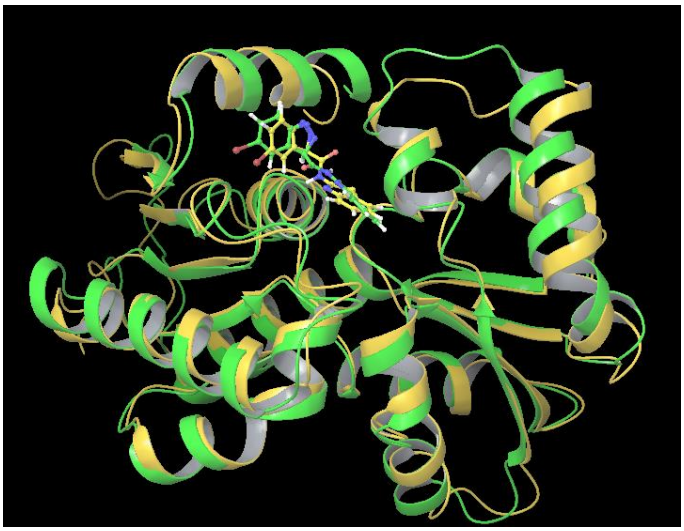

Figure 5.52: Docking pose of active molecule **IN_ 11** in **site 1** of *M. tuberculosis* (5HJ7) and *B. subtilis* (1ZUW) in superimposed view. Yellow color represents protein and ligand in 5HJ7 whereas green represents 1ZUW.

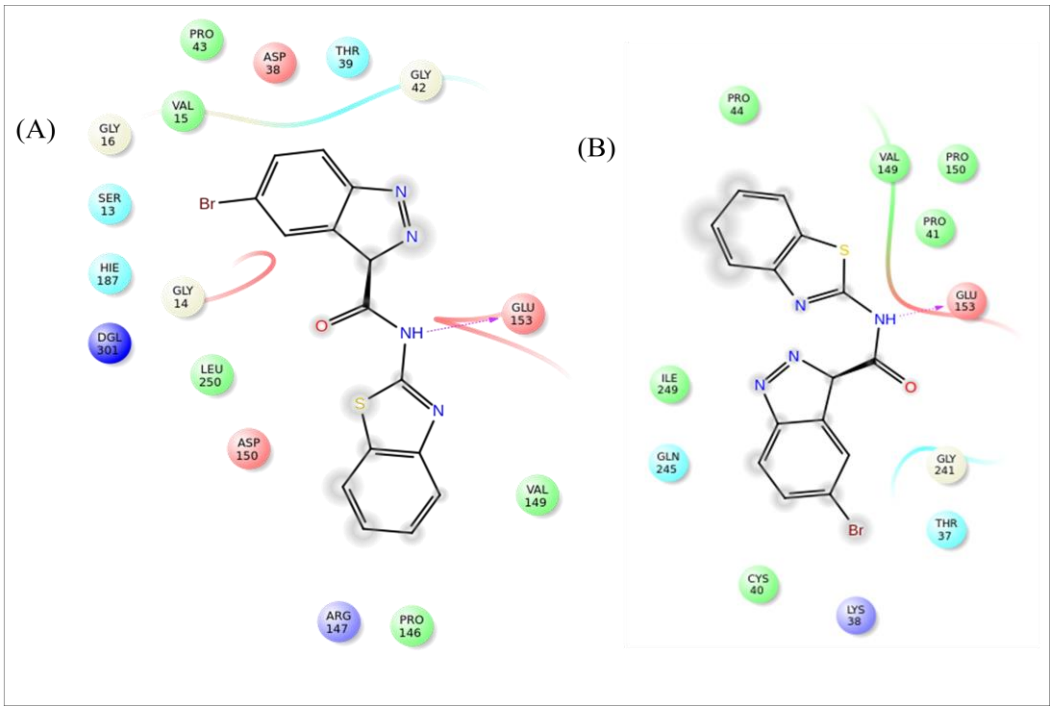

Figure 5.53: Binding pose and interaction pattern of compound **IN_11** in (A) *M. tuberculosis* and (B) *B. subtilis*

Compound **IN_11** in 5HJ7 and 1ZUW protein complexes were subjected to a 10 ns simulation. The rmsd analysis plots for the protein-ligand complexes have been carried out so as to measure the distance between atoms during simulation (**Figure 5.54**).Rmsd for 1ZUW, C_{α} and ligand were within the average of ~1.7 Å and ~1.0 Å and for 5HJ7 both C_{α} and ligand were within average of ~1.5 Å and ~1.1 Å respectively during 10 ns simulation trajectory. The root mean square fluctuation (rmsf) analysis shows the fluctuation range undergone by every residue in the protein during simulation. Rmsf plot for compound **IN_11** in both protein complexes was shown in (**Figure 5.55**). The figure shows least fluctuations of the ligand binding site residues with rmsf values in an average of ~1.3 Å and 1.8 Å respectively for 5HJ7 and 1ZUW.

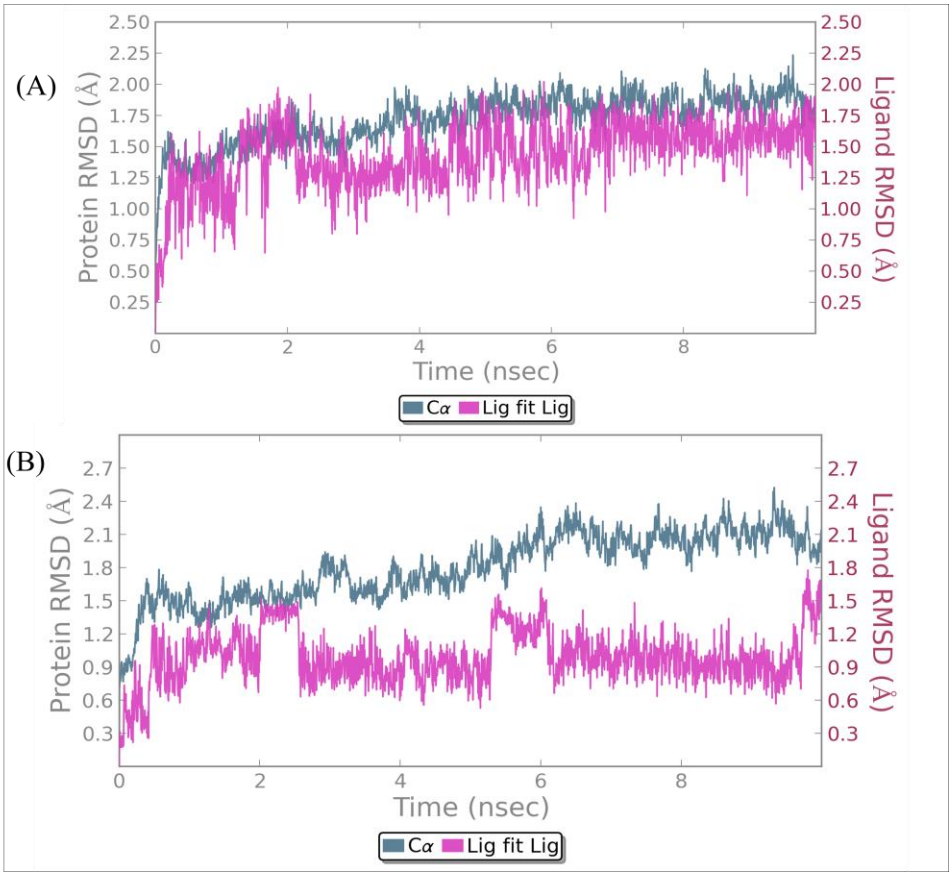

Figure 5.54: Rmsd plots of GR inbound state with compounds **IN_11** as a function of time in *M. tuberculosis* (A) and (B) *B. subtilis.*

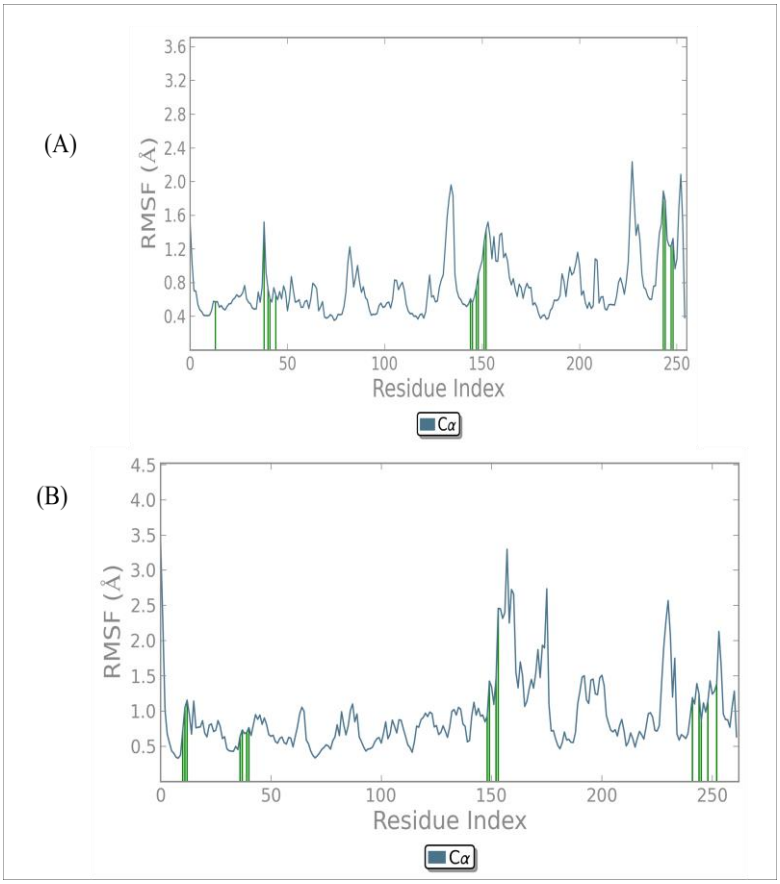

Figure 5.55: Rmsf plots of GR inbound state with compounds **IN_11** as a function of time in *M. tuberculosis* (A) and (B) *B. subtilis.*

Mode of inhibition of active compound was characterized using thermal shift assay. The melt temperature pattern of most active molecule **IN_22** indicated that it follows the non-competitive mode of inhibition. It showed a shift in ΔT_m by ~3.5 ^oC with native protein and when tested with protein-substrate complex there was a shift ~4.9 ^oC with native protein and ~4.1 ^oC with protein and D-glu complex (**Figure 5.56**). This indicates that the protein and protein-substrate complex were more stabilized in the presence of compound **IN_22** when compared to **lead 5**.

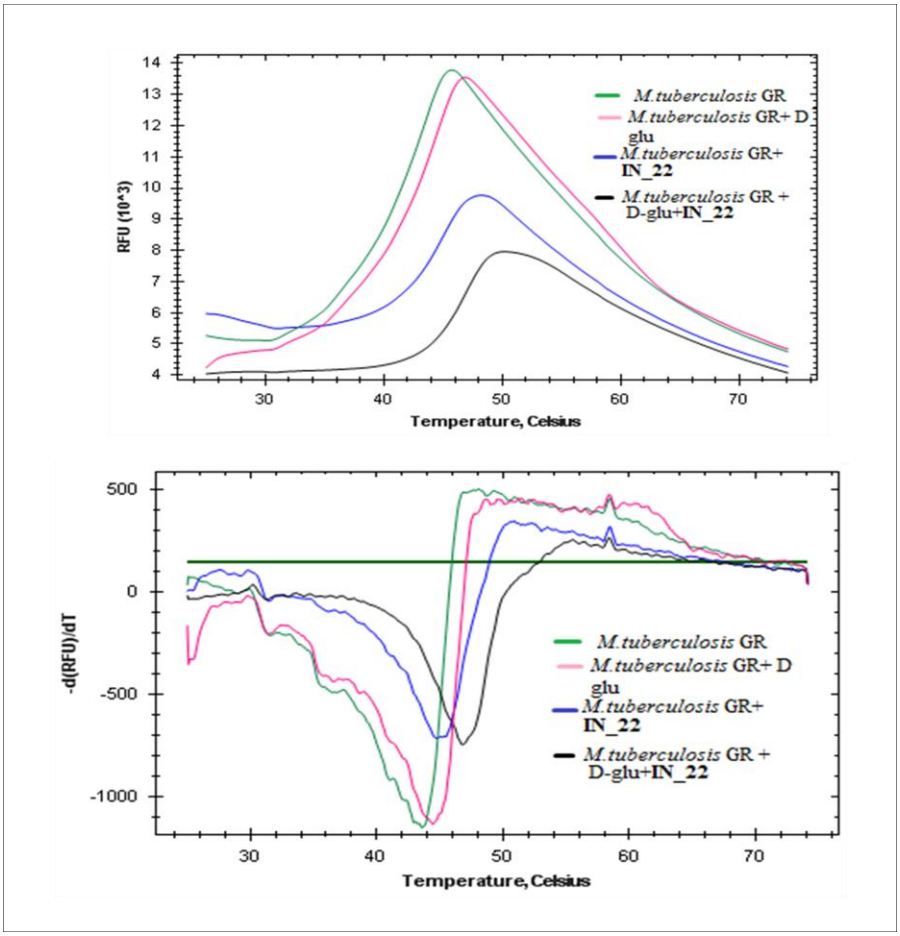

Figure 5.56: Thermal stability curves of *M. tuberculosis* GR depicting the non-competitive inhibition by compound **IN_22.**

5.2.5.6. *In vitro* active and nutrient-starved dormant *M. tuberculosis* assay models

All the synthesized molecules were screened *in vitro* for their activity against replicating *M. tuberculosis* using microplate alamar blue assay (MABA) with drug concentrations from 50 µg/mL to 0.78 µg/mL and the minimum inhibitory concentration (MIC) was determined for each compound MIC values of the synthesized compounds and the standard drugs (Isoniazid, Ethambutol and Rifampicin) for comparison were represented in **Table 5.15**. None of the compounds have shown good inhibitory activity against whole cell bacteria. Assuming efflux of the drug by bacteria as the major reason for their inactivity, compounds **IN_5, IN_11, IN_13, IN_16** and **IN_ 20** that showed activity in enzyme assay were tested for susceptibility in the presence of efflux pump inhibitors like verapamil and piperine. Among all the compound **IN_5** has shown drastic improvement in activity in the presence of verapamil (2.05 µM) and piperine

(16.23 µM) (**Table 5.15**). It has shown better activity than standard drugs (Isoniazid, Ethambutol and Rifampicin) in the presence of verapamil.

In this model, *M. tuberculosis* cultures were starved of nutrients in phosphate buffer saline (PBS) for 6 weeks. After 6 weeks, the culture was treated with the synthesized test compounds and standard drugs at a concentration of 10 µg/mL. Considering the IC_{50} and MIC values of the synthesized compounds **IN_ 11** and **IN_22** were selected for testing in nonreplicating *M. tuberculosis* assays. INH, RIF and MOXI were selected for standard comparison. INH, RIF and MOXI have shown an inhibition of 1, 1.8 and 2.2 log reduction respectively compared with control (**Figure 5.57**). Test compounds **IN_11** and **IN_22** have shown a log reduction of 1.4 and 1.3 respectively. This indicates that test compounds were showing better activities than INH on dormant culture.

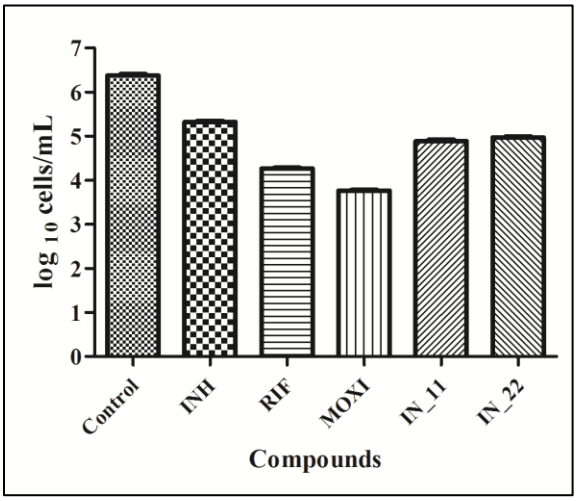

Figure 5.57: Activity profile of compounds in the nutrient starvation model. Bacterial count (Mean ± S.E., n=3) for control and treated groups was estimated through MPN (most probable number) assay.

5.2.5.7. Determination of kill kinetics using nutrient starved culture of *M. tuberculosis*

We have evaluated compounds at different concentrations on bacteria obtained after 2 weeks of nutrient starvation at 0, 7, 14, 21 days after drug treatment. Compounds **IN_11** and **IN_22** showing good inhibition in above study on nutrient starved culture have shown MBC more than

fourfold of their MIC values indicating that they are bacteriostatic. The kinetic graph of compound **IN_22** was shown in **Figure 5.58**.

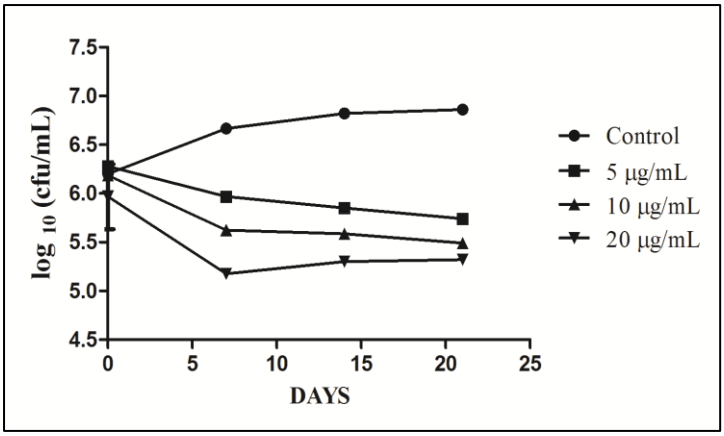

Figure 5.58: Kill kinetic curve of compound **IN_22** depicting bacteriostatic inhibition.

5.2.4.8. Inhibitory studies on persistent *M. tuberculosis* bacteria (biofilm) and cytotoxicity assay

Compounds **11** and **22** were tested for their activity on biofilm at concentration of10 µg/mL. Standards INH, RIF and MOXI have shown a log reduction of 1, 1.2 and 1.8 respectively compared to control. Test compounds **11** and **22** have shown log reduction of 1.2 and 0.8 respectively as shown in **Figure 5.59**. All the compounds were tested at a concentration of 25 µM and the percentage inhibition was found to be in varied ranges. However, most of the compounds were not toxic at 25 µM (**Table 5.15**). Hence most of the compounds are devoid of effects on metabolism.

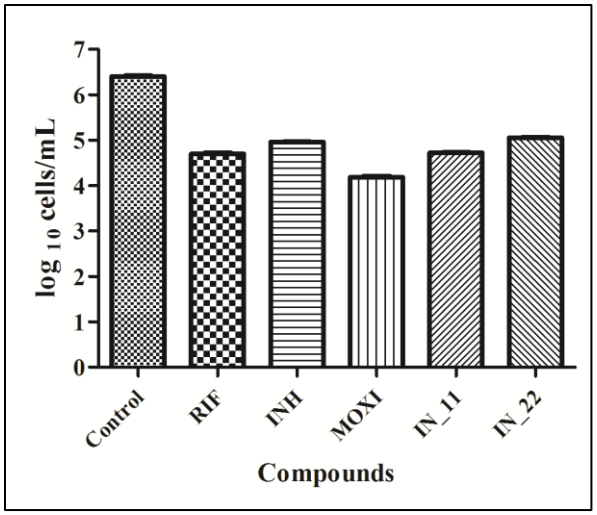

Figure 5.59: Comparative biofilm inhibitory activity plots of compounds **IN_11** and **IN_22** against *M. tuberculosis* along with standards. Bacterial count estimation (Mean ± S.D., n = 4) for control and treated groups was conducted by using the MPN assay.

5.2.5.9. Highlights of the study

In present work, we attempted to modify Indazole leads to increase efficiency against *M. tuberculosis* by targeting GR enzyme. We were able to identify compounds which have efficacy against both replicating and non-replicating stages of *M. tuberculosis*. **IN_22** has shown considerable activity against the active stage of tuberculosis, additionally, they have the advantage of potency against the persistent phase of tuberculosis (**Figure 5.60**). Further, there is a need of optimization to develop them into much more promising agents against the disease. As the urge for new antitubercular drugs is increasing day by day the present class of drugs would be a suitable class for further drug development studies.

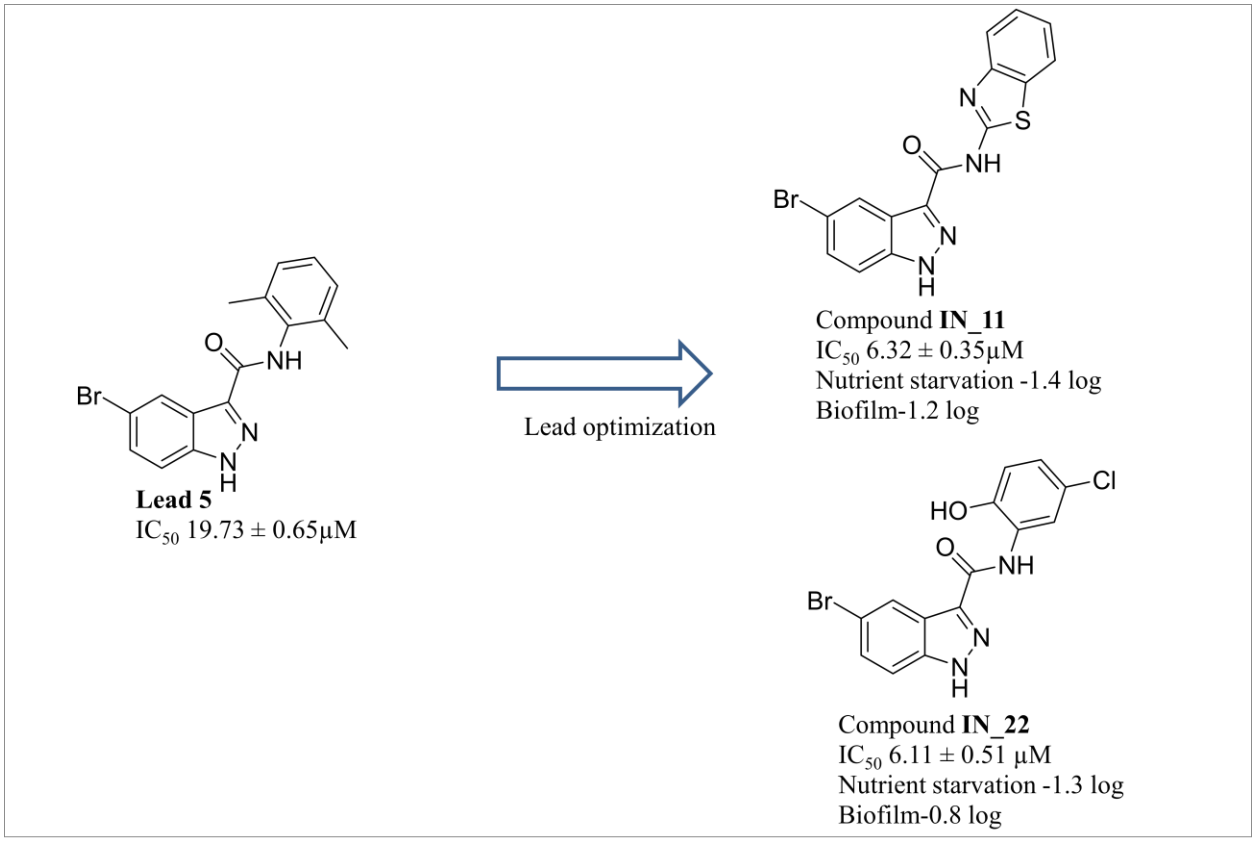

Figure 5.60: Chemical structure and biological activity of the most active compounds **IN_11** and **IN_22**

Summary and Conclusion

Findings of WHO review on antimicrobial resistance revealed that one person in every three seconds will be affected with superbugs which accounts for 10 million lives by 2050. Superbugs are nothing but microbes which acquired resistance to all available antibiotics. Tuberculosis and malaria would cause devastating blow on mankind as superbugs. All these observations throw limelight on need for development of new drugs especially in case of Tuberculosis. Despite END TB Strategy efforts by WHO TB still remains among top 10 leading causes of deaths worldwide.

About one third of world population has been infected with latent TB and has lifetime risk of 10% to develop into active TB. Risk factors such as co-infection with HIV, use of immunosuppressant, smoking will aggravate condition of latent TB. Current treatment regimens for latent TB are too long and have associated side effects. New drugs are required in TB with enhanced efficacy against resistant forms and which can reduce treatment duration due to their potency to eliminate persistent phase of TB. Literature review shows that Pantothenate kinase and Glutamate racemase are attractive and less exploited targets of *M. tuberculosis*.

In first section we reported the design logic and screening of database using e-pharmacophore and further testing for their inhibitory activity of *M. tuberculosis* PanK which was unsuccessful. We haven't proceeded with the study further. In the second section we have detailed about the studies performed targeting *M. tuberculosis* GR, we synthesized total of 117 compounds by lead derivatization technique for GR and evaluated them by various biological assays. In Benzthiazole series, compound **BT_25** (1-(3-(benzo[*d*]thiazol-2-yl)phenyl)-3-(*p*-tolyl)thiourea) has shown very good activity in *B. subtilis* enzyme assay. Further evaluation in molecular docking supported that this compound also showed similar interactions with *B. subtilis* and TB bacteria with non competitive mode of inhibition in TB bacteria (thermal shift assay results). Compounds **BT_10, BT_23, BT_24** and **BT_25** have shown activity in MABA assay, some compounds which doesn't show activity in enzyme assay has shown activity in MABA and vice versa in case of some compounds. The same set of above mentioned compounds have shown activity in nutrient starvation also. Where as in biofilm study compound **BT_10, BT_24** and **BT_25** have shown log reduction and in killkinetics compound **BT_10** has shown concentration dependant bactericidal inhibition. Compound **BT_25** has shown potent activity in *in vivo* study

on zebrafish. All the results suggest that these compounds are active in replicating and non replicating M. *tuberculosis*.

In Benzoxazole series compounds which showed good *in vitro* and *in vivo* activities belong to thiourea family. Compound **BO_22** (1-(4-chlorophenyl)-3-(3-(5-methylbenzo[*d*]oxazol-2-yl)phenyl)thiourea) was proven to be the most potent molecule of series in both *in vitro* and *in vivo* evaluation studies. This data was supported by molecular docking and simulation studies, both the compounds retained similar kind of interactions with amino acid residues. There were some compounds which are active in vitro but were unsuccessful on whole cell organism, one of the drawback can be the strong efflux nature of cell wall. Further there were few compounds showing very food whole organism inhibition than enzyme inhibition, these might be targeting an additional pathway for inhibition. These compounds need further studies to answer all questions in drug discovery. Further optimization of compounds can results in still better compounds for treating tuberculosis. All these parameters make it a better candidate for further development.

In flourothiazole series, comparing the overall assays tested for, compounds **FT_24** 4-(5-fluoro-2-(4-methylpiperazin-1-yl)thiazol-4-yl)-*N*-(2-hydroxyethyl)benzamide and **FT_25** 4-(5-fluoro-2-(4-methylpiperazin-1-yl)thiazol-4-yl)benzamide have shown potent activities in enzyme assay as well as against active and dormant culture. The above conclusions were supported by molecular docking and simulation studies, both the compounds retained similar kind of interactions with amino acid residues. There were few compounds showing very food whole organism inhibition than enzyme inhibition, these might be targeting an additional pathway for inhibition.

In Oxoquinazoline and Indazole series, we were able to identify compounds which have efficacy against both replicating and nonreplicating stages of *M.tuberculosis*. **QA_16, QA_19** and **IN 22** results show that they are equally effective as standard drugs against active stage of tuberculosis, additionally, they have the advantage of potency against the persistent phase of tuberculosis.

Our studies open a new window to a set of NCE which can be further developed into a novel drug candidate.

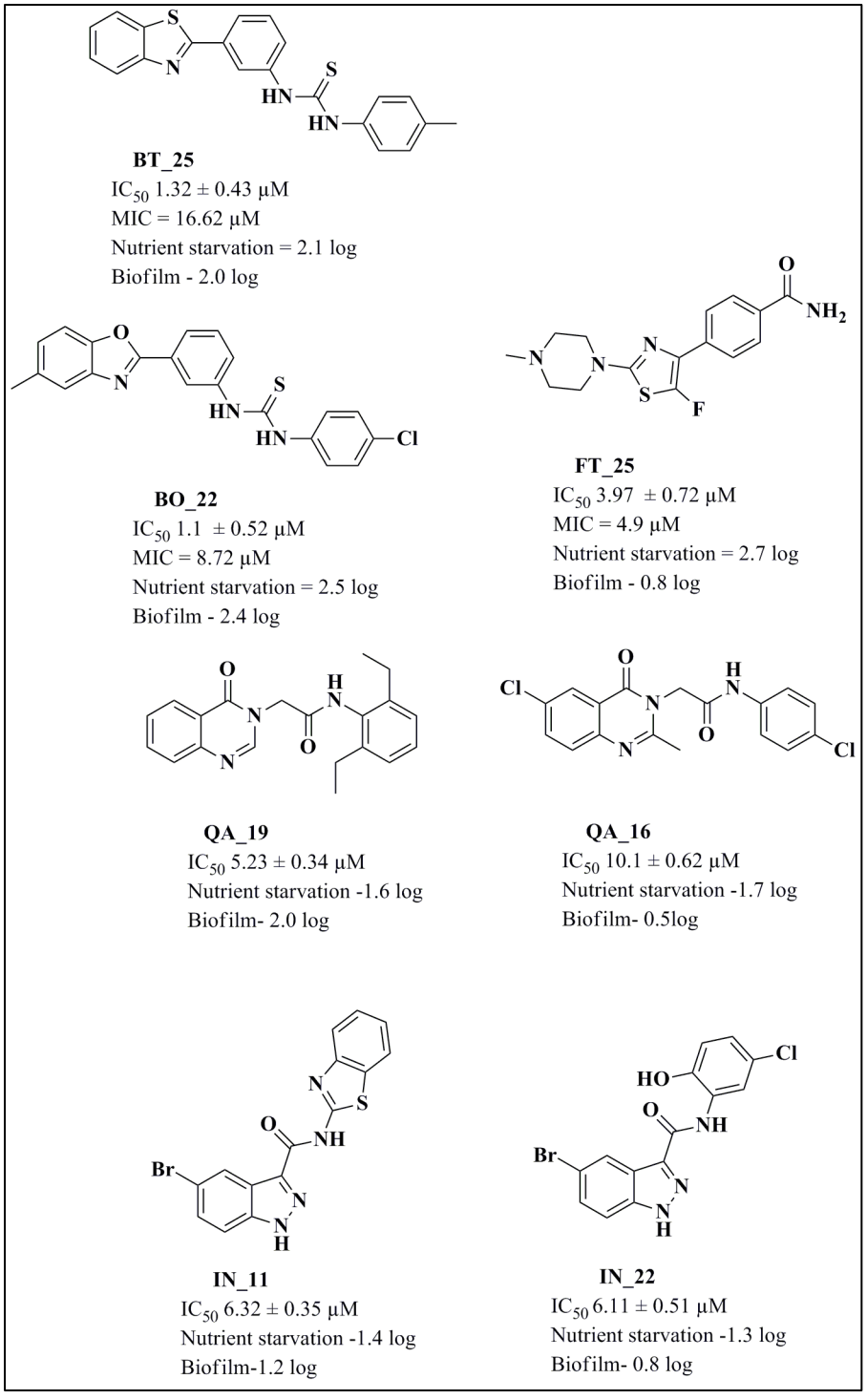

Figure 6.1: Structures of most potent compounds from each series

Future Perspectives

The Pantothenate kinase and Glutamate racemase biosynthetic pathways are absent in humans but essential in microbial pathogens, suggesting that it provides potential targets for the development of novel antibacterial compounds with minimal mammalian toxicity. The present study focused on utilizing the less and unexploited targets such as PanK and GR as potential anti-tubercular target thus offering an excellent opportunity to address the ever increasing problem of latent tuberculosis.

The compounds reported here displayed excellent enzyme inhibitory potency and potency against *M. tuberculosis* H37Rv strain. Compounds were found to be more effective in dormant models such as nutrient starvation model, biofilm model, Nutrient starved and kill kinetics model. Although these results are encouraging, further optimization is still needed.

Also some of the active anti-mycobacterial compounds reported in this thesis were screened for their *in vivo* activity using adult zebra fish. Extensive pharmacodynamics and pharmacokinetic studies of the safer compounds have to be undertaken in higher animal models.

Extensive toxic and side effect profile of all the synthesized compounds may be studied. The advancement of any of the candidate molecules presented in this thesis along a drug development track would require a substantial investment in medicinal chemistry, preclinical and clinical studies.

Cost effective and minimizing the number of steps involved in the synthesis of compounds reported in this thesis should be optimized.

References

Awasthy, D., Ambady, A., Bhat, J., Sheikh, G., Ravishankar, S., Subbulakshmi, V., & Sharma, U. (2010). Essentiality and functional analysis of type I and type III Pantothenate kinases of Mycobacterium tuberculosis. *Microbiology*, *156*(9), 2691-2701.

Banks, J. L., Beard, H. S., Cao, Y., Cho, A. E., Damm, W., Farid, R., & Murphy, R. (2005). Integrated modeling program, applied chemical theory (IMPACT). *Journal of computational chemistry*, *26*(16), 1752-1780.

Betts, J. C., Lukey, P. T., Robb, L. C., McAdam, R. A., & Duncan, K. (2002). Evaluation of a nutrient starvation model of *Mycobacterium tuberculosis* persistence by gene and protein expression profiling. *Molecular microbiology*, *43*(3), 717-731.

Bittker, J. A., & Ross, N. T. (Eds.). (2016). *High throughput screening methods: evolution and refinement* (Vol. 1). Royal Society of Chemistry.

Björkelid, C., Bergfors, T., Raichurkar, A. K. V., Mukherjee, K., Malolanarasimhan, K., Bandodkar, B., & Jones, T. A. (2013). Structural and biochemical characterization of compounds inhibiting Mycobacterium tuberculosis PanK. *Journal of Biological Chemistry*, jbc-M113.

Centers for Disease Control and Prevention. (2012). The difference between latent TB infection and TB disease. *CDC Report*.

Chetnani, B., Das, S., Kumar, P., Surolia, A., & Vijayan, M. (2009). Mycobacterium tuberculosis pantothenate kinase: possible changes in location of ligands during enzyme action. *Acta Crystallographica Section D: Biological Crystallography*, *65*(4), 312-325.

Chetnani, B., Kumar, P., Surolia, A., & Vijayan, M. (2010). M. tuberculosis pantothenate kinase: dual substrate specificity and unusual changes in ligand locations. *Journal of molecular biology*, *400*(2), 171-185.

Chetnani, B., Kumar, P., Abhinav, K. V., Chhibber, M., Surolia, A., & Vijayan, M. (2011). Location and conformation of pantothenate and its derivatives in Mycobacterium tuberculosis pantothenate kinase: insights into enzyme action. *Acta Crystallographica Section D: Biological Crystallography*, *67*(9), 774-783.

Clark-Curtiss, J. E., & Haydel, S. E. (2003). Molecular genetics of Mycobacterium tuberculosis pathogenesis. *Annual Reviews in Microbiology*, *57*(1), 517-549.

Collins, L. A., & Franzblau, S. G. (1997). Microplate alamar blue assay versus BACTEC 460 system for high-throughput screening of compounds against Mycobacterium tuberculosis and Mycobacterium avium. *Antimicrobial agents and chemotherapy*, *41*(5), 1004-1009.

Cronan, M. R., & Tobin, D. M. (2014). Fit for consumption: zebrafish as a model for tuberculosis. *Disease models & mechanisms*, *7*(7), 777-784.

D'Ambrosio, L., Centis, R., Sotgiu, G., Pontali, E., Spanevello, A., & Migliori, G. B. (2015). New anti-tuberculosis drugs and regimens: 2015 update. *ERJ Open Research*, *1*(1), 00010-2015.

De Man, J. C. (1975). The probability of most probable numbers. *European journal of applied microbiology and biotechnology*, *1*(1), 67-78.

Dheda, K., Warren, R. M., Zumla, A., & Grobusch, M. P. (2010). Extensively drug-resistant tuberculosis: epidemiology and management challenges.*Infectious Disease Clinics of North America*, *24*(3), 705-725.

Das, S., Kumar, P., Bhor, V., Surolia, A., & Vijayan, M. (2006). Invariance and variability in bacterial PanK: a study based on the crystal structure of Mycobacterium tuberculosis PanK. *Acta Crystallographica Section D: Biological Crystallography*, *62*(6), 628-638.

Das, S., Kumar, P., Bhor, V., Surolia, A., & Vijayan, M. (2005). Expression, purification, crystallization and preliminary X-ray crystallographic analysis of pantothenate kinase from Mycobacterium tuberculosis. *Acta Crystallographica Section F: Structural Biology and Crystallization Communications*, *61*(1), 65-67.

Dover, L. G., & Coxon, G. D. (2011). Current status and research strategies in tuberculosis drug development: miniperspective. *Journal of medicinal Chemistry*, *54*(18), 6157-6165.

Dubos, R. J., & Davis, B. D. (1946). Factors affecting the growth of tubercle bacilli in liquid media. *The Journal of experimental medicine*, *83*(5), 409.

Flynn, J. L., & Chan, J. (2001). Immunology of tuberculosis. *Annual review of immunology*, *19*(1), 93-129.

Franzblau, S. G., Witzig, R. S., McLaughlin, J. C., Torres, P., Madico, G., Hernandez, A., ... & Gilman, R. H. (1998). Rapid, low-technology MIC determination with clinical Mycobacterium tuberculosis isolates by using the microplate Alamar Blue assay. *Journal of clinical microbiology*, *36*(2), 362-366.

Friesner, R. A., Murphy, R. B., Repasky, M. P., Frye, L. L., Greenwood, J. R., Halgren, T. A., ... & Mainz, D. T. (2006). Extra precision glide: Docking and scoring incorporating a model of hydrophobic enclosure for protein− ligand complexes. *Journal of medicinal chemistry*, *49*(21), 6177-6196.

Gerlier, D., & Thomasset, N. (1986). Use of MTT colorimetric assay to measure cell activation. *Journal of immunological methods*, *94*(1-2), 57-63.

Ginsburg, A. S., Grosset, J. H., & Bishai, W. R. (2003). Fluoroquinolones, tuberculosis, and resistance. *The Lancet infectious diseases*, *3*(7), 432-442.

Ginsberg, A. M., & Spigelman, M. (2007). Challenges in tuberculosis drug research and development. *Nature medicine*, *13*(3), 290-294.

Glavas, S., & Tanner, M. E. (2001). Active site residues of glutamate racemase. *Biochemistry*, *40*(21), 6199-6204.

Green, K., & Garneau-Tsodikova, S. (2013). Resistance in tuberculosis: what do we know and where can we go?. *Frontiers in Microbiology*, *4*, 208.

Haydel, S. E. (2010). Extensively drug-resistant tuberculosis: a sign of the times and an impetus for antimicrobial discovery. *Pharmaceuticals*, *3*(7), 2268-2290.

Houben, R. M., Sumner, T., Grant, A. D., & White, R. G. (2014). Ability of preventive therapy to cure latent Mycobacterium tuberculosis infection in HIV-infected individuals in high-burden settings. *Proceedings of the National Academy of Sciences*, *111*(14), 5325-5330.

Hwang, K. Y., Cho, C. S., Kim, S. S., Sung, H. C., Yu, Y. G., & Cho, Y. (1999). Structure and mechanism of glutamate racemase from Aquifex pyrophilus. *Nature structural biology*, *6*(5).

Ivey, R. A., Zhang, Y. M., Virga, K. G., Hevener, K., Lee, R. E., Rock, C. O., ... & Park, H. W. (2004). The structure of the pantothenate kinase· ADP· pantothenate ternary complex reveals the relationship between the binding sites for substrate, allosteric regulator, and antimetabolites. *Journal of Biological Chemistry*, *279*(34), 35622-35629.

Israyilova, A., Buroni, S., Forneris, F., Scoffone, V. C., Shixaliyev, N. Q., Riccardi, G., & Chiarelli, L. R. (2016). Biochemical Characterization of Glutamate Racemase—A New Candidate Drug Target against Burkholderia cenocepacia Infections. *PloS one*, *11*(11), e0167350.

Jasmer, R. M., Nahid, P., & Hopewell, P. C. (2002). Latent tuberculosis infection. *New England Journal of Medicine*, *347*(23), 1860-1866.

Jorgensen, W. L., Chandrasekhar, J., Madura, J. D., Impey, R. W., & Klein, M. L. (1983). Comparison of simple potential functions for simulating liquid water. *The Journal of chemical physics*, *79*(2), 926-935.

Jorgensen, W. L., Maxwell, D. S., & Tirado-Rives, J. (1996). Development and testing of the OPLS all-atom force field on conformational energetics and properties of organic liquids. *J. Am. Chem. Soc*, *118*(45), 11225-11236.

Kim, K. H., Bong, Y. J., Park, J. K., Shin, K. J., Hwang, K. Y., & Kim, E. E. (2007). Structural basis for glutamate racemase inhibition. *Journal of molecular biology*, *372*(2), 434-443.

Kräutler, V., Van Gunsteren, W. F., & Hünenberger, P. H. (2001). A fast SHAKE algorithm to solve distance constraint equations for small molecules in molecular dynamics simulations. *Journal of computational chemistry*, *22*(5), 501-508.

Kulka, K., Hatfull, G., & Ojha, A. K. (2012). Growth of *Mycobacterium tuberculosis* biofilms. *JoVE* , (60), e3820-e3820.

Leonardi, R., Chohnan, S., Zhang, Y. M., Virga, K. G., Lee, R. E., Rock, C. O., & Jackowski, S. (2005). A pantothenate kinase from Staphylococcus aureus refractory to feedback regulation by coenzyme A. *Journal of Biological Chemistry*, *280*(5), 3314-3322.

Lundqvist, T., Fisher, S. L., Kern, G., Folmer, R. H., Xue, Y., Newton, D. T., ... & de Jonge, B. L. (2007). Exploitation of structural and regulatory diversity in glutamate racemases. *Nature*, *447*(7146), 817.

Lyon, R. H., Lichstein, H. C., & Hall, W. H. (1963). Effect of Tween 80 on the growth of tubercle bacilli in aerated cultures. *Journal of bacteriology*, *86*(2), 280-284.

O'Donnell, M. R., Padayatchi, N., Kvasnovsky, C., Werner, L., Master, I., & Horsburgh Jr, C. R. (2013). Treatment outcomes for extensively drug-resistant tuberculosis and HIV co-infection. *Emerg Infect Dis*, *19*(3), 416-424.

Parida, S. K., Axelsson-Robertson, R., Rao, M. V., Singh, N., Master, I., Lutckii, A., & Maeurer, M. (2015). Totally drug-resistant tuberculosis and adjunct therapies. *Journal of Internal Medicine*, *277*(4), 388-405.

Parish, T., & Stoker, N. G. (Eds.). (1998). Mycobacteria protocols pg 269-279.

Pai, M., Behr, M., Dowdy, D., Dheda, K., Divangahi, M., Boehme, C., Ginsberg, A., Swaminathan, S., Spigelman, M., Getahun, H., Menzies, D., & Raviglione M9. (2016). Tuberculosis. *Nature Reviews. Disease Primers*, 2, 16076.

Pieters, J. (2008). Mycobacterium tuberculosis and the macrophage: maintaining a balance. *Cell host & microbe*, *3*(6), 399-407.

Poen, S., Nakatani, Y., Opel-Reading, H. K., Lassé, M., Dobson, R. C., & Krause, K. L. (2016). Exploring the structure of glutamate racemase from Mycobacterium tuberculosis as a template for anti-mycobacterial drug discovery. *Biochemical Journal*, *473*(9), 1267-1280.

Prosser, G. A., Rodenburg, A., Khoury, H., de Chiara, C., Howell, S., Snijders, A. P., & de Carvalho, L. P. S. (2016). Glutamate racemase is the primary target of β-chloro-D-alanine in Mycobacterium tuberculosis. *Antimicrobial agents and chemotherapy*, *60*(10), 6091-6099.

Salam, N. K., Nuti, R., & Sherman, W. (2009). Novel method for generating structure-based pharmacophores using energetic analysis. *Journal of chemical information and modeling*, *49*(10), 2356-2368.

Salina, E., Ryabova, O., Kaprelyants, A., & Makarov, V. (2014). New 2-thiopyridines as potential candidates for killing both actively growing and dormant *Mycobacterium tuberculosis* cells. *Antimicrobial agents and chemotherapy*, *58*(1), 55-60.

Scudiero, D. A., Shoemaker, R. H., Paull, K. D., Monks, A., Tierney, S., Nofziger, T. H., ... & Boyd, M. R. (1988). Evaluation of a soluble tetrazolium/formazan assay for cell growth and drug sensitivity in culture using human and other tumor cell lines. *Cancer research*, *48*(17), 4827-4833.

Sengupta, S., Shah, M., & Nagaraja, V. (2006). Glutamate racemase from Mycobacterium tuberculosis inhibits DNA gyrase by affecting its DNA-binding. *Nucleic acids research*, *34*(19), 5567-5576.

Sengupta, S., Ghosh, S., & Nagaraja, V. (2008). Moonlighting function of glutamate racemase from Mycobacterium tuberculosis: racemization and DNA gyrase inhibition are two independent activities of the enzyme. *Microbiology*, *154*(9), 2796-2803.

Schleifer, K. H., & Kandler, O. (1972). Peptidoglycan types of bacterial cell walls and their taxonomic implications. *Bacteriological reviews*, *36*(4), 407.

Sharma, S. K., & Mohan, A. (2013). Tuberculosis: From an incurable scourge to a curable disease-journey over a millennium. *The Indian journal of medical research*, *137*(3), 455.

Shelley, J. C., Cholleti, A., Frye, L. L., Greenwood, J. R., Timlin, M. R., & Uchimaya, M. (2007). Epik: a software program for pKa prediction and protonation state generation for drug-like molecules. *Journal of computer-aided molecular design*, *21*(12), 681-691.

Singh, K. D., Hadjadj-Aoul, Y., & Rubino, G. (2012, January). Quality of experience estimation for adaptive HTTP/TCP video streaming using H. 264/AVC. In *Consumer Communications and Networking Conference (CCNC), 2012 IEEE* (pp. 127-131). IEEE.

Spry, C., Kirk, K., & Saliba, K. J. (2007). Coenzyme A biosynthesis: an antimicrobial drug target. *FEMS microbiology reviews*, *32*(1), 56-106.

Sridevi, J. P., Anantaraju, H. S., Kulkarni, P., Yogeeswari, P., & Sriram, D. (2014). Optimization and validation of *Mycobacterium marinum*-induced adult zebrafish model for evaluation of oral anti-tuberculosis drugs. *International journal of mycobacteriology*, *3*(4), 259-267.

Reddy, B. K., Landge, S., Ravishankar, S., Patil, V., Shinde, V., Tantry, S., ... & Ambady, A. (2014). Assessment of Mycobacterium tuberculosis pantothenate kinase vulnerability through target knockdown and mechanistically diverse inhibitors. *Antimicrobial agents and chemotherapy*, *58*(6), 3312-3326.

Reece, R. J., & Maxwell, A. (1991). Probing the limits of the DNA breakage-reunion domain of the Escherichia coli DNA gyrase A protein. *Journal of Biological Chemistry*, *266*(6), 3540-3546.

Reck, F., Alm, R., Brassil, P., Newman, J., DeJonge, B., Eyermann, C. J., ... & Davis, H. (2011). Novel N-linked aminopiperidine inhibitors of bacterial topoisomerase type II: broad-spectrum antibacterial agents with reduced hERG activity. *Journal of medicinal chemistry*, *54*(22), 7834-7847.

Ruzheinikov, S. N., Taal, M. A., Sedelnikova, S. E., Baker, P. J., & Rice, D. W. (2005). Substrate-induced conformational changes in Bacillus subtilis glutamate racemase and their implications for drug discovery. *Structure*, *13*(11), 1707-1713.

Thomas, J., & Cronan, J. E. (2010). Antibacterial activity of N-pentylpantothenamide is due to inhibition of coenzyme A synthesis. *Antimicrobial agents and chemotherapy*, *54*(3), 1374-1377.

Vallari, D. S., Jackowski, S., & Rock, C. O. (1987). Regulation of pantothenate kinase by coenzyme A and its thioesters. *Journal of Biological Chemistry*, *262*(6), 2468-2471.

van Leeuwen, L. M., van der Sar, A. M., & Bitter, W. (2015). Animal models of tuberculosis: zebrafish. *Cold Spring Harbor perspectives in medicine*, *5*(3), a018580.

Venkatraman, J., Bhat, J., Solapure, S. M., Sandesh, J., Sarkar, D., Aishwarya, S., ... & Das, K. S. (2012). Screening, identification, and characterization of mechanistically diverse inhibitors of

the Mycobacterium tuberculosis enzyme, pantothenate kinase (CoaA). *Journal of biomolecular screening*, *17*(3), 293-302.

Wang, F., Sambandan, D., Halder, R., Wang, J., Batt, S. M., Weinrick, B., ... & Hassani, M. (2013). Identification of a small molecule with activity against drug-resistant and persistent tuberculosis. *Proceedings of the National Academy of Sciences*, *110*(27), E2510-E2517.

WHO Global tuberculosis report, 2016.

Worthington, A. S., & Burkart, M. D. (2006). One-pot chemo-enzymatic synthesis of reporter-modified proteins. *Organic & biomolecular chemistry*, *4*(1), 44-46.

Appendix

LIST OF PUBLICATIONS

From Thesis work

1. **Malapati P**, Siva Krishna V, Nallangi R, Meda N, Reshma Srilakshmi R, Sriram D. "Identification and development of benzoxazole derivatives as novel bacterial glutamate racemase inhibitors" *Eur J Med Chem*. 2018, 145:23-34.
2. **Malapati P**, Siva Krishna V, Nallangi R, Meda N, Reshma Srilakshmi R, Sriram D. "Lead identification and optimization of bacterial glutamate racemase inhibitors" *Bioorg Med Chem*. 2018, 26(1):177-190.
3. **Malapati P**, Siva Krishna V, Sriram D. "Identification and development of novel indazole derivatives as potent bacterial peptidoglycan synthesis inhibitors" *Int J Mycobacteriol*. 7 (1): 76-80.
4. **Malapati P**, Siva Krishna V, Sriram D. "Identification and development of oxoquinazoline derivatives as novel mycobacterial inhibitors targeting cell wall synthesis enzyme" *Biomed Biotechnol Res J*. 2 (1): 31-35.

Other publications

1. Dhar A, Udumula MP, Medapi B, Bhat A, Dhar I, **Malapati P**, Babu MS, Kalra J, Sriram D, Desai KM. (2016). "Pharmacological evaluation of novel alagebrium analogs as methylglyoxal scavengers in vitro in cardiac myocytes and in vivo in SD rats" *Int J Cardiol*. 223: 581-589.

Papers presented at National/International Conferences

- **Prasanthi M**, Vagolu S.K, Radhika N, Nikhila M, Rudraraju R. S., Dharmarajan S "Lead identification and optimization of bacterial Glutamate racemase inhibitors" presented at ATMOS held at BITS-Pilani Hyderabad Campus, 29 Oct 2017
- **Prasanthi M**, Reshma R, Priyanka S, Vijay S, D Sriram " Design and identification of *Mycobacterium tuberculosis* Glutamate racemase inhibitors. 6^{th} International Symposium on "Current Trends in Drug Discovery & Research", CSIR-CDRI, Lucknow, Feb. 25^{th} – 28^{th}, 2016

BIOGRAPHY OF D. SRIRAM

D. Sriram is presently working in the capacity of Professor at Department of Pharmacy, Birla Institute of Technology & Science, Pilani, Hyderabad campus. He received his Ph.D. in 2000 from Banaras Hindu University (IIT-BHU), Varanasi. He has been involved in teaching and research for last 17 years. He has 330 peer-reviewed research publications, 5 patents and 1 book to his credit. He has collaborations with various national and international organizations such as Karolinska Institute, Sweden; Institute of Science and Technology for Tuberculosis, Porto Allegre, Brazil; National Institute of Immunology, New Delhi etc. He was awarded the Young Pharmacy Teacher of the year award of 2006 by the Association of Pharmacy Teachers of India. He received ICMR Centenary year award in 2011. Prof. D Sriram has been selected for the prestigious Tata Innovation Fellowship of the Department of Biotechnology, Government of India for the year 2015-16 in recognition of his outstanding research contributions.He has guided 19 Ph.D. students and 8 students are pursuing Ph.D. currently. His research is funded by agencies like the UGC, CSIR, ICMR, DBT and DST.

BIOGRAPHY OF PRASANTHI MALAPATI

Ms. Prasanthi Malapati completed her Bachelor of Pharmacy from Jawaharlal Nehru Technological University, Kakinada. She has obtained her M.S. (Pharm.) from National Institute of Education and Research (NIPER) Hyderabad campus. She has been awarded DST-Inspire Junior Research Fellowship and started working from Jan 2015 onwards at Birla Institute of Technology & Science, Pilani, and Hyderabad campus under the supervision of Prof. D. Sriram. She has five scientific papers in well-renowned international journals and also presented papers at international conferences.